Novel Insights into Cardiac Imaging in Cardiovascular Disease

J.M.J. Boogers

The research described in this thesis was performed at the departments of cardiology, radiology and nuclear medicine of the Leiden University Medical Center, Leiden, the Netherlands.

Lay-out: Optima Grafische Communicatie, Rotterdam, the Netherlands

Printed by: Optima Grafische Communicatie, Rotterdam, the Netherlands

ISBN: 978-90-9026746-3

Financial support for the costs involved in publication of this thesis was gratefully received from: J.E. Jurriaanse Stichting, Bronovo Research Foundation, GE Healthcare BV, Servier Nederland Farma BV, Merck Sharp & Dohme BV, Boehringer Ingelheim BV, Medis Medical Imaging Systems BV, Bracco Imaging Europe BV, Toshiba Medical Systems BV.

Novel Insights into Cardiac Imaging in Cardiovascular Disease

Proefschrift

de graad van Doctor aan de Universiteit Leiden,
op gezag van Rector Magnificus prof.mr. P.F. van der Heijden
volgens besluit van het College van Promoties
te verdedigen op donderdag 14 juni 2012

klokke 10:00 uur

door

Johannes Maria Josephus Boogers
geboren te Tilburg
in 1983

Promotiecommissie

Promotores:	Prof. dr. J.W. Jukema
	Prof. dr. J.J. Bax
Overige leden:	Prof. dr. M.J. Schalij
	Prof. dr. E.E. van der Wall
	Prof. dr. A. de Roos
	Prof. dr. J.H.C. Reiber
	Prof. dr. B.L.F. van Eck-Smit *(Academic Medical Center, Amsterdam)*
	dr. P.V. Oemrawsingh *(Medical Center Haaglanden, the Hague)*

The research activities described in this thesis were supported by the Interuniversity Cardiology Institute of the Netherlands, Utrecht, the Netherlands. Part of the research described in this thesis was supported by a grant of the Dutch Heart Foundation (DHF-2006T102). Financial support by the Dutch Heart Foundation for publication of this thesis is gratefully acknowledged.

Te weten dat je onwetend bent
is het begin van alle wijsheid

Table of Contents

Chapter **1**

General Introduction and Outline of the Thesis

Cardiovascular Disease

Although considerable improvements in diagnosis, therapeutic interventions and prognostification of patients with cardiovascular disease have been made over the last several decades, cardiovascular disease remains one of the foremost challenges of public health these days.[1-3]

Based upon National Health Surveys, the World Health Organization (WHO) has reported that cardiovascular disease affects approximately 17.3 million individuals worldwide, with an estimated 7.3 million people who are suffering from ischemic heart disease.[3] The WHO has stated that 4.6 million Europeans have been diagnosed with cardiovascular disease, including 2.2 million individuals with ischemic heart disease across European countries.[3] Even though the age-adjusted incidence of cardiovascular disease may appear constant over the last couple of years, its prevalence is expected to grow considerably in the upcoming years as the population ages over time due to further improvements in early diagnosis, treatment options along with advances in risk stratification of patients with cardiovascular disease. Additionally, the world-wide under-recognition and under-treatment of individuals with risk factors for atherosclerosis will lead to an even further increase in cardiovascular disease, predominantly ischemic heart disease.[2]

At present, cardiac imaging has contributed significantly to the currently applied diagnostic, therapeutic and prognostic algorithms for patients with cardiovascular disease. Among available cardiac imaging techniques, computed tomography (CT) has emerged as one of most potent cardiac imaging techniques for non-invasive evaluation of coronary atherosclerosis. However, despite the presence of highly advanced image acquisition techniques for cardiac CT, the evaluation of coronary artery disease (CAD) is usually based on a rather simple dichotomous visual approach. Based upon visual analysis of cardiac CT images, coronary lesions with ≥50% luminal narrowing are usually defined as lesions with significant coronary stenosis.

Accordingly, the use of automated quantitative algorithms for post-processing of cardiac CT images may help to improve ***diagnosis*** *of coronary atherosclerosis by cardiac CT (Part I)*. A detailed assessment of coronary atherosclerosis on cardiac CT can be used to guide patient referral for percutaneous coronary intervention or coronary artery bypass grafting surgery.

Beyond advances in diagnosis of cardiovascular disease, cardiac imaging has also been used to improve the selection of patients who will benefit from specific **therapeutic interventions**. Cardiac imaging has been applied to guide clinicians in the selection of heart failure patients for cardiac resynchronization therapy (CRT). Even though several cardiac imaging techniques are already available in clinical practice, the selection of heart failure patients who will gain benefit from dedicated cardiac device therapies remains difficult.

Phase analysis on gated myocardial perfusion single photon emission computed tomography (SPECT) (GMPS) provides potential important information in patients with heart failure referred for CRT. *Novel insights in GMPS with phase analysis may further improve the selection of heart failure patients who will benefit from CRT (Part II)*.

Finally, cardiac imaging can be used to **risk stratify** patients with cardiovascular disease for future adverse events. Although significant improvements in prognostification of patients with cardiovascular disease have been made in recent years, appropriate selection of patients at risk for adverse cardiac events remains a main challenge these days. *Recent developments in sympathetic nerve imaging with 123-iodine metaiodobenzylguanidine (123-I MIBG) imaging may be used to improve risk stratification of patients with cardiovascular disease (Part III)*.

Dedicated Automated Quantitative Computed Tomography in Patients with Coronary Artery Disease (Part I)

The presence of coronary artery disease can be detected by direct anatomic assessment of coronary atherosclerosis and luminal narrowing using cardiac CT, which has emerged as a potent non-invasive imaging technique since it provides excellent image quality and high diagnostic accuracy for visualization of CAD when compared to invasive coronary angiography.[4-6]

Although invasive coronary angiography is primarily restricted to luminography, cardiac CT offers the ability for a comprehensive evaluation of CAD by assessment of location, extent and severity as well as composition of atherosclerotic lesions, rather than the degree of coronary artery stenosis alone.[6] A complete analysis of coronary atherosclerosis may provide important information to identify patients at risk for adverse cardiovascular events[7], and importantly, may be used to guide future therapeutic interventions such as percutaneous coronary intervention or coronary artery bypass grafting surgery. Despite the rapid developments in CT acquisition technology, cardiac CT angiography images are most commonly post-processed and evaluated by an expert CT reader using a rather simple visual and dichotomous approach, in which ≥50% luminal narrowing is usually defined as a significant coronary stenosis.

In this perspective, the introduction of new dedicated algorithms for automated quantification of coronary atherosclerosis (Figure 1) may further improve diagnostic accuracy of cardiac CT, and interestingly, may lead to a more time-efficient post-processing of cardiac CT images. Moreover, even though the number of cardiac CT scans with ambiguous or inconclusive results has become considerably smaller with the introduction of modern CT

scanners and image acquisition protocols, the use of dedicated post-processing techniques may result in a further decrease in the number of inconclusive or misinterpreted cardiac CT scans.

Additionally, one should acknowledge that cardiac CT is still hampered by reduced positive predictive values due to image artifacts along with a tendency to overestimate coronary stenosis in calcified lesions.[5, 6, 8] Visual analysis of heavily calcified lesions can lead to (severe) overestimation of luminal narrowing due to blooming artifacts, which in turn, results in false-positive findings on invasive coronary angiography. Accordingly, the development of novel automated quantitative approaches for cardiac CT has gained increasingly interest over the recent years.

Current preliminary data for quantitative CT have been derived from semi-manual or manually-assisted cardiac CT approaches, rather than automated dedicated algorithms for quantification of coronary atherosclerosis.[9-14] As compared to intravascular ultrasound (IVUS), these quantitative approaches were limited by substantial variability and large limits of agreement.[9-14] The use of sophisticated automated post-processing algorithms for quantification of coronary atherosclerosis may lead to improved diagnostic accuracy and reproducibility of cardiac CT. *Such quantitative information can be used to improve diagnosis of coronary atherosclerosis, and for this reason, may improve the patient referral*

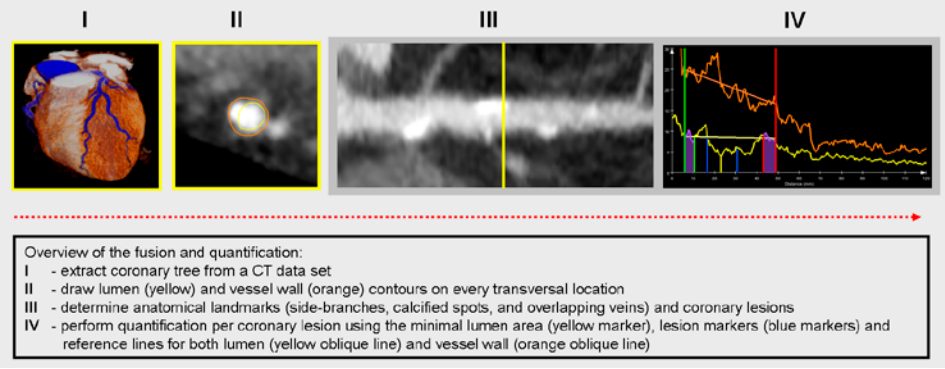

Figure 1. Schematic illustration of consecutive processing steps involved in automated quantification using dedicated quantitative post-processing software for cardiac computed tomography (CT).

for percutaneous coronary intervention or coronary artery bypass grafting surgery.

Myocardial Perfusion SPECT for Selection of Heart Failure Patients Referred for Cardiac Resynchronization Therapy (Part II)

Within the last 10 to 15 years, multiple randomized controlled trials have clearly demonstrated the benefits of biventricular pacing on morbidity and mortality rates in patients with moderate-to-severe heart failure who remain symptomatic despite optimal pharmacological treatment.[15, 16] Based on several landmark trials[15-19], international guidelines have recommended CRT with a class I indication in patients with symptomatic drug-refractory systolic heart failure New York Heart Association (NYHA) functional class III and IV, ventricular dyssynchrony (prolonged QRS duration ≥120 ms), reduced LV ejection fraction (LVEF) ≤35% and sinus rhythm.[20, 21]

Although considerable improvements in heart failure symptoms, exercise capacity, mitral regurgitation and LV dimensions have been observed in heart failure patients receiving CRT[17-19, 21-24], a consistent proportion of patients who meet the current selection criteria for CRT fail to respond to CRT.[24, 25]

As a consequence, numerous clinical studies have been conducted that were designed to improve current selection of patients referred to CRT by identification of potential determinants for response to CRT.[24-28] Among the multiple pathophysiologic mechanisms involved in heart failure, the presence of LV systolic dyssynchrony has been identified as one of the major determinants of CRT response.[29, 30] It has been shown that LV systolic dyssynchrony can affect biomechanics and performance of the LV considerably.[31]

At present, many cardiac imaging techniques have been applied in clinical practice to assess the presence and extent of LV systolic dyssynchrony in heart failure patients, wherein echocardiographic techniques such as 2D echocardiography with tissue Doppler imaging (TDI) have been used most widely for detection of LV systolic dyssynchrony.[29, 30] At present however, no consensus exists on the echocardiographic definition of LV systolic dyssynchrony, an issue which can be addressed by nuclear imaging techniques since phase analysis on GMPS allows assessment of mechanical dyssynchrony using an automated and reproducible post-processing algorithm.

Moreover, non-synchrony issues such as location, extent and severity of scar tissue have been identified as (important) determinants affecting the likelihood of response to CRT.[25, 32-34] Additionally, the relation between LV lead position and site of latest mechanical activation has been shown to play an important role in prediction of CRT response.[35] Accordingly, SPECT may be of interest, since it provides information on cardiac dyssynchrony (by phase analysis of gated SPECT data) along with assessment of presence, location and extent of scar tissue.

As indicated in Figure 2, phase analysis is performed on standard GMPS short-axis images and involves several processing steps. A histogram is generated that provides information on LV systolic (dys) synchrony for the entire ventricle. A total of 5 quantitative parameters for LV systolic dyssynchrony can be derived from the phase histogram, including histogram bandwidth (HBW), phase standard deviation (SD), histogram kurtosis, skewness and peakedness. HBW (including 95% of the phase angles) and phase SD (SD of the phase distribution) have been validated against echocardiographic techniques for assessment of LV systolic dyssynchrony.[36, 37] Along with LV systolic dyssynchrony, phase analysis can be used for assessment of LV diastolic dyssynchrony by detection of changes in myocardial counts during the diastolic phase of the LV. Additionally, phase analysis on GMPS can be used to

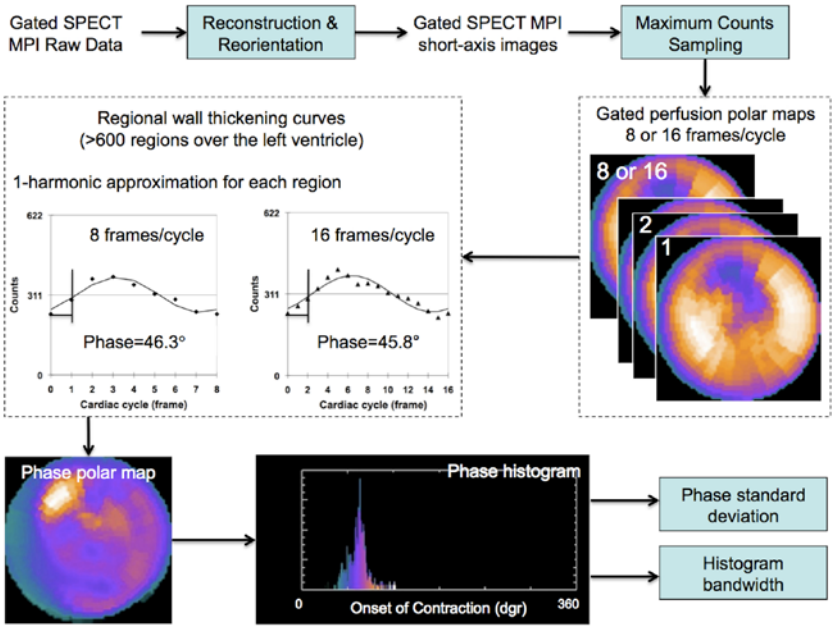

Figure 2: Phase analysis on gated myocardial perfusion single photon emission computed tomography (SPECT) (GMPS) allows integrated assessment of left ventricular (LV) systolic dyssynchrony, myocardial infarction and site of latest mechanical activation. Phase analysis is performed on standard GMPS reconstructed short-axis images and involves several processing steps: (1) detection of maximal counts in 3D for each temporal frame, (2) count-based wall-thickening curves are created from regional count changes during the R-R cycle, (3) approximation of separate sample points into a continuous curve using first Fourier Harmonic function (middle, left panel). As indicated below, the phase polar map (bottom, left panel) shows a considerable phase delay (bright region) at the anterior and apical segments of the LV. Subsequently, the phase histogram (bottom, mid panel) shows the degree of systolic dyssynchrony or synchrony for the entire LV, in which histogram bandwidth (HBW) and phase standard deviation (SD) are the most commonly used indicators of LV (dys) synchrony.

identify the site of latest mechanical activation (and whether this region is viable) which may help in selecting the optimal LV lead position. Thus, GMPS with phase analysis is a potent cardiac imaging technique that provides important information in patients with heart failure referred for CRT. *In part II, the role of phase analysis on GMPS for selection of heart failure patients for CRT will be addressed.*

Cardiac Sympathetic Nerve Scintigraphy with 123-I Metaiodobenzylguanidine for Risk Stratification of Patients with Cardiovascular Disease (Part III)

Among patients with cardiovascular disease, the clinical syndrome of heart failure is a common pathophysiologic disorder, with an estimated prevalence of approximately 5.3 million individuals in the United States.[38] The risk for newly diagnosed heart failure is considerably high in the western population, with a life-time risk of 1 out of 5 in patients aged 40 years. Importantly, heart failure patients are suffering from a serious pathophysiologic condition as 20% of patients will die within the first year after the beginning of heart failure.[38] Moreover, heart failure patients also exhibit a considerably high long-term mortality rate, with an estimated 5-year mortality rate of 59% in men and 45% in women.[39]

Even though considerable advances in risk stratification of patients with heart failure have been made in recent years, identification of heart failure patients who will suffer from serious adverse events remains a difficult issue.

The cardiac sympathetic nervous system may serve as an important determinant for risk stratification in heart failure as it is directly involved in preservation of cardiovascular homeostasis by regulation of heart frequency, electrical conduction and cardiac contractility.[40] A chronic dysfunctional cardiac sympathetic nervous system exerts pleiotropic detrimental effects on the structural and functional integrity of the myocardium, including stimulation of cardiomyocyte hypertrophy, fibroblast and smooth muscle cell proliferation, which altogether contribute to a worse cardiovascular outcome.[41, 42] As a consequence, the cardiac sympathetic nervous system can been used for risk stratification of patients with cardiovascular disease, most commonly in the setting of chronic heart failure.[41-45]

Although plasma norepinephrine levels and the rate of norepinephrine spillover can be used as determinants for identification of patients at risk for adverse cardiovascular outcome[41, 42], a direct assessment of cardiac sympathetic innervation by nuclear imaging may represent a more sensitive marker for risk stratification of patients with heart failure.[45]

Among nuclear imaging techniques, SPECT can be used for mapping the cardiac sympathetic nervous system as it provides enough sensitivity to assess distinct aspects of the cardiac neurotransmission itself, including norepinephrine uptake at the presynaptic site (sympathetic innervation) as well as binding of norepinephrine at the post-synaptic site.[46-48] Moreover, the rate in which radionuclide SPECT tracers are washed out of the myocardium provides information on the degree of sympathetic activity within the heart.

The norepinephrine analogue metaiodobenzylguanidine labeled to iodine-123 (123-I MIBG) has been used most commonly as a SPECT radionuclide tracer for assessment of cardiac sympathetic innervation (Figure 3).[44, 45] Thus far, a large number of studies have demonstrated the predictive value of cardiac 123-I MIBG imaging in patients with heart failure.[44, 45, 49] Agostini et al.[50] evaluated whether 123-I MIBG scintigraphy allowed risk stratification of 290 heart failure patients. Patients with adverse events (n=67) showed significantly lower cardiac 123-I MIBG uptake on late planar imaging (as expressed as the heart-to-mediastinum (H/M) ratio) when compared to patient without adverse events (n=223) ($p<0.001$). Moreover, both H/M ratio (on late planar 123-I MIBG scintigraphy) and LVEF were significant predictors for adverse cardiac events. More recently, the prospective multicenter AdreView Myocardial Imaging for Risk Evaluation in Heart Failure (ADMIRE-HF) study has evaluated the predictive value of cardiac neuronal status as derived from cardiac 123-I MIBG scintigraphy in 961 patients with NYHA functional class II or III. Heart failure patients with a late H/M ratio of <1.60 experienced significantly more adverse events than heart failure patients with a late H/M ratio of ≥1.60 ($p<0.001$).[45]

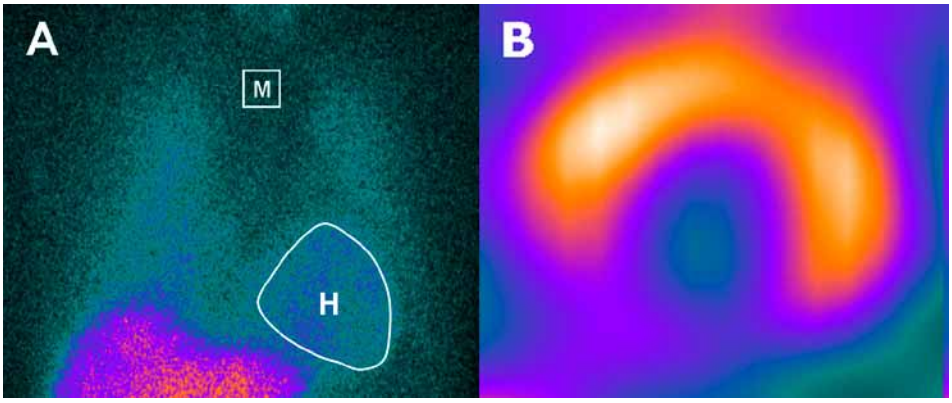

Figure 3. 123-iodine metaiodobenzylguanidine (123-I MIBG) for assessment of cardiac sympathetic innervation using planar imaging (panel A) and single photon emission computed tomography (SPECT) (panel B). Planar imaging is used for assessment of global sympathetic innervation patterns by calculation of the heart-to-mediastinum (H/M) ratio, in which the mean counts per pixel within the heart (H) is divided by the mean counts per pixel within the upper mediastinum (M). Regional defects in sympathetic innervation of the myocardium can be assessed using SPECT, as depicted in panel B.

Beyond prediction of cardiac death or worsening heart failure, some studies have also postulated the use of cardiac 123-I MIBG scintigraphy for identification of patients at risk for adverse arrhythmogenic events, including lethal ventricular arrhythmias and sudden cardiac death.[44, 45] It has been shown that parasympathetic stimulation of the ventricles exerts anti-fibrillatory effects on the myocardium, while ventricular sympathetic activation emerged to have a pro-arrhythmogenic effect on the myocardium.[51] Moreover, activation of the cardiac sympathetic nervous system contributes to cardiac arrhythmogenesis as regions with abnormalities in cardiac sympathetic innervation may show a denervation supersensitivity response to circulating catecholamines with an enhanced automaticity of cardiomyocytes and a reduction of ventricular effective refraction period.[51-53] Finally, co-existence of sympathetic denervated regions alongside regions with preserved sympathetic innervation may lead to inhomogeneous neuronal release of neurotransmitter norepinephrine, which subsequently, can cause considerable changes in action potential duration and configuration with associated electrophysiologic heterogeneity of the myocardium.[51-53]

Accordingly, cardiac 123-I MIBG scintigraphy may provide important information to risk stratify patients with cardiovascular disease by assessment of cardiac sympathetic innervation and activation.

More specifically, cardiac 123-I MIBG scintigraphy may serve as a potent imaging technique for identification of patients at risk for future ventricular arrhythmia or sudden cardiac death, which potentially, could help to improve the current selection of patients indicated for implantable cardioverter-defibrillator (ICD) treatment (Part III).

Objective and Outline of the Thesis

Although cardiac imaging has already contributed significantly in the evaluation of patients with cardiovascular disease, novel insights into cardiac imaging techniques may further improve diagnostic and therapeutic algorithms as well as prognostification of patients with cardiovascular disease. More specifically, the current thesis describes the role of novel insights into cardiac imaging for diagnosis (Part I), treatment (Part II) and risk stratification (Part III) of patients with cardiovascular disease.

In **part I**, the value of automated quantitative CT for evaluation of coronary atherosclerosis is described. Chapter 2 provides an overview of the currently available approaches for quantification of coronary atherosclerosis. Additionally, chapter 2 describes the potential role of quantitative CT to guide percutaneous coronary intervention procedures. In chapter 3, the validation of a dedicated CT algorithm for automated quantification of coronary stenosis severity is discussed. Chapter 4 shows the feasibility of automated coronary plaque quantification using dedicated CT software in comparison with IVUS. At last, the feasibility of cardiac CT to assess diastolic function is described in chapter 5.

In **part II**, the potentials of nuclear imaging with GMPS in heart failure patients referred for CRT are described. Chapter 6 reviews the role of phase analysis on GMPS for assessment of LV systolic dyssynchrony, myocardial infarction and viability. Chapter 7 describes the validation of a dedicated algorithm for phase analysis on GMPS in a direct comparison with echocardiography using TDI for assessment of LV systolic dyssynchrony. Chapter 8 evaluates the relation between the site of latest mechanical activation as derived from GMPS, LV lead position and response to CRT. In chapter 9, the feasibility of GMPS with phase analysis to assess LV diastolic dyssynchrony in a direct comparison with TDI is evaluated. Finally, chapter 10 evaluates the prediction of response to CRT by LV diastolic dyssynchrony as assessed from GMPS with phase analysis.

In **part III**, the role of cardiac sympathetic nerve imaging with 123-I MIBG for risk stratification of patients with cardiovascular disease is described. Chapter 11 describes the value of cardiac 123-I MIBG scintigraphy for prognostification of patients with heart failure. The potentials of cardiac 123-I MIBG imaging for identification of patients at risk for ventricular arrhythmias are described in chapter 12. In chapter 13, the relation between contrast-enhanced magnetic resonance imaging (MRI) and 123-I MIBG/perfusion scintigraphy for assessment of infarct size and infarct border zone, referred to as myocardium at risk for ventricular arrhythmias, is evaluated.

Reference List

(1) Yusuf S, Reddy S, Ounpuu S, Anand S. Global burden of cardiovascular diseases: part I: general considerations, the epidemiologic transition, risk factors, and impact of urbanization. Circulation 2001;104:2746-2753.

(2) Sanz J, Fayad ZA. Imaging of atherosclerotic cardiovascular disease. Nature 2008;451:953-957.

(3) World Health Organization. Report on global burden of disease. 2008.

(4) Miller JM, Rochitte CE, Dewey M, rbab-Zadeh A, Niinuma H, Gottlieb I, Paul N, Clouse ME, Shapiro EP, Hoe J, Lardo AC, Bush DE, de Roos A, Cox C, Brinker J, Lima JA. Diagnostic performance of coronary angiography by 64-row CT. N Engl J Med 2008;359:2324-2336.

(5) Meijboom WB, Meijs MF, Schuijf JD, Cramer MJ, Mollet NR, van Mieghem CA, Nieman K, van Werkhoven JM, Pundziute G, Weustink AC, de Vos AM, Pugliese F, Rensing B, Jukema JW, Bax JJ, Prokop M, Doevendans PA, Hunink MG, Krestin GP, de Feyter PJ. Diagnostic accuracy of 64-slice computed tomography coronary angiography: a prospective, multicenter, multivendor study. J Am Coll Cardiol 2008;52:2135-2144.

(6) Achenbach S, Raggi P. Imaging of coronary atherosclerosis by computed tomography. Eur Heart J 2010;31:1442-1448.

(7) Bamberg F, Sommer WH, Hoffmann V, Achenbach S, Nikolaou K, Conen D, Reiser MF, Hoffmann U, Becker CR. Meta-analysis and systematic review of the long-term predictive value of assessment of coronary atherosclerosis by contrast-enhanced coronary computed tomography angiography. J Am Coll Cardiol 2011;57:2426-2436.

(8) Budoff MJ, Dowe D, Jollis JG, Gitter M, Sutherland J, Halamert E, Scherer M, Bellinger R, Martin A, Benton R, Delago A, Min JK. Diagnostic performance of 64-multidetector row coronary computed tomographic angiography for evaluation of coronary artery stenosis in individuals without known coronary artery disease: results from the prospective multicenter ACCURACY (Assessment by Coronary Computed Tomographic Angiography of Individuals Undergoing Invasive Coronary Angiography) trial. J Am Coll Cardiol 2008;52:1724-1732.

(9) Achenbach S, Ropers D, Hoffmann U, MacNeill B, Baum U, Pohle K, Brady TJ, Pomerantsev E, Ludwig J, Flachskampf FA, Wicky S, Jang IK, Daniel WG. Assessment of coronary remodeling in stenotic and nonstenotic coronary atherosclerotic lesions by multidetector spiral computed tomography. J Am Coll Cardiol 2004;43:842-847.

(10) Achenbach S, Moselewski F, Ropers D, Ferencik M, Hoffmann U, MacNeill B, Pohle K, Baum U, Anders K, Jang IK, Daniel WG, Brady TJ. Detection of calcified and noncalcified coronary atherosclerotic plaque by contrast-enhanced, submillimeter multidetector spiral computed tomography: a segment-based comparison with intravascular ultrasound. Circulation 2004;109:14-17.

(11) Leber AW, Knez A, von Ziegler F, Becker A, Nikolaou K, Paul S, Wintersperger B, Reiser M, Becker CR, Steinbeck G, Boekstegers P. Quantification of obstructive and nonobstructive coronary lesions by 64-slice computed tomography: a comparative study with quantitative coronary angiography and intravascular ultrasound. J Am Coll Cardiol 2005;46:147-154.

(12) Leber AW, Becker A, Knez A, von Ziegler F, Sirol M, Nikolaou K, Ohnesorge B, Fayad ZA, Becker CR, Reiser M, Steinbeck G, Boekstegers P. Accuracy of 64-slice computed tomography to classify and quantify plaque volumes in the proximal coronary system: a comparative study using intravascular ultrasound. J Am Coll Cardiol 2006;47:672-677.

(13) Otsuka M, Bruining N, Van Pelt NC, Mollet NR, Ligthart JM, Vourvouri E, Hamers R, De Jaegere P, Wijns W, van Domburg RT, Stone GW, Veldhof S, Verheye S, Dudek D, Serruys PW, Krestin GP, de Feyter PJ. Quantification of coronary plaque by 64-slice computed tomography: a comparison with quantitative intracoronary ultrasound. Invest Radiol 2008;43:314-321.

(14) Schepis T, Marwan M, Pflederer T, Seltmann M, Ropers D, Daniel WG, Achenbach S. Quantification of noncalcified coronary atherosclerotic plaques with Dual Source Computed Tomography: comparison to intravascular ultrasound. Heart 2010;96:610-615.

(15) Bristow MR, Saxon LA, Boehmer J, Krueger S, Kass DA, De Marco T, Carson P, DiCarlo L, DeMets D, White BG, DeVries DW, Feldman AM. Cardiac-resynchronization therapy with or without an implantable defibrillator in advanced chronic heart failure. N Engl J Med 2004;350:2140-2150.
(16) Cleland JG, Daubert JC, Erdmann E, Freemantle N, Gras D, Kappenberger L, Tavazzi L. The effect of cardiac resynchronization on morbidity and mortality in heart failure. N Engl J Med 2005;352:1539-1549.
(17) Cazeau S, Leclercq C, Lavergne T, Walker S, Varma C, Linde C, Garrigue S, Kappenberger L, Haywood GA, Santini M, Bailleul C, Daubert JC. Effects of multisite biventricular pacing in patients with heart failure and intraventricular conduction delay. N Engl J Med 2001;344:873-880.
(18) Auricchio A, Stellbrink C, Sack S, Block M, Vogt J, Bakker P, Huth C, Schondube F, Wolfhard U, Bocker D, Krahnefeld O, Kirkels H. Long-term clinical effect of hemodynamically optimized cardiac resynchronization therapy in patients with heart failure and ventricular conduction delay. J Am Coll Cardiol 2002;39:2026-2033.
(19) Abraham WT, Fisher WG, Smith AL, Delurgio DB, Leon AR, Loh E, Kocovic DZ, Packer M, Clavell AL, Hayes DL, Ellestad M, Trupp RJ, Underwood J, Pickering F, Truex C, McAtee P, Messenger J. Cardiac resynchronization in chronic heart failure. N Engl J Med 2002;346:1845-1853.
(20) Epstein AE, DiMarco JP, Ellenbogen KA, Estes NA, III, Freedman RA, Gettes LS, Gillinov AM, Gregoratos G, Hammill SC, Hayes DL, Hlatky MA, Newby LK, Page RL, Schoenfeld MH, Silka MJ, Stevenson LW, Sweeney MO, Smith SC, Jr., Jacobs AK, Adams CD, Anderson JL, Buller CE, Creager MA, Ettinger SM, Faxon DP, Halperin JL, Hiratzka LF, Hunt SA, Krumholz HM, Kushner FG, Lytle BW, Nishimura RA, Ornato JP, Page RL, Riegel B, Tarkington LG, Yancy CW. ACC/AHA/HRS 2008 Guidelines for Device-Based Therapy of Cardiac Rhythm Abnormalities: a report of the American College of Cardiology/American Heart Association Task Force on Practice Guidelines: developed in collaboration with the American Association for Thoracic Surgery and Society of Thoracic Surgeons. Circulation 2008;117:e350-e408.
(21) Vardas PE, Auricchio A, Blanc JJ, Daubert JC, Drexler H, Ector H, Gasparini M, Linde C, Morgado FB, Oto A, Sutton R, Trusz-Gluza M. Guidelines for cardiac pacing and cardiac resynchronization therapy: The Task Force for Cardiac Pacing and Cardiac Resynchronization Therapy of the European Society of Cardiology. Developed in collaboration with the European Heart Rhythm Association. Eur Heart J 2007;28:2256-2295.
(22) Ypenburg C, Lancellotti P, Tops LF, Boersma E, Bleeker GB, Holman ER, Thomas JD, Schalij MJ, Pierard LA, Bax JJ. Mechanism of improvement in mitral regurgitation after cardiac resynchronization therapy. Eur Heart J 2008:757-765.
(23) St John SM, Ghio S, Plappert T, Tavazzi L, Scelsi L, Daubert C, Abraham WT, Gold MR, Hassager C, Herre JM, Linde C. Cardiac resynchronization induces major structural and functional reverse remodeling in patients with New York Heart Association class I/II heart failure. Circulation 2009;120:1858-1865.
(24) Bax JJ, Abraham T, Barold SS, Breithardt OA, Fung JW, Garrigue S, Gorcsan J, III, Hayes DL, Kass DA, Knuuti J, Leclercq C, Linde C, Mark DB, Monaghan MJ, Nihoyannopoulos P, Schalij MJ, Stellbrink C, Yu CM. Cardiac resynchronization therapy: Part 1-issues before device implantation. J Am Coll Cardiol 2005;46:2153-2167.
(25) Gorcsan J, III. Finding pieces of the puzzle of nonresponse to cardiac resynchronization therapy. Circulation 2011;123:10-12.
(26) Yu CM, Fung JW, Zhang Q, Chan CK, Chan YS, Lin H, Kum LC, Kong SL, Zhang Y, Sanderson JE. Tissue Doppler imaging is superior to strain rate imaging and postsystolic shortening on the prediction of reverse remodeling in both ischemic and nonischemic heart failure after cardiac resynchronization therapy. Circulation 2004;110:66-73.
(27) Bax JJ, Bleeker GB, Marwick TH, Molhoek SG, Boersma E, Steendijk P, Van der Wall EE, Schalij MJ. Left ventricular dyssynchrony predicts response and prognosis after cardiac resynchronization therapy. J Am Coll Cardiol 2004;44:1834-1840.

(28) Bommel van R, Delgado V, Schalij MJ, Bax JJ. Critical appraisal of the use of cardiac resynchronization therapy beyond current guidelines. J Am Coll Cardiol 2010;56:754-762.
(29) Gorcsan J, III, Abraham T, Agler DA, Bax JJ, Derumeaux G, Grimm RA, Martin R, Steinberg JS, Sutton MS, Yu CM. Echocardiography for cardiac resynchronization therapy: recommendations for performance and reporting--a report from the American Society of Echocardiography Dyssynchrony Writing Group endorsed by the Heart Rhythm Society. J Am Soc Echocardiogr 2008;21:191-213.
(30) Delgado V, Bax JJ. Assessment of systolic dyssynchrony for cardiac resynchronization therapy is clinically useful. Circulation 2011;123:640-655.
(31) Kass DA. Pathobiology of cardiac dyssynchrony and resynchronization. Heart Rhythm 2009;6:1660-1665.
(32) Bleeker GB, Kaandorp TA, Lamb HJ, Boersma E, Steendijk P, de Roos A, van der Wall EE, Schalij MJ, Bax JJ. Effect of posterolateral scar tissue on clinical and echocardiographic improvement after cardiac resynchronization therapy. Circulation 2006;113:969-976.
(33) Ypenburg C, Schalij MJ, Bleeker GB, Steendijk P, Boersma E, Dibbets-Schneider P, Stokkel MP, van der Wall EE, Bax JJ. Extent of viability to predict response to cardiac resynchronization therapy in ischemic heart failure patients. J Nucl Med 2006;47:1565-1570.
(34) Ypenburg C, Schalij MJ, Bleeker GB, Steendijk P, Boersma E, Dibbets-Schneider P, Stokkel MP, van der Wall EE, Bax JJ. Impact of viability and scar tissue on response to cardiac resynchronization therapy in ischaemic heart failure patients. Eur Heart J 2007;28:33-41.
(35) Ypenburg C, Van Bommel RJ, Delgado V, Mollema SA, Bleeker GB, Boersma E, Schalij MJ, Bax JJ. Optimal left ventricular lead position predicts reverse remodeling and survival after cardiac resynchronization therapy. J Am Coll Cardiol 2008;52:1402-1409.
(36) Henneman MM, Chen J, Ypenburg C, Dibbets-Schneider P, Bleeker GB, Boersma E, Stokkel MP, van der Wall EE, Garcia EV, Bax JJ. Phase analysis of gated myocardial perfusion single-photon emission computed tomography compared with tissue Doppler imaging for the assessment of left ventricular dyssynchrony. J Am Coll Cardiol 2007;49:1708-1714.
(37) Marsan NA, Henneman MM, Chen J, Ypenburg C, Dibbets-Schneider P, Ghio S, Bleeker GB, Stokkel MP, van der Wall EE, Tavazzi L, Garcia EV, Bax JJ. Real-time 3-dimensional Echocardiography as a Novel Approach to Quantify Left Ventricular Dyssynchrony: A Comparison Study with Phase Analysis of Gated Myocardial Perfusion Single Photon Emission Computed Tomography. J Am Soc Echocardiogr 2008;21:801-807.
(38) Rosamond W, Flegal K, Furie K, Go A, Greenlund K, Haase N, Hailpern SM, Ho M, Howard V, Kissela B, Kittner S, Lloyd-Jones D, McDermott M, Meigs J, Moy C, Nichol G, O'Donnell C, Roger V, Sorlie P, Steinberger J, Thom T, Wilson M, Hong Y. Heart disease and stroke statistics-2008 update: a report from the American Heart Association Statistics Committee and Stroke Statistics Subcommittee. Circulation 2008;117:e25-146.
(39) Levy D, Kenchaiah S, Larson MG, Benjamin EJ, Kupka MJ, Ho KK, Murabito JM, Vasan RS. Long-term trends in the incidence of and survival with heart failure. N Engl J Med 2002;347:1397-1402.
(40) Braunwald E, Fauci AS, Kasper DL, Hauser SL, Longo DL, Jameson JL. Principles of internal medicine. Harrison's 15 ed. 2001:1316-1323.
(41) Cohn JN, Levine TB, Olivari MT, Garberg V, Lura D, Francis GS, Simon AB, Rector T. Plasma norepinephrine as a guide to prognosis in patients with chronic congestive heart failure. N Engl J Med 1984;311:819-823.
(42) Kaye DM, Lefkovits J, Jennings GL, Bergin P, Broughton A, Esler MD. Adverse consequences of high sympathetic nervous activity in the failing human heart. J Am Coll Cardiol 1995;26:1257-1263.
(43) Merlet P, Valette H, Dubois-Rande JL, Moyse D, Duboc D, Dove P, Bourguignon MH, Benvenuti C, Duval AM, Agostini D. Prognostic value of cardiac metaiodobenzylguanidine imaging in patients with heart failure. J Nucl Med 1992;33:471-477.

(44) Verberne HJ, Brewster LM, Somsen GA, Van Eck-Smit BL. Prognostic value of myocardial 123I-metaiodobenzylguanidine (MIBG) parameters in patients with heart failure: a systematic review. Eur Heart J 2008;29:1147-1159.
(45) Jacobson AF, Senior R, Cerqueira MD, Wong ND, Thomas GS, Lopez VA, Agostini D, Weiland F, Chandna H, Narula J. Myocardial Iodine-123 Meta-Iodobenzylguanidine Imaging and Cardiac Events in Heart Failure Results of the Prospective ADMIRE-HF (AdreView Myocardial Imaging for Risk Evaluation in Heart Failure) Study. J Am Coll Cardiol 2010;55:2212-2221.
(46) Carrio I. Cardiac neurotransmission imaging. J Nucl Med 2001;42:1062-1076.
(47) Flotats A, Carrio I. Cardiac neurotransmission SPECT imaging. J Nucl Cardiol 2004;11:587-602.
(48) Flotats A, Carrio I. Radionuclide noninvasive evaluation of heart failure beyond left ventricular function assessment. J Nucl Cardiol 2009;16:304-315.
(49) Boogers MJ, Borleffs CJW, Henneman MM, Van Bommel RJ, Van Ramshorst J, Boersma E, Dibbets-Schneider P, Stokkel MP, van der Wall EE, Schalij MJ, Bax JJ. Cardiac sympathetic denervation assessed with 123-I MIBG Imaging predicts ventricular arrhythmias in Implantable cardioverter-defibrillator patients. J Am Coll Cardiol 2010;55:2769-2777.
(50) Agostini D, Verberne HJ, Burchert W, Knuuti J, Povinec P, Sambuceti G, Unlu M, Estorch M, Banerjee G, Jacobson AF. I-123-mIBG myocardial imaging for assessment of risk for a major cardiac event in heart failure patients: insights from a retrospective European multicenter study. Eur J Nucl Med Mol Imaging 2008;35:535-546.
(51) Zipes DP, Rubart M. Neural modulation of cardiac arrhythmias and sudden cardiac death. Heart Rhythm 2006;3:108-113.
(52) Zipes DP. Sympathetic stimulation and arrhythmias. N Engl J Med 1991;325:656-657.
(53) Podrid PJ, Fuchs T, Candinas R. Role of the sympathetic nervous system in the genesis of ventricular arrhythmia. Circulation 1990;82:I103-I113.

Part I:

Automated Quantitative Computed Tomography in Patients with CAD

Chapter **2**

Quantification of Stenosis Severity on Multi-Detector Row Computed Tomography

Mark J. Boogers, MD[1, 2], Joanne D. Schuijf, PhD[1]

[1]Department of Cardiology, Leiden University Medical Center, Leiden, the Netherlands; [2]The Interuniversity Cardiology Institute of the Netherlands, Utrecht, the Netherlands.

Abstract

A comprehensive evaluation of coronary anatomy and atherosclerosis can be provided by multidetector row computed tomography (CT). Currently, several studies have used either manual or semi-automated algorithms for quantification of different plaque characteristics, in particular the degree of luminal narrowing. Although the feasibility of previously used quantitative algorithms has been demonstrated, further refinement of quantitative CT algorithms is currently indicated to allow a comprehensive yet fully automated analysis of plaque characteristics.

Introduction

Multidetector row computed tomography (MDCT) allows non-invasive evaluation of coronary artery disease (CAD) with excellent image quality and diagnostic accuracy as compared to invasive coronary angiography.[1-3] In recent years, rapid technological advances have led to an enormous increase in the use of MDCT for non-invasive evaluation of patients with known or suspected coronary atherosclerosis.

One of the advantages of MDCT is the fact that it provides a detailed overview of coronary anatomy (including the location of coronary ostia, coronary tree dominancy, tortuosity and coronary angulation) as well as comprehensive analysis of coronary stenosis (extent, distribution and location). Moreover, the technique is not restricted to luminography and additional important information on coronary plaques can be easily derived, including plaque morphology, degree of plaque remodeling, plaque burden and the longitudinal length of atherosclerotic lesions. Such an integrated analysis of coronary atherosclerotic disease may provide important information to risk stratify patients for potential forthcoming cardiovascular events, and while it can also be used to guide future therapeutic clinical interventions, including percutaneous coronary intervention.

At present, MDCT images are most commonly post-processed and evaluated by an experienced reader using a visual approach. However, the introduction of dedicated algorithms for automated quantification of plaque characteristics may further improve diagnostic accuracy and reproducibility of MDCT. Moreover, automated quantitative approaches may reduce the amount of time required to evaluate MDCT images. Accordingly, the development and validation of novel quantitative approaches for MDCT are increasingly attracting interest.

The current review will provide an overview of the currently available approaches for MDCT to quantify plaque characteristics, with particular focus on the quantification of stenosis severity. Additionally, the review will discuss the potential role of quantitative MDCT analyses to guide percutaneous coronary intervention procedures.

Quantification of Coronary Artery Stenosis

Invasive coronary angiography is considered the golden standard for evaluation of stenosis severity in clinical cardiology.[4] As compared to the standard of reference, MDCT has been shown in several studies, including large multicenter trials, to be an accurate technique for detection of significant coronary artery luminal narrowing (≥50% stenosis).[1-3] However, despite these promising results, one of the major drawbacks of MDCT remains the fact that the degree of coronary stenosis is most often determined visually using a dichotomous scoring system with 50% lumen diameter stenosis as a cutoff.[3, 5] This binary approach restricts the amount of potential useful information that can be derived from MDCT with regard to stenosis severity. For clinical purposes, an accurate discrimination between low, intermediate

and high-grade stenotic coronary plaques is of importance. In recent years, a large number of studies have evaluated the performance of quantitative MDCT approaches to assess the degree of coronary stenosis in a direct comparison to invasive imaging techniques, including invasive coronary angiography and gray-scale intravascular ultrasound (IVUS).[5-10] An interesting study was performed by Leber et al.[6] who have evaluated the accuracy of a manual quantification approach for assessment of the degree of lumen diameter stenosis as compared to invasive angiographic evaluation with quantitative coronary angiography (QCA) and gray-scale IVUS. Using MDCT images, the grade of stenosis was determined by dividing the minimal lumen diameter at the level of the stenosis through the lumen diameter at the adjacent non-diseased region. Quantitative measurements were performed in longitudinal multi-planar curved reconstructions in 2 projections similar as those used for QCA. In total, MDCT and invasive coronary angiography were performed in 55 consecutive patients with known or suspected coronary atherosclerosis, of whom 18 patients underwent a combined examination with gray-scale IVUS. Reliable quantitative analysis could be performed in 825 coronary segments (using the 15-segment model). Overall, MDCT showed an only moderate correlation with QCA (r=0.54) and IVUS (r=0.61) for quantification of the degree of coronary stenosis. Importantly, sub-analysis showed that quantification was particularly challenging in distal coronary tree segments (segment 8 and 13) and marginal coronary branches (segment 12, 14 and 15). Additionally, coronary segments with heavily calcified lesions showed more often misclassifications when compared to coronary segments without severe calcified lesions. Moreover, it is important to note that the degree of luminal obstruction was significantly underestimated with MDCT as compared to gray-scale IVUS (41.1%±22.7% vs. 50.4%±14.0%, $p<0.01$). More recently, Cheng et al.[11] sought to determine the relation between a visual multi-tiered grading system, semi-automated MDCT quantification of stenosis severity and QCA in 84 patients who had undergone invasive coronary angiography and MDCT. Only interpretable native coronary segments with a diameter stenosis of ≥25% were included. All non-stented coronary segments were evaluated by 2 experienced and blinded MDCT readers who visually graded segments as follows: 0 = 0%, 1 = 1 - 24%, 2 = 25 - 49%, 3 = 50 - 69%, 4 = 70 - 89%, 5 = 90 - 100%. All coronary segments were also quantified by a semi-automated approach using a manually determined proximal and distal reference region, representing an approximation of the normal coronary vessel tapering. The reference regions were used to determine luminal narrowing at the level of maximal diameter stenosis (lesion marker) on longitudinal images. Consecutively, the degree of coronary stenosis, as derived from visual and semi-automated MDCT analysis, was compared to QCA. In total, 278 coronary segments with ≥25% diameter stenosis were included. Overall, the multi-tiered visual scoring system showed good correlation to QCA (Kendall's tau-b 0.76, weighted kappa 0.70, $p<0.05$). Of note, the semi-automated MDCT approach showed no improvement in diagnostic accuracy when compared to expert visual grading. One of the potential explanations for these findings may be the fact that the use of

semi-automated quantification was associated with large variability introduced by manual interference. The minimal luminal diameter, the proximal and distal reference points were assessed manually, as indicated in Figure 1, whereas a computed-assisted approach could have improved the accuracy of the quantitative measurements.

Recently, Joshi et al.[10] have aimed to determine the performance of quantitative computer-assisted MDCT analysis in 48 patients using gray-scale IVUS as the standard of reference. Quantitative coronary angiographic MDCT analysis was used to calculate percentage diameter stenosis on cross-sectional images. At first, semi-automated detection of coronary lumen centerline was performed with the use of vessel calipers, which could be manually adapted to ensure true coronary lumen detection. Consecutively, proximal and distal reference regions were defined by hand, after which the program automatically calculated minimal lumen diameter and minimal lumen area as well as the degree of percentage diameter stenosis. In this study, a moderate correlation between MDCT and IVUS was found for minimal lumen area (r^2=0.41, p<0.01), whereas no correlation was found between MDCT and QCA for minimal lumen diameter (r^2=0.01, p=0.57) or diameter stenosis (r^2=0.02, p=0.31). For moderate to severe calcified lesions, MDCT showed no correlation for minimal lumen diameter (r^2<0.01) and area (r^2<0.01) as well as percentage diameter stenosis (r^2=0.06) as compared to IVUS. However, for mildly calcified or non-calcified lesions, MDCT showed

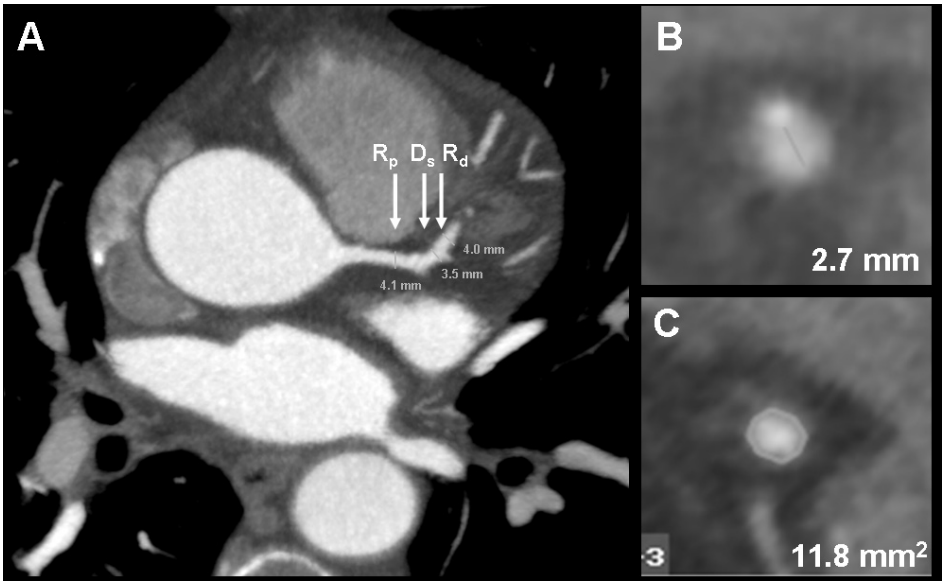

Figure 1. Quantification of stenosis severity on multidetector row computed tomography (MDCT). Diameter coronary stenosis can be manually determined by assessing the lumen diameter at the lesion site and proximal/distal reference sites using either axial slices (panel A) or cross-sectional images perpendicular to the centerline of the vessel (panel B). Similarly, area stenosis can be calculated by tracing lumen areas on the cross-sectional images (panel C).

significantly improved correlations with IVUS for minimal lumen diameter (r^2=0.40) and minimal lumen area (r^2=0.68).

Currently, the majority of studies have used semi-manual MDCT approaches rather than dedicated automated segmentation algorithms to quantify stenosis severity. Recently, the feasibility of a novel dedicated algorithm for automated quantification of the degree of coronary stenosis was shown in a subset of 93 patients with known and suspected CAD.[12] In this study, performance of the novel quantitative algorithm was evaluated against QCA measurements in 282 coronary lesions. Quantitative analysis involved several automated processing steps, with less manual interference when compared to previous attempts to calculate the degree of stenosis (Figure 2). A 3D centerline of the region of interest (ranging from proximal to distal marker) was obtained with the use of a fast vessel tracking algorithm, which consisted of: (1) pre-segmentation of the coronary vessel and (2) fastest path back-tracking from distal to the proximal point. The 3D centerline was used to generate a multi-planar reconstructed volume and 4 longitudinal cross-sections of the region of interest. Finally, coronary lumen borders were detected by a model guided minimum cost approach (MCA) and used to quantify the percentage diameter stenosis. The MCA used spatial first-, and second-derivative gradient filters combined with knowledge of the expected intracoronary CT intensity to detect the contours. The study showed good correlations for quantification of percentage diameter stenosis on a vessel- (n=282, r=0.83, p<0.01) and patient basis (n=93, r=0.86, p<0.01), as shown in Figure 3. Importantly, MDCT scans were also visually scored using a binary scoring system with 50% diameter stenosis as a cutoff. An

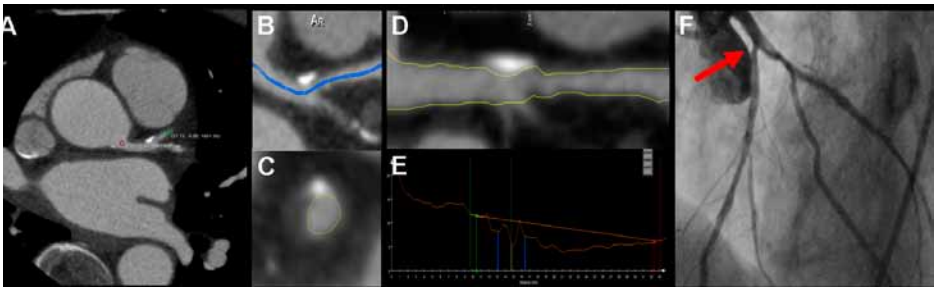

Figure 2. Illustration of automated quantification of stenosis severity on multidetector row computed tomography (MDCT). The automated process involved several consecutive processing steps: (A) Determination of proximal (red) and distal (green) reference markers on axial slices; (B) Automated generation of the lumen centerline ranging from the proximal to distal reference marker; (C) Automated detection of lumen contours in transversal and (D) longitudinal planes; (E) Quantification of stenosis severity was based on the interrelation between lumen diameter at the site of minimal lumen diameter (yellow line, panel E) and the corresponding reference diameter (oblique orange line, panel E). (E) The reference line was generated from proximal (green markers) and distal reference (red markers) regions. For this lesion (indicated by the blue markers, panel E), the maximal degree of stenosis was 39.0%. Corresponding invasive coronary angiography view was shown in panel F. Data based on reference 12.

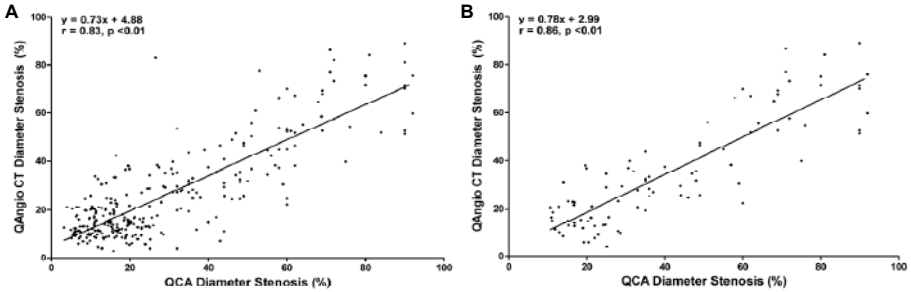

Figure 3. Automated quantification of diameter stenosis (%) using dedicated software (QAngioCT) showed good correlation with quantitative coronary angiography (QCA) on a vessel basis (panel A) (n=282, r=0.83, p<0.01) and patient-basis (panel B) (n=93, r=0.86, p<0.01). Data based on reference 12.

improved diagnostic accuracy (95% vs. 87%, p=0.08) and positive predictive value (100% vs. 78%, p<0.05) was found for assessment of significant lesions (≥50% diameter stenosis) using quantitative MDCT analysis as compared to visual analysis.

Despite these promising results, one has to take into consideration that the use of quantitative MDCT algorithms is currently only feasible in data sets with good or moderate image quality. In case of severe cardiac motion artifacts, decreased image/noise ratio or suboptimal contrast arrival, the consistency of quantitative analyses may be distorted, and if so, visual interpretation may be preferred in these data sets. Additionally, quantification of atherosclerotic lesions located at coronary bifurcations remains challenging. In such lesions, visual analysis to evaluate stenosis severity may be preferred, rather than automated quantitative MDCT analysis. However, further improvement in quantitative MDCT algorithms may enhance the diagnostic accuracy of automated quantification and extend the analysis to more difficult cases. Moreover, rapid technological developments have led to considerable improvement in spatial and temporal resolution of the currently available MDCT scanners. Potentially, the introduction of new MDCT scanners as well as the continuous refinement of acquisition and post-processing protocols may even further improve diagnostic image quality of MDCT coronary angiography, resulting in an increased number of data sets suitable for automated MDCT quantification.

Quantitative Analysis of Coronary Plaque Characteristics

MDCT enables a comprehensive non-invasive evaluation of coronary atherosclerosis beyond the isolated detection of significant coronary artery stenosis. It provides information on location, extent and distribution of coronary atherosclerotic plaques as well as a wide variety of additional geometric plaque characteristics, including plaque volume, plaque

length and the degree of remodeling (Figure 4). These variables may be valuable for risk stratification as well as for planning of therapeutic coronary interventions.[13, 14]

Currently, comprehensive evaluation of the presence and extent of coronary atherosclerosis is usually performed by visual analysis of MDCT images. However, one of the major limitations of visual MDCT analysis of plaque characteristics remains the fact that it is observer dependent and requires substantial reading experience. Accordingly, several attempts have been made that sought to determine the performance of automated or computed-based algorithms for quantification of plaque characteristics without extensive manual interference. The use of automated quantitative algorithms may potentially improve the robustness and reproducibility of MDCT analyses, and importantly, the combined post-processing and interpretation of MDCT data sets may become less time-consuming. Moreover, quantification of plaque characteristics (e.g. plaque volume) with an automated and robust approach becomes of special interest when using MDCT to assess progression of coronary atherosclerosis.

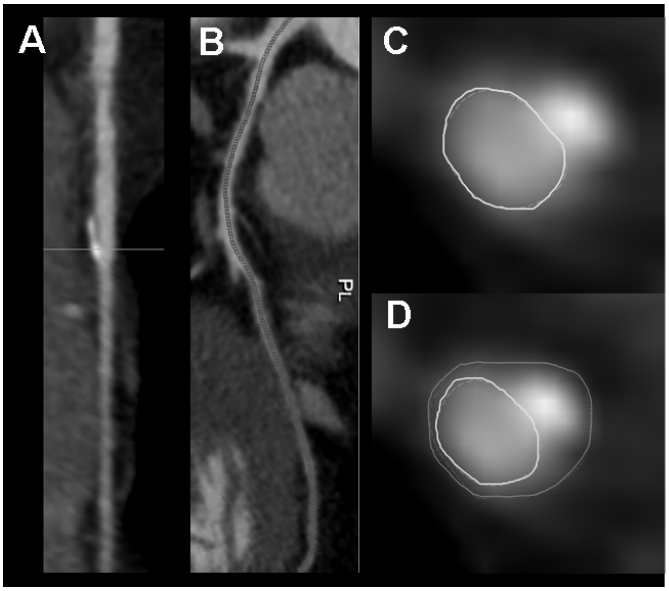

Figure 4. Multidetector row computed tomography (MDCT) provides a comprehensive overview of the coronary anatomy and coronary atherosclerosis. The location, extent and morphology of atherosclerotic plaques can be derived using multi-planar reconstructed volumes (panel A and B). Additionally, with the use of quantitative algorithms, detection of lumen (panel C) and outer vessel wall (panel D) contours can be performed based on image gradients and lumen center lines. Consecutively, the detected contours allow evaluation of stenosis severity, plaque burden, plaque length and the degree of remodeling.

Plaque Morphology

In recent years, the non-invasive evaluation of plaque morphology and plaque configuration gained increasingly interest in clinical cardiology, as these variables may be important predictors for plaque rupture and acute coronary events.[13, 15] For this reason, several studies have sought to evaluate the potential of MDCT to quantify coronary plaque composition.[16-18] Schroeder et al.[16] has evaluated the diagnostic accuracy of plaque composition analysis on MDCT using IVUS as the standard of reference. In total, 34 coronary plaques of 15 patients with chronic stable anginal complaints were identified on both imaging modalities, including non-calcified (n=12), mixed (n=5) and calcified (n=17) atherosclerotic lesions. Differentiation of plaque composition was performed visually by an expert observer. For each plaque type, the mean attenuation (expressed in Hounsfield units (HU)) of 16 randomly selected locations within the intracoronary plaque (defined as >40% luminal narrowing) was measured using a dedicated post-processing software. On MDCT, the mean attenuation was 14±26 HU for non-calcified lesions, whereas mixed and calcified lesions showed a mean attenuation of 91±21 HU and 419±194 HU, respectively. Moreover, the mean attenuation values on MDCT were significantly different for each IVUS-derived plaque type ($p<0.05$). More recently, Leber et al.[18] performed a study that aimed to assess the accuracy of plaque type characterization on MDCT in 46 patients with an increased risk profile. For each coronary plaque, density measurements (HU) were performed at each 3-mm coronary section using axial slices. After a raster consisting of 1 mm^2 boxes was placed for each 3-mm section, density measurements were performed on 5 randomly selected locations. In this study, the mean attenuation values were 49±22 HU (hypo-echoic), 91±22 HU (hyperechoic) and 391±156 HU (calcified lesions). Accordingly, these studies have indicated that MDCT can be used to quantify different types of plaque morphology. However, it has also been demonstrated that further classification of plaque type using MDCT can be difficult. Using IVUS, Pohle et al.[19] have demonstrated that mean MDCT density was significantly lower in lesions consisting mainly of fibrofatty tissue as compared to fibrotic lesions. Nevertheless, between individual lesions, substantial overlap in density values was noted. Similar findings were reported by Choi et al.[20], evaluating 80 non-calcified plaques and compared findings to IVUS radiofrequency analysis (VH-IVUS). In addition, differences in acquisition characteristics, including flow rate and contrast agent, as well as patient characteristics such as cardiac output and body weight, may substantially influence individual measurements. Finally, one should also be aware of the restrictions in spatial resolution of MDCT. In calcified lesions, the blooming effect of the calcium may result in overestimation of the extent of calcium and inaccurate classification of adjacent plaque areas. Vice versa, one has to take into consideration that plaques deemed to be entirely non-calcified on MDCT may contain small amounts of calcium.[21]

Plaque Volume, Burden and Remodeling Index

A large number of studies have aimed to quantify plaque volume, burden and the degree of remodeling using semi-automated MDCT approaches.[7, 9, 13, 22] Leber et al.[7] sought to determine the accuracy of plaque volume measurements using MDCT as compared to invasive gray-scale IVUS in 20 patients. For both techniques, the total plaque volume was measured by adding the semi-automated detected plaque area per coronary section. The study showed a good correlation for plaque volume (r^2=0.69, p<0.01) (Figure 5) between both imaging modalities, with a significant underestimation for mixed (47.7±87.5 mm^3 vs. 57.5±99.4 mm^3, p<0.05) and non-calcified (59.8±76.6 mm^3 vs. 67.7±67.9 mm^3, p<0.05) plaques. Calcified lesions were slightly overestimated on MDCT when compared to IVUS (65.8±110.0 mm^3 vs. 53.2±90.3 mm^3, p=0.19). In addition, Bruining and colleagues[9] have used an automated MDCT approach with limited manual interference to assess plaque volume using IVUS as the standard of reference. In 48 symptomatic patients, computed-assisted coronary plaque MDCT measurements were performed by 2 independent observers. After the regions of interest were matched for both techniques, they were extracted from the 3D data set with the use of semi-automated vessel extraction software (CURAD). Thereafter, for each region of interest, lumen borders were automatically detected on the basis of an edge-detection method using a dedicated filter (digital Deriche filter) which calculated the gradient of the images. Of note, the automated edge-detection method could only be used for detection of lumen borders, whereas the vessel wall borders were manually outlined. Using this approach, plaque volume was significantly overestimated on MDCT when compared to IVUS (222±121 mm^3 vs. 189±93 mm^3, p<0.01). Importantly, for both readers, good correlations were found between MDCT and IVUS for plaque volume (r=0.74 and r=0.79). Similarly, Otsuka et al.[22] have evaluated the accuracy of quantitative plaque volume MDCT

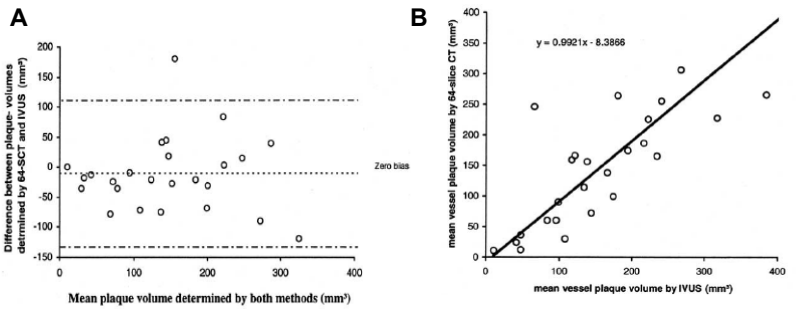

Figure 5. Semi-automated quantification of plaque volume as assessed with multidetector row computed tomography (MDCT) and intravascular ultrasound (IVUS). A. Plaque volume was systematically underestimated with MDCT as compared to IVUS as shown in the Bland-Altman Analysis (p<0.05). B. Good correlation was found for quantification of plaque volume between both techniques (r^2=0.69, p<0.01). Data based on reference 7.

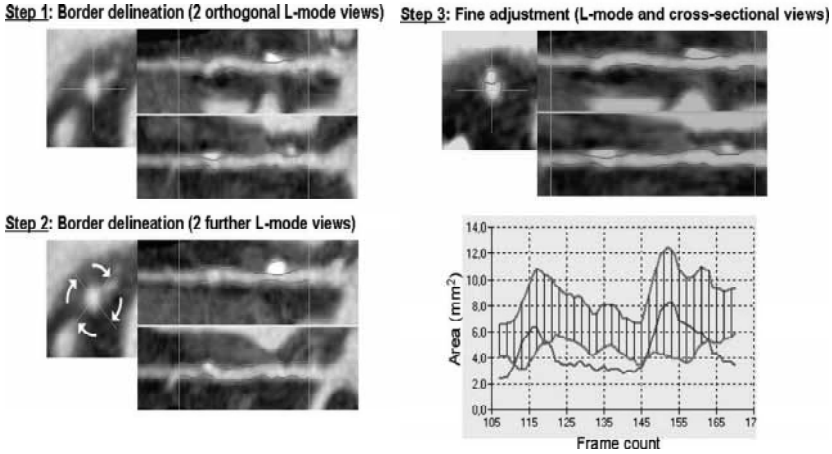

Figure 6. Schematic illustration of plaque burden quantification as assessed with multidetector row computed tomography (MDCT). Coronary arteries were extracted using semi-automated vessel extraction software. For each coronary artery, lumen plaque interface (red lines) and the outer vessel wall border (green lines) were identified and manually delineated in at least 4 orthogonal L -mode views with rotational display of the extracted coronary artery (step 1 and 2). Further refinement of the contour tracing was performed by referring to the corresponding transversal images (step 3). Finally, plaque burden (blue line) was derived from the interrelation of vessel wall area (green line) and lumen area (red line). Reprinted with permission from reference 22.

measurements in 47 patients as compared to IVUS. After coronary-tree extraction was performed, plaque volume and plaque burden were measured using manually-traced MDCT lumen and vessel wall contours (Figure 6). The study found good correlations for regional plaque burden ($r=0.96$, $p<0.01$) and plaque volume ($r=0.98$, $p<0.01$) between quantitative CT and IVUS. In addition, good reproducibility was observed as indicated by a Pearson's correlation coefficient of 0.98 ($p<0.001$) and 0.91 ($p<0.001$), respectively, for intraobserver and interobserver correlation.

Coronary plaque remodeling has also been recognized as an important plaque characteristic that has been linked to increased vulnerability.[13, 15] With IVUS as the standard of reference, several studies have explored the potential of MDCT to assess coronary plaque remodeling.[13, 23] Achenbach et al.[23] evaluated the feasibility of MDCT to evaluate remodeling index in 44 patients with known atherosclerotic plaques. In this study, plaque remodeling was calculated by dividing the manually-traced cross-sectional vessel wall area at the level of maximal luminal narrowing by the cross-sectional vessel wall area at the proximal non-diseased reference region, as indicated in Figure 7. Interestingly, the study demonstrated that the degree of remodeling was significantly higher in patients with non-stenotic lesions as compared to patients with stenotic lesions (1.3±0.2 vs. 1.0±0.2, $p<0.01$). Moreover, remodeling index as derived from MDCT showed good correlation with IVUS ($r^2=0.82$, $p<0.01$).

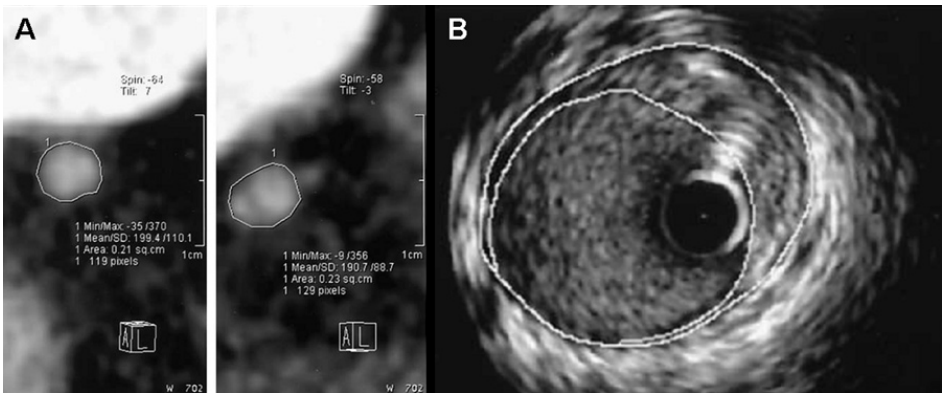

Figure 7. Quantitative approach for assessment of coronary plaque remodeling using multidetector row computed tomography (MDCT) (panel A) and IVUS (panel B). With MDCT, remodeling index was calculated using manually-traced outer vessel wall area at the site of maximal luminal narrowing (right panel) and non-diseased proximal reference region (left panel). A similar approach was used to calculate the degree of plaque remodeling on IVUS. For both imaging modalities, the degree of remodeling was calculated by dividing the vessel wall area at the level of the maximal stenosis by the proximal reference vessel wall area. Reprinted with permission from reference 23.

Future Challenges

A systematic evaluation of atherosclerotic lesions requires the detection of both lumen and outer vessel wall borders throughout the coronary tree. Although the feasibility for automated detection of luminal borders has been demonstrated[12], the automated detection of outer vessel wall borders remains a challenge as it is usually hampered by subtle differences in image gradients, particularly in peripheral coronary segments. A fully automated approach for detection of outer vessel wall borders has not been validated yet for clinical practice. Accordingly, the feasibility to quantify plaque volume, burden and remodeling index have only been demonstrated using semi-automated vessel wall border detection.[7, 9, 13, 22] With the currently applied algorithms, extensive manual interference is still required to generate reliable outer vessel wall borders. Potentially, the introduction of advanced quantitative algorithms in combination with developments in scanner technology may further improve the consistency of vessel wall and reference contour detection, leading to improved quantification of plaque characteristics.

Quantitative Computed Tomography Angiography to Guide Percutaneous Coronary Interventions

Non-invasive evaluation of coronary atherosclerosis with the use of MDCT provides important information which can be used to guide percutaneous coronary interventions. MDCT provides integrated information on extent, location and distribution of coronary atherosclerosis, beyond the isolated assessment of coronary stenosis severity. More in-depth

pre-procedural evaluation of coronary plaques (stenosis severity, plaque location and length) may be valuable for procedural planning and may increase procedural success. For example, it has been recently demonstrated that depicting the degree of calcification and the length of an occluded segment on MDCT (which can be difficult on invasive coronary angiography but can be easily derived from MDCT) may predict the success of percutaneous treatment of chronic total coronary artery occlusions.[24] Bifurcation lesions represent another challenge in interventional cardiology. One of the underlying mechanisms of the observed lower angiographic success rate of these lesions is the occurrence of coronary plaque shifting or rupture, which may lead an occlusion of coronary side branches. Pre-interventional MDCT assessment of the coronary angulation and tortuosity as well as plaque location, severity and composition could potentially prevent difficult and high-risk percutaneous procedures.

Conclusions

MDCT provides a comprehensive evaluation of coronary anatomy and atherosclerosis. The majority of studies have used semi-automated algorithms to quantify a wide variety of plaque characteristics, predominantly focusing on the degree of luminal narrowing. Despite promising findings, further refinement of the quantitative MDCT algorithms is currently indicated. With the introduction of such improved quantitative post-processing algorithms, however, fully automated analysis of plaque characteristics may become feasible and may provide valuable information for the diagnosis and management of patients with CAD.

Reference List

(1) Hoffmann MH, Shi H, Schmitz BL, Schmid FT, Lieberknecht M, Schulze R, Ludwig B, Kroschel U, Jahnke N, Haerer W, Brambs HJ, Aschoff AJ. Noninvasive coronary angiography with multislice computed tomography. JAMA 2005;293:2471-2478.

(2) Miller JM, Rochitte CE, Dewey M, rbab-Zadeh A, Niinuma H, Gottlieb I, Paul N, Clouse ME, Shapiro EP, Hoe J, Lardo AC, Bush DE, de Roos A, Cox C, Brinker J, Lima JA. Diagnostic performance of coronary angiography by 64-row CT. N Engl J Med 2008;359:2324-2336.

(3) Meijboom WB, Meijs MF, Schuijf JD, Cramer MJ, Mollet NR, van Mieghem CA, Nieman K, van Werkhoven JM, Pundziute G, Weustink AC, de Vos AM, Pugliese F, Rensing B, Jukema JW, Bax JJ, Prokop M, Doevendans PA, Hunink MG, Krestin GP, de Feyter PJ. Diagnostic accuracy of 64-slice computed tomography coronary angiography: a prospective, multicenter, multivendor study. J Am Coll Cardiol 2008;52:2135-2144.

(4) Scanlon PJ, Faxon DP, Audet AM, Carabello B, Dehmer GJ, Eagle KA, Legako RD, Leon DF, Murray JA, Nissen SE, Pepine CJ, Watson RM, Ritchie JL, Gibbons RJ, Cheitlin MD, Gardner TJ, Garson A, Jr., Russell RO, Jr., Ryan TJ, Smith SC, Jr. ACC/AHA guidelines for coronary angiography. A report of the American College of Cardiology/American Heart Association Task Force on practice guidelines (Committee on Coronary Angiography). Developed in collaboration with the Society for Cardiac Angiography and Interventions. J Am Coll Cardiol 1999;33:1756-1824.

(5) Raff GL, Gallagher MJ, O'Neill WW, Goldstein JA. Diagnostic accuracy of noninvasive coronary angiography using 64-slice spiral computed tomography. J Am Coll Cardiol 2005;46:552-557.

(6) Leber AW, Knez A, von Ziegler F, Becker A, Nikolaou K, Paul S, Wintersperger B, Reiser M, Becker CR, Steinbeck G, Boekstegers P. Quantification of obstructive and nonobstructive coronary lesions by 64-slice computed tomography: a comparative study with quantitative coronary angiography and intravascular ultrasound. J Am Coll Cardiol 2005;46:147-154.

(7) Leber AW, Becker A, Knez A, von Ziegler F, Sirol M, Nikolaou K, Ohnesorge B, Fayad ZA, Becker CR, Reiser M, Steinbeck G, Boekstegers P. Accuracy of 64-slice computed tomography to classify and quantify plaque volumes in the proximal coronary system: a comparative study using intravascular ultrasound. J Am Coll Cardiol 2006;47:672-677.

(8) Husmann L, Gaemperli O, Schepis T, Scheffel H, Valenta I, Hoefflinghaus T, Stolzmann P, Desbiolles L, Herzog BA, Leschka S, Marincek B, Alkadhi H, Kaufmann PA. Accuracy of quantitative coronary angiography with computed tomography and its dependency on plaque composition: plaque composition and accuracy of cardiac CT. Int J Cardiovasc Imaging 2008;24:895-904.

(9) Bruining N, Roelandt JR, Palumbo A, La Grutta L, Cademartiri F, de Feijter PJ, Mollet N, van Domburg RT, Serruys PW, Hamers R. Reproducible coronary plaque quantification by multislice computed tomography. Catheter Cardiovasc Interv 2007;69:857-865.

(10) Joshi SB, Okabe T, Roswell RO, Weissman G, Lopez CF, Lindsay J, Pichard AD, Weissman NJ, Waksman R, Weigold WG. Accuracy of computed tomographic angiography for stenosis quantification using quantitative coronary angiography or intravascular ultrasound as the gold standard. Am J Cardiol 2009;104:1047-1051.

(11) Cheng V, Gutstein A, Wolak A, Suzuki Y, Dey D, Gransar H, Thomson LE, Hayes SW, Friedman JD, Berman DS. Moving beyond binary grading of coronary arterial stenoses on coronary computed tomographic angiography: insights for the imager and referring clinician. JACC Cardiovasc Imaging 2008;1:460-471.

(12) Boogers MJ, Schuijf JD, Kitslaar PH, van Werkhoven JM, de Graaf FR, Boersma E, van Velzen JE, Dijkstra J, Adame IM, Kroft LJ, de Roos A, Schreur JHM, Heijenbrok MW, Jukema JW, Reiber JHC, Bax JJ. Novel Dedicated Approach for Automated Quantification of Stenosis Severity on 64-Slice Multi-slice Computed Tomography: A Comparison with Quantitative Coronary Angiography. JACC Cardiovasc Imaging 2010;3:699-709.

(13) Motoyama S, Kondo T, Sarai M, Sugiura A, Harigaya H, Sato T, Inoue K, Okumura M, Ishii J, Anno H, Virmani R, Ozaki Y, Hishida H, Narula J. Multislice computed tomographic characteristics of coronary lesions in acute coronary syndromes. J Am Coll Cardiol 2007;50:319-326.
(14) Bluemke DA, Achenbach S, Budoff M, Gerber TC, Gersh B, Hillis LD, Hundley WG, Manning WJ, Printz BF, Stuber M, Woodard PK. Noninvasive coronary artery imaging: magnetic resonance angiography and multidetector computed tomography angiography: a scientific statement from the american heart association committee on cardiovascular imaging and intervention of the council on cardiovascular radiology and intervention, and the councils on clinical cardiology and cardiovascular disease in the young. Circulation 2008;118:586-606.
(15) Virmani R, Burke AP, Farb A, Kolodgie FD. Pathology of the vulnerable plaque. J Am Coll Cardiol 2006;47(8 Suppl):C13-C18.
(16) Schroeder S, Kopp AF, Baumbach A, Meisner C, Kuettner A, Georg C, Ohnesorge B, Herdeg C, Claussen CD, Karsch KR. Noninvasive detection and evaluation of atherosclerotic coronary plaques with multislice computed tomography. J Am Coll Cardiol 2001;37:1430-1435.
(17) Hur J, Kim YJ, Lee HJ, Nam JE, Choe KO, Seo JS, Choi DH, Kim JS, Choi BW. Quantification and characterization of obstructive coronary plaques using 64-slice computed tomography: a comparison with intravascular ultrasound. J Comput Assist Tomogr 2009;33:186-192.
(18) Leber AW, Knez A, Becker A, Becker C, von Ziegler F, Nikolaou K, Rist C, Reiser M, White C, Steinbeck G, Boekstegers P. Accuracy of multidetector spiral computed tomography in identifying and differentiating the composition of coronary atherosclerotic plaques: a comparative study with intracoronary ultrasound. J Am Coll Cardiol 2004;43:1241-1247.
(19) Pohle K, Achenbach S, MacNeill B, Ropers D, Ferencik M, Moselewski F, Hoffmann U, Brady TJ, Jang IK, Daniel WG. Characterization of non-calcified coronary atherosclerotic plaque by multi-detector row CT: comparison to IVUS. Atherosclerosis 2007;190:174-180.
(20) Choi BJ, Kang DK, Tahk SJ, Choi SY, Yoon MH, Lim HS, Kang SJ, Yang HM, Park JS, Zheng M, Hwang GS, Shin JH. Comparison of 64-slice multidetector computed tomography with spectral analysis of intravascular ultrasound backscatter signals for characterizations of noncalcified coronary arterial plaques. Am J Cardiol 2008;102:988-993.
(21) Pundziute G, Schuijf JD, Jukema JW, Decramer I, Sarno G, Vanhoenacker PK, Reiber JH, Schalij MJ, Wijns W, Bax JJ. Head-to-head comparison of coronary plaque evaluation between multislice computed tomography and intravascular ultrasound radiofrequency data analysis. JACC Cardiovasc Interv 2008;1:176-182.
(22) Otsuka M, Bruining N, Van Pelt NC, Mollet NR, Ligthart JM, Vourvouri E, Hamers R, De Jaegere P, Wijns W, van Domburg RT, Stone GW, Veldhof S, Verheye S, Dudek D, Serruys PW, Krestin GP, de Feyter PJ. Quantification of coronary plaque by 64-slice computed tomography: a comparison with quantitative intracoronary ultrasound. Invest Radiol 2008;43:314-321.
(23) Achenbach S, Ropers D, Hoffmann U, MacNeill B, Baum U, Pohle K, Brady TJ, Pomerantsev E, Ludwig J, Flachskampf FA, Wicky S, Jang IK, Daniel WG. Assessment of coronary remodeling in stenotic and nonstenotic coronary atherosclerotic lesions by multidetector spiral computed tomography. J Am Coll Cardiol 2004;43:842-847.
(24) Garcia-Garcia HM, van Mieghem CA, Gonzalo N, Meijboom WB, Weustink AC, Onuma Y, Mollet NR, Schultz CJ, Meliga E, van der Ent M, Sianos G, Goedhart D, den Boer A, de Feyter P, Serruys PW. Computed tomography in total coronary occlusions (CTTO registry): radiation exposure and predictors of successful percutaneous intervention. EuroIntervention 2009;4:607-616.

Chapter **3**

Automated Quantification of Stenosis Severity on 64-slice CT: a Comparison with Quantitative Coronary Angiography

Mark J. Boogers, MD[1, 2], Joanne D. Schuijf, PhD[1], Pieter H. Kitslaar, MSc[3], Jacob M. van Werkhoven, MSc[1, 2], Fleur R. de Graaf, MD[1], Eric Boersma, PhD[4], Joëlla E. van Velzen, MD[1, 2], Jouke Dijkstra, PhD[3], Isabel M. Adame, PhD[5], Lucia J. Kroft, MD, PhD[6], Albert de Roos, MD, PhD[6], Joop H. M. Schreur, MD, PhD[7], Mark W. Heijenbrok, MD[8], J. Wouter Jukema, MD, PhD[1], Johan H. C. Reiber, PhD[3, 5], Jeroen J. Bax, MD, PhD[1].

[1]Department of Cardiology, Leiden University Medical Center, Leiden, the Netherlands; [2]The Interuniversity Cardiology Institute of the Netherlands, Utrecht, the Netherlands; [3]Department of Radiology, Division of Image Processing, Leiden University Medical Center, Leiden, the Netherlands; [4]Department of Epidemiology and Statistics, Erasmus University, Rotterdam, the Netherlands; [5]Medis medical imaging systems B.V., Leiden, the Netherlands; [6]Department of Radiology, Leiden University Medical Center, Leiden, the Netherlands; [7]Department of Cardiology, Medical Center Haaglanden, the Hague, the Netherlands; [8]Department of Radiology, Medical Center Haaglanden, the Hague, the Netherlands.

Abstract

Background Limited information is available on quantification of coronary stenosis while previous attempts using semi-automated approaches were suboptimal.

Objectives To demonstrate the feasibility of a novel dedicated algorithm for automated quantification of stenosis severity on multi-slice computed tomography (MSCT) in comparison to quantitative coronary angiography (QCA).

Methods In patients who had undergone 64-slice MSCT and invasive coronary angiography, the most severe lesion on QCA was quantified per coronary artery using quantitative computed tomography (QAngioCT) software. Additionally, visual grading of stenosis severity using a binary approach (50% stenosis as a cutoff) was performed. Diameter stenosis (percentage) was obtained from detected lumen contours at the minimal lumen area and corresponding reference diameter values obtained from an automatic trend analysis of the vessel areas within the artery.

Results One-hundred patients (53 men, 59.8±8.0 yrs) were evaluated and 282 (94%) vessels were analyzed. Good correlations for diameter stenosis were observed for vessel-based ($n=282$, $r=0.83$, $p<0.01$) and patient-based ($n=93$, $r=0.86$, $p<0.01$) analyses. Mean differences between QAngioCT and QCA were -3.0±12.3% and -6.2±12.4%. Furthermore, good agreement was observed between QAngioCT and QCA for semi-quantitative assessment of diameter stenosis (accuracy of 95%). Diagnostic accuracy for assessment of ≥50% diameter stenosis was higher using QAngioCT as compared to visual analysis (95% vs. 87%, $p=0.08$). Moreover, a significantly higher positive predictive value was observed with QAngioCT when compared to visual analysis (100% vs. 78%, $p<0.05$). Although the visual approach showed a reduced diagnostic accuracy for data sets with moderate image quality, QAngioCT performed equally well in patients with moderate or good image quality. However, in data sets with good image quality, QAngioCT tended to have a reduced sensitivity as compared to visual analysis.

Conclusions Good correlations were found for quantification of stenosis severity between QAngioCT and QCA. QAngioCT showed an improved positive predictive value when compared to visual analysis.

Introduction

Multi-slice computed tomography (MSCT) has emerged as a promising non-invasive modality to detect coronary artery disease (CAD).[1-3] High diagnostic accuracy for detection of significant CAD as compared to invasive coronary angiography has been reported in studies using 64-MSCT.[1-3] Moreover, high negative predictive values have been reported in studies using 64-slice MSCT and as a result MSCT is increasingly used in the evaluation of CAD.[1-3]

However, a major limitation of the technique remains the fact that at present stenosis severity on MSCT can only be assessed visually; most frequently a dichotomous score system with a cutoff value of 50% stenosis is used. A fully automated approach to quantify stenosis severity, similar to quantitative coronary angiography (QCA) would be preferred to further improve the diagnostic accuracy and reproducibility. However, such an automated quantitative approach is currently not available. In the majority of previous studies, attempts to quantify stenosis severity have used semi-manual approaches rather than dedicated automated segmentation algorithms. Unfortunately, these semi-manual approaches suffer from limited diagnostic accuracy and poor reproducibility, and as a result, results were suboptimal in the majority of studies.[4-7]

Recently, novel software has become available for automated quantification of stenosis severity which involves several automated processing steps with less manual interference as compared with previous attempts to quantify stenosis severity. Accordingly, this study aimed to demonstrate the feasibility of this novel dedicated algorithm for automated quantification of stenosis severity in comparison to QCA.

Methods

Study Population

The study population consisted of patients who underwent 64-slice MSCT and invasive coronary angiography sequentially, within 4 months. Patients were clinically referred for MSCT because of known or suspected CAD. Known CAD was defined as a history of myocardial infarction, revascularization or evidence of CAD on previous diagnostic tests.

No adverse cardiac events or hospitalizations were documented between MSCT and invasive coronary angiography. Patients underwent comprehensive imaging as part of an ongoing study registry addressing the value of MSCT in relation to other imaging modalities. Referral for invasive coronary angiography was based on clinical presentation and/or imaging results. Patients were excluded in case of atrial fibrillation, renal dysfunction (glomerular filtration rate <30 mL/min), documented iodine-containing contrast allergy and pregnancy. Risk factors for CAD were derived from existing patient medical record data.

Conventional Invasive Coronary Angiography

Acquisition and Analysis

Conventional invasive coronary angiography was performed according to the standard protocols. QCA was performed offline by an independent and blinded observer, using a dedicated and validated software package (QAngioXA 7.1, Medis medical imaging systems, Leiden, the Netherlands). Coronary arteries were evaluated according to the 17-segment model as previously described[8], and measurements were performed on a projection without superimposition of other coronary artery segments or cardiac structures as well as showing the stenosis in the tightest view. After catheter-based image calibration, side branches and coronary ostia were used as anatomical markers for accurate segment definition (17-segment model).[8] Image calibration was performed in two end-diastolic frames with a catheter diameter of 6F. Subsequently, the centerline was automatically defined followed by automated detection of lumen contours and calculation of luminal diameter function. From these data, the reference diameter function was derived and reference contours were reconstructed. The reference diameter function was obtained from a linear regression fit on the lumen diameter function. This regression fit approximates best the normal vessel tapering. Abnormal sections of a segment were excluded from the regression analysis by a user-interactive flagging procedure. At the site of minimal luminal diameter, the percentage diameter stenosis was calculated as: (1 – minimal luminal diameter / corresponding reference diameter) x 100%.[9] Accordingly, in the current study, diameter stenosis refers to percentage diameter stenosis as previously described.[9]

MSCT Examination

Acquisition

MSCT examinations were performed with a 64-slice CT scanner (Aquilion 64, Toshiba Medical Systems, Tokyo, Japan; General Electrics (GE) Lightspeed VR 64, Milwaukee, Wisconsin, USA). Patients with an elevated heart rate (≥65 beats/min) were administered metoprolol 50 or 100 mg orally, if not contra-indicated. The contrast-enhanced helical scan was performed using a bolus of 95 to 130 mL of nonionic contrast medium (Iomeron 400; Bracco, Milan, Italy) followed by a bolus of saline flush (50 mL).

Prior to the helical scan, all patients underwent a non-enhanced electrocardiographic (ECG)-gated scan to assess the coronary calcium score. For the 64-slice GE Lightspeed system, the following parameters were used for the coronary calcium scan: 4 x 3.0 mm or 2.5 mm, rotational time 350-500 ms, tube voltage 120 kV and tube current 200-250 mA. The following parameters were used for the helical scan: collimation of 64 x 0.625 mm, rotation time 350 ms, tube voltage 120 kV, and tube current 600 mA. Scan parameters for the Aquilion 64 CT scanner have been published previously.[3] The ECG was obtained

simultaneously for retrospective gating of the raw data. Images were reconstructed with a slice thickness of 0.5 mm and a reconstruction interval of 0.3 mm, for the 64-slice Toshiba Aquilion system. For the 64-slice GE Lightspeed system, data were reconstructed at an effective slice thickness of 0.625 mm.

MSCT Examination

Coronary Artery Calcium Score

The non-helical scans performed with the Toshiba multislice Aquilion 64 system or the 64-slice GE Lightspeed system were analyzed using dedicated offline software (Vitrea 2, Vital Images, Plymouth, Minnesota, USA or Advantage, GE Healthcare, Milwaukee, Wisconsin, USA, respectively). An overall Agatston score was calculated for each patient.[10]

Computed Tomography Coronary Angiography

The MSCT angiography examinations were evaluated by an independent and experienced observer who was blinded to quantitative data, as derived from QAngioCT and QCA. Coronary arteries were divided into 17 segments according to the American Heart Association classification.[8]

The most severely diseased segment per coronary artery was evaluated for the presence of significant (≥50% diameter stenosis) or non-significant (<50% diameter stenosis) diameter stenosis with the use of axial images and curved multiplanar reconstructions in at least 2 orthogonal planes.

Automated quantitative computed tomography angiography (QAngioCT) was performed by an independent observer, blinded to QCA data, using dedicated software (QAngioCT 1.1, Medis medical imaging systems, Leiden, the Netherlands). Using the 17-segment model[8], quantitative measurements were performed on the most severely diseased segment for each coronary artery, as defined with QCA. A single coronary stenosis was assigned per coronary segment. To ensure that similar segments were analyzed with QCA and QAngioCT, accurate segment definition (defined with proximal and distal markers) was based on the 17-segment model. Side branches and coronary ostia were used as anatomical markers. Before automatic quantification, image quality of coronary segments was classified using the following scale: 1 = good image quality, 2 = moderate image quality, 3 = poor image quality. Data sets with moderate image quality showed either motion artifacts or increased image noise. Data sets with poor image quality were non-diagnostic. In addition, atherosclerotic plaques were classified as non-calcified (lesions with lower density compared with contrast-enhanced lumen), mixed (lesions having elements of both non-calcified and calcified lesions) or calcified (lesions with high density).

Consecutively, automated quantification of diameter stenosis was performed. A fast vessel tracking algorithm was used to obtain the three dimensional centerline (ranging from

the proximal to distal marker) of the coronary artery. This vessel tracking step consists of: (1) a pre-segmentation of the vessel between the proximal and distal point; and (2) a fastest path back-tracking from distal to the proximal point through the center of the segmentation. Based on this centerline, a stretched multi planar reformatted (MPR) volume was created of the segment of interest. MPR volumes allowed analysis of curved coronary arteries as straight vessels. Next, four longitudinal cross-sections were extracted from the MPR volume at 45º degrees angular intervals. Subsequently, lumen borders in these four longitudinal images were detected by a model guided minimum cost approach (MCA).[11] A comprehensive overview of the whole coronary segment of interest was provided by these four longitudinal images and corresponding longitudinal contours. Consecutively, the lumen border contours were detected in each transversal slice of the MPR volume using MCA with a circular lumen model. The MCA method uses a combination of spatial first-, and second-derivative gradient filters in combination with knowledge of the expected CT intensity values in the arteries. Therefore, the MCA method is insensitive to differences in attenuation values between data sets. During this step, the intersection points of each transversal slice with the earlier obtained longitudinal contours were used to guide the contour detection in each particular slice. Based on the cross-sectional area of the obtained transversal contours a diameter function along the vessel course was derived using the formula for circular cross sections. Finally, from these data, the reference diameter function, minimal lumen diameter and the degree of stenosis were obtained similar to the QCA method (Figure 1). The minimal detectable diameter is approximately 0.25 mm with the currently used settings for coronary analyses in QAngioCT. This is the image resolution at which the CTA data set is re-sampled along the vessel within the stretched image. Automated quantitative processing steps were independent from the standard viewing settings (window level 1024, width 0). Only limited manual input was used to improve the automated processing steps. Corrections could be made in the longitudinal contour detection to improve contour detection in a limited number of transversal slices (less than 5 minutes per patient). If indicated, coronary flagging of particular segments was performed to improve the luminal reference line (less than 1 minute per patient).

Reproducibility of QAngioCT was evaluated by assessment of inter- and intraobserver variability. A second blinded observer performed QAngioCT measurements in 20 patients (58 interpretable vessels) who were randomly identified. To assess intraobserver variability measurements were performed twice by the same observer in a subset of 20 randomly selected patients (58 interpretable vessels).

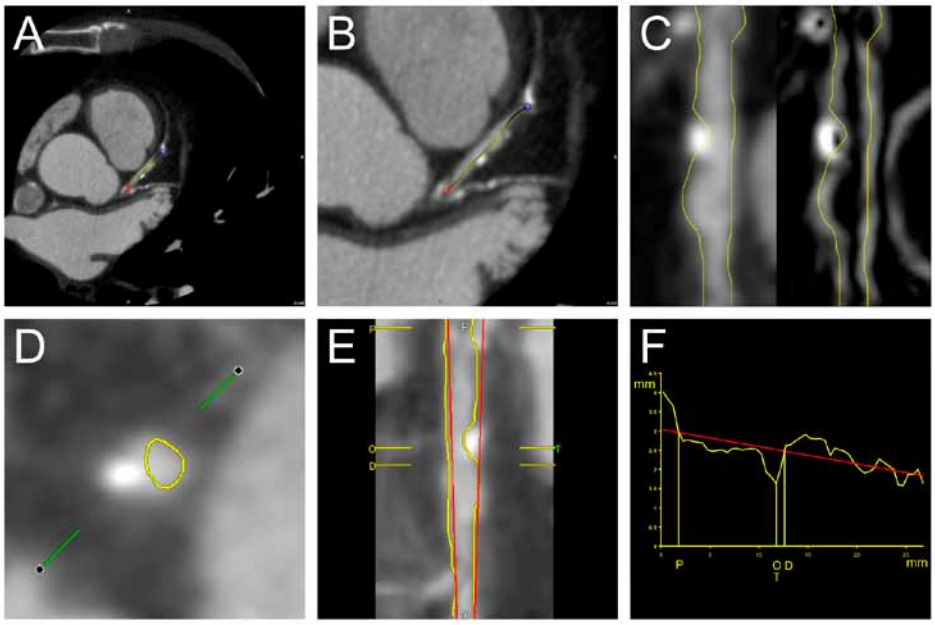

Figure 1. Process of automated quantification of stenosis severity on 64-slice multi-slice computed tomography (MSCT). Automated quantification of stenosis severity on MSCT. Initially, accurate segment definition was performed using proximal and distal markers (Panel A and B). Automated contour detection was performed in longitudinal (Panel C) and transversal (Panel D) views. The longitudinal contours provide an initial approximation of the lumen border locations and are used to guide the automatic transversal contour detection. The right side of panel C shows the gradient image which is used to provide an intensity independent border description. Lumen quantification is only based on the transversal contours. Finally, in Panel E and F, quantification of stenosis was based on differences between reference line (red line) and contour area (yellow line). Reference line represented an estimate of normal tapering of the coronary artery. Diameter stenosis was 35.0% on QAngioCT which corresponded with 41.5% on QCA.

Statistical Analysis

Continuous data are presented as mean ± standard deviation, and categorical data are presented as absolute numbers or percentages. QAngioCT and QCA were compared on a vessel and patient basis using Pearson's linear regression analysis. Segments with the most severe lesion per coronary vessel were included in de vessel-based analysis, whereas segments with the most severe lesion per patient were included in the patient-based analysis. Additionally, a segment-based analysis on a subset of 10 randomly selected patients was performed to evaluate the performance of QAngioCT in a wide range of stenosis and to avoid potential bias towards the most severe stenosis. For the segment-based analysis, each location of luminal narrowing per coronary segment was identified and analyzed using both quantitative approaches. Pearson's linear regression analysis was used to compare

QAngioCT and QCA on a segment basis. Furthermore, separate analyses were performed for non-calcified, mixed and calcified lesions. When appropriate, wilcoxon signed-rank tests were used to compare percentage diameter stenosis as derived from QAngioCT and QCA. Limits of agreement between QAngioCT and QCA were calculated with Bland-Altman analyses showing the mean value of differences of each pair plotted against the average value of each pair. In addition, separate analyses were performed for non-calcified, mixed and calcified lesions.

Diagnostic accuracy for assessment of significant coronary artery stenosis (≥50% diameter stenosis) was assessed for QAngioCT and visual analysis. Corresponding sensitivity, specificity, negative and positive predictive values were calculated. The 95% confidence intervals were calculated using the following formula: p±1.96 x standard error (SE) and the SE was estimated by $\sqrt{[p\ (1 - p) / n]}$. Agreement between quantitative and visual analysis was evaluated using Cohen's Kappa statistics, and *k* values were qualified as poor (<0.40), moderate (0.40-0.75) or good (>0.75) agreement. Inter- and intraobserver variability were determined with Bland-Altman analyses (GraphPad Prism software, version 5.01, GraphPad software Inc, San Diego, California, USA). Analyses were performed with statistical software (SPSS version 16.0, SPSS inc., Chicago, Illinois, USA). A p value <0.05 was considered statistically significant.

Results

Study Population and Baseline Results

One-hundred patients (53 men, 59.8±8.0 yrs) who underwent 64-slice MSCT and invasive coronary angiography were enrolled retrospectively. The mean duration between both examinations was 38.0±49.3 days. Baseline characteristics of the study population are listed in Table 1. Fifty patients underwent a 64-slice Toshiba Aquilion MSCT examination (Leiden University Medical Center, Leiden, the Netherlands) and 50 patients underwent a 64-slice GE Lightspeed MSCT examination (Medical Center Haaglanden, the Hague, the Netherlands).

In total, 282 (94%) vessels were included in the vessel-based analysis. Eighteen (6%) vessels from 18 patients were excluded because of poor image quality, including motion artifacts on MSCT (n=7), reduced contrast arrival on MSCT (n=7) or the presence of a total occlusion (n=4). Good image quality was documented in 212 (71%) vessels, whereas moderate image quality was documented in 70 (23%) vessels. Mean values of diameter stenosis and minimal lumen diameter for vessel-based analysis are shown in Table 2.

On a patient basis, 93 (93%) patients were included, whereas in 7 (7%) patients, the vessel with the most severe lesion was excluded because of poor image quality, including

motion artifacts (n=3) or total occlusion (n=4). Of the 93 patients, good image quality was observed in 62 (62%) patients and moderate image quality in 31 (31%) patients.

Table 1. Baseline characteristics of study population (n=100)

Men	53
Age (yrs)	59.8±8.0
Heart rate (bpm)	61.1±9.8
Calcium score	366±728
Suspected CAD	93
Known CAD	7
Previous coronary angioplasty	4
Indications of CAD on previous tests	3
Clinical presentation prior to MSCT	
Atypical angina pectoris	70
Typical angina pectoris	24
Cardiovascular risk factors	
Diabetes mellitus	16
Systemic hypertension	65
Hypercholesterolemia	62
Current smoking	33
Obesity	23
Positive family history	36

Data are presented as mean ± standard deviation or as number. CAD = coronary artery disease; MSCT = multislice computed tomography

Table 2. Diameter stenosis (%) and minimal lumen diameter (mm) derived from QAngioCT and QCA for all vessels (n=282), non-calcified (n=146), mixed (n=81) and calcified lesions (n=55)

	QAngioCT	QCA
Diameter stenosis (%)		
All vessels	26.4±19.4	29.4±22.0*
Non-calcified lesions	16.8±11.9	20.1±15.3*
Mixed lesions	35.1±21.5	38.5±23.2*
Calcified lesions	39.2±19.0	40.9±24.4
Minimal lumen diameter (mm)		
All vessels	2.4±0.8	2.2±1.0*
Non-calcified lesions	2.7±0.7	2.5±0.9*
Mixed lesions	2.1±0.9	1.9±1.1*
Calcified lesions	2.0±0.7	1.7±0.9*

Data are presented as mean ± standard deviation. QAngioCT = quantitative computed tomography angiography; QCA = quantitative coronary angiography. *$p<0.05$.

Agreement between Visual Analysis and QCA

The agreement between visual analysis and QCA for semi-quantitative assessment of significant coronary stenosis (using ≥50% diameter stenosis as a cutoff) was determined on a patient basis (Table 3). In total, 30 vessels were identified as significant stenosis on QCA, of which 25 vessels were also classified as having significant stenosis on visual analysis (sensitivity 83%, 95% CI 70-97%). Of the 63 vessels which were classified as non-significant using QCA, visual analysis incorrectly classified 7 vessels as having a significant stenosis (specificity 89%, 95% CI 81-97%). The corresponding negative and positive predictive values were 92% (95% CI 85-99%) and 78% (95% CI 64-93%). The agreement between the visual analysis and QCA was 87% (95% CI 80-94%), with a *k* value of 0.71 using ≥50% diameter stenosis as a cutoff for significant lesions.

Table 3. Diagnostic accuracy of QAngioCT and visual analysis for assessment of significant coronary artery stenosis (≥50% diameter stenosis) on a patient basis (n=93)

	TN	TP	FN	FP	Se	Sp	NPV	PPV	Accuracy
Visual score	56	25	5	7	83	89	92	78	87
95% CI					(70-97)	(81-97)	(85-99)	(64-93)	(80-94)
QAngioCT	63	25	5	0	83	100	93	100	95
95% CI					(70-97)		(87-99)		(90-99)

CI = confidence interval; FN = false negative; FP = false positive; NPV = negative predictive value; PPV = positive predictive value; QAngioCT = quantitative computed tomography angiography; Se = sensitivity; Sp = specificity; TN = true negative; TP = true positive.

In addition, further analysis of the agreement between visual analysis and QCA was performed in relation to image quality. In Table 4, corresponding sensitivity, specificity, negative and positive predictive values are provided.

Table 4. Diagnostic accuracy of QAngioCT and visual analysis for assessment of significant coronary artery stenosis (≥50% diameter stenosis) for data sets with good (n=62) or moderate (n=31) image quality.

	TN	TP	FN	FP	Se	Sp	NPV	PPV	Accuracy
Visual analysis									
Good quality	43	13	1	5	93	90	98	72	90
95% CI					(79-100)	(81-98)	(93-100)	(52-93)	(83-98)
Moderate quality	13	12	4	2	75	87	76	86	81
95% CI					(54-96)	(70-100)	(56-97)	(67-100)	(67-95)
QAngioCT									
Good quality	48	11	3	0	79	100	94	100	95
95% CI					(57-100)		(88-100)		(90-100)
Moderate quality	15	14	2	0	88	100	88	100	94
95% CI					(71-100)		(73-100)		(85-100)

CI = confidence interval; FN = false negative; FP = false positive; NPV = negative predictive value; PPV = positive predictive value; QAngioCT = quantitative computed tomography angiography; Se = sensitivity; Sp = specificity; TN = true negative; TP = true positive.

Agreement between QAngioCT and QCA

Good correlations for diameter stenosis were observed between QAngioCT and QCA on a vessel basis (n=282, r=0.83, p<0.01) and a patient basis (n=93, r=0.86, p<0.01) (Figures 2 and 3). Additionally, the segment-based analysis which provided information regarding the performance of QAngioCT in a wide range of percentage diameter stenosis showed a good correlation between QAngioCT and QCA for diameter stenosis (n=127, r=0.82, p<0.01).

In addition, limits of agreement between QAngioCT and QCA for assessment of diameter stenosis were assessed. On a vessel basis, mean value of differences ± standard deviation was -3.0±12.3% with 95% limits of agreement ranging from -27.1 to 21.0% (Figure 2), whereas on a patient basis mean value of differences ± standard deviation was -6.2±12.4% with 95% limits of agreement ranging from -30.5 to 18.1% (Figure 3). For the segment-based analysis, mean value of differences ± standard deviation was -0.1±8.2% with 95% limits of agreement ranging from -16.2 to 16.0%.

Evaluation of inter- and intraobserver variability revealed mean value of differences ± standard deviations of -1.4±7.4% and -1.9±7.2%.

The agreement between QAngioCT and QCA for assessment of significant (≥50% diameter stenosis) or non-significant (<50% diameter stenosis) was calculated on a patient basis (Table 3). In 30 vessels a significant stenosis was identified on QCA, of which 25 vessels were classified similarly using QAngioCT (sensitivity 83%, 95% CI 70-97%). In 5 vessels a non-significant stenosis was identified with QAngioCT, whereas QCA showed a significant stenosis. Importantly, the majority of the lesions that were underestimated with QAngioCT showed <70% stenosis on QCA (n=4). Moreover, of the 63 non-significant lesions on QCA,

63 lesions were also classified as non-significant using QAngioCT (specificity 100%). No lesions were overestimated on QAngioCT as compared to QCA, yielding an accuracy of 95% (95% CI 90-99%) and a *k* value of 0.87. Using ≥50% diameter stenosis as a cutoff, corresponding negative and positive predictive values were 93% (95% CI 87-99%) and 100%.

Finally, further analysis of the agreement between QAngioCT and QCA was performed in relation to image quality (Table 4). QAngioCT performed equally well in patients with moderate or good image quality (diagnostic accuracy 94% vs. 95%, p=NS). However, as compared to visual analysis, QAngioCT tended to have a reduced sensitivity in data sets with good image quality. Corresponding sensitivity, specificity, negative and positive predictive values are shown in Table 4.

Figure 2. Comparison between quantitative computed tomography angiography (QAngioCT) and quantitative coronary angiography (QCA) for assessment of diameter stenosis on a vessel basis.

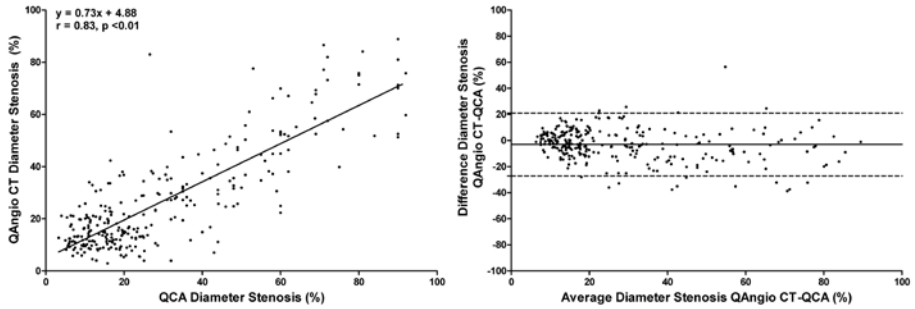

Linear regression (left panel) and Bland-Altman (right panel) analyses for diameter stenosis on a vessel basis (n=282). QAngioCT and QCA showed good correlation and agreement for diameter stenosis.

Figure 3. Comparison between quantitative computed tomography angiography (QAngioCT) and quantitative coronary angiography (QCA) for assessment of diameter stenosis on a patient basis.

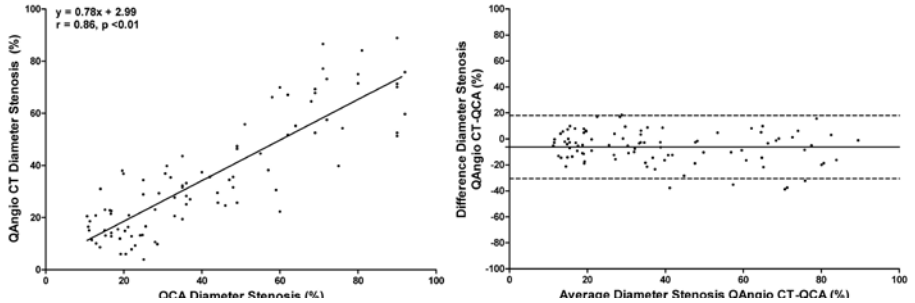

Linear regression (left panel) and Bland-Altman (right panel) analyses for diameter stenosis on a patients basis (n=93). QAngioCT and QCA showed good correlation and agreement for diameter stenosis.

Influence of Plaque Composition

In addition, non-calcified (n=146), mixed (n=81) or calcified lesions (n=55) were analyzed separately. Mean diameter stenosis and minimal lumen diameter for different plaque types are shown in Table 2. A good correlation for non-calcified (n=146, r=0.79, p<0.01), mixed (n=81, r=0.80, p<0.01) and calcified (n=55, r=0.77, p<0.01) lesions was observed (Figures 4-6). For non-calcified lesions, mean value of differences ± standard deviation was -3.2±9.4% with 95% limits of agreement ranging from -21.6 to 15.1%. Furthermore, for mixed lesions, mean value of differences ± standard deviation was -3.5±14.2% with 95% limits of agreement ranging from -31.3 to 24.4%. Mean value of differences ± standard deviation for calcified lesions was -1.8±15.7% with 95% limits of agreement ranging from -32.5 to 29.0% (Figures 4-6).

Figure 4. Comparison between quantitative computed tomography angiography (QAngioCT) and quantitative coronary angiography (QCA) to assess diameter stenosis of segments with non-calcified lesions.

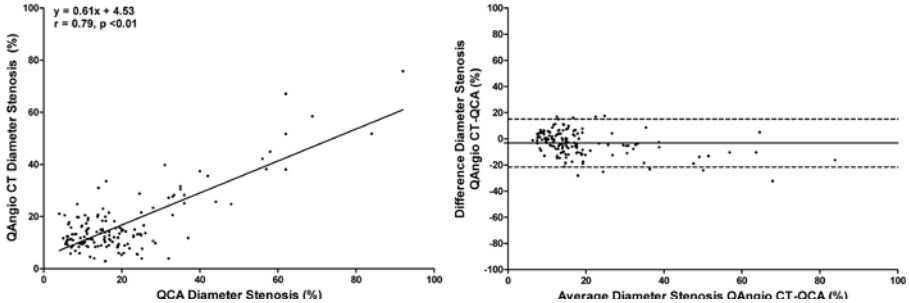

Linear regression (left panel) and Bland-Altman (right panel) analyses of diameter stenosis of segments with non-calcified lesions (n=146). Good correlation and agreement were observed for assessment of diameter stenosis.

Figure 5. Comparison between quantitative computed tomography angiography (QAngioCT) and quantitative coronary angiography (QCA) to assess diameter stenosis of segments with mixed lesions.

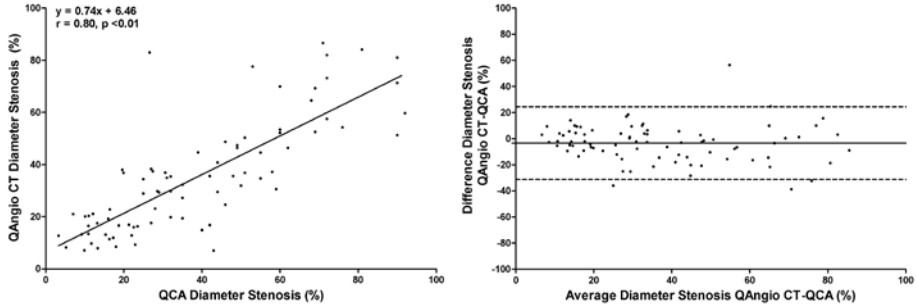

Linear regression (left panel) and Bland-Altman (right panel) analyses of diameter stenosis of segments with mixed lesions (n=81). Good correlation and agreement were observed for assessment of diameter stenosis.

Figure 6. Comparison between quantitative computed tomography angiography (QAngioCT) and quantitative coronary angiography (QCA) to assess diameter stenosis of segments with calcified lesions.

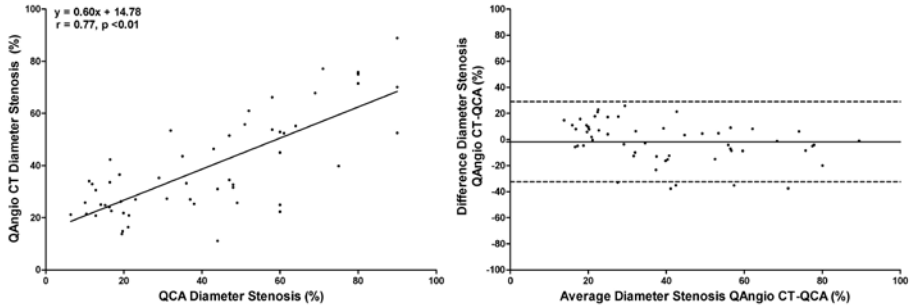

Linear regression (left panel) and Bland-Altman (right panel) analyses of diameter stenosis of segments with calcified lesions (n=55). Good correlation and agreement were observed for assessment of diameter stenosis.

Discussion

The main findings of the study are as follows: novel automated dedicated QAngioCT software and QCA showed good correlations for quantification of stenosis severity on vessel- and patient-based analysis. In addition, QAngioCT and QCA showed good agreement for semi-quantitative assessment of stenosis severity (accuracy of 95%, *k* value of 0.87). Moreover, a tendency towards improved diagnostic accuracy was observed with QAngioCT when compared to visual analysis of stenosis severity. Importantly, the positive predictive value was significantly higher with QAngioCT when compared to visual analysis for the assessment of significant coronary artery stenosis.

MSCT has appeared as a potent imaging technique for non-invasive evaluation of coronary atherosclerosis. Most of the studies have used visual and, moreover, binary approaches (≥50% luminal narrowing based on visual assessment) to identify significant stenoses on MSCT. However, quantification of stenosis severity may be preferred in terms of diagnostic accuracy and reproducibility. In addition, quantification of stenosis severity with an automated and robust approach may become particularly interesting when using MSCT to evaluate progression of coronary atherosclerosis.

At present however, limited evidence is available on quantification of stenosis severity on MSCT.[5, 7, 13] Thus far, results of quantitative studies using a semi-automated CT approach for assessment of stenosis severity are lacking consistency. In addition, these semi-quantitative approaches resulted frequently in modest correlations between QCA and MSCT for the quantification of stenosis severity.[5, 7] An important study was performed by Leber et al.[5] who determined the diagnostic accuracy of 64-slice MSCT for quantification of stenosis severity in comparison to QCA. In 55 patients, 825 cardiac segments (15-segment model) could be visualized and analyzed using a semi-automated quantitative approach. Overall, moderate correlations were observed for stenosis severity between 64-slice MSCT and QCA (r=0.54). Also, stenosis severity as assessed with intravascular ultrasound (IVUS) was moderately correlated with 64-slice MSCT (r=0.61). Likewise, Raff and colleagues[4] evaluated the diagnostic accuracy of a semi-automated quantitative CT approach in comparison to invasive quantitative analyses in 70 patients with suspected CAD. Quantitative MSCT showed high diagnostic accuracy for the assessment of significant stenosis as compared to QCA. Importantly, however, significant variability in stenosis severity was observed between QCA and quantitative MSCT. In particular, lesions of intermediate severity on QCA (30-70% diameter stenosis) showed high variability when compared to quantitative MSCT. Interestingly, Cheng et al.[14] have recently showed that a multi-tiered visual grading system was more accurate as compared to semi-manual quantification of MSCT.

A potential explanation for the limited accuracy observed for these semi-manual quantification approaches may be the large variation that is introduced due to manual interference. For instance, in the study by Cheng et al.[14], manual input was required to assess the

minimal luminal diameter at the site of stenosis (in addition to proximal and distal points). Furthermore, measurements were performed in a single longitudinal image. In the present study however, an automated quantification algorithm was used for assessment of diameter stenosis in which only limited manual input was used to guide the automated processing steps. Manual input was limited to accurate segment definition using proximal and distal markers. In this respect, Marquering et al.[15] have demonstrated that deviations were minimal in extracted centerlines when varying the position of placed proximal and distal markers. In addition, the manual corrections made in the longitudinal contour detection were only used to improve the detected transversal contours in a limited number of locations in the transversal slice. Accordingly, quantification of stenosis severity was performed by an automated dedicated approach consisting of several consecutive programmed processing steps. Nevertheless, small corrections could also be made to improve the luminal reference line by flagging particular coronary segments, similar as performed with QCA. Interestingly, this approach resulted in good correlations between QAngioCT and QCA for assessment of diameter stenosis on vessel- and patient-based analysis.

In the study by Bruining and colleagues[16] an automated approach with limited manual interference was also used to determine its diagnostic accuracy and reproducibility. Quantitative CT analysis was performed in 48 symptomatic patients who underwent invasive coronary angiography and IVUS. Measurements were performed by two independent observers using a coronary artery extraction method with computed-assisted quantitative volumetric analysis. Both observers found good correlations between MSCT and IVUS for lumen (r=0.76 and r=0.95) and plaque volumes (r=0.74 and r=0.79).

Another important finding of the present study was that no influence of plaque type was observed and that the algorithm performed equally well in non-calcified, mixed and calcified lesions. In contrast, previous studies have reported that algorithms may quantify stenosis severity of non-calcified, mixed and calcified plaques with variable accuracy.[6, 12, 13] Overall, a tendency to underestimate stenosis severity of non-calcified lesions versus an overestimation of calcified lesions has been observed in many studies.[6, 12] In a previous study by Leber and colleagues[6], non-calcified and mixed plaque volumes were significantly underestimated on quantitative MSCT (59.8±76.6 mm^3 vs. 67.7±67.9 mm^3 and 47.7±87.5 mm^3 vs. 57.5±99.4 mm^3, $p<0.03$) as compared to IVUS derived plaque volumes, whereas calcified plaques were systematically overestimated (65.8±110.0 mm^3 vs. 53.2±90.3 mm^3, p=0.19) on MSCT when compared to IVUS. In this study, a slight underestimation of stenosis severity using QAngioCT for non-calcified and mixed plaques was found. Also, for calcified lesions, although showing the lowest mean value of differences, a systematic underestimation of stenosis severity was observed in comparison to QCA. In contrast, calcified lesions are usually overestimated with cardiac CT possibly due to the blooming effect of calcium. With the use of an automatic quantification algorithm however, the influence of blooming artifacts may be reduced, leading to a better estimate of stenosis severity.

In this study, results of the Bland-Altman analysis revealed smaller limits of agreement for vessel-based and patient-based analysis, as compared to previously performed studies using semi-quantitative measurements of coronary stenosis.[7, 13] These findings underline the feasibility of this novel automated quantitative algorithm to assess stenosis severity, although further improvements are needed.

Moreover, semi-quantitative assessment of the presence of significant coronary artery stenosis (≥50% diameter stenosis) revealed a good agreement (overall agreement of 95%). Only 5 lesions with ≥50% diameter stenosis on QCA were underestimated by QAngioCT; the majority of these significant lesions were not severe and showed <70% diameter stenosis on QCA. Importantly, the current study showed a tendency towards improved diagnostic accuracy for assessment of significant lesions with QAngioCT when compared to visual CT analysis (95% vs. 87%, p=0.08). In particular, a significantly improved positive predictive value was observed using QAngioCT when compared to visual analysis (100% vs. 78%, p<0.05).

In addition, the performance of QAngioCT and visual analysis was analyzed in data sets with different image quality. Although the visual approach showed a reduced diagnostic accuracy for data sets with moderate image quality, QAngioCT performed equally well in patients with moderate or good image quality. These findings demonstrate the feasibility of QAngioCT for evaluation of coronary artery stenosis in data sets with variable image quality. Only in data sets with good image quality, sensitivity tended to be lower with QAngioCT as compared to visual analysis.

Finally, the present study has demonstrated low inter- and intraobserver variability for automated quantification of stenosis severity. This is an important finding, since previous quantitative approaches were largely limited due to poor reproducibility.[4-7, 13] Accordingly, the current study provides important information on the use of automated quantification of stenosis severity on MSCT. Still, more studies are needed to elucidate the precise role of automated quantification in clinical cardiology.

Limitations

The current study should be considered as a feasibility study, validating a novel approach for automated quantification of stenosis severity. Integration of other plaque characteristics (remodeling index, plaque burden, eccentricity and plaque length) would be preferred in evaluation of coronary atherosclerosis, however, the study was only designed to demonstrate feasibility of the new approach. Further studies are needed to validate automated quantification of different plaque characteristics. In the present study, IVUS may have been a more reliable reference standard as compared to QCA as IVUS is considered to be a true tomographic atherosclerosis imaging technique. Indeed, MSCT may be more suited for the evaluation of atherosclerosis rather than stenosis. However, conventional coronary angiography represents the validated standard for detection of CAD in clinical cardiology.

Finally, in the current study the prevalence of significant CAD was relatively low and the performance of QAngioCT should be tested in more challenging populations with higher disease prevalence as well.

Conclusion

The novel automated QAngioCT approach and QCA showed good correlation for quantification of stenosis severity on vessel and patient basis. Good agreement was observed for semi-quantitative assessment of significant coronary artery stenosis (≥50% diameter stenosis). The use of an automated quantification algorithm improves the positive predictive value of MSCT when compared to visual assessment of stenosis severity.

Reference List

(1) Miller JM, Rochitte CE, Dewey M, et al. Diagnostic performance of coronary angiography by 64-row CT. N Engl J Med 2008; 359:2324-36.

(2) Meijboom WB, Meijs MF, Schuijf JD, et al. Diagnostic accuracy of 64-slice computed tomography coronary angiography: a prospective, multicenter, multivendor study. J Am Coll Cardiol 2008; 52:2135-44.

(3) Schuijf JD, Pundziute G, Jukema JW, et al. Diagnostic accuracy of 64-slice multislice computed tomography in the noninvasive evaluation of significant coronary artery disease. Am J Cardiol 2006; 98:145-8.

(4) Raff GL, Gallagher MJ, O'Neill WW, Goldstein JA. Diagnostic accuracy of noninvasive coronary angiography using 64-slice spiral computed tomography. J Am Coll Cardiol 2005; 46:552-7.

(5) Leber AW, Knez A, von Ziegler F, et al. Quantification of obstructive and nonobstructive coronary lesions by 64-slice computed tomography: a comparative study with quantitative coronary angiography and intravascular ultrasound. J Am Coll Cardiol 2005; 46:147-54.

(6) Leber AW, Becker A, Knez A, et al. Accuracy of 64-slice computed tomography to classify and quantify plaque volumes in the proximal coronary system: a comparative study using intravascular ultrasound. J Am Coll Cardiol 2006; 47:672-7.

(7) Dewey M, Rutsch W, Schnapauff D, Teige F, Hamm B. Coronary artery stenosis quantification using multislice computed tomography. Invest Radiol 2007; 42:78-84.

(8) Austen WG, Edwards JE, Frye RL, et al. A reporting system on patients evaluated for coronary artery disease. Report of the Ad Hoc Committee for Grading of Coronary Artery Disease, Council on Cardiovascular Surgery, American Heart Association. Circulation 1975; 51:5-40.

(9) Reiber JHC, Tuinenburg JC, Koning G, et al. Chapter 2.2: Quantitative coronary arteriography.In: Coronary Radiology 2nd Revised Edition, Oudkerk M, Reiser MF (Eds.), Series: Medical Radiology, Sub series: Diagnostic Imaging, Baert AL, Knauth M, Sartor K (Eds.). Springer-Verlag, Berlin-Heidelberg 2009; 41-65.

(10) Agatston AS, Janowitz WR, Hildner FJ, Zusmer NR, Viamonte M, Jr., Detrano R. Quantification of coronary artery calcium using ultrafast computed tomography. J Am Coll Cardiol 1990;15:827-32.

(11) van de Zwet PMJ, van Land CD, Loois G, Gerbrands JJ, Reiber JHC. An on-line system for the quantitative analysis of coronary arterial segments. Comp Cardiol 1990;19:157-60.

(12) Otsuka M, Bruining N, Van Pelt NC, et al. Quantification of coronary plaque by 64-slice computed tomography: a comparison with quantitative intracoronary ultrasound. Invest Radiol 2008; 43:314-21.

(13) Husmann L, Gaemperli O, Schepis T, et al. Accuracy of quantitative coronary angiography with computed tomography and its dependency on plaque composition: plaque composition and accuracy of cardiac CT. Int J Cardiovasc Imaging 2008; 24:895-904.

(14) Cheng V, Gutstein A, Wolak A, et al. Moving beyond binary grading of coronary arterial stenoses on coronary computed tomographic angiography: insights for the imager and referring clinician. JACC Cardiovasc Imaging 2009; 1:460-71.

(15) Marquering HA, Dijkstra J, de Koning PJ, Stoel BC, Reiber JH. Towards quantitative analysis of coronary CTA. Int J Cardiovasc Imaging 2005; 21:73-84.

(16) Bruining N, Roelandt JR, Palumbo A, et al. Reproducible coronary plaque quantification by multislice computed tomography. Catheter Cardiovasc Interv 2007; 69:857-65.

Chapter **4**

Automated Quantification of Coronary Plaque with Computed Tomography: Comparison with IVUS using a Dedicated Registration Algorithm for Fusion-Based Quantification

Mark J. Boogers, MD[1, 2]; Alexander Broersen, PhD[3]; Joëlla E. van Velzen, MD[1, 2]; Fleur R. de Graaf, MD[1]; Heba M. El-Naggar, MD[1]; Pieter H. Kitslaar, MSc[3]; Jouke Dijkstra, PhD[3]; Victoria Delgado, MD[1]; Eric Boersma, PhD[4]; Albert de Roos, MD, PhD[5]; Joanne D. Schuijf, PhD[1]; Martin J. Schalij, MD, PhD[1]; Johan H.C. Reiber, PhD[3, 6]; Jeroen J. Bax, MD, PhD[1]; J. Wouter Jukema, MD, PhD[1]

[1]Department of Cardiology, Leiden University Medical Center, Leiden, the Netherlands; [2]The Interuniversity Cardiology Institute of the Netherlands, Utrecht, the Netherlands; [3]Department of Radiology, Division of Image Processing, Leiden University Medical Center, Leiden, the Netherlands; [4]Department of Epidemiology and Statistics, Erasmus University, Rotterdam, the Netherlands; [5]Department of Radiology, Leiden University Medical Center, Leiden, the Netherlands; [6]Medis medical imaging systems B.V., Leiden, the Netherlands.

Abstract

Aims Previous studies have only used semi-automated approaches for coronary plaque quantification on multi-detector row computed tomography (CT), while an automated quantitative approach using a dedicated registration algorithm is currently lacking. Accordingly, the study aimed to demonstrate the feasibility and accuracy of automated coronary plaque quantification on cardiac CT using dedicated software with a novel 3D coregistration algorithm of CT and intravascular ultrasound (IVUS) datasets.

Methods Patients who had undergone CT and IVUS were enrolled. Automated lumen and vessel wall contour detection was performed for both imaging modalities. Dedicated automated quantitative software (QCT) with a unique registration algorithm was used to fuse a complete IVUS run with a CT angiography volume using true anatomical markers. At the level of the minimal lumen area (MLA), percentage lumen area stenosis, plaque burden and degree of remodeling were obtained on CT. Additionally, mean plaque burden was assessed for the whole coronary plaque. At the identical level within the coronary artery, the same variables were derived from IVUS.

Results Fifty-one patients (40 men, 58±11 yrs, 103 coronary arteries) with 146 lesions were evaluated. QCT and IVUS showed good correlation for MLA ($n=146$, $r=0.75$, $p<0.001$). At the level of the MLA, both techniques were well-correlated for lumen area stenosis ($n=146$, $r=0.79$, $p<0.001$) and plaque burden ($n=146$, $r=0.70$, $p<0.001$). Mean plaque burden ($n=146$, $r=0.64$, $p<0.001$) and remodeling index ($n=146$, $r=0.56$, $p<0.001$) showed significant correlations between QCT and IVUS.

Conclusion Automated quantification of coronary plaque on CT is feasible using dedicated quantitative software with a novel 3D registration algorithm.

Introduction

Multi-detector row computed tomography (CT) permits non-invasive evaluation of coronary artery disease (CAD) with excellent image quality and diagnostic accuracy as compared to invasive coronary angiography.[1-3] The degree of coronary luminal narrowing is commonly used to guide diagnosis and therapeutic interventions in clinical cardiology.[3-5] However, cardiac CT is not restricted to coronary luminography as it provides additional information on the coronary atherosclerotic plaque itself, including plaque morphology, plaque burden and the degree of plaque remodeling. However, one of the current drawbacks of cardiac CT remains the fact that coronary plaque characteristics are most commonly evaluated by a visual approach, which is observer dependent and requires substantial reading experience.

Automated quantification of coronary plaque characteristics would be preferred to further improve the diagnostic accuracy, reproducibility and time-efficiency of cardiac CT. At present however, the feasibility of automated quantification of coronary luminal narrowing using cardiac CT has only been demonstrated in a small number of studies.[6, 7] Earlier attempts that aimed to measure other coronary plaque characteristics have used either manually-based or semi-automated techniques, rather than automated dedicated quantitative algorithms.[8-10] Moreover, in these previous studies, a visual approach was used to match coronary lesions on the different imaging techniques which may introduce inaccuracies.

Recently, dedicated automated quantitative computed tomography (QCT) software with a unique 3D registration algorithm has been developed to enable accurate matching of imaging modalities along the longitudinal and transversal axis of coronary arteries. The novel 3D registration algorithm allows fusion of cardiac imaging techniques using a slice-by-slice comparison of each location along the longitudinal and transversal axis of the coronary arteries and may improve detection and quantification of coronary plaques on cardiac CT when compared to previous quantitative CT studies using a visual approach.

At present, no study has evaluated the feasibility of automated coronary plaque quantification on cardiac CT using an automated 3D registration algorithm of CT and intravascular ultrasound (IVUS) datasets. Accordingly, the current study aimed to demonstrate the feasibility and accuracy of automated quantification of coronary plaque on cardiac CT using dedicated software with a novel 3D registration algorithm of CT and IVUS datasets.

Material and Methods

Patient Population and Study Protocol

The patient population consisted of patients who had undergone cardiac CT and conventional invasive coronary angiography with IVUS within a period of 4 months. Clinical data were

prospectively entered in the departmental Cardiology Information System (EPD-Vision®, Leiden University Medical Center). A total of 80 consecutive patients with known (n=32) or suspected (n=48) coronary atherosclerosis who were referred for cardiac CT were selected. From these 80 patients, 51 patients were referred within a period of 4 months for invasive coronary angiography with IVUS, because of patient's clinical symptoms and/or imaging results to further evaluate the extent and severity of CAD. Accordingly, 29 patients who were not referred to invasive coronary angiography with IVUS (n=18) or did not undergo invasive coronary angiography along with IVUS (n=11) were excluded from further analyses. A flow chart of the patient inclusion is provided in Figure 1.

In each of the 51 patients, IVUS was performed in 1 to 3 coronary arteries during invasive coronary angiography. Of the 153 coronary arteries, IVUS was performed in 103 coronary arteries, whereas IVUS studies were not acquired in 50 coronary arteries due to vessel tortuosity (n=15), severe luminal narrowing (n=9), (subtotal) vessel occlusion (n=11) or time constraints (n=15).

Figure 1. Flow chart of the patient inclusion. A total of 80 patients referred for cardiac computed tomography (CT) because of known or suspected coronary artery disease (CAD) were selected, of which 51 patients underwent invasive coronary angiography with intravascular ultrasound (IVUS).

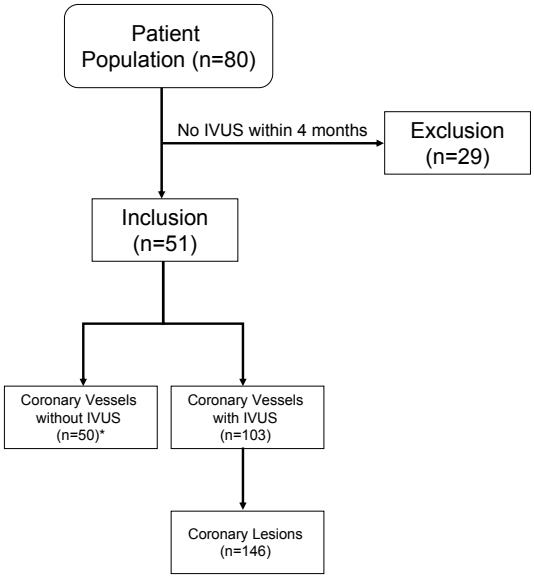

*IVUS examinations could not be performed in 50 coronary arteries due to vessel tortuosity (n=15), severe luminal narrowing (n=9), (subtotal) vessel occlusion (n=11) or time constraints (n=15).

Conventional Invasive Coronary Angiography with Gray-Scale IVUS

Data Acquisition and Analysis

Invasive coronary angiography was performed according to the standard protocol.[11] Vascular access was obtained via the femoral artery using the Seldinger technique with a 6 or 7F sheath. During invasive coronary angiography, IVUS examinations were performed in 103 coronary arteries using a dedicated IVUS-console (Volcano Corporation, Rancho, Cordova, CA, USA). After administration of intracoronary nitrates, IVUS runs were acquired using a 20 MHz, 2.9F phases-array IVUS catheter (Eagle Eye, Volcano Corporation, Rancho Cordova, CA, USA) which was positioned in the distal coronary segments. Consecutively, the IVUS catheter was pulled back towards the coronary ostium at a continuous speed of 0.5 mm/s using an automated pullback device. Images were acquired with a frame rate of 15 frames/s. Data sets were stored for offline post-processing analyses. Consecutively, lumen-intima and media-adventitia borders were obtained by dedicated post-processing software as described in the appendix.

Computed Tomography

Data Acquisition and Analysis

Cardiac CT was performed using either a 64-detector row helical scanner (Aquilion 64, Toshiba Medical Systems, Otawara, Japan) or a 320-detector row volumetric scanner (Aquilion ONE, Toshiba Medical Systems, Otawara, Japan). One hour prior to cardiac CT, all patients with an elevated heart rate (≥65 beats/min) were given metoprolol 50 or 100 mg orally, unless contra-indicated. Additionally, patients received sublingual nitroglycerine (0.4 mg/dose, one dose per patient) directly before the CTA examination.

For the 64-detector and 320-detector row CT examination, patients underwent both a non-enhanced and contrast-enhanced scan. Prior to the contrast-enhanced helical scan, a non-enhanced electrocardiographic (ECG)-triggered scan was performed to assess the coronary calcium score. The non-enhanced and contrast-enhanced scans were performed as previously described.[6, 12]

Reconstructed images were transferred to a remote dedicated workstation with post-processing software (Vitrea FX 1.0, Vital Images, Minnetonka, MN, USA). The non-enhanced scans were used to assess the total amount of coronary calcium according to the Agatston approach.[13]

CT angiography data sets were evaluated by an independent and experienced observer, who was blinded to the IVUS data. Prior to the automated quantitative analyses, image quality was evaluated using the following ordinal scale: (1) good image quality, (2) moderate image quality or (3) poor image quality. Data sets with good quality showed no motion artifacts and no image noise, whereas data sets were classified as moderate in case of motion

artifacts or increased image noise. Non-diagnostic scans were classified as data sets with poor image quality. Furthermore, coronary lesions were classified by an independent and blinded observer as either non-calcified (no coronary calcium) or calcium-containing (any presence of coronary calcium) lesions.

Automated quantitative computed tomography angiography (QCT)[14] was performed by an independent observer who was blinded to IVUS data. A dedicated and extended version of the QAngioCT software (QAngioCT 1.1, Medis medical imaging systems, Leiden, the Netherlands) was used to perform quantitative CT analyses. On CT data sets, the dedicated software was able to detect both lumen and vessel wall contours which were used for automated quantitative measurements of coronary plaques, as depicted in Figure 2, upper panel. A detailed description of the lumen and vessel contour detection process is provided in the appendix.

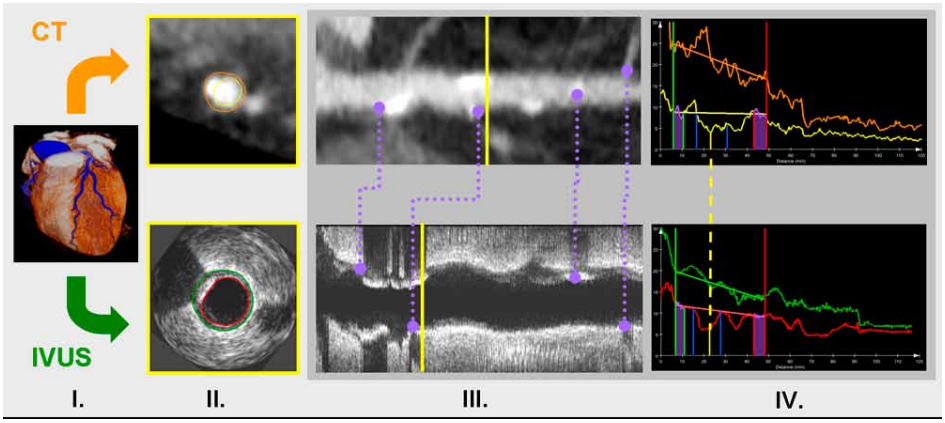

Figure 2. Schematic illustration of automated quantification of coronary plaque on multi-detector row computed tomography (CT) (QCT) in a direct comparison to quantitative intravascular ultrasound (IVUS). QCT was based on several consecutive processing phases. After the 3-D centerline was generated from the CT data set using a fast vessel-tracking algorithm (panel I), automated lumen and vessel wall contour detection was performed for both imaging modalities (panel II). Consecutively, dedicated quantitative software with a unique registration algorithm was used to fuse a complete pullback series of IVUS images with a computed tomography angiography (CTA) volume using true anatomical markers (panel III). Finally, fusion-based quantification of atherosclerotic lesions was based on the lumen and vessel wall contours as well as the corresponding reference lines (estimate of normal tapering of the coronary artery), as shown in panel IV. At the level of the minimal lumen area (MLA) (yellow lines), lumen area, lumen area stenosis, plaque burden and remodeling index could be derived for both imaging techniques. Additionally, the mean plaque burden was derived for the whole coronary lesion, ranging from the proximal to distal lesion marker (blue markers).

Registration and Fusion-based Quantification of Coronary Plaque

Dedicated quantitative software with a unique registration algorithm was developed for automated fusion of a complete pullback series of high-resolution IVUS images with CT angiography.[15] The novel registration algorithm enabled an accurate matching of both imaging modalities along the longitudinal and transversal axis of the coronary arteries. IVUS images were fused on the corresponding slices within the CT data using a two-step 3D fusion process. First, the stack of IVUS images was mapped onto the longitudinal CT image along the centerline of the vessel by locating corresponding anatomical landmarks. The anatomical landmarks (side-branches, coronary ostia, calcified plaques, and overlapping veins) were located and marked within both imaging modalities. Second, the individual IVUS images were translated and rotated until they fit best onto the corresponding cross-sections of the CT image. The fitting procedure was based on the location of the center of the vessel in both images. In addition, the presence of anatomical landmarks (side-branches, calcified spots, and overlapping veins) in each image was used to identify the correct rotation of the IVUS image on top of the CT image. In between anatomical landmarks, IVUS images were aligned to the corresponding locations of the MPR volume of the CT data with the use of interpolation. For this reason, deviations within the motorized pullback speed of the IVUS catheter were corrected.

After both imaging modalities were aligned, fusion-based quantification of coronary lesions was performed using automated detected lumen and vessel wall contours as well as corresponding reference lines (Figure 2). In both modalities, the reference line represented an estimate of the normal proximal-to-distal tapering of the coronary artery. Reference lines were generated from proximal and distal non-diseased reference regions, in which the mean value of these regions was used to define a reference slope for both lumen and vessel wall contours. In the current study, proximal and distal reference regions were not positioned at coronary bifurcations. Importantly, the use of an average reference value results in a reduction of isolated discrepancies between sequential contours.

Per coronary lesion, fusion-based quantification was performed at the level of the minimal lumen area (MLA) and for the whole lesion, ranging from the proximal to distal lesion marker. At first, the level of the MLA and lesion markers was automatically identified within the coronary artery using the detected lumen contours on CT. At the level of the MLA, plaque burden was calculated by the following equation: (vessel wall area – lumen area)/vessel wall area x 100%. Using the same formula, the mean plaque burden was calculated for the whole coronary lesion. The percentage lumen area stenosis (%) was defined at the level of the MLA by: 1-(MLA/corresponding reference lumen area). In addition, at the level of the MLA, the degree of remodeling was calculated as reported previously.[16] Positive remodeling was defined as a remodeling index ≥1.0.[16]

Both MLA and lesion markers were automatically set on the same level within the IVUS run using the dedicated registration algorithm (Figure 2 and 3). Consecutively, the

corresponding plaque variables on IVUS were automatically derived for each coronary lesion using the markers set at precisely the same level as used for cardiac CT.

Reproducibility of QCT for assessment of coronary plaque characteristics was evaluated in 10 randomly selected patients with 25 coronary lesions. To evaluate the reproducibility of QCT, automated lumen and vessel wall contour detection as well as plaque quantification were performed twice by the same observer. Quantification of coronary plaques was based on lesion as well as reference markers which were positioned at a similar level within the coronary artery in both CT data sets.

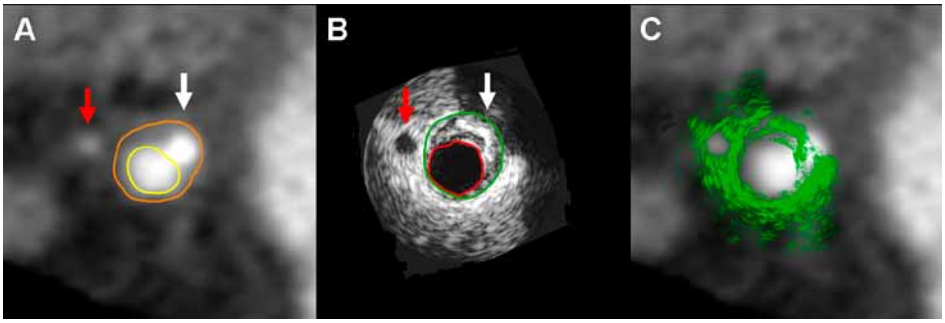

Figure 3. Dedicated quantitative software with a novel registration tool was used to merge a complete pullback IVUS run with a computed tomography angiography (CTA) volume. Fusion of both imaging modalities was based on the identification of true anatomical markers along the coronary artery. In this example, multi-detector row computed tomography (CT) (panel A) was aligned to the corresponding IVUS run (panel B) using a calcified spot (white arrow) and coronary side-branch (red arrow). Consecutively, the IVUS run (green color) was projected on the corresponding CT image (panel C). The IVUS overlay in panel C was color-coded in green to improve the visual appearance of the fusion process.

Statistical Analysis

Continuous data were expressed as mean ± standard deviation, and categorical data are presented as absolute numbers or percentages. Kolmogorov-Smirnov tests were used to evaluate the distribution of the data. When non-normally distributed, data were presented as medians and 25^{th} and 75^{th} percentiles. Comparison of both quantitative techniques was performed using Pearson's linear regression analysis (or spearman's rho correlation) and Bland-Altman analyses (GraphPad Prism software, version 5.01, GraphPad software Inc, San Diego, California, USA). The 95% confidence intervals for the correlations were calculated using Fisher z-transformation.

QCT and IVUS were compared on a lesion and vessel basis, in which lesion-based analysis was based on each coronary lesion, whereas vessel-based analysis was based on the most severe lesion per coronary vessel. Bland-Altman graphs showed the mean value of

differences of each pair plotted against the average value of each pair, in which IVUS was subtracted from the QCT measurements.

In addition, in the lesion-based analysis, comparisons between both quantitative techniques were performed using generalized estimating equations in order to correct for the intra-patient correlation. The difference between QCT and IVUS was calculated for each quantitative parameter (MLA, lumen area stenosis, mean plaque burden, plaque burden at the MLA and remodeling index) and was entered as dependent variable. The 95% confidence intervals for these analyses were calculated.

Furthermore, the accuracy of QCT for assessment of coronary plaque remodeling was assessed using a binary approach (using 1.0 as a cutoff) with IVUS as reference method. For this analysis, corresponding sensitivity, specificity, negative and positive predictive values were calculated. Additionally, the influence of image quality (good, moderate or poor) on the performance of QCT was determined using Pearson's linear regression. Reproducibility of QCT was determined on a lesion basis (25 lesions) using intra-class correlation (ICC) analyses. Excellent agreement was defined as an ICC coefficient of >0.8. All p-values were two-sided and a p-value <0.05 was considered to indicate statistical significance. Statistical analyses were performed with the use of statistical software (SPSS version 16.0, SPSS inc., Chicago, Illinois, USA).

Results

Patient Population

Baseline characteristics of the patient population are described in Table 1. Fifty-one patients (40 men, mean age 58.0±10.6 yrs) who had undergone cardiac CT and invasive coronary angiography with IVUS were enrolled. Patients had undergone either a 320-row volumetric (n=12) or a 64-row helical scan (n=39) to evaluate coronary atherosclerosis non-invasively. In the population consisting of 51 patients, IVUS studies were acquired in 103 coronary arteries in which a total of 146 non-stented coronary lesions were identified on both imaging modalities. The mean heart rate during cardiac CT was 60.9±11.0 bpm. Only the MLA data as derived from QCT and IVUS were non-normally distributed.

Table 1. Baseline characteristics of study population (n=51)

Men	40 (78)
Age (yrs)	58.0±10.6
Calcium score	595±1386
Known CAD	11 (22)
Clinical presentation	
Atypical anginal complaints	31 (61)
Typical anginal complaints	20 (39)
Cardiovascular risk factors	
Diabetes	11 (22)
Systemic hypertension	32 (63)
Hypercholesterolemia	28 (55)
Current smoking	23 (45)
Obesity	8 (16)
Positive family history	15 (29)
Medication	
Beta-blocker	27 (53)
Angiotensin converting enzyme / Angiotensin II blocker	18 (35)
Diuretic	13 (25)
Nitrate	11 (22)
Calcium antagonist	10 (20)

Data are presented as mean ± standard deviation or as number (percentage). CAD = coronary artery disease.

Minimal Lumen Area and Lumen Area Stenosis

On a lesion basis, good correlations were observed between QCT and IVUS for assessment of MLA (n=146, r=0.75, p<0.001) (95% CI 0.67-0.81) (Figure 4A) and lumen area stenosis (n=146, r=0.79, p<0.001) (95% CI 0.72-0.84) (Figure 5A). Lesions with a small MLA showed improved correlations between QCT and IVUS when compared to lesions with a large MLA. Similarly, vessel-based analysis showed good correlation between both quantitative techniques for assessment of MLA (n=103, r=0.73, p<0.001) (95% CI 0.63-0.81) and lumen area stenosis (n=103, r=0.82, p<0.001) (95% CI 0.75-0.88).

On a lesion basis, the mean bias between techniques for quantification of MLA was -3.0 mm^2 with 95% limits of agreement ranging from -7.5 to 1.4 mm^2 (Figure 4B). QCT significantly underestimated the MLA when compared to IVUS (3.6 mm^2 [2.3 - 5.0] vs. 6.4 mm^2 [4.3 - 9.3]; 95% CI of the mean difference was -3.4 to -2.5; p<0.001).

On a lesion basis, the mean bias was 9.8% for lumen area stenosis with 95% limits of agreement ranging from -13.9% to 33.6% (Figure 5B). The lumen area stenosis was significantly overestimated by QCT as compared to IVUS (44.4±19.6% vs. 34.6±17.8%; 95% CI of the mean difference 7.9 to 11.7; p<0.001).

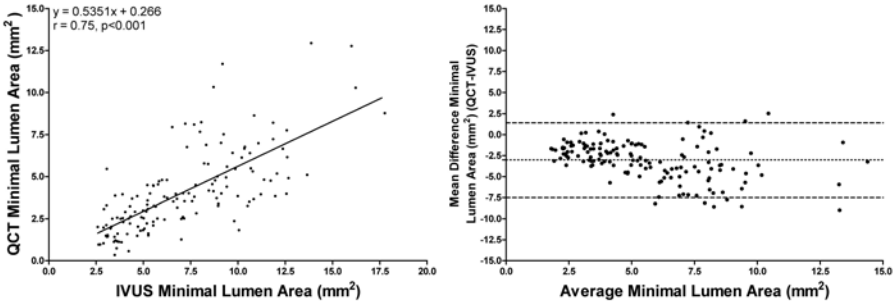

Figure 4. Quantitative computed tomography (QCT) was compared to quantitative coronary ultrasound (IVUS) for assessment of minimal lumen area (MLA). Linear regression (panel A) and Bland-Altman analyses (panel B) for MLA on a lesion basis (n=146). The mean value of differences ± standard deviation was -3.0±2.3 mm^2 with 95% limits of agreement ranging from -7.5 to 1.4 mm^2.

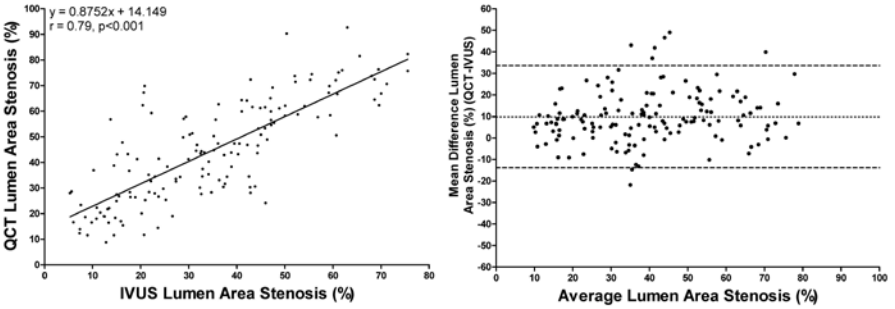

Figure 5. Quantitative computed tomography (QCT) was compared to quantitative coronary ultrasound (IVUS) for assessment of percentage lumen area stenosis. Linear regression (panel A) and Bland-Altman analyses (panel B) for percentage lumen area stenosis on a lesion basis (n=146). The mean value of differences ± standard deviation was 9.8±12.1% with 95% limits of agreement ranging from -13.9 to 33.6%.

Coronary Plaque Burden

Mean plaque burden (n=146, r=0.64, p<0.001) (95% CI 0.53-0.73) showed a good correlation between QCT and IVUS on a lesion basis. On a vessel basis, QCT was correlated to IVUS for the assessment of mean plaque burden (n=103, r=0.62, p<0.001) (95% CI 0.49-0.73). Bland-Altman analyses showed a mean bias for mean plaque burden of 12.3% with 95% limits of agreement ranging from -13.8 to 38.5%. Based on linear mixed models, the mean plaque burden was significantly overestimated with QCT as compared to IVUS (61.1±16.1% vs. 48.8±15.4%; 95% CI of the mean difference 14.8 - 19.6; p<0.001).

For plaque burden at the MLA, good correlations were found between QCT and IVUS on a lesion (n=146, r=0.70, p<0.001) (95% CI 0.61-0.77) and vessel (n=103, r=0.68, p<0.001) (95% CI 0.56-0.77) basis. For plaque burden at the MLA, Bland-Altman analyses

showed mean bias of 17.2%, with 95% limits of agreement extending from -9.1 to 43.6%. Plaque burden at the MLA was significantly overestimated with QCT as compared to IVUS (69.4±17.7% vs. 52.1±16.8%; 95% CI of the mean difference 9.7 - 15.0; p<0.001) on a lesion basis.

Remodeling Index

On a lesion basis, a significant correlation was observed between QCT and IVUS for assessment of remodeling index (n=146, r=0.56, p<0.001) (95% CI 0.44-0.66). Both quantitative approaches showed an improved correlation on a vessel basis (n=103, r=0.58, p<0.001) (95% CI 0.44-0.70). Bland-Altman analyses showed a mean bias of 0.05 with 95% limits of agreement ranging from -0.30 to 0.40. There was a trend towards overestimation of remodeling index by QCT as compared to IVUS with linear regression mixed models (0.94±0.21 vs. 0.90±0.14; 95% CI of the mean difference 0.01 - 0.08; p=0.005).

Additionally, the accuracy of QCT for assessment of coronary plaque remodeling was calculated using a binary approach on a vessel basis. In total, 20 coronary arteries showed positive remodeling on IVUS, of which 15 were classified similarly on QCT, yielding a sensitivity of 75% (95% CI 0.51-0.90). Of the 83 coronary vessels with negative plaque remodeling on IVUS, 66 were scored appropriately on QCT (specificity of 80%, 95% CI 0.69-0.87). Furthermore, the negative and positive predictive values were 93% (95% CI 0.85-0.97) and 47% (95% CI 0.31-0.64), respectively. Importantly, using IVUS as a reference method, the overall accuracy of QCT for assessment of plaque remodeling was modest (79%).

Influence of Image Quality on Automated Quantification

A sub-analysis was performed to evaluate the influence of image quality on the performance of QCT (Table 2). The image quality of CT data sets was classified as either good (n=49), moderate (n=63) or poor (n=34). For the MLA, good correlations between both quantitative approaches were observed for data sets with good (r=0.81, p<0.001) (95% CI 0.69-0.89) or moderate (r=0.75, p<0.001) (95% CI 0.62-0.84) quality, whereas they showed a moderate correlation for data sets with poor (r=0.68, p<0.001) (95% CI 0.44-0.83) quality. For the assessment of lumen area stenosis, QCT showed a slightly improved correlation with IVUS for data sets with good (r=0.84, p<0.001) (95% CI 0.73-0.91) and moderate (r=0.79, p<0.001) (95% CI 0.67-0.87) quality when compared to data sets with poor (r=0.78, p<0.001) (95% CI 0.60-0.89) image quality. Mean plaque burden showed a decreased correlation in data sets with suboptimal quality; good quality (r=0.70, p<0.001) (95% CI 0.52-0.82), moderate quality (r=0.65, p<0.001) (95% CI 0.48-0.77) and poor quality (r=0.60, p<0.001) (95% CI 0.32-0.78). However, the influence of image quality for the assessment of plaque burden at the MLA was minimal; IVUS and QCT were well-correlated for data sets with good (r=0.70, p<0.001) (95% CI 0.52-0.82), moderate (r=0.71, p<0.001) (95% CI 0.56-0.81) or poor

(r=0.68, p<0.001) (95% CI 0.44-0.83) image quality. Additionally, image quality showed no effect on the assessment of plaque remodeling. Remodeling index showed significant but moderate correlations for data sets with good (r=0.42, p=0.002) (95% CI 0.16-0.63), moderate (r=0.62, p<0.001) (95% CI 0.44-0.75) and poor (r=0.55, p<0.001) (95% CI 0.26-0.75) quality.

Table 2. Influence of image quality on automated quantification of coronary plaque characteristics using quantitative computed tomography (QCT) in a direct comparison with quantitative coronary ultrasound (IVUS). QCT and IVUS were compared on a lesion basis for data sets with good (n=49), moderate (n=63) or poor (n=34) image quality. For each comparison the corresponding Pearson's regression coefficients are shown.

	Good quality (n=49)	Moderate quality (n=63)	Poor quality (n=34)
MLA (mm^2)	0.81	0.75	0.68
Lumen area stenosis (%)	0.84	0.79	0.78
Mean plaque burden (%)	0.70	0.65	0.60
Plaque burden MLA (%)	0.70	0.71	0.68
Remodeling index	0.42	0.62	0.55

MLA = minimal lumen area. All correlations showed a p<0.05.

Influence of Coronary Calcium

Coronary lesions were classified as either non-calcified (lesions with no coronary calcium) or calcium-containing (any presence of coronary calcium) lesions. Of the 146 coronary lesions, 76 (52%) lesions were classified as calcium-containing lesions, whereas the remaining 70 (48%) lesions were classified as non-calcified lesions. The correlation between QCT and IVUS was similar between non-calcified and calcium-containing lesions for assessment of MLA (r=0.70, 95% CI 0.56-0.80; r=0.73, 95% CI 0.60-0.82) and lumen area stenosis (r=0.77, 95% CI 0.65-0.85; r=0.75, 95% CI 0.63-0.83; both p<0.001).

Furthermore, as compared to IVUS, QCT showed a smaller underestimation of MLA in calcium-containing lesions than in non-calcified lesions, as reflected by mean value of differences of -2.9±2.2 mm^2 and -3.1±2.3 mm^2, respectively. In addition, the overestimation of lumen area stenosis on CT was higher in calcium-containing lesions than in non-calcified lesions (mean value of differences of 12.0±12.8% and 7.4±11.0%, respectively).

Accordingly, no substantial differences in coronary plaque quantification were observed between QCT and IVUS, except for a small overestimation of lumen area stenosis by QCT in calcium-containing lesions.

Reproducibility of Quantitative Computed Tomography

Reproducibility of QCT for coronary plaque quantification was evaluated in 10 randomly selected patients with 25 coronary lesions. On a lesion basis, QCT showed a good reproducibility for assessment of MLA (ICC 0.91, 95% CI 0.78-0.96) and lumen area stenosis (ICC 0.86, 95% CI 0.37-0.95). Furthermore, on a lesion basis, QCT was reproducible for the assessment of mean plaque burden (ICC 0.88, 95% CI 0.74-0.95) as well as plaque burden at the MLA (ICC 0.92, 95% CI 0.78-0.96). Finally, the quantification of plaque remodeling showed good reproducibility with QCT, as reflected by an ICC of 0.84 (95% CI 0.63-0.93).

Discussion

The current study is the first study that has demonstrated the feasibility of automated quantification of coronary plaque on cardiac CT using dedicated quantitative software with a novel 3D registration algorithm of CT and IVUS datasets.

Automated quantitative CT and IVUS were well-correlated for the assessment of MLA, lumen area stenosis and plaque burden on a vessel- and lesion basis. Coronary plaque remodeling showed a significant but moderate correlation between quantitative CT and IVUS on a vessel- and lesion basis. When using a binary approach, the accuracy of QCT for assessment of coronary plaque remodeling was fair. Finally, MLA was significantly underestimated by QCT when compared to IVUS, whereas lumen area stenosis was significantly overestimated by QCT in comparison with IVUS.

Non-invasive imaging of coronary atherosclerosis with the use of cardiac CT provides important information for patient diagnosis, evaluation of therapeutic options as well as for risk stratification of patients for potential adverse cardiovascular events.[1-3] Rapid developments in CT technology have led to an improvement in image quality and diagnostic accuracy for detection of coronary atherosclerosis.[1-3] Despite its advances, one of the current drawbacks of cardiac CT is the fact that evaluation of coronary atherosclerosis is most commonly based on a visual approach, which is observer dependent and requires substantial reading experience. A fully automated approach to quantify plaque characteristics would be preferred to further improve the diagnostic accuracy and reproducibility of cardiac CT. Moreover, automated quantification could potentially decrease the amount of post-processing time required for cardiac CT. Accordingly, substantial effort has been invested in the development of quantitative strategies for CT.[6-9, 17-19]

Thus far, quantitative studies have used manually-based or semi-automated algorithms for detection of lumen and vessel wall contours, rather than dedicated automated algorithms for contour detection. Furthermore, previous studies were hampered since comparisons between cardiac imaging techniques were based on visual assessment of coronary plaques as well as manual fusion of imaging modalities. The current study is the first study that allows

comparison of cardiac CT and IVUS using a novel dedicated quantitative algorithm, which allows automated detection of both lumen and outer vessel wall from CT data sets fused with IVUS data along its longitudinal and transversal axis. Additionally, the currently applied novel 3D registration algorithm represents a unique fusion imaging technique as it allows comparison between cardiac imaging techniques using a slice-by-slice comparison of each location along the transversal axis of the coronary arteries in both CT and IVUS images. The novel 3D registration algorithm allows improved detection of various (anatomical) landmarks in both longitudinal and transversal axis of the coronary arteries, which are used to obtain an accurate fusion between imaging modalities, and as a consequence, improved quantification of coronary plaque. Accordingly, a detailed fusion-based imaging view is available, which permits a simultaneous quantification of the entire segmented coronary artery in both CT and IVUS.

At present, only a limited number of studies have aimed to quantify lumen area or lumen area stenosis using cardiac CT with variable results.[8, 18, 20, 21] Leber et al.[8] have evaluated the performance of cardiac CT for quantification of coronary lesions in 55 patients with stable CAD, of whom 18 patients underwent IVUS. Quantification of lumen area and lumen area stenosis was performed on cross sectional reconstructions derived from cardiac CT images. Even though lumen area showed a good correlation with IVUS ($r=0.81$, $p<0.01$), lumen area stenosis showed only a modest correlation between quantitative CT and IVUS ($r=0.61$, $p<0.05$). Another study from Joshi et al.[18] has shown a modest correlation between IVUS and quantitative CT for assessment of lumen area ($r^2=0.41$, $p<0.05$) in 48 patients with 67 coronary lesions. Accordingly, previous investigations which aimed to quantify lumen area stenosis or lumen area on cardiac CT have shown a large variability. One of the potential explanations may be the fact that in these studies most often semi-manual approaches were used, rather than dedicated quantitative algorithms. Moreover, a visual approach to match coronary lesions identified on CT with IVUS was used, which may have led to an inaccurate alignment of coronary plaques on both imaging modalities. In the current study however, a novel registration algorithm was used permitting an accurate matching of lesions on both imaging modalities along the longitudinal and transversal axis of the coronary arteries. After both imaging modalities were aligned using true anatomical markers, fusion-based quantification showed a good correlation between CT and IVUS for MLA ($r=0.75$, $p<0.001$) and lumen area stenosis ($r=0.79$, $p<0.001$). Moreover, the quantification process itself was performed with the use of automated dedicated CT software, which represents a more robust approach for coronary plaque quantification as compared to manually-based or semi-automated approaches. Furthermore, Bland-Altman analysis showed an underestimation of MLA (and overestimation of lumen area stenosis) as assessed with QCT when compared to IVUS. These findings may be related to the quantification of high-degree, heavily calcified lesions. In addition, QCT and IVUS showed a better correlation for lesions with a small MLA

than lesions with a large MLA. This could be explained by the calculation of lumen areas, in which small changes in radius can result in considerable changes in MLA for a large radius.

Beyond coronary luminography, cardiac CT provides information on plaque burden and the degree of plaque remodeling.[3, 9] Previous studies have shown a good correlation between cardiac CT and IVUS for assessment of plaque volume. In these studies, the overall plaque volume was significantly underestimated with CT as compared to IVUS.[9, 22] Although the current study showed a good correlation for assessment of plaque burden with quantitative CT, a significant overestimation of plaque burden with cardiac CT was observed when compared to IVUS. The differences in study findings may be explained by the fact that the current population consisted of patients with advanced and heavily calcified lesions, which may have led to an overestimation of plaque burden with CT as compared to IVUS. In line with the current study, Bruining et al.[19] have shown a significant overestimation of plaque volume with quantitative CT as compared to IVUS (222±121 mm^3 vs.189±93 mm^3, $p<0.05$). The study by Bruining et al.[19] have used a quantitative CT approach with limited manual interference to assess plaque volume. In 48 patients with clinical symptoms of CAD, a semi-automated vessel extraction software was used to derive the region of interest, in which lumen contours were detected with an automated edge-detection method. However, it is important to note that Bruining et al.[19] have used manually drawn vessel wall contours, rather than automated detected vessel wall contours. Furthermore, in the study by Bruining et al.[19], the investigators were allowed to alter the window and level image settings during the quantification process, whereas the automated processing steps in the current study were independent from standard viewing settings. Accordingly, even though a significant overestimation of lumen area stenosis, mean plaque burden, plaque burden at the MLA and remodeling index on CT was observed, the present study showed that coronary plaque quantification using an automated approach was highly reproducible, as indicated by a high intra-class correlation value for assessment of MLA, lumen area stenosis, mean plaque burden, plaque burden at the MLA and remodeling index. This may represent an important advantage over previous quantification methods.[9, 23]

In addition, a sub-analysis was performed to determine the influence of image quality on the performance of automated quantitative CT. Although quantitative CT showed a slightly decreased performance in data sets with poor image quality for assessment of MLA and lumen area stenosis, no significant influence of image quality was observed for the quantification of plaque burden and remodeling index. Accordingly, these findings show the feasibility of automated quantification of coronary plaques in data sets with different image quality.

Finally, the study has evaluated the influence of coronary calcium on the accuracy of atherosclerotic plaque quantification using QCT. In line with previous observations[21], the current study has shown that calcium-containing lesions showed a larger overestimation of lumen area stenosis when compared to non-calcified lesions. Although small differences

between non-calcified and calcium-containing lesions were observed, the current study has demonstrated that overall the QCT algorithm performed equally well in non-calcified and calcium-containing lesions.

Study Limitations and Clinical Perspectives

Some limitations need to be considered. In the current study, automated quantitative CT was only applied to non-stented coronary segments, whereas segments with coronary stents were excluded. Although a sub-analysis on stented segments would have provided additional information, the current study was only designed to demonstrate the feasibility of QCT for evaluation of coronary plaque. Moreover, IVUS was only performed in 103 (67%) coronary arteries as it could not be performed in 50 (33%) coronary arteries due to vessel tortuosity, severe luminal narrowing, (subtotal) vessel occlusion or severe time constraints.

In addition, even though both quantitative techniques showed good correlations for coronary plaque characteristics, a significant bias for quantitative plaque parameters was observed. However, the bias between both quantitative imaging modalities was consistent as indicated by a high intra-class correlation coefficient in the reproducibility analyses for assessment of MLA, lumen area stenosis, mean plaque burden, plaque burden at the MLA as well as remodeling index. Accordingly, the study showed the feasibility of QCT for automated coronary plaque quantification. Furthermore, the study showed only a moderate correlation between CT and IVUS for assessment of coronary plaque remodeling. However, when using a binary approach, the study showed a modest accuracy of QCT for assessment of plaque remodeling, indicating that quantitative CT allows assessment of coronary plaque remodeling. This is an important finding as outward remodeling of coronary lesions, which is commonly referred to as positive remodeling, represents one of the plaque characteristics that has been associated with an increased risk for plaque rupture and acute coronary syndromes.[5, 24] Finally, although QCT was reproducible for assessment of coronary plaque parameters, reproducibility was only tested in a limited number of patients.

In addition, the influence of coronary calcium on the accuracy of QCT has been evaluated in the current analysis. The study has demonstrated that QCT performed equally well in non-calcified and calcium-containing lesions when compared to IVUS. Although both techniques can be used for assessment of coronary calcium, IVUS represents a more accurate technique due to its superior spatial and temporal resolution. However, despite these potentials, IVUS studies are usually performed in only a limited number of patients (patients with a high likelihood of having a significant stenosis) due to the invasive nature of the technique. In contrast, cardiac CT allows non-invasive evaluation of plaque morphology in a wide variety of patients, predominantly patients with a low (or intermediate) pre-test likelihood of CAD and an early stage of CAD. One of limitations of cardiac CT remains its relatively low positive predictive value which may be caused by the overestimation of heavily calcified

lesions due to blooming artifacts. In the current study, the use of an automated quantitative algorithm may have resulted in only a small overestimation of calcium-containing lesions.

Conclusions

The current study demonstrated the feasibility of automated quantification of coronary plaque on cardiac CT using dedicated quantitative software with a novel 3D registration algorithm of CT and IVUS datasets. Both quantitative CT and IVUS showed good correlations for automated assessment of MLA, lumen area stenosis and plaque burden. Finally, even though QCT showed underestimation of MLA and overestimation of lumen area stenosis along with plaque burden, QCT was reproducible for quantification of MLA, lumen area stenosis, mean plaque burden, plaque burden at the MLA and remodeling index.

Appendix

IVUS

Lumen and Vessel Wall Contour Detection

Coronary plaque characteristics were evaluated on IVUS data sets by an independent and blinded observer using offline dedicated post-processing software (IVUS CMS 4.0, Medis Medical Imaging Systems, Leiden, the Netherlands). Along the full length of the IVUS run, lumen-intima and media-adventitia interface were identified in longitudinal and transversal views by an automatic contour detection algorithm. A limited number of individual cross-sectional frames were manually adapted to optimize lumen and vessel wall contour detection. IVUS contour detection was performed independently from the contour detection derived from CT.

Computed Tomography

Lumen and Vessel Wall Contour Detection

On cardiac CT data sets, the dedicated software was able to detect both lumen and vessel wall contours which were used for automated quantitative measurements of coronary plaques, as depicted in Figure 1, upper panel. At first, a fast vessel-tracking algorithm was used to obtain the 3-dimensional centerline (ranging from the proximal to distal marker) of each coronary artery. This vessel-tracking step consists of: (1) a pre-segmentation of the vessel between the proximal and distal point and (2) a fast path backtracking from distal

to the proximal point through the center of the segmentation. Based on this centerline, a stretched multi-planar reformatted (MPR) volume was created of the segment of interest. MPR volumes allow the analysis of curved coronary arteries as straight vessels. Next, four longitudinal cross-sections were extracted from the MPR volume at 45 degrees angular intervals. Subsequently, lumen borders in these four longitudinal images were detected by a model guided minimum cost approach (MCA). The MCA method uses a combination of spatial first-, and second-derivative gradient filters in combination with knowledge of the expected CT intensity values in the arteries. Therefore, the MCA method is not sensitive to differences in attenuation values between different data sets. The longitudinal detection allows a smooth interpolation between the proximal and distal sites of coronary bifurcations. The MCA with a circular lumen model was used to detect the lumen border contours in each transversal slice of the MPR volume. In this step, the intersection points of each transversal slice with the earlier obtained longitudinal contours were used to guide the contour detection.

Additionally, the vessel wall borders were detected in these longitudinal images by a similar MCA with a different model. The applied model was based on several pre-defined constraints concerning the location of longitudinal vessel wall contours; contours were positioned outside the detected longitudinal lumen contours and the regions with high intensity values (e.g. calcified regions) were included according to a relative weighting scheme. Consecutively, transversal vessel wall contours were fitted on the transversal slices using the intersection of the longitudinal contours with each slice as attraction point. These automated processing steps were independent from the standard viewing settings (window level 1024, width 0).

Reference List

(1) Hoffmann MH, Shi H, Schmitz BL, Schmid FT, Lieberknecht M, Schulze R, Ludwig B, Kroschel U, Jahnke N, Haerer W, Brambs HJ, Aschoff AJ. Noninvasive coronary angiography with multislice computed tomography. JAMA 2005;293:2471-2478.

(2) Miller JM, Rochitte CE, Dewey M, rbab-Zadeh A, Niinuma H, Gottlieb I, Paul N, Clouse ME, Shapiro EP, Hoe J, Lardo AC, Bush DE, de Roos A, Cox C, Brinker J, Lima JA. Diagnostic performance of coronary angiography by 64-row CT. N Engl J Med 2008;359:2324-2336.

(3) Mark DB, Berman DS, Budoff MJ, Carr JJ, Gerber TC, Hecht HS, Hlatky MA, Hodgson JM, Lauer MS, Miller JM, Morin RL, Mukherjee D, Poon M, Rubin GD, Schwartz RS. ACCF/ACR/AHA/NASCI/SAIP/SCAI/SCCT 2010 expert consensus document on coronary computed tomographic angiography: a report of the American College of Cardiology Foundation Task Force on Expert Consensus Documents. Circulation 2010;121:2509-2543.

(4) Virmani R, Burke AP, Farb A, Kolodgie FD. Pathology of the vulnerable plaque. J Am Coll Cardiol 2006;47:C13-C18.

(5) Motoyama S, Kondo T, Sarai M, Sugiura A, Harigaya H, Sato T, Inoue K, Okumura M, Ishii J, Anno H, Virmani R, Ozaki Y, Hishida H, Narula J. Multislice computed tomographic characteristics of coronary lesions in acute coronary syndromes. J Am Coll Cardiol 2007;50:319-326.

(6) Boogers MJ, Schuijf JD, Kitslaar PH, van Werkhoven JM, de Graaf FR, Boersma E, van Velzen JE, Dijkstra J, Adame IM, Kroft LJ, de Roos A, Schreur JHM, Heijenbrok MW, Jukema JW, Reiber JHC, Bax JJ. Novel Dedicated Approach for Automated Quantification of Stenosis Severity on 64-Slice Multi-slice Computed Tomography: A Comparison with Quantitative Coronary Angiography. JACC Cardiovasc Imaging 2010;3:699-709.

(7) Korosoglou G, Mueller D, Lehrke S, Steen H, Hosch W, Heye T, Kauczor HU, Giannitsis E, Katus HA. Quantitative assessment of stenosis severity and atherosclerotic plaque composition using 256-slice computed tomography. Eur Radiol 2010;20:1841-1850.

(8) Leber AW, Knez A, von Ziegler F, Becker A, Nikolaou K, Paul S, Wintersperger B, Reiser M, Becker CR, Steinbeck G, Boekstegers P. Quantification of obstructive and nonobstructive coronary lesions by 64-slice computed tomography: a comparative study with quantitative coronary angiography and intravascular ultrasound. J Am Coll Cardiol 2005;46:147-154.

(9) Leber AW, Becker A, Knez A, von Ziegler F, Sirol M, Nikolaou K, Ohnesorge B, Fayad ZA, Becker CR, Reiser M, Steinbeck G, Boekstegers P. Accuracy of 64-slice computed tomography to classify and quantify plaque volumes in the proximal coronary system: a comparative study using intravascular ultrasound. J Am Coll Cardiol 2006;47:672-677.

(10) Achenbach S, Ropers D, Hoffmann U, MacNeill B, Baum U, Pohle K, Brady TJ, Pomerantsev E, Ludwig J, Flachskampf FA, Wicky S, Jang IK, Daniel WG. Assessment of coronary remodeling in stenotic and nonstenotic coronary atherosclerotic lesions by multidetector spiral computed tomography. J Am Coll Cardiol 2004;43:842-847.

(11) Scanlon PJ, Faxon DP, Audet AM, Carabello B, Dehmer GJ, Eagle KA, Legako RD, Leon DF, Murray JA, Nissen SE, Pepine CJ, Watson RM, Ritchie JL, Gibbons RJ, Cheitlin MD, Gardner TJ, Garson A, Jr., Russell RO, Jr., Ryan TJ, Smith SC, Jr. ACC/AHA guidelines for coronary angiography. A report of the American College of Cardiology/American Heart Association Task Force on practice guidelines (Committee on Coronary Angiography). Developed in collaboration with the Society for Cardiac Angiography and Interventions. J Am Coll Cardiol 1999;33:1756-1824.

(12) de Graaf FR, Schuijf JD, van Velzen JE, Kroft LJ, de Roos A, Reiber JH, Boersma E, Schalij MJ, Spano F, Jukema JW, van der Wall EE, Bax JJ. Diagnostic accuracy of 320-row multidetector computed tomography coronary angiography in the non-invasive evaluation of significant coronary artery disease. Eur Heart J 2010;31:1908-1915.

(13) Agatston AS, Janowitz WR, Hildner FJ, Zusmer NR, Viamonte M, Jr., Detrano R. Quantification of coronary artery calcium using ultrafast computed tomography. J Am Coll Cardiol 1990;15:827-832.

(14) Marquering HA, Dijkstra J, de Koning PJ, Stoel BC, Reiber JH. Towards quantitative analysis of coronary CTA. Int J Cardiovasc Imaging 2005;21:73-84.
(15) Marquering HA, Dijkstra J, Besnehard QJA, Duthé JPM, Schuijf JD, Bax JJ, Reiber JHC. Coronary CT angiography: IVUS image fusion for quantitative plaque and stenosis analyses. Medical Imaging: Visualization, Image-guided Procedures, and Modeling 2008;6918:1G1-1G10.
(16) Mintz GS, Nissen SE, Anderson WD, Bailey SR, Erbel R, Fitzgerald PJ, Pinto FJ, Rosenfield K, Siegel RJ, Tuzcu EM, Yock PG. American College of Cardiology Clinical Expert Consensus Document on Standards for Acquisition, Measurement and Reporting of Intravascular Ultrasound Studies (IVUS). A report of the American College of Cardiology Task Force on Clinical Expert Consensus Documents. J Am Coll Cardiol 2001;37:1478-1492.
(17) Pohle K, Achenbach S, MacNeill B, Ropers D, Ferencik M, Moselewski F, Hoffmann U, Brady TJ, Jang IK, Daniel WG. Characterization of non-calcified coronary atherosclerotic plaque by multi-detector row CT: comparison to IVUS. Atherosclerosis 2007;190:174-180.
(18) Joshi SB, Okabe T, Roswell RO, Weissman G, Lopez CF, Lindsay J, Pichard AD, Weissman NJ, Waksman R, Weigold WG. Accuracy of computed tomographic angiography for stenosis quantification using quantitative coronary angiography or intravascular ultrasound as the gold standard. Am J Cardiol 2009;104:1047-1051.
(19) Bruining N, Roelandt JR, Palumbo A, La Grutta L, Cademartiri F, de Feijter PJ, Mollet N, van Domburg RT, Serruys PW, Hamers R. Reproducible coronary plaque quantification by multislice computed tomography. Catheter Cardiovasc Interv 2007;69:857-865.
(20) Caussin C, Larchez C, Ghostine S, Pesenti-Rossi D, Daoud B, Habis M, Sigal-Cinqualbre A, Perrier E, Angel CY, Lancelin B, Paul JF. Comparison of coronary minimal lumen area quantification by sixty-four-slice computed tomography versus intravascular ultrasound for intermediate stenosis. Am J Cardiol 2006;98:871-876.
(21) Hur J, Kim YJ, Lee HJ, Nam JE, Choe KO, Seo JS, Choi DH, Kim JS, Choi BW. Quantification and characterization of obstructive coronary plaques using 64-slice computed tomography: a comparison with intravascular ultrasound. J Comput Assist Tomogr 2009;33:186-192.
(22) Schepis T, Marwan M, Pflederer T, Seltmann M, Ropers D, Daniel WG, Achenbach S. Quantification of non-calcified coronary atherosclerotic plaques with dual-source computed tomography: comparison with intravascular ultrasound. Heart 2009;96:610-615.
(23) Otsuka M, Bruining N, Van Pelt NC, Mollet NR, Ligthart JM, Vourvouri E, Hamers R, De Jaegere P, Wijns W, van Domburg RT, Stone GW, Veldhof S, Verheye S, Dudek D, Serruys PW, Krestin GP, de Feyter PJ. Quantification of coronary plaque by 64-slice computed tomography: a comparison with quantitative intracoronary ultrasound. Invest Radiol 2008;43:314-321.
(24) Schoenhagen P, Ziada KM, Kapadia SR, Crowe TD, Nissen SE, Tuzcu EM. Extent and direction of arterial remodeling in stable versus unstable coronary syndromes : an intravascular ultrasound study. Circulation 2000;101:598-603.

Chapter **5**

Feasibility of Diastolic Function Assessment with Cardiac CT: Feasibility Study in Comparison with Tissue Doppler Imaging

Mark J. Boogers, MD[1,2]; Jacob M. van Werkhoven, MSc[1,2]; Joanne D. Schuijf, PhD[1]; Victoria Delgado, MD[1]; Heba M. El-Naggar, MD[1]; Eric Boersma, PhD[3], Gaetano Nucifora, MD[1]; Rob J. van der Geest, MSc[4,5]; Bernard P. Paelinck, MD, PhD[6], Lucia J. Kroft, MD, PhD[4]; Johan H.C. Reiber, PhD[4,5]; Albert de Roos, MD, PhD[4]; Jeroen J. Bax, MD, PhD[1]; Hildo J. Lamb, MD, MSc, PhD[4]

[1]Department of Cardiology, Leiden University Medical Center, Leiden, the Netherlands; [2]The Interuniversity Cardiology Institute of the Netherlands, Utrecht, the Netherlands; [3]Department of Epidemiology and Statistics, Erasmus University, Rotterdam, the Netherlands; [4]Department of Radiology, Leiden University Medical Center, Leiden, the Netherlands; [5]Department of Radiology, Division of Image Processing, Leiden University Medical Center, Leiden, the Netherlands; [6]Department of Cardiology, Antwerp University Hospital.

Abstract

Objectives This study aimed to demonstrate the feasibility of multidetector row computed tomography (CT) for assessment of diastolic function in comparison with 2-dimensional (2D) echocardiography using tissue Doppler imaging (TDI).

Background Diastolic left ventricular (LV) function plays an important role in patients with cardiovascular disease. Currently, 2D echocardiography using TDI has been used most commonly to evaluate diastolic LV function. Although the role of cardiac CT for evaluation of coronary atherosclerosis has been explored extensively, its feasibility to evaluate diastolic function has not been studied.

Methods Patients who had undergone 64-multidetector row CT and 2D echocardiography with TDI were enrolled. Diastolic function was evaluated using early (E) and late (A) transmitral peak velocity (cm/s) and peak mitral septal tissue velocity (Ea) (cm/s). Peak transmitral velocity (cm/s) was calculated by dividing peak diastolic transmitral flow (mL/s) by the corresponding mitral valve area (cm^2). Mitral septal tissue velocity was calculated from changes in LV length per cardiac phase. Subsequently, the estimation of LV filling pressures (E/Ea) was determined.

Results Seventy patients (46 men, mean age 55±11 years) who had undergone cardiac CT and 2D echocardiography with TDI were included. Good correlations were observed between cardiac CT and 2D echocardiography for assessment of E ($r=0.73$, $p<0.01$), E/A ($r=0.87$, $p<0.01$), Ea ($r=0.82$, $p<0.01$) and E/Ea ($r=0.81$, $p<0.01$). Moreover, a good diagnostic accuracy (79%) was found for detection of diastolic dysfunction using cardiac CT. Finally, the study showed a low intra- and interobserver variability for assessment of diastolic function on cardiac CT.

Conclusions Cardiac CT showed good correlations for transmitral velocity, mitral septal tissue velocity and the estimation of LV filling pressures when compared to 2D echocardiography. Additionally, cardiac CT and 2D echocardiography were comparable for assessment of diastolic dysfunction. Accordingly, cardiac CT may provide information on diastolic dysfunction.

Introduction

Diastolic left ventricular (LV) function plays an important role in the evaluation of clinical symptoms, therapeutic options and prognosis in patients with cardiovascular disease.[1, 2] More specifically, it has been shown that diastolic dysfunction represents an important pathological condition in patients with coronary artery disease (CAD).[3, 4]

Currently, Doppler echocardiography is the most commonly used imaging technique for evaluation of diastolic function.[5-10] For the evaluation of diastolic function, transmitral velocity has been used frequently as a non-invasive alternative to directly measured LV filling pressures.[5, 7] However, it is important to note that several confounding factors may influence transmitral velocity and consequently transmitral velocity alone may not be the best marker for diastolic LV dysfunction.[6, 7, 11] Combined assessment of early peak transmitral velocity and early peak mitral septal tissue velocity may be more accurate for the evaluation of diastolic LV function, predominantly in patients with depressed or increased LV filling pressures.[6, 10, 11]

Cardiac computed tomography (CT) has emerged as a potent non-invasive imaging modality for the evaluation of coronary atherosclerosis.[12, 13] In specific subsets of patients, multiphase CT may be indicated to ensure diagnostic image quality for visualization of the coronary arteries. Thus far, multiphase CT studies have been restricted to LV systolic function analysis[14], and no information is available on the feasibility of cardiac CT to assess diastolic LV function. Accordingly, the present study aimed to evaluate the feasibility of cardiac CT for assessment of diastolic function in a direct comparison with 2D echocardiography using TDI.

Methods

Patient Population, Study Design

Seventy consecutive patients who had been referred for 64-CT imaging were retrospectively selected from our clinical registry. Cardiac CT was performed to evaluate known or established CAD, and 2D echocardiography with TDI was performed to evaluate therapeutic options. Both examinations had been performed sequentially, in random order. Known CAD was defined as previous myocardial infarction, revascularization or evidence of CAD on previous diagnostic tests. Patients without evidence of CAD on previous diagnostic tests were suspected to have CAD (and therefore referred for CT angiography). Patients were derived from our ongoing clinical registry if they met the following selection criteria: (1) presence of multiphase cardiac CT (information acquired of the entire cardiac cycle), (2) availability of multiphase CT and 2D echocardiography with TDI within 3 months, (3) diagnostic image

quality of multiphase CT and 2D echocardiography with TDI, (4) sinus rhythm and (5) absence of valvulopathy (aortic or mitral valvulopathy, grade ≥I). Additionally, patients with unstable angina pectoris or acute coronary syndrome were excluded from further analysis. Our Institutional Review Board does not require its approval for retrospective technical analysis of clinically obtained data, as was the case in this study.

Cardiac CT - Data Acquisition and Analysis

Multidetector row CT (MDCT) was performed with a 64-slice CT scanner (Aquilion 64, Toshiba Medical Systems, Otawara, Japan). Prior to MDCT, patients were monitored for blood pressure and heart rate. Patients with a heart rate ≥65 beats/min were given metoprolol 50 or 100 mg orally, unless contra-indicated. Patients did not receive nitroglycerin before cardiac CT.

For the contrast-enhanced helical scan, collimation was 64x0.5 mm with a rotation time of 400 ms. Tube current and voltage were 350 mA and 120 kV. At an injection rate of 5 mL/min, 95 to 130 mL of nonionic contrast medium (Iomeron 400; Bracco, Milan, Italy) was infused in the antecubital vein. After start of contrast infusion, recurrent low-dose examinations were performed to monitor contrast arrival within the region of interest, placed in the descending aorta. The electrocardiogram (ECG) was registered simultaneously for retrospective gating of the data. The entire cardiac cycle was scanned without dose modulation. The ECG gated helical scan was automatically triggered once the predetermined threshold level of baseline +100 Hounsfield units was reached. After a preset delay of 2 seconds, scanning was performed during an inspiratory breath hold of 8 to 12 seconds.

Data were reconstructed with a slice thickness of 1 mm and a reconstruction interval of 1 mm. With the use of half reconstruction algorithms, the actual temporal resolution was 200 milliseconds. Segmented reconstruction algorithms yielded a temporal resolution of up to 50 milliseconds, depending on the actual imaging acquisition conditions (pitch, rotation time and heart rate). ECG-gated post processing software was used to reconstruct data in short-axis orientation. Images were reconstructed at 20 intervals (0% to 95% of the R-R interval) and transferred to a separate workstation with dedicated cardiac function analysis software (Mass V2008-EXP, LKEB, Leiden, the Netherlands).[15] Contrast-enhanced scans were analyzed by an independent observer who was blinded to all other data. Significant coronary artery stenosis was defined as ≥50% luminal narrowing, whereas non-significant stenosis was defined as <50% luminal narrowing.

The evaluation of LV diastolic function was based on the assessment of transmitral velocity (15 minutes per patient) and mitral septal tissue velocity (5 minutes per patient). Accordingly, the assessment of LV diastolic function was performed within 20 minutes per patient.

Cardiac CT - Transmitral Velocity

Peak transmitral velocity (cm/s) was measured in early (E) and late (A) diastole. The peak value represents the highest mean value of the measurements obtained during early and late diastole. Late peak transmitral velocity (cm/s) was measured at atrial contraction. Transmitral velocity (cm/s) measurements were based on several processing steps (Figure 1). At first, LV volumes were calculated for 20 cardiac phases (each phase represented 5% of the cardiac cycle). For each phase, automatic contour detection was performed on 1 mm sliced reconstructed short-axis images ranging from mitral valve annulus to the apex (Figure 1A, left panel). Manual corrections could be made to improve contour detection. Papillary muscles were regarded as part of the LV cavity and were included in the LV volume analyses.[16] Automatic contour detection was performed using dedicated in-house developed MASS research software package (Mass V2008-EXP, LKEB, Leiden, the Netherlands).[15] Next, LV volumes were plotted in a volume versus time curve (Figure 1A, right upper curve). In addition, changes in LV volumes between two consecutive phases (first derivative) were derived and used to calculate the transmitral flow (mL/s) per phase (Figure 1A, right lower curve). Subsequently, the maximal transmitral flow (mL/s) in early and late diastole was derived using the transmitral flow versus time curve. To allow direct comparison with 2D echocardiography, the maximal transmitral flow (mL/s) in early and late diastole was divided by their corresponding mitral valve area (cm^2) (which was measured during early and late diastole, as described below), yielding an early and late peak transmitral velocity (cm/s) and the E/A.

Cardiac CT - Mitral Septal Tissue Velocity

Myocardial tissue velocity (cm/s) was measured at the septal level of the mitral valve annulus attachment. Measurements of peak mitral septal tissue velocity (cm/s) during early diastole (Ea) are illustrated (Figure 1B). For 20 phases, LV length (mm) was calculated as the distance between two anatomical markers: (1) mitral septal annulus (MA) (the annular attachment of the septal mitral valve leaflet) and (2) cardiac apex (AP) (Figure 1B, left panel). Anatomical markers were positioned at reconstructed 4-chamber views. Reconstruction of a 4-chamber view was based on several reconstruction steps. At first, a 2-chamber view was reconstructed from axial slices, directing the image slice (cardiac axis) through the cardiac apex. Consecutively, a 4-chamber view was reconstructed by positioning the image slice at two-third of the mitral valve annulus (perpendicular to the interventricular septum) using the 2-chamber view.

A. Transmitral Flow

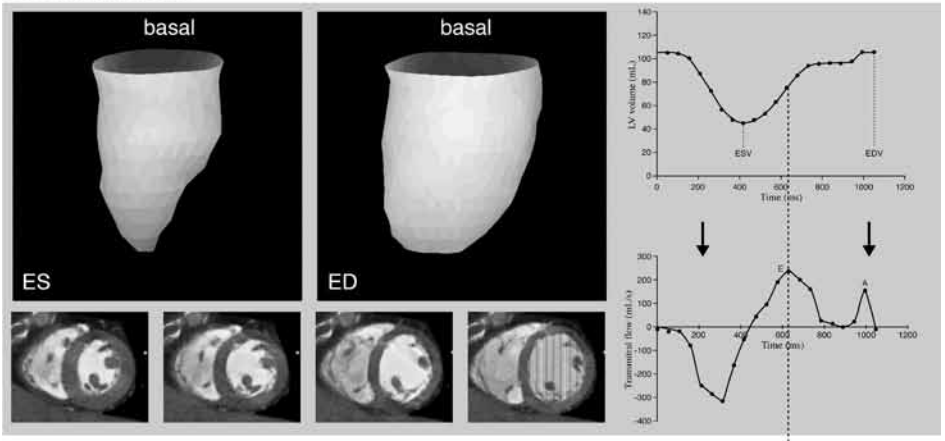

B. Mitral Septal Tissue Velocity

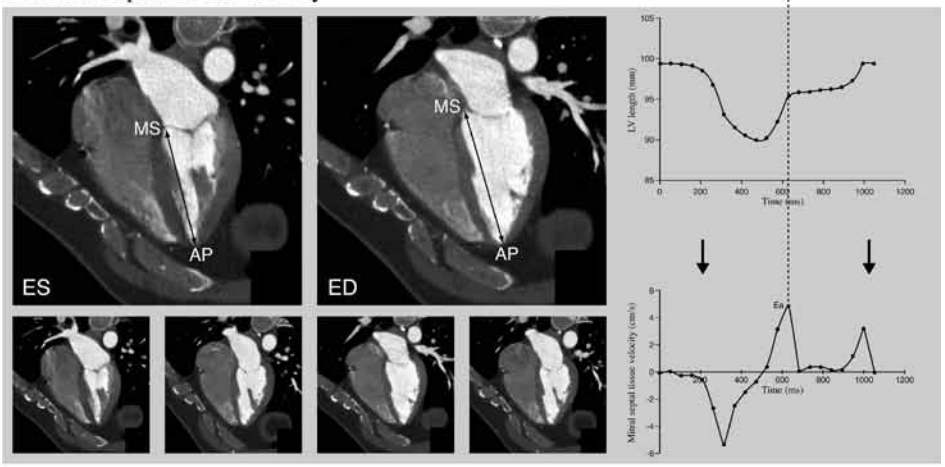

C. Mitral Valve Area

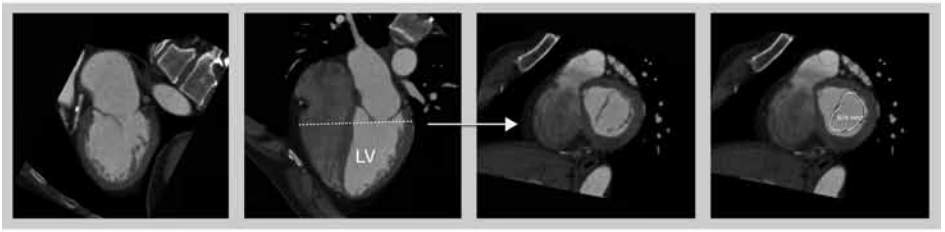

$$\text{Transmitral velocity} = \frac{\text{Transmitral flow (mL / s)}}{\text{Mitral valve area (mm}^2\text{)}} = \frac{\text{cm}^3 / \text{s}}{\text{cm}^2} = \frac{\text{cm}}{\text{s}}$$

Figure 1. Diastolic left ventricular (LV) function assessed with multidetector row computed tomography (CT).

A Transmitral flow. LV volumes (mL) were measured for 20 phases per cardiac cycle. LV volumes (mL) were measured using short-axis images by outlining endocardial contours in each phase. LV volumes (mL) were plotted in a volume versus time curve (right upper panel). These curves were used to define the diastole, ranging from end-systolic (ES) to end-diastolic (ED) phase. Consecutively, changes in LV volumes between two consecutive phases were plotted against time (transmitral flow versus time curve) (right lower curve). Subsequently, early and late peak transmitral flow (mL/s) were derived.

B Mitral septal tissue velocity. Anatomical markers were positioned at the mitral septal annulus (MA) and cardiac apex (AP). LV length (mm) (distance between anatomical markers) was calculated for each phase (left panel). LV length (mm) was plotted in a LV length versus time curve (right upper curve). Next, changes in LV length between two consecutive phases were calculated. Based on these numbers, mitral septal tissue velocities (cm/s) were calculated for each phase (velocity versus time curve, right lower panel). The early peak mitral septal tissue velocity (cm/s) (Ea) represented the maximal tissue velocity during early diastole.

C Mitral valve area. Measurements were performed at the most distal level of the mitral valve leaflets (smallest mitral valve area) using reconstructed images at peak early and late transmitral velocity. LV axis was positioned perpendicular to mid-mitral valve annulus on sagital and coronal views (left panel), yielding a 2-chamber view (panel 1). Consecutively, the 4-chamber view was reconstructed (panel 2) and mitral valve area was measured at the tip of the leaflets (panels 3 and 4) on short-axis views. To allow direct comparison, transmitral velocity (cm/s) was calculated using the following formula: peak diastolic transmitral flow (mL/s) divided by the corresponding mitral valve area (cm2).

The LV length (mm) per phase was plotted in a LV length versus time curve (Figure 1B, right upper panel). Changes in LV length between two consecutive phases were calculated and used to generate a velocity versus time curve (Figure 1B, right lower panel). In this curve, mitral septal tissue velocities were plotted against time. For each phase, mitral septal tissue velocity (cm/s) was computed using changes in LV length and heart rate. The maximal tissue velocity (cm/s) during early diastole represented early peak mitral septal tissue velocity (cm/s) (Ea). Measurements were performed using the MASS software.[15] Finally, the estimation of LV filling pressures (E/Ea) was calculated by dividing early transmitral velocity (E) (cm/s) by the mitral septal tissue velocity (Ea) (cm/s).

Cardiac CT - Mitral Valve Area

Mitral valve area (cm^2) was measured to enable direct comparison of volumetric indices derived from cardiac CT with velocity-based parameters as assessed with 2D echocardiography. In Figure 1C, the processing steps involved in mitral valve area (cm^2) measurements are illustrated. Images were reconstructed with a slice thickness of 0.5 mm and a reconstruction interval of 0.3 mm.

Mitral valve area (cm^2) measurements were based on different steps: the LV axis was positioned perpendicular to mid-mitral valve annulus on sagital and coronal views, yielding a 2-chamber view (panel 1). Subsequently, a 4-chamber view (panel 2) was reconstructed and manual contour detection was performed at the most distal level of the mitral valve leaflets in short-axis views (panel 3 and 4). Measurements were performed during early and late peak transmitral flow (mL/s) using a dedicated workstation (Vitrea 2; Vital Images, Minnetonka, Minnesota, USA).

The mitral valve area (cm^2) was calculated to enable direct comparison with 2D echocardiography. Transmitral velocity (cm/s) was calculated by the following formula: transmitral velocity = transmitral flow (mL/s) / corresponding mitral valve area (cm^2) (Figure 1).

Intra- and Interobserver Reproducibility

Intra- and interobserver reproducibility for assessment of transmitral velocity was evaluated in a subset of 15 patients who were randomly selected from the patient population. Transmitral velocity was measured twice by the same observer in these 15 patients. Subsequently, transmitral velocity measurements were performed by a second independent observer in the same subset of patients. In addition, intra- and interobserver reproducibility for assessment of mitral septal tissue velocity was evaluated in another random sample of 15 patients. Mitral septal tissue velocity was measured twice by the same observer in these patients according to the standardized protocol, as described above. Additionally, a second independent observer performed the mitral septal tissue velocity measurements in the same subset of patients.

Finally, the intra- and interobserver reproducibility of the mitral valve area measurements was evaluated in a subset of 20 patients who were randomly selected from the patient population. In these patients, the mitral valve area was measured twice by the same observer using the same processing steps, as described above. Furthermore, a second blinded observer performed the mitral valve measurements in the same subset of 20 patients.

Transthoracic 2D Echocardiography Using Tissue Doppler Imaging

Acquisition

Transthoracic 2D echocardiography was performed in left lateral decubitus position using a commercially available system (Vingmed Vivid-7, General Electric, Horten, Norway).

Standard parasternal (long- and short-axis) and apical views (2- and 4-chamber) were obtained. In addition, continuous-wave and pulsed-wave Doppler examinations were performed. From the 4-chamber view, TDI was obtained with color Doppler frame rates exceeding 115 frames/second, depending on the sector width of the range of interest. Aliasing velocities varied between 16 and 32 cm/s and resulted from pulse repetition frequencies ranging from 500 Hz and 1 kHz. Echocardiographic analyses were performed by an independent and blinded observer.

2D Echocardiography - Transmitral Velocity

Transmitral velocity (cm/s) was recorded at the end of respiratory expiration (Figure 2, upper panel). Transmitral velocity (cm/s) measurements were performed using dedicated offline software (EchoPAC 7.0.0.; General Electric, Horten, Norway). Standard pulsed-wave Doppler imaging was performed to assess early (E) and late (A) peak transmitral peak velocity (cm/s). Early and late peak transmitral velocity (cm/s) were used to calculate the E/A. Doppler sample volume was placed at the tip of the mitral valve leaflets, on a 4-chamber view .[17] Subsequently, early and late peak transmitral velocities (cm/s) were obtained in diastole.

2D Echocardiography - Mitral Septal Tissue Velocity

Early peak mitral septal tissue velocity (cm/s) (Ea) was assessed using color-coded TDI on a 4-chamber view. Images were obtained in end-expiration in a patient in left lateral decubitus position. Doppler velocities (cm/s) were measured from the apical 4-chamber view using a 6x6 mm sample volume positioned at the basal septal mitral valve annulus, as illustrated in Figure 2 (lower panel).[17] Color-coded images from three consecutive heartbeats were analyzed using dedicated offline software (EchoPAC 7.0.0.; General Electric, Horten, Norway). Reliable tissue Doppler curves were obtained in 67 patients.

Detection of Diastolic Dysfunction

To evaluate the accuracy of cardiac CT to detect diastolic dysfunction, diastolic function was graded in four categories using the following criteria; normal diastolic function (≥1 E/A <2 and E/Ea ≤8), impaired relaxation pattern (diastolic dysfunction grade I) (E/A <1 and E/Ea ≤8), pseudonormal pattern (diastolic dysfunction grade II) (≥1 E/A <2 and ≥9 E/Ea ≤12) and restrictive filling pattern (diastolic dysfunction grade III) (E/A ≥2 and E/Ea ≥13).[18] Based on these criteria, the patient population was divided into two groups; patients with normal diastolic function and patients with diastolic dysfunction (including impaired LV relaxation, pseudonormal and restrictive LV filling pattern).

Statistical Analysis

Continuous data are presented as mean ± standard deviation, and categorical data are presented as absolute numbers or percentages. Kolmogorov-Smirnov tests were used to evaluate

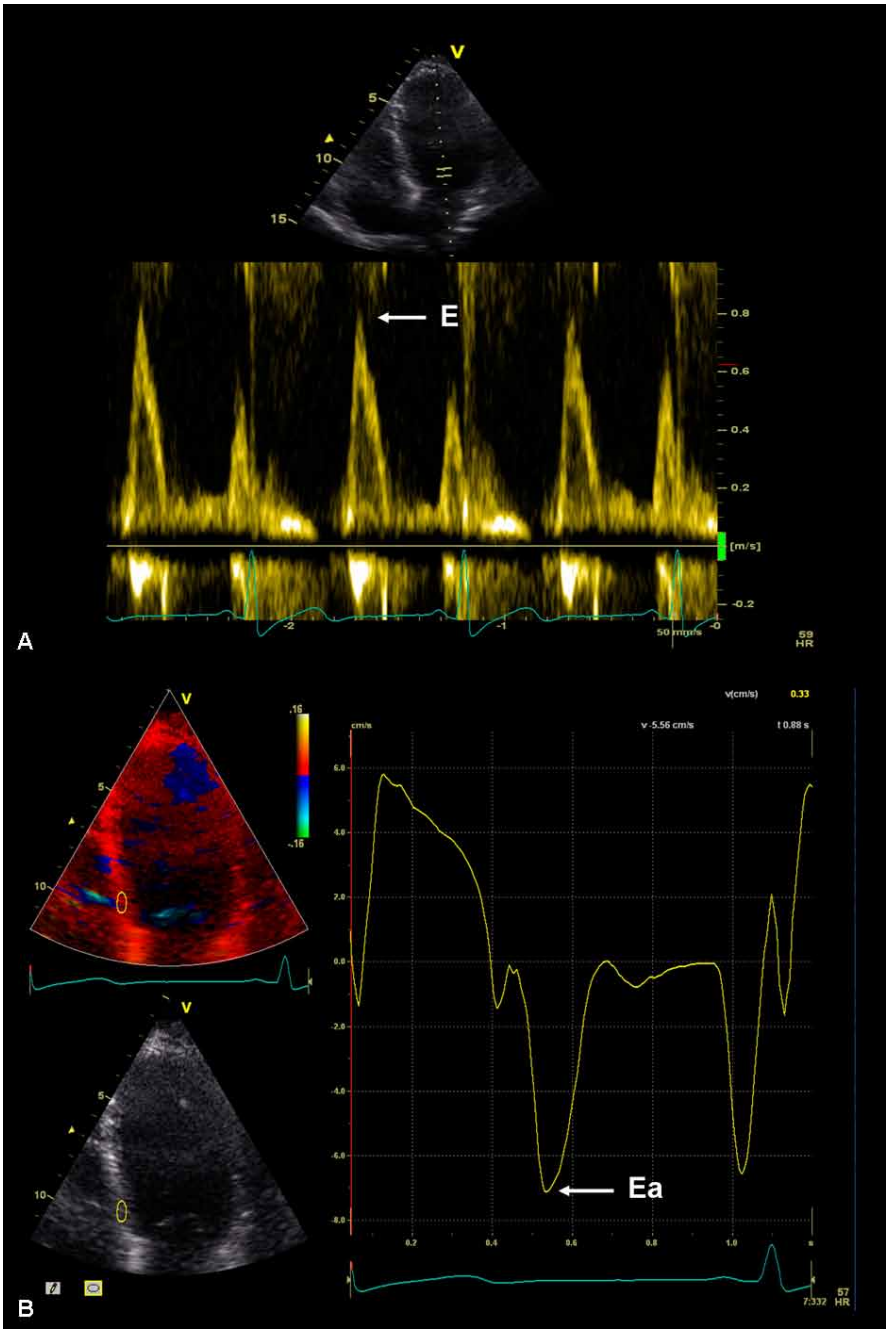

Figure 2. Evaluation of diastolic function with 2-dimensional (2D) echocardiography using tissue Doppler imaging (TDI). 2D echocardiographic assessment of pulsed-wave Doppler of early (E) transmitral velocity (cm/s) (white arrow, panel A) and early diastolic peak mitral septal tissue velocity (cm/s) (Ea) (white arrow, panel B) at basal septal segment by TDI.

the distribution of the data. All variables were normally distributed except for the estimation of LV filling pressures (E/Ea) on cardiac CT and 2D echocardiography with TDI. Data for E/Ea were presented as medians and 25th and 75th percentiles. When appropriate, paired *t* tests or Wilcoxon signed-rank tests were used to compare diastolic function parameters as derived from cardiac CT and 2D echocardiography with TDI.

Comparison of cardiac CT and 2D echocardiography with TDI was performed using Pearson's linear regression analysis or spearman's rho correlation. The 95% limits of agreement were calculated using Bland-Altman analysis that plotted the mean value of differences of each pair against the average value of similar pair of data. Cardiac CT was subtracted from 2D echocardiography with TDI as the latter was considered the clinical standard. Reproducibility was evaluated by calculating the intraclass correlation coefficients (ICC) and an excellent agreement was defined as an ICC >0.8. Diagnostic accuracy of cardiac CT for detection of diastolic dysfunction was assessed using a binary approach; normal diastolic function and diastolic dysfunction (including impaired LV relaxation, pseudonormal and restrictive LV filling pattern). Corresponding sensitivity and specificity values were calculated. For these values, the 95% confidence intervals (CI) were calculated using the following formula: p±1.96 x standard error (SE) and the SE was estimated by $\sqrt{}$ [p (1–p)/n]. Statistical analyses were performed with SPSS release 16.0 (SPSS Inc, Chicago, Illinois, USA). All tests $p<0.05$ were considered statistically significant. Bland-Altman analyses were performed with dedicated Prism software (GraphPad Prism software, version 5.01, GraphPad software Inc, San Diego, California, USA).

Results

Patient Population

A total of 80 patients had undergone multiphase cardiac CT and 2D echocardiography with TDI within 3 months. Of these 80 patients, 10 patients were excluded due to the absence of sinus rhythm (n=2) or the presence of non-diagnostic image quality of either cardiac CT (n=7) or 2D echocardiography with TDI (n=1). Accordingly, a total of 70 patients (46 (66%) men, mean age 55±11 years) were included. Baseline characteristics of the patient population are listed in Table 1. Cardiac CT and 2D echocardiography were performed within 3 months, in which no acute coronary events or worsening of angina occurred. No changes in the use of medication occurred between both examinations. The mean duration between cardiac CT and 2D echocardiography was 34.1±25.0 days. Clinical referral for cardiac CT was based on suspected CAD in 58 patients and known CAD in 12 patients. Patients with known CAD included patients with previous myocardial infarction (n=10), percutaneous coronary intervention (n=7) and patients with indications of CAD on earlier diagnostic tests

Table 1. Baseline characteristics of study population (n=70)

Men	46 (66)
Age (yrs)	55±11
Suspected CAD	58 (83)
Known CAD	12 (17)
Significant coronary stenosis	21 (30)
Cardiovascular risk factors	
Diabetes mellitus	35 (50)
Systemic hypertension	43 (61)
Hypercholesterolemia	40 (57)
Current smoking	11 (16)
Positive family history	27 (39)
Medication use	
Beta-blockers	24 (34)
ACE-I / AT II antagonists	35 (50)
Statins	29 (41)
Diuretics	15 (21)
Anticoagulants	30 (43)
Cardiac CT	
Heart rate (bpm)	58±10
LV end-systolic volume (mL)	70±50
LV end-diastolic volume (mL)	149±52
LV ejection fraction (%)	56±13

Data are presented as mean ± standard deviation or as number (%). ACE-I = angiotensin converting enzyme - inhibitor; AT = angiotensin; CAD = coronary artery disease; LV = left ventricle; CT = computed tomography.

Table 2. Diastolic function parameters for cardiac CT and 2D echocardiography

	Cardiac CT	2D echocardiography
Transmitral velocity		
E (cm/s)	59.0±16.6	61.8±14.5*
A (cm/s)	56.2±17.4	64.8±18.2*
E/A	1.1±0.4	1.1±0.5*
Mitral septal tissue velocity		
Ea (cm/s)	6.6±2.7	6.2±2.3*
E/Ea	8.8 (6.4-13.1)	9.7 (7.5-14.0)**

Data are presented as mean values ± standard deviation or as numbers. Data for E/Ea are presented as medians and corresponding 25^{th} and 75^{th} percentiles. 2D = 2-dimensional; CT = computed tomography. *Paired t-test showed a p-value <0.05. ** Wilcoxon signed-rank test showed a p-value <0.05.

(n=3). Significant coronary artery stenosis (≥50% luminal narrowing) was reported in 21 (30%) patients. In total, 31 (44%) patients received beta-blocking therapy prior to cardiac CT.

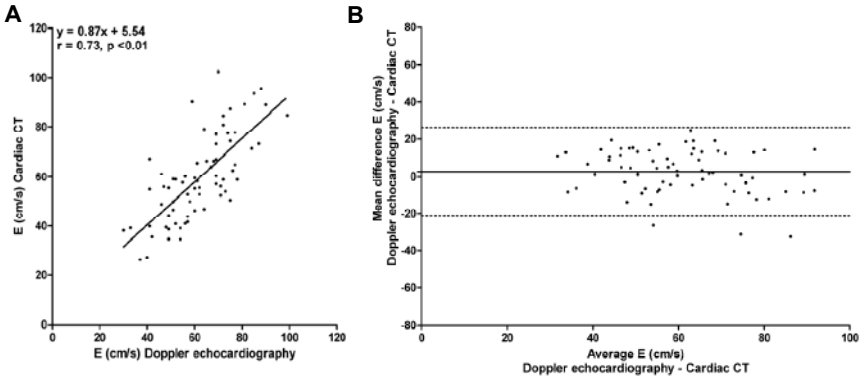

Figure 3. Comparison between 2-dimensional (2D) echocardiography and multidetector row computed tomography (CT) for assessment of early maximal diastolic transmitral velocity (E). A. Good correlation was observed between both techniques. B. Bland-Altman analysis showing the difference of each pair plotted against the average value of same pair of values. Dotted lines represent 95% limits of agreement.

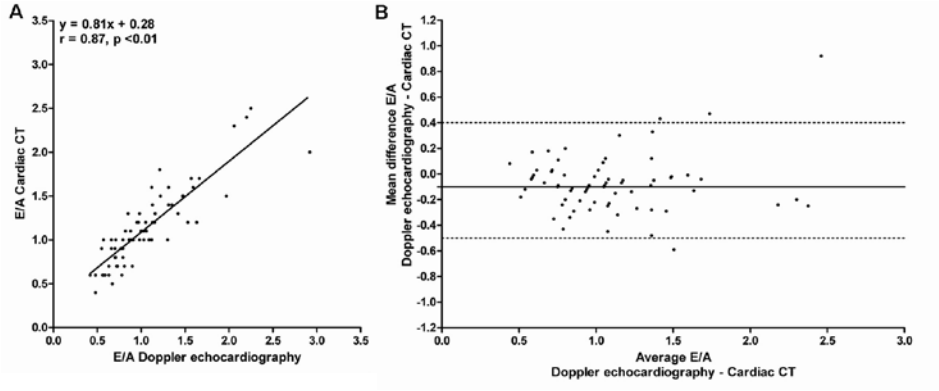

Figure 4. Comparison between 2-dimensional (2D) echocardiography and multidetector row computed tomography (CT) for E/A. A. Good correlation was observed between both techniques. B. Bland-Altman analysis showing the difference of each pair plotted against the average value of same pair of values. Dotted lines represent 95% limits of agreement.

Transmitral Velocity

Transmitral flow versus time curves were obtained in all patients. Mean LV end-systolic and LV end-diastolic volumes were 70±50 mL and 149±52 mL on cardiac CT. Accordingly, the mean LV ejection fraction was 56±13% (Table 1). Mean values for early and late peak transmitral velocity are shown in Table 2. The mean diastolic transmitral velocity was 24.3±8.5 cm/s. Pearson's correlation showed a good correlation for E (r=0.73, p<0.01) and E/A (r=0.87, p<0.01) (Figures 3A and 4A). Bland-Altman analysis for E showed a mean difference of 2.4±12.0 cm/s, with 95% limits of agreement ranging from -21.2 to 26.0 cm/s, whereas for E/A the mean value of difference was -0.1±0.2 with 95% limits of agreement ranging from -0.5 to 0.4 (Figures 3B and 4B).

A low intra- and interobserver variability was observed for assessment of early (ICC 0.97, 95% CI 0.91-0.99 and ICC 0.93, 95% CI 0.78-0.97) and late (ICC 0.98, 95% CI 0.94-0.99

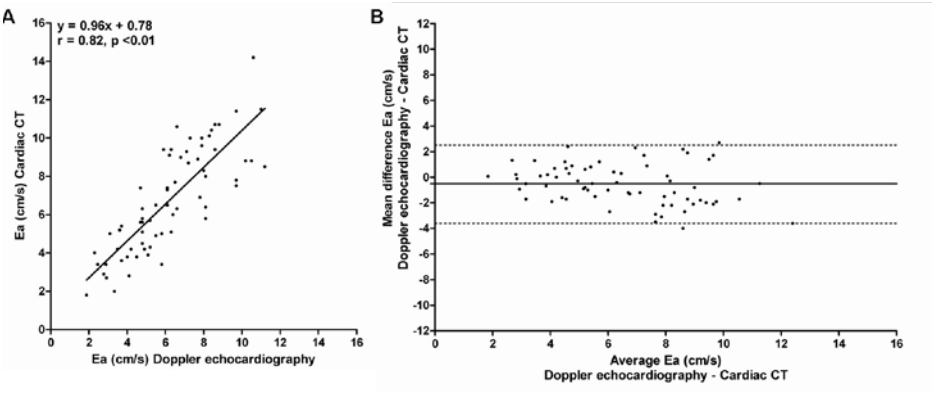

Figure 5. Comparison between 2-dimensional (2D) echocardiography and multidetector row computed tomography (CT) for assessment of early peak mitral septal tissue velocity (Ea). A. Good correlation was observed between both imaging techniques. B. Bland-Altman analysis showing the difference of each pair plotted against the average value of same pair of values. Dotted lines represent 95% limits of agreement.

and ICC 0.91, 95% CI 0.51-0.98) peak transmitral velocity. Moreover, the assessment of E/A showed a low intra- and interobserver variability (ICC 0.95, 95% CI 0.84-0.98 and ICC 0.95, 95% CI 0.85-0.98)

Finally, the intra- and interobserver reproducibility of mitral valve area measurements was evaluated. In a subset of 15 patients, an excellent intra- and interobserver reproducibility was observed for assessment of mitral valve area (ICC 0.94, 95% CI 0.83-0.98 and ICC 0.92, 95% CI 0.80-0.97, respectively).

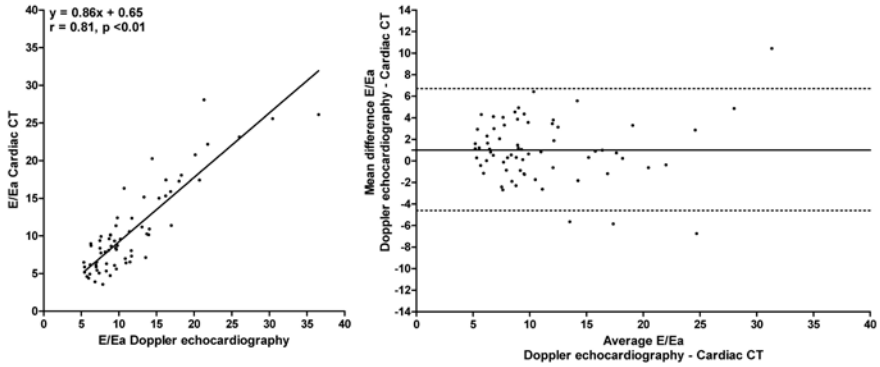

Figure 6. Comparison between 2-dimensional (2D) echocardiography and multidetector row computed tomography (CT) for E/Ea. A. Good correlation for E/Ea was observed between both techniques. B. Bland-Altman analysis showing the difference of each pair plotted against the average value of same pair of values. Dotted lines represent 95% limits of agreement.

Mitral Septal Tissue Velocity

Velocity versus time curves were obtained for all patients. Mean values for Ea are shown in Table 2. In addition, the medians and corresponding 25th and 75th percentiles for E/Ea are shown in Table 2. A good correlation (r=0.82, p<0.01) (Figure 5A) for Ea was found. Bland-Altman analysis showed a mean value of difference of -0.5±1.6 cm/s with 95% limits of agreement ranging from -3.6 to 2.5 cm/s (Figure 5B). In addition, good correlation (r=0.81, p<0.01, Figure 6A) was reported for E/Ea with a mean value of difference of 1.0±2.9 and 95% limits of agreement ranging from -4.6 to 6.7 (Figure 6B).

An excellent intra- and interobserver reproducibility was observed for assessment of mitral septal tissue velocity (ICC 0.95, 95% CI 0.85-0.98 and ICC 0.89, 95% CI 0.69-0.96) and estimation of LV filling pressures (E/Ea) (ICC 0.96, 95% CI 0.87-0.99) and ICC 0.93, 95 % CI 0.80-0.98).

Detection of Diastolic Dysfunction

The diagnostic accuracy of cardiac CT to detect diastolic dysfunction in comparison to 2D echocardiography with TDI was calculated.[18] In total, 19 (27%) patients showed normal diastolic function, whereas 51 (73%) patients showed diastolic dysfunction using 2D echocardiography. Of the patients with diastolic dysfunction on 2D echocardiography, 40 patients were scored similarly using cardiac CT, yielding a sensitivity of 78% (95% CI 67-89%). Normal diastolic function was found in 15 of the 19 patients using cardiac CT, yielding a specificity of 79% (95% CI 61-97%). Overall, diagnostic accuracy for assessment of diastolic dysfunction was 79% (95% CI 69-89%).

Discussion

This study demonstrated good correlations for transmitral velocity (E and E/A) and mitral septal tissue velocity (Ea). Additionally, combined assessment of transmitral and mitral septal tissue velocity (E/Ea) representing an estimation of LV filling pressures showed good correlation between cardiac CT and 2D echocardiography with TDI. Finally, the study showed that cardiac CT and 2D echocardiography were comparable for assessment of diastolic dysfunction. Accordingly, cardiac CT may provide information on diastolic dysfunction.

The importance of diastolic function in patients with coronary atherosclerosis has been demonstrated in several studies.[3, 4] A recent meta-analysis pooled 3396 patients with documented myocardial infarction from 12 prospective studies and demonstrated that patients with a restrictive LV filling pattern had a significantly higher mortality rate than patients with a non-restrictive LV filling pattern (28.7% vs. 11.3 %, $p<0.01$).[3, 4] Although invasive measurements of LV filling pressure are considered the most accurate approach for evaluation of diastolic LV function, they are not ideal for widespread application and follow-up examinations. Consequently, several cardiac imaging techniques (particularly 2D echocardiography) have been used to assess transmitral velocity as a noninvasive alternative.[5, 7] Even though complex interacting pathophysiologic mechanisms may underlie diastolic dysfunction, evaluation of diastolic LV function is most frequently based on transmitral velocity measurements alone.[5, 7, 11]

Transmitral Velocity

Doppler echocardiography has been validated for the assessment of transmitral velocity as a noninvasive alternative of direct LV filling pressures.[5] Additionally, Doppler echocardiography has been compared to magnetic resonance imaging (MRI) for assessment of transmitral velocity.[9, 10] The present study demonstrated that cardiac CT can be used for assessment of LV diastolic function as was indicated by good correlations between cardiac CT and Doppler echocardiography for early transmitral velocity ($r=0.73$, $p<0.01$) and E/A ratio

(r=0.87, p<0.01). In line with the study by Hartiala et al.[9], a systematic underestimation of transmitral velocity was observed when compared to Doppler echocardiography (Table 2). One of the potential explanations of this underestimation could be related to the sampling rate of cardiac CT. As the data sets were sampled in 20 cardiac phases, each sampling took place in 5% steps of the RR interval. Accordingly, the sampling rate of cardiac CT was markedly lower as compared to 2D echocardiography, and this may resulted in an underestimation of transmitral velocity on CT as the peak transmitral velocity as derived from 2D echocardiography could be present in between 2 sampled cardiac phases. In both studies, correlations were not excellent for transmitral velocity and this may be related to other parameters that could influence transmitral velocity measurements, including filling pressures, degree of LV relaxation, myocardial elastic recoil and stiffness.[7, 8] To overcome these limitations, additional measurements have been proposed, including the evaluation of pulmonary venous velocity, M-mode echocardiography flow velocity curves, and altering pre- and afterload conditions (Vasalva maneuver or nitroglycerin administration).[19, 20] In the current study however, these measurements were not performed as this study was only performed to evaluate the feasibility of cardiac CT.

Additionally, it has been suggested to combine transmitral velocity and mitral septal tissue velocity measurements when evaluating diastolic heart function. Importantly, the combined assessment of transmitral velocity and mitral septal tissue velocity represents a better estimate of LV filling pressures as it is a normalization of LV filling gradient for filling LV volume.[6, 10, 11]

Mitral Septal Tissue Velocity

Ommen and colleagues[6] have studied the clinical use of TDI for evaluation of diastolic LV function in 100 patients. Comparison between invasive LV filling pressures and combined assessment of early transmitral velocity and mitral septal tissue velocity showed improved correlation (r=0.64) as compared to transmitral velocity (r=0.59) or mitral septal tissue velocity (r=0.36) alone.[6] In addition, MRI has been compared to TDI for assessment of tissue velocities.[10] Paelinck et al.[10] have used phase-contrast MRI and Doppler echocardiography to measure transmitral and mitral septal tissue velocities in 18 patients with hypertrophic cardiomyopathy. Importantly, combined assessment of early transmitral velocity and mitral septal tissue velocity (E/Ea) showed a good correlation between Doppler echocardiography and MRI (r=0.89, p<0.01). Moreover, invasive measurements were well correlated to E/Ea derived from Doppler echocardiography (r=0.85, p<0.01) and MRI (r=0.80, p<0.01). Likewise, the current study has reported good correlations for transmitral velocity (E/A, r=0.87, p<0.01) and E/Ea (r=0.81, p<0.01). Furthermore, both studies have shown that mitral septal tissue velocity was slightly overestimated when compared to 2D echocardiography with TDI. With tissue Doppler echocardiography, tissue velocities are quantified using changes in Doppler signal over time. Doppler patterns are only displayed for the region of interest

(sample volume), located at the basal septal mitral valve annulus. With cardiac CT however, tissue velocities are measured using a different region of interest; ranging from the basal septal mitral valve annulus to the apex. The different regions of interest may have caused a slight overestimation of tissue velocity using cardiac CT.

Diastolic Left Ventricular Function

Cardiac CT and 2D echocardiography with TDI were comparable for detection of diastolic dysfunction. This represents an important finding as the assessment of diastolic dysfunction provides important diagnostic, therapeutic and prognostic information in patients with cardiovascular disease, and more specifically, in patients with coronary atherosclerosis.[1-4] Additionally, it has been shown that patients with coronary atherosclerosis and normal LV systolic function may already exhibit diastolic dysfunction.[21] Accordingly, additional post-processing for diastolic dysfunction may have the potential to enhance the clinical evaluation derived from cardiac CT, particularly in patients with evidence of coronary atherosclerosis but normal LV systolic function. Moreover, the feasibility of cardiac CT for assessment of diastolic function is of particular interest as the number of patients referred for noninvasive evaluation of known or suspected coronary atherosclerosis with cardiac CT has increased substantially over the recent years.

At present, prospective triggering techniques are commonly used in patients referred for cardiac CT, particularly for ruling out the presence of significant CAD in young patients. However, cardiac CT is also used in patients with advanced CAD or elderly patients for detailed characterization of coronary and cardiac anatomy. In these patients, multiphase CT images may still be acquired using retrospective ECG gating to ensure diagnostic image quality for coronary visualization. The additional information derived from this examination can be used for additional purposes, including the retrospective evaluation of systolic and, as demonstrated in the current manuscript, diastolic function. Accordingly, the information that is needed for evaluation of diastolic function can be derived from conventional multiphase CT, without additional image acquisition or radiation dose.

Moreover, with the recent developments in acquisition and reconstruction algorithms, multiphase imaging may be performed at considerably lower radiation dose when compared to the currently available imaging protocols.

Limitations

At first, the study represents a retrospective study, whereas a prospective study design would be more preferred. Secondly, transmitral velocity parameters were assessed with Doppler echocardiography and cardiac CT as a noninvasive alternative to directly measured LV filling pressures. Although direct measurements of LV filling pressures would have been preferred, they are not ideal for routine clinical examination. Furthermore, patients with valvular regurgitation were excluded. Severe valvular regurgitation may disturb accurate velocity

measurements, leading to an inaccurate diastolic LV function analysis. Future studies are needed to evaluate this potential confounding effect. Additionally, cardiac CT and 2D echocardiography with TDI were performed within a period of maximal 3 months. However, to ensure optimal comparability between both examinations the study only included patients with stable hemodynamic conditions; patients with unstable angina pectoris or acute coronary syndromes were excluded. Also, in the current study, diastolic function indices were derived from multiphase CT data sets acquired without tube current modulation. To what extent tube modulation may influence the measurements of the mitral valve area and other diastolic function parameters needs to be addressed in additional studies. Finally, it is important to note that the effect of intravenous infusion of contrast media during cardiac CT angiography on diastolic function indices is currently unknown.[22]

Conclusions

Cardiac CT showed good correlations for transmitral velocity, mitral septal tissue velocity and estimation of LV filling pressures when compared to 2D echocardiography using TDI. Accordingly, cardiac CT may provide information on diastolic dysfunction in selected patients imaged by retrospectively ECG gated CT.

Reference List

(1) Zile MR, Brutsaert DL. New concepts in diastolic dysfunction and diastolic heart failure: Part I: diagnosis, prognosis, and measurements of diastolic function. Circulation 2002;105:1387-93.

(2) Bhatia RS, Tu JV, Lee DS, et al. Outcome of heart failure with preserved ejection fraction in a population-based study. N Engl J Med 2006;355:260-9.

(3) Perrone-Filardi P, Bacharach SL, Dilsizian V, Bonow RO. Impaired left ventricular filling and regional diastolic asynchrony at rest in coronary artery disease and relation to exercise-induced myocardial ischemia. Am J Cardiol 1991;67:356-60.

(4) Moller JE, Whalley GA, Dini FL, et al. Independent prognostic importance of a restrictive left ventricular filling pattern after myocardial infarction: an individual patient meta-analysis: Meta-Analysis Research Group in Echocardiography acute myocardial infarction. Circulation 2008;117:2591-8.

(5) Nishimura RA, Appleton CP, Redfield MM, et al. Noninvasive doppler echocardiographic evaluation of left ventricular filling pressures in patients with cardiomyopathies: a simultaneous Doppler echocardiographic and cardiac catheterization study. J Am Coll Cardiol 1996;28:1226-33.

(6) Ommen SR, Nishimura RA, Appleton CP, et al. Clinical utility of Doppler echocardiography and tissue Doppler imaging in the estimation of left ventricular filling pressures: A comparative simultaneous Doppler-catheterization study. Circulation 2000;102:1788-94.

(7) Nishimura RA, Tajik AJ. Evaluation of diastolic filling of left ventricle in health and disease: Doppler echocardiography is the clinician's Rosetta Stone. J Am Coll Cardiol 1997;30:8-18.

(8) Oh JK, Appleton CP, Hatle LK, Nishimura RA, Seward JB, Tajik AJ. The noninvasive assessment of left ventricular diastolic function with two-dimensional and Doppler echocardiography. J Am Soc Echocardiogr 1997;10:246-70.

(9) Hartiala JJ, Mostbeck GH, Foster E, et al. Velocity-encoded cine MRI in the evaluation of left ventricular diastolic function: measurement of mitral valve and pulmonary vein flow velocities and flow volume across the mitral valve. Am Heart J 1993;125:1054-66.

(10) Paelinck BP, de Roos A, Bax JJ, et al. Feasibility of tissue magnetic resonance imaging: a pilot study in comparison with tissue Doppler imaging and invasive measurement. J Am Coll Cardiol 2005;45:1109-16.

(11) Nagueh SF, Middleton KJ, Kopelen HA, Zoghbi WA, Quinones MA. Doppler tissue imaging: a noninvasive technique for evaluation of left ventricular relaxation and estimation of filling pressures. J Am Coll Cardiol 1997;30:1527-33.

(12) Raff GL, Gallagher MJ, O'Neill WW, Goldstein JA. Diagnostic accuracy of noninvasive coronary angiography using 64-slice spiral computed tomography. J Am Coll Cardiol 2005;46:552-7.

(13) Mollet NR, Cademartiri F, van Mieghem CA, et al. High-resolution spiral computed tomography coronary angiography in patients referred for diagnostic conventional coronary angiography. Circulation 2005;112:2318-23.

(14) Henneman MM, Bax JJ, Schuijf JD, et al. Global and regional left ventricular function: a comparison between gated SPECT, 2D echocardiography and multi-slice computed tomography. Eur J Nucl Med Mol Imaging 2006;33:1452-60.

(15) van der Geest RJ, Reiber JH. Quantification in cardiac MRI. J Magn Reson Imaging 1999;10:602-8.

(16) Pattynama PM, Lamb HJ, van der Velde, van der Wall EE, de Roos A. Left ventricular measurements with cine and spin-echo MR imaging: a study of reproducibility with variance component analysis. Radiology 1993;187:261-8.

(17) Lester SJ, Tajik AJ, Nishimura RA, Oh JK, Khandheria BK, Seward JB. Unlocking the mysteries of diastolic function: deciphering the Rosetta Stone 10 years later. J Am Coll Cardiol 2008;51:679-89.

(18) Nagueh SF, Appleton CP, Gillebert TC, et al. Recommendations for the evaluation of left ventricular diastolic function by echocardiography. J Am Soc Echocardiogr 2009;22:107-33.
(19) Nishimura RA, Abel MD, Hatle LK, Tajik AJ. Relation of pulmonary vein to mitral flow velocities by transesophageal Doppler echocardiography. Effect of different loading conditions. Circulation 1990;81:1488-97.
(20) Takatsuji H, Mikami T, Urasawa K, et al. A new approach for evaluation of left ventricular diastolic function: spatial and temporal analysis of left ventricular filling flow propagation by color M-mode Doppler echocardiography. J Am Coll Cardiol 1996;27:365-71.
(21) Garcia-Fernandez MA, Azevedo J, Moreno M, et al. Regional diastolic function in ischaemic heart disease using pulsed wave Doppler tissue imaging. Eur Heart J 1999;20:496-505.
(22) Stern L, Firth BG, Dehmer GJ, et al. Effect of selective coronary arteriography on left ventricular volumes and ejection fraction in man. Am J Cardiol 1980;46:827-31.

Part II

GMPS for Selection of Heart Failure Patients Referred for Cardiac Resynchronization Therapy

Chapter **6**

Role of Nuclear Imaging in Cardiac Resynchronization Therapy

Mark M. Boogers, MD[1, 2], Ji Chen, PhD[3], Jeroen J. Bax, MD, PhD[1].

[1]Department of Cardiology, Leiden University Medical Center, Leiden, the Netherlands; [2]The Interuniversity Cardiology Institute of the Netherlands, Utrecht, the Netherlands; [3]Department of Radiology, Emory University School of Medicine, Atlanta, Georgia.

Abstract

Cardiac resynchronization therapy (CRT) has become an integrated treatment option for patients with drug-refractory heart failure. Selection of patients for CRT is based on moderate to severe heart failure (New York Heart Association, NYHA functional class III-IV), depressed left ventricular (LV) systolic function ≤35% and prolonged QRS interval ≥120 ms. However, 30-40% of selected patients do not exhibit improvement in heart failure symptoms or LV systolic performance.

Efforts have been made to improve patient selection criteria and several studies using echocardiography have demonstrated the significance of LV dyssynchrony for prediction of CRT response as an additional selection criterium. In addition, (location and extent of) viability and scar tissue are important for outcome after CRT. Nuclear imaging with ECG-gated myocardial perfusion SPECT (GMPS) permits assessment of viability, scar tissue and LV dyssynchrony from 1 dataset. The potential value of GMPS in CRT patients is discussed in this review. In addition, the use of nuclear imaging (and particularly positron emission tomography, PET) for evaluation of changes in blood flow, metabolism and innervation after CRT is addressed.

Introduction

Heart failure represents a major problem in the Western health care system. In the United States, heart failure affects 5.3 million patients and each year approximately 660,000 patients are diagnosed with heart failure.[1] Furthermore, (decompensated) heart failure is responsible for more than one million hospital admissions per year and direct and indirect costs accounted for $34.8 billion in 2008.[1] Despite advanced treatment options for heart failure, the 5-year mortality rate still exceeds 50%.

In recent years, cardiac resynchronization therapy (CRT) has been integrated in the treatment of patients with drug-refractory heart failure. The evidence for success of CRT in heart failure patients is mainly based on results of eight large clinical trials that have demonstrated beneficial effects of CRT on heart failure symptoms, quality of life, and exercise capacity.[2-7] In addition, a reduction in left ventricular (LV) volumes (indicating reverse remodeling) along with an improvement in LV ejection fraction (LVEF) and mitral regurgitation were observed in patients undergoing CRT.[2-7] Besides clinical and echocardiographic end-points, two large clinical trials have demonstrated an improvement in survival with a reduction in morbidity in patients undergoing CRT as compared to patients on optimal medical therapy.[8, 9]

Current ACC/AHA/ESC guidelines recommend CRT in patients with advanced heart failure (NYHA class III or IV), prolonged QRS duration (≥120 ms), depressed LV systolic function (LVEF ≤35%) and sinus rhythm.[10, 11] However, multiple clinical trials have demonstrated that a substantial group of patients (30-40%), who were selected according to current criteria on CRT, did not show significant improvement in heart failure symptoms or LV systolic performance.[5, 12, 13] Hence, refinement of selection criteria is needed and several studies have emphasized the importance of cardiac dyssynchrony for response to CRT.[13-15] Cardiac dyssynchrony includes atrioventricular dyssynchrony, interventricular dyssynchrony and intraventricular (LV) dyssynchrony, and most studies suggested that the latter may be most powerful for prediction of response to CRT.[13, 14, 16] In this regard, QRS duration is of limited value for prediction of response to CRT, mainly since QRS duration reflects interventricular rather than intraventricular dyssynchrony.[13, 14, 17, 18]

At present, detection of LV dyssynchrony can be performed with several cardiac imaging techniques, including echocardiography[13, 14, 19-21], magnetic resonance imaging[22, 23] and nuclear imaging.[24-30] The majority of clinical studies on LV dyssynchrony and the prediction of response to CRT used echocardiography.[14, 16] These predominantly single-center studies have clearly demonstrated that LV dyssynchrony has additional value in selection of patients for CRT. Since all studies used different echocardiographic techniques and different criteria for LV dyssynchrony, it is currently unclear which are the precise cut-off values that could be used for prediction of CRT response. This issue has been addressed in the Predictors of Response to Cardiac Resynchronization Therapy (PROSPECT) trial, which was the first multicenter prospective trial using echocardiography for identification of predictors of response

to CRT.[31] The study has shown only a modest value of echocardiography to predict response to CRT, and an important problem posed the limited intra- and interobserver variability.[32] Another aspect that may have influenced the study results is the heterogeneous study population included. A substantial cohort of patients included had a LV ejection fraction >35% without severe LV dilatation. These patients were not able to demonstrate cardiac remodeling, one of major endpoints of the study. In addition, other issues could have contributed to the disappointing results, including myocardial scar tissue, LV lead positioning and accessibility of the venous anatomy.

Accordingly, more sophisticated and reproducible imaging techniques are needed for assessment of LV dyssynchrony for selection of CRT candidates.

One of these techniques may be nuclear imaging. Particularly, ECG-gated myocardial perfusion SPECT (GMPS) has emerged as a reasonable technique to determine LV dyssynchrony. Moreover, nuclear imaging is already used extensively in heart failure patients to detect LVEF, LV volumes, ischemia, viability and scar tissue. Accordingly, the addition of LV dyssynchrony to previously mentioned clinical data, provides heart failure clinicians tools to direct therapeutic strategy in the individual heart failure patient (medical therapy, revascularization or CRT). Beyond LV dyssynchrony, viability and scar tissue are particularly important in CRT patients, since the location and extent of scar tissue is also predictive of (non-) response to CRT.

In this review, the potential role of GMPS for prediction of response to CRT is addressed. Moreover, nuclear imaging (and particularly positron emission tomography, PET) is also important in the evaluation of changes in perfusion, metabolism and innervation after CRT, which is also discussed in this review.

Nuclear Imaging to Assess Left Ventricular Dyssynchrony

Several nuclear imaging techniques can be used for detection of cardiac dyssynchrony, including multi-gated equilibrium blood-pool scintigraphy[24, 25], gated blood-pool SPECT[26, 27] and GMPS.[28-30, 33, 34]

Initially, gated blood-pool scintigraphy was used for assessment of the myocardial contraction pattern. In gated blood-pool imaging, labeled erythrocytes are used for generating count-based volume-time curves. Images are obtained from one left-anterior oblique view (LAO) in 16 to 64 frames per cardiac cycle and can be smoothed with spatial and temporal filtering in order to reduce noise.[35] Subsequently, regions of interest (ROI) are drawn automatically or manually on the left and right ventricles respectively. For each pixel in the ROI, a time-activity curve is generated by approximation of discrete sample points into a continuous curve using the first Fourier Harmonic (FFH) function. The phase angle of the first FFH function corresponds to the timing of contraction at the particular region. The standard deviation (SD) of phase angles over the ventricle represents the intra-ventricular dyssynchrony, and the difference between the means of the phase angles of the two

ventricles represents inter-ventricular dyssynchrony. The major limitation of this method is that determination of ROI from planar images is less accurate due to overlap of non-cardiac structures. Gated blood-pool SPECT, with the similar principles of phase analysis as gated blood-pool scintigraphy, allows assessment of inter- and intraventricular dyssynchrony in 3 dimensions (3D).[26, 27] The major limitation of this method is that it lacks standard processing procedures due to the complexity of generation time-activity curves from gated blood-pool SPECT images.

Recently, phase analysis of GMPS has attracted considerable attention. GMPS is frequently applied in heart failure patients to evaluate for ischemia, viability and scar tissue to direct patient management (revascularization or medical therapy), and the current possibility to derive information on cardiac dyssynchrony from the same dataset has emerged as an appropriate alternative to assess cardiac dyssynchrony.[28-30, 33, 34]

The phase analysis of GMPS studies is based on the partial-volume effect in which changes in segmental maximal counts is proportional to cardiac wall thickening.[36, 37] Phase analysis is performed on standard GMPS images without any additional acquisition. For each frame of the gated short-axis image, a 3D sampling algorithm is used to search for regional maximal counts. Next, a count-based wall-thickening curve is generated for each segment and then approximated using the FFH function. The phase angle of the FFH function represents the onset of mechanical activation of the region. Hetero- or homogeneity of the phase distribution over the entire LV represents LV dys- or synchrony. Peak phase (maximum of phase histogram), phase standard deviation (standard deviation (SD) of phase distribution), histogram bandwidth (bandwidth which includes 95% of phase angles), kurtosis (degree of peakedness of histogram) and skewness (symmetry of histogram) are used to quantify the phase distribution. In Figure 1, an example of a patient with a synchronous

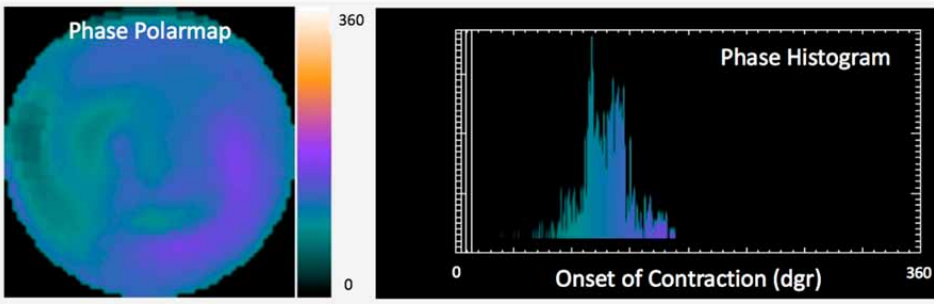

Figure 1A. Heart failure patient with minimal left ventricular (LV) dyssynchrony as evidenced by the homogeneous phase angle distribution (polar map, left panel) and a narrow phase histogram (right panel). This patient did not improve in symptoms or LV systolic function after 6 months of cardiac resynchronization therapy (CRT); particularly, LV ejection fraction did not improve (30% at baseline vs. 29% at follow-up).

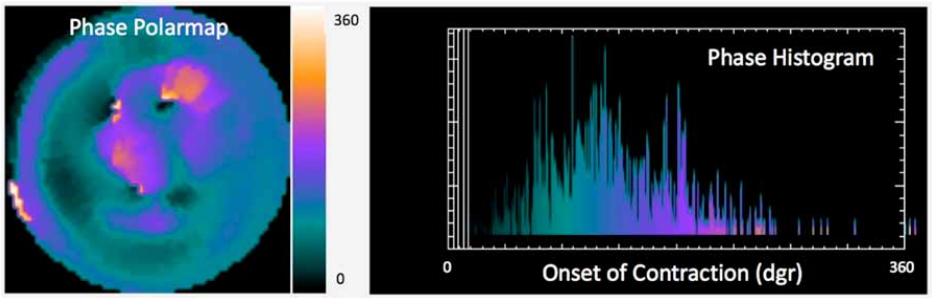

Figure 1B. Heart failure patient with extensive left ventricular (LV) dyssynchrony as evidenced by heterogeneous phase distribution (polar map, left panel) and a broad phase histogram (right panel). This patient improved in symptoms and LV ejection fraction (from 28% to 40%) after 6 months of cardiac resynchronization therapy (CRT).

LV contraction pattern is illustrated in upper panel, whereas an example of a patient with extensive LV dyssynchrony is illustrated in the lower panel.

In general, GMPS studies are perceived with poor temporal resolution since data acquisition is based on 8 or 16 frames per cardiac cycle. However, phase analysis on GMPS is able to improve temporal resolution by replacing 8 or 16 discrete points into a continuous FFH curve.[38] It has been shown that in clinical settings (≥10 counts per pixel) phase analysis using either first, second or third harmonics, phase analysis was able to detect phase difference of 5.6 degrees, reflecting 1/64 of the cardiac cycle.[38] GMPS has been validated against echocardiography for assessment of LV dyssynchrony. Henneman and coworkers[39] have published on the agreement between echocardiography with tissue Doppler imaging (TDI) and GMPS. Good correlations between LV dyssynchrony as measured by TDI and histogram bandwidth ($r=0.89$, $P<0.0001$) or phase SD ($r=0.80$, $P<0.0001$) as measured by phase analysis of GMPS were presented. Moreover, good correlations between LV dyssynchrony indices on 3D echocardiography and GMPS were recently reported. The systolic dyssynchrony index (derived from real-time 3D echocardiography) correlated well with histogram bandwidth ($r=0.76$, $P<0.0001$) and phase SD ($r=0.80$, $P<0.0001$) as illustrated in Figure 2.[20]

Henneman and colleagues[40] have evaluated 42 heart failure patients who underwent CRT with GMPS. After 6 months of CRT, a significant improvement in NYHA class, quality of life score and exercise capacity was noted. The authors demonstrated that LV dyssynchrony derived from GMPS was related to CRT response. Particularly, histogram bandwidth (175 ± 63 versus 117 ± 51, $P<0.05$) and phase SD (56.3 ± 19.9 versus 37.1 ± 14.4, $P<0.05$) were significantly larger in responders as compared to non-responders to CRT. Receiver operating characteristic curve analysis revealed good predictive values for CRT response using histogram bandwidth (AUC 0.78) or phase SD (AUC 0.81) as markers of LV dyssynchrony (Figure 3). For histogram bandwidth, a cut-off value of 135° had a sensitivity and specificity

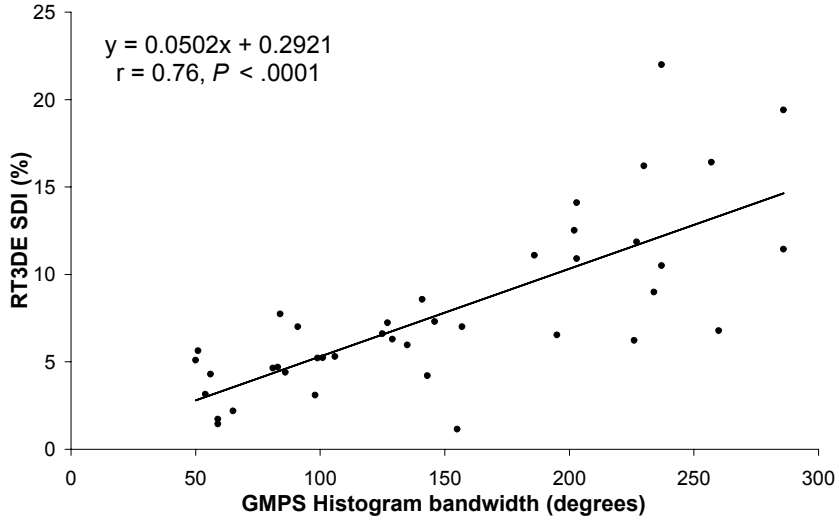

Figure 2A. Comparison between left ventricular (LV) dyssynchrony derived from real-time 3 dimensional echocardiography (RT3DE) and gated myocardial perfusion single photon emission computed tomography (SPECT) (GMPS). The systolic dyssynchrony index (SDI) from RT3DE correlated well with histogram bandwidth derived from GMPS. Reprinted with permission from reference 20.

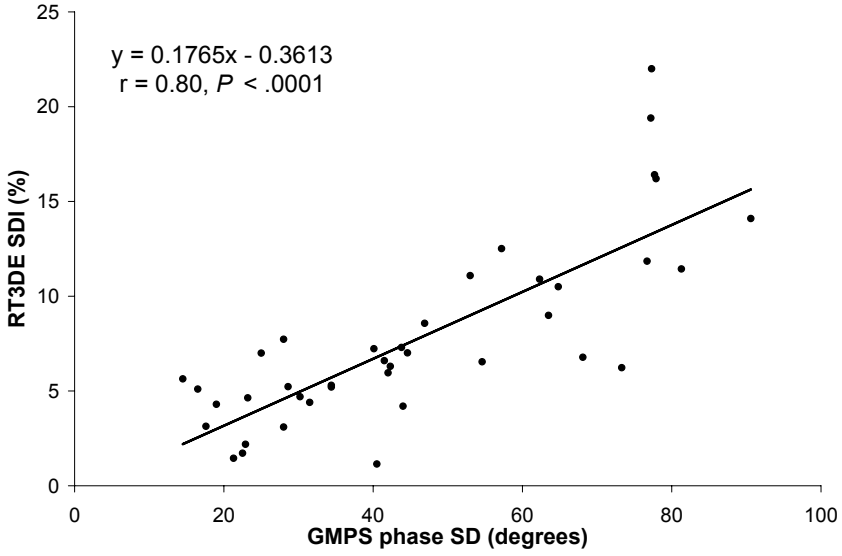

Figure 2B. Comparison between left ventricular (LV) dyssynchrony derived from real-time 3 dimensional echocardiography (RT3DE) and gated myocardial perfusion single photon emission computed tomography (SPECT) (GMPS). Good correlation was observed between systolic dyssynchrony index (SDI) from RT3DE and phase standard deviation (SD) derived from GMPS. Reprinted with permission from reference 20.

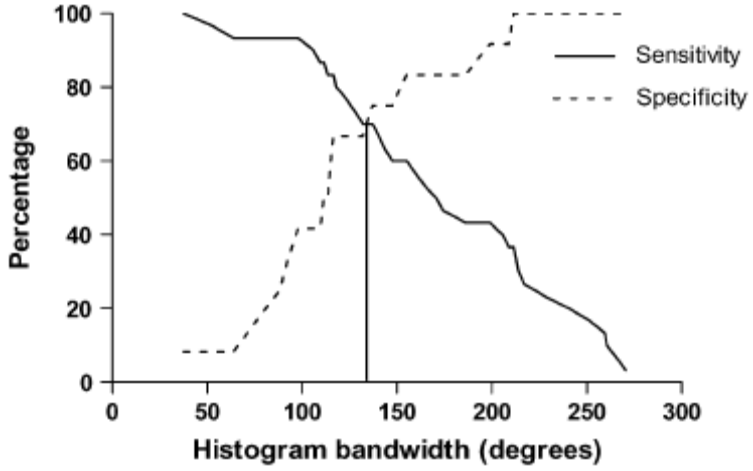

Figure 3A. Receiver operating characteristic curve analysis on histogram bandwidth demonstrated a good predictive value (AUC 0.78) for response to cardiac resynchronization therapy (CRT). A cut-off value of 135° for histogram bandwidth showed a sensitivity and specificity of 70%. Reprinted with permission from reference 40.

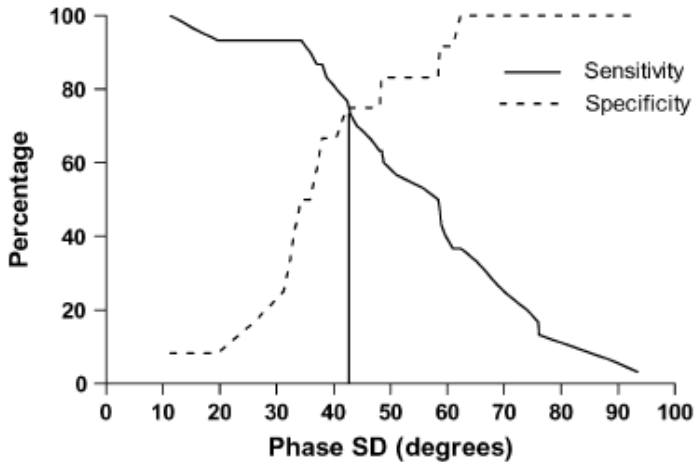

Figure 3B. Receiver operating characteristic curve analysis on phase standard deviation (SD) showed a good predictive value (AUC 0.81) for response to cardiac resynchronization therapy (CRT). A cut-off value of 43° for phase SD yielded a sensitivity and specificity of 74%. Reprinted with permission from reference 40.

of 70%; for phase SD, a threshold of 43° yielded a sensitivity and specificity of 74% for prediction of CRT response.

One important advantage of phase analysis of GMPS for assessment of LV dyssynchrony is that this method is largely automatic and has superior reproducibility to echocardiography. Trimble and colleagues[33] have evaluated phase analysis of GMPS with 10 normal subjects and 10 patients with LV dysfunction and showed that intra-observer and inter-observer reproducibility of phase analysis of GMPS is very robust with correlation coefficients of 1.00 and 0.99 respectively.

Nuclear Imaging to Assess Viability and Scar Tissue

It appears that viability and scar tissue are important for response to CRT. In particular, the presence of scar tissue in the region where the LV pacing lead is positioned is of importance. Bleeker et al.[41] have demonstrated in an elegant study with contrast-enhanced magnetic resonance imaging that patients with scar tissue in the posterolateral region (where the LV lead was positioned in these patients) was associated with non-response to CRT[41]; the authors hypothesized that transmural scar tissue in the LV pacing region resulted in ineffective pacing prohibiting LV resynchronization. Another important issue in patients considered for CRT is identification of the region of latest activation for optimal LV lead positioning.[42-44] Recently, Ypenburg and colleagues[44] have evaluated echocardiographic response to CRT in patients with LV lead positioned at the region of latest activation (concordant) and in patients with LV lead positioned at other regions than the area of latest activation (discordant). Patients with concordant LV lead positioning (n=153) showed significant reduction in LV end-systolic volume, whereas patients with discordant LV lead position (n=91) demonstrated no significant reduction in LV end-systolic volume.

In addition to the area of latest activation and its viability, the balance between the total extent of viable myocardium and scar tissue in the left ventricle is important.[45-47] In 61 patients with ischemic cardiomyopathy, Ypenburg and colleagues[45] have shown that the extent of viable myocardium (assessed with F18-fluorodeoxyglucose, FDG) and SPECT) was directly related to improvement in LVEF ($r=0.56$, $P<0.05$) after 6 months of CRT, whereas the extent of scar tissue was inversely related to change in LVEF ($r=-0.56$, $P<0.05$) at 6 months follow-up. Also, responders to CRT had significantly more viable segments as compared to non-responders (12±3 vs. 7±3 viable segments respectively, $P<0.01$). Based on these data, receiver operating characteristic curve analysis was performed, and a cutoff value of 11 viable segments was defined to predict CRT response with a sensitivity of 74% and a specificity of 87%.

Adelstein et al.[48] have reported similar findings in 50 heart failure patients undergoing SPECT. Larger extent of scar tissue and the presence of scar tissue in the region where the LV pacing lead was positioned were inversely related to improvement in LVEF after CRT.

Similar findings were reported with FDG PET in 39 patients with ischemic cardiomyopathy undergoing CRT, confirming a direct relation between the extent of viable tissue and cardiac performance after CRT (r=0.64, P<0.001).[49] The optimal threshold for prediction of hemodynamic response (improvement in cardiac index >15%) after LV pacing was defined at 3 viable segments, yielding a sensitivity of 72% with a specificity of 71% (AUC 0.80) to predict hemodynamic improvement after CRT.

Of note, these studies found different cutoff values for prediction of response to CRT. One of potential explanations for the observed discrepancy is the fact that different scoring models were used. In the study by Ypenburg and colleagues[45], the 17-segment model was used for assessment of the number of viable and infarcted segments, whereas Van Campen et al.[49] used a 13-segment model. Moreover, different definitions for response to CRT were used in these studies. Patients with an improvement in ≥1 NYHA class were considered responders to CRT in the study by Ypenburg et al.[45], while Van Campen and colleagues[49] considered patients as responders to CRT in the presence of >15% improvement in cardiac index.

Nuclear Imaging to Evaluate CRT Effects on Blood Flow, Metabolism and Innervation

The effects of CRT on myocardial blood flow, metabolism and sympathetic innervation have been studied using nuclear imaging.[50-61] To evaluate the beneficial effects of CRT, particularly correction of LV dyssynchrony, the etiology of heart failure plays an important role as different mechanism may be involved. In this regard, two concepts are important, including cardiac dyssynchrony and cardiac dyssynnergy; cardiac dyssynchrony results from different timing of contraction between cardiac segments, whereas cardiac dyssynnergy refers to heterogeneous contractile capacity (contractile disparity) between cardiac segments with similar contraction timing. The former may play an important role in patients with congestive heart failure and left bundle branch block, whereas cardiac dyssynnergy may play a more evident role in ischemic heart failure patients. The effect of CRT in patients with cardiac dyssynchrony based on disparity in activation timing can be expected, however, the precise mechanisms of effects of CRT in patients with cardiac contractile disparity are less clear. Several studies on nuclear imaging have been performed to evaluate the beneficial effects of CRT on myocardial blood flow, oxidative metabolism, glucose utilization and sympathetic innervation. Particularly the effects of CRT on myocardial blood flow have been extensively studied with PET.[50-57] Different studies demonstrated that global blood flow did not change after CRT.[50-57] However, an inhomogeneous distribution of blood flow was observed in heart failure patients, with lower values in the septum as compared to the lateral wall. After CRT a more homogeneous distribution of blood flow was detected. Knaapen and coworkers[54] have evaluated 14 heart failure patients who underwent CRT with O15-labeled water and PET. Myocardial blood flow was inhomogeneously distributed as reflected by a

baseline septal-to-lateral blood flow ratio of 0.77±0.27, which increased to 0.97±0.34 after 3 months of CRT. Similarly, a heterogeneous distribution of glucose utilization was observed in heart failure patients, with lower glucose utilization in the septum as compared to the lateral wall.[57, 58] Nowak and colleagues[58] have used FDG PET in 15 patients with dilated cardiomyopathy and left bundle branch block configuration on the ECG, and demonstrated low FDG uptake in the septum as compared to the lateral wall (56±12% versus 89±6%, P<0.001). The septal-to-lateral FDG ratio improved significantly after CRT (0.62±0.12 versus 0.91±0.26, P<0.001) indicating more homogeneous tracer uptake.

The effect of CRT on myocardial efficiency has been evaluated by Ukkonen and colleagues.[59] The authors used C11-acetate with PET and showed an improvement in cardiac efficiency after CRT.

Finally, sympathetic innervation has been evaluated with 123-I-metaiodobenzylguanidine (MIBG) and SPECT in patients undergoing CRT, suggesting that patients with more preserved innervation had better response to CRT.[60, 61]

Conclusions

In heart failure patients, nuclear imaging with GMPS can provide information on myocardial ischemia, viability and scar tissue; in addition, precise information on LV function and LV volumes can be derived. With current technology of phase analysis, assessment of LV dyssynchrony is possible from the same dataset. It provides a comprehensive overview for the heart failure specialist, permitting therapeutic decision making. At present, large trials are needed to determine the precise role of GMPS for assessment of LV dyssynchrony and outcome after CRT.

Future Perspectives

Accurate prediction of response to CRT remains challenging. Different issues need to be concerned for appropriate patient selection for CRT, in particular the assessment of LV dyssynchrony. Most frequently, echocardiography has been proposed to provide information on LV dyssynchrony, however the results from the PROSPECT trial are disappointing; a major issue was the reproducibility of echo analyses, with large inter- and intraobserver variability of dyssynchrony measurements. GMPS has the potential to provide objective, reproducible parameters on LV dyssynchrony. In clinical cardiology, many heart failure patients undergo nuclear imaging for assessment of myocardial perfusion state and simultaneous detection of mechanical dyssynchrony will add important information for therapeutic strategies. Although GMPS is promising, limited data are available on the use of GMPS for selection of CRT candidates and larger trials are needed to define to final role of GMPS in CRT. As a consequence, echocardiography remains the first choice for patient selection to CRT,

however, depending on upcoming studies GMPS may be incorporated in the clinical workup of patient selection for CRT.

Reference List

(1) Rosamond W, Flegal K, Furie K et al. Heart disease and stroke statistics--2008 update: a report from the American Heart Association Statistics Committee and Stroke Statistics Subcommittee. Circulation.2008;117: 25-146.

(2) Lozano I, Bocchiardo M, Achtelik M et al. Impact of biventricular pacing on mortality in a randomized crossover study of patients with heart failure and ventricular arrhythmias. Pacing Clin Electrophysiol.2000;23:1711-1712.

(3) Cazeau S, Leclercq C, Lavergne T et al. Effects of multisite biventricular pacing in patients with heart failure and intraventricular conduction delay. N Engl J Med.2001;344:873-880.

(4) Auricchio A, Stellbrink C, Sack S et al. Long-term clinical effect of hemodynamically optimized cardiac resynchronization therapy in patients with heart failure and ventricular conduction delay. J Am Coll Cardiol.2002;39:2026-2033.

(5) Abraham WT, Fisher WG, Smith AL et al. Cardiac resynchronization in chronic heart failure. N Engl J Med.2002;346:1845-1853.

(6) Auricchio A, Stellbrink C, Butter C et al. Clinical efficacy of cardiac resynchronization therapy using left ventricular pacing in heart failure patients stratified by severity of ventricular conduction delay. J Am Coll Cardiol.2003;42:2109-2116.

(7) Young JB, Abraham WT, Smith AL et al. Combined cardiac resynchronization and implantable cardioversion defibrillation in advanced chronic heart failure: the MIRACLE ICD Trial. JAMA.2003;289:2685-2694.

(8) Cleland JG, Daubert JC, Erdmann E et al. The effect of cardiac resynchronization on morbidity and mortality in heart failure. N Engl J Med.2005;352:1539-1549.

(9) Bristow MR, Saxon LA, Boehmer J et al. Cardiac-resynchronization therapy with or without an implantable defibrillator in advanced chronic heart failure. N Engl J Med.2004;350:2140-2150.

(10) Epstein AE, DiMarco JP, Ellenbogen KA et al. ACC/AHA/HRS 2008 Guidelines for Device-Based Therapy of Cardiac Rhythm Abnormalities: a report of the American College of Cardiology/American Heart Association Task Force on Practice Guidelines (Writing Committee to Revise the ACC/AHA/NASPE 2002 Guideline Update for Implantation of Cardiac Pacemakers and Antiarrhythmia Devices): developed in collaboration with the American Association for Thoracic Surgery and Society of Thoracic Surgeons. Circulation.2008;117:350-408.

(11) Swedberg K, Cleland J, Dargie H et al. Guidelines for the diagnosis and treatment of chronic heart failure: executive summary (update 2005): The Task Force for the Diagnosis and Treatment of Chronic Heart Failure of the European Society of Cardiology. Eur Heart J.2005;26:1115-1140.

(12) Bax JJ, Van der Wall EE, Schalij MJ. Cardiac resynchronization therapy for heart failure. N Engl J Med.2002;347:1803-1804.

(13) Bax JJ, Abraham T, Barold SS et al. Cardiac resynchronization therapy: Part 1--issues before device implantation. J Am Coll Cardiol.2005;46:2153-2167.

(14) Bax JJ, Bleeker GB, Marwick TH et al. Left ventricular dyssynchrony predicts response and prognosis after cardiac resynchronization therapy. J Am Coll Cardiol.2004;44:1834-1840.

(15) Suffoletto MS, Dohi K, Cannesson M, Saba S, Gorcsan J. Novel speckle-tracking radial strain from routine black-and-white echocardiographic images to quantify dyssynchrony and predict response to cardiac resynchronization therapy. Circulation.2006;113:960-968.

(16) Yu CM, Fung WH, Lin H, Zhang Q, Sanderson JE, Lau CP. Predictors of left ventricular reverse remodeling after cardiac resynchronization therapy for heart failure secondary to idiopathic dilated or ischemic cardiomyopathy. Am J Cardiol.2003;91:684-688.

(17) Achilli A, Sassara M, Ficili S et al. Long-term effectiveness of cardiac resynchronization therapy in patients with refractory heart failure and "narrow" QRS. J Am Coll Cardiol.2003;42:2117-2124.

(18) Bleeker GB, Holman ER, Steendijk P et al. Cardiac resynchronization therapy in patients with a narrow QRS complex. J Am Coll Cardiol.2006;48:2243-2250.

(19) Tops LF, Suffoletto MS, Bleeker GB et al. Speckle-tracking radial strain reveals left ventricular dyssynchrony in patients with permanent right ventricular pacing. J Am Coll Cardiol.2007;50:1180-1188.
(20) Marsan NA, Henneman MM, Chen J et al. Real-time 3-dimensional Echocardiography as a Novel Approach to Quantify Left Ventricular Dyssynchrony: A Comparison Study with Phase Analysis of Gated Myocardial Perfusion Single Photon Emission Computed Tomography. J Am Soc Echocardiogr.2008;21:801-807.
(21) Ajmone MN, Henneman MM, Chen J et al. Left ventricular dyssynchrony assessed by two three-dimensional imaging modalities: phase analysis of gated myocardial perfusion SPECT and tri-plane tissue Doppler imaging. Eur J Nucl Med Mol Imaging.2008;35:166-173.
(22) Lardo AC, Abraham TP, Kass DA. Magnetic resonance imaging assessment of ventricular dyssynchrony: current and emerging concepts. J Am Coll Cardiol.2005;46:2223-2228.
(23) Westenberg JJ, Lamb HJ, van der Geest RJ et al. Assessment of left ventricular dyssynchrony in patients with conduction delay and idiopathic dilated cardiomyopathy: head-to-head comparison between tissue doppler imaging and velocity-encoded magnetic resonance imaging. J Am Coll Cardiol.2006;47:2042-2048.
(24) O'Connell JW, Schreck C, Moles M et al. A unique method by which to quantitate synchrony with equilibrium radionuclide angiography. J Nucl Cardiol.2005;12:441-450.
(25) Somsen GA, Verberne HJ, Burri H, Ratib O, Righetti A. Ventricular mechanical dyssynchrony and resynchronization therapy in heart failure: a new indication for Fourier analysis of gated blood-pool radionuclide ventriculography. Nucl Med Commun.2006;27:105-112.
(26) Botvinick EH, O'Connell JW, Kadkade PP et al. Potential added value of three-dimensional reconstruction and display of single photon emission computed tomographic gated blood pool images. J Nucl Cardiol.1998;5:245-255.
(27) Vilain D, Daou D, Casset-Senon D, Faraggi M, Le GD. Optimal 3-dimensional method for right and left ventricular fourier phase analysis in electrocardiography-gated blood-pool SPECT. J Nucl Cardiol.2001;8:371-378.
(28) Chen J, Garcia EV, Folks RD et al. Onset of left ventricular mechanical contraction as determined by phase analysis of ECG-gated myocardial perfusion SPECT imaging: development of a diagnostic tool for assessment of cardiac mechanical dyssynchrony. J Nucl Cardiol.2005;12:687-695.
(29) Garcia EV, Faber TL, Cooke CD, Folks RD, Chen J, Santana C. The increasing role of quantification in clinical nuclear cardiology: the Emory approach. J Nucl Cardiol.2007;14:420-432.
(30) Chen J, Henneman MM, Trimble MA et al. Assessment of left ventricular mechanical dyssynchrony by phase analysis of ECG-gated SPECT myocardial perfusion imaging. J Nucl Cardiol.2008;15:127-136.
(31) Yu CM, Abraham WT, Bax J et al. Predictors of response to cardiac resynchronization therapy (PROSPECT)--study design. Am Heart J.2005;149:600-605.
(32) Chung ES, Leon AR, Tavazzi L et al. Results of the Predictors of Response to CRT (PROSPECT) trial. Circulation.2008;117:2608-2616.
(33) Trimble MA, Velazquez EJ, Adams GL et al. Repeatability and reproducibility of phase analysis of gated single-photon emission computed tomography myocardial perfusion imaging used to quantify cardiac dyssynchrony. Nucl Med Commun.2008;29:374-381.
(34) Trimble MA, Borges-Neto S, Velazquez EJ et al. Emerging role of myocardial perfusion imaging to evaluate patients for cardiac resynchronization therapy. Am J Cardiol.2008;102:211-217.
(35) Bonow RO, Bacharach SL, Crawford-Green C, Green MV. Influence of temporal smoothing on quantitation of left ventricular function by gated blood pool scintigraphy. Am J Cardiol.1989;64:921-925.
(36) Hoffman EJ, Huang SC, Phelps ME. Quantitation in positron emission computed tomography: 1. Effect of object size. J Comput Assist Tomogr.1979;3:299-308.
(37) Galt JR, Garcia EV, Robbins WL. Effects of myocardial wall thickness on SPECT quantification. IEEE Trans Med Imaging.1990;9:144-150.

(38) Chen J, Faber TL, Cooke CD, Garcia EV. Temporal resolution of multiharmonic phase analysis of ECG-gated myocardial perfusion SPECT studies. J Nucl Cardiol.2008;15:383-391.
(39) Henneman MM, Chen J, Ypenburg C et al. Phase analysis of gated myocardial perfusion single-photon emission computed tomography compared with tissue Doppler imaging for the assessment of left ventricular dyssynchrony. J Am Coll Cardiol.2007;49:1708-1714.
(40) Henneman MM, Chen J, Dibbets-Schneider P et al. Can LV dyssynchrony as assessed with phase analysis on gated myocardial perfusion SPECT predict response to CRT? J Nucl Med.2007;48:1104-1111.
(41) Bleeker GB, Kaandorp TA, Lamb HJ et al. Effect of posterolateral scar tissue on clinical and echocardiographic improvement after cardiac resynchronization therapy. Circulation.2006;113:969-976.
(42) Helm RH, Byrne M, Helm PA et al. Three-dimensional mapping of optimal left ventricular pacing site for cardiac resynchronization. Circulation.2007;115.953-961.
(43) Bilchick KC, Dimaano V, Wu KC et al. Magnetic Resonance Imaging Analysis of Dyssynchrony and Myocardial Scar Predicts Function Class Improvement following Cardiac Resynchronization Therapy. J Am Coll Cardiol Img.2008;1:561-568.
(44) Ypenburg C, van Bommel RJ, Delgado V et al. Optimal left ventricular lead position predicts reverse remodeling and survival after cardiac resynchronization therapy. J Am Coll Cardiol.2008;52:1402-1409.
(45) Ypenburg C, Schalij MJ, Bleeker GB et al. Extent of viability to predict response to cardiac resynchronization therapy in ischemic heart failure patients. J Nucl Med.2006;47:1565-1570.
(46) Ypenburg C, Schalij MJ, Bleeker GB et al. Impact of viability and scar tissue on response to cardiac resynchronization therapy in ischaemic heart failure patients. Eur Heart J.2007;28:33-41.
(47) Ypenburg C, Roes SD, Bleeker GB et al. Effect of total scar burden on contrast-enhanced magnetic resonance imaging on response to cardiac resynchronization therapy. Am J Cardiol.2007;99:657-660.
(48) Adelstein EC, Saba S. Scar burden by myocardial perfusion imaging predicts echocardiographic response to cardiac resynchronization therapy in ischemic cardiomyopathy. Am Heart J.2007;153:105-112.
(49) Van Campen CM, Visser FC, van der Weerdt AP et al. FDG PET as a predictor of response to resynchronisation therapy in patients with ischaemic cardiomyopathy. Eur J Nucl Med Mol Imaging.2007;34:307-308.
(50) Braunschweig F, Sorenson J, von Bibra H et al. Effects of biventricular pacing on myocardial blood flow and oxygen consumption using carbon- 11 acetate positron emission tomography in patients with heart failure. Am J Cardiol.2003;92:95-99.
(51) Nielsen JC, Bottcher M, Jensen HK, Nielsen TT, Pedersen AK, Mortensen PT. Regional myocardial perfusion during chronic biventricular pacing and after acute change of the pacing mode in patients with congestive heart failure and bundle branch block treated with an atrioventricular sequential biventricular pacemaker. Eur J Heart Fail.2003;5:179-186.
(52) Sundell J, Engblom E, Koistinen J et al. The effects of cardiac resynchronization therapy on left ventricular function, myocardial energetics, and metabolic reserve in patients with dilated cardiomyopathy and heart failure. J Am Coll Cardiol.2004;43:1027-1033.
(53) Nowak B, Stellbrink C, Sinha AM et al. Effects of cardiac resynchronization therapy on myocardial blood flow measured by oxygen-15 water positron emission tomography in idiopathic-dilated cardiomyopathy and left bundle branch block. Am J Cardiol.2004;93:496-499.
(54) Knaapen P, van Campen LM, de Cock CC et al. Effects of cardiac resynchronization therapy on myocardial perfusion reserve. Circulation.2004;110:646-651.
(55) Lindner O, Vogt J, Kammeier A et al. Effect of cardiac resynchronization therapy on global and regional oxygen consumption and myocardial blood flow in patients with non-ischaemic and ischaemic cardiomyopathy. Eur Heart J.2005;26:70-76.

(56) Lindner O, Vogt J, Kammeier et al. Cardiac re-synchronization therapy: effects on myocardial perfusion at rest, after vasodilation and oxygen consumption. Nuklearmedizin.2006;45:10-14.
(57) Neri G, Zanco P, Zanon F, Buchberger R. Effect of biventricular pacing on metabolism and perfusion in patients affected by dilated cardiomyopathy and left bundle branch block: evaluation by positron emission tomography. Europace.2003;5:111-115.
(58) Nowak B, Sinha AM, Schaefer WM et al. Cardiac resynchronization therapy homogenizes myocardial glucose metabolism and perfusion in dilated cardiomyopathy and left bundle branch block. J Am Coll Cardiol.2003;41:1523-1528.
(59) Ukkonen H, Beanlands RS, Burwash IG et al. Effect of cardiac resynchronization on myocardial efficiency and regional oxidative metabolism. Circulation.2003;107:28-31.
(60) Burri H, Sunthorn H, Somsen A et al. Improvement in cardiac sympathetic nerve activity in responders to resynchronization therapy. Europace.2008;10:374-378.
(61) Nishioka SA, Martinelli Filho M, Brandão SC et al. Cardiac sympathetic activity pre and post resynchronization therapy evaluated by 123I-MIBG myocardial scintigraphy. J Nucl Cardiol.2007;14:852-859.

Chapter **7**

Quantitative Gated SPECT-Derived Phase Analysis on Gated Myocardial Perfusion SPECT Detects Left Ventricular Dyssynchrony and Predicts Response to Cardiac Resynchronization Therapy

Mark M. Boogers, MD[1,2], Serge D. Van Kriekinge, PhD[3,4], Maureen M. Henneman, MD[1], Claudia Ypenburg, MD[1], Rutger J. Van Bommel, MD[1], Eric Boersma, PhD[5], Petra Dibbets-Schneider, MSc[6], Marcel P. Stokkel, MD, PhD[6], Martin J. Schalij, MD, PhD[1], Daniel S. Berman, MD[4, 7], Guido Germano, PhD[3,4], Jeroen J. Bax, MD, PhD[1].

[1]Department of Cardiology, Leiden University Medical Center, Leiden, the Netherlands; [2]The Interuniversity Cardiology Institute of the Netherlands, Utrecht, the Netherlands; [3]Artificial Intelligence in Medicine Program, Cedars-Sinai Medical Center, Los Angeles, CA, USA; [4]David Geffen School of Medicine, University of California, Los Angeles, CA, USA, [5]Department of Epidemiology and Statistics, Erasmus University, Rotterdam, the Netherlands; [6]Department of Nuclear Medicine, Leiden University Medical Center, Leiden, the Netherlands, [7]Department of Imaging, Cedars-Sinai Medical Center, Los Angeles, CA, USA.

Abstract

Introduction The significance of LV dyssynchrony for prediction of response to cardiac resynchronization therapy (CRT) has been demonstrated. Parameters reflecting LV dyssynchrony (phase SD, histogram bandwidth) can be derived from gated myocardial perfusion SPECT (GMPS) using phase analysis. The feasibility of LV dyssynchrony assessment with phase analysis on GMPS using Quantitative Gated SPECT (QGS) software has not been demonstrated in patients undergoing CRT. The aim of the present study was to validate the QGS algorithm for phase analysis on GMPS in a direct comparison with echocardiography using tissue Doppler imaging (TDI) for LV dyssynchrony assessment. In addition, prediction of response to CRT using GMPS and phase analysis was evaluated.

Methods Patients (n=40) with severe heart failure (NYHA class III-IV), LV ejection fraction ≤35%, QRS complex ≥120 ms were evaluated for LV dyssynchrony using GMPS and echocardiography with TDI. At baseline and after 6 months of CRT, clinical status, LV volumes and LV ejection fraction were evaluated. Patients with functional improvement were classified as CRT responders.

Results Both histogram bandwidth ($r=0.69$, $r^2=0.48$, SEE 25.4, $p<0.01$) and phase SD ($r=0.65$, $r^2=0.42$, SEE 26.8, $p<0.01$) derived from GMPS correlated significantly with TDI for assessment of LV dyssynchrony. At baseline, CRT responders showed significantly larger histogram bandwidth as compared to non-responders (94±23° vs. 68±21°, $p<0.01$) and larger phase SD (26±6° vs. 18±5°, $p<0.01$). Receiver operating characteristic (ROC) curve analysis identified an optimal cutoff value of 72.5° for histogram bandwidth to predict CRT response, yielding a sensitivity of 83% with a specificity of 81%. Similar sensitivity and specificity were obtained at a cutoff value of 19.6° for phase SD.

Conclusions QGS phase analysis on GMPS was significantly correlated with TDI for assessment of LV dyssynchrony. Moreover, a high accuracy for prediction of response to CRT was obtained using either histogram bandwidth or phase SD.

Introduction

Cardiac resynchronization therapy (CRT) has become an established therapeutic option for patients with drug-refractory heart failure. Thus far, several clinical trials have been reported, which demonstrated the beneficial effect of CRT on heart failure symptoms, quality of life score, and exercise capacity.[1, 2] In addition, CRT improved left ventricular ejection fraction (LVEF), reduced severity of mitral regurgitation and decreased LV volumes (reverse remodeling).[1, 2] Moreover, it has been demonstrated that CRT resulted in a superior survival with a reduction in heart failure hospitalization rate.[3, 4]

Although considerable benefit of CRT has been observed, one third of the patients meeting the current selection criteria do not respond to CRT.[5-8] Hence, attention has shifted towards improved patient selection for CRT.[9, 10] Particularly, observational trials have shown the significance of LV dyssynchrony for prediction of response to CRT.[6-8] LV dyssynchrony can be detected using different imaging modalities, including echocardiography with tissue Doppler imaging (TDI)[6-8], or strain (rate) imaging[11], magnetic resonance imaging (MRI)[12] or nuclear imaging with single photon emission computed tomography (SPECT).[13-18] Particularly, phase analysis of gated myocardial perfusion SPECT (GMPS) has been evaluated recently for assessment of LV dyssynchrony.[14-18] Recently, the Quantitative Gated SPECT (QGS) algorithm has been expanded to provide quantitative parameters for the assessment of LV (dys)synchrony, in addition to previously reported functional parameters.[14, 18] With this algorithm, quantification of LV (dys)synchrony is based on phase calculations for each LV surface sampling point. The aim of the current study was to further validate the QGS modified algorithm for phase analysis on GMPS, in a direct comparison with echocardiography using TDI for the assessment of LV dyssynchrony. Moreover, outcome after 6 months of CRT was evaluated and related to baseline LV dyssynchrony on GMPS.

Materials and Methods

Study Population and Protocol

The study population consisted of 40 consecutive drug-refractory heart failure patients who were scheduled for implantation of a CRT device. Eligibility for CRT was based on advanced heart failure (New York Heart Association (NYHA) functional class III-IV), depressed systolic LV function (LVEF ≤35%), prolonged QRS duration (≥120 ms) and sinus rhythm. Patients with decompensated heart failure, recent myocardial infarction (<3 months) or previously implanted pacemaker were excluded.

Before CRT implantation, all patients underwent evaluation of clinical status, GMPS with ^{99m}technetium tetrofosmin and 2-dimensional (2D) echocardiography with TDI as part of

the clinical evaluation to determine therapeutic options. The clinical status was evaluated by assessment of NYHA functional class, exercise capacity (6-minute walk test) and quality of life score [using the Minnesota Quality-of-Life (QoL) Questionnaire].[19]

Six months after CRT implantation, assessment of clinical status and 2D echocardiography with TDI were repeated. Patients with an improvement of 1 grade or more in NYHA class were classified as responders to CRT. Patients without improvement in NYHA class were considered non-responders; patients who died of progressive heart failure were also considered non-responders.

Gated Myocardial Perfusion SPECT: Data Acquisition

Resting ECG-gated GMPS with ^{99m}technetium tetrofosmin (500 MBq, injected at rest) was performed with a triple-head SPECT camera system (GCA 9300/HG; Toshiba Corporation, Tokyo, Japan). High-resolution, low-energy collimators were used and a 20% window was centered around the 140-keV energy peak of ^{99m}technetium tetrofosmin. Over a 360-degree circular orbit, 90 projections (step and shoot method, 35 s/projection, 64 x 64 matrix, total imaging time 23 min) were obtained in which data acquisition involved 16 frames per cardiac cycle. Data were reformatted into gated short-axis images by reconstruction with filtered back projection and reorientation. No attenuation correction was used. Data were displayed in polar map format and analyzed using a 17-segment model.[20] Cardiac segments with <50% tracer uptake were considered as segments with a perfusion defect.

Phase Calculations

These reconstructed images were analyzed by a modified version of the QGS algorithm[21] that provides quantitative parameters for the assessment of LV dyssynchrony, in addition to previously described functional parameters.[14] QGS operates by first computing a mid-myocardial LV surface, then computing endo- and epicardial surfaces using count-profile as well as thickening information derived from myocardial mass conservation combined with count increases caused by partial volume effects. All surfaces are generated as two-dimensional meshes in an ellipsoidal coordinate system with a fixed number of latitudinal and longitudinal samples.[21] The current version of QGS uses 36 longitudinal and 28 latitudinal samples, leading to a maximum of 1008 sampling points (usually fewer due to surface truncation by the valve plane). Subsequent phase calculations are performed using regional maximal counts obtained by searching between the endo- and epicardial surfaces, normally to the mid-myocardial surface, for each surface sampling point. A unidimensional array is created for each spatial sampling point containing the image counts at each interval. This array represents a time-varying, periodic function to which a cosine curve can be fitted. For the purposes of this analysis the constant component can be ignored, and therefore this process is equivalent to reducing the periodic function to its first Fourier harmonic (FFH), characterized by an amplitude and phase angle. Once the phase angle has been calculated

for each mid-myocardial surface point, a 2D median filter is applied to eliminate spurious variations. The window size of the filter (9 longitudinal samples out of 36, 7 latitudinal samples out of 28) was selected empirically. As phase measurements are essentially ill-defined for signals that exhibit low temporal variations[22], 5% of the samples for which the amplitude is lowest are eliminated.

(Dys)synchrony Parameters

Once phase information has been calculated for all sampling points, global and regional (dys)synchrony measures can be computed. For this study, a histogram was constructed from the phase values for the entire LV and phase standard deviation (SD) and bandwidth were calculated and examined as the global (dys)synchrony measures. Phase SD was calculated in the usual manner. Bandwidth was calculated to include 95% of histogram elements as previously reported by Chen et al.[15] Timing values can be expressed in milliseconds (ms), angles in degrees (0^o – 360^o) or as a percentage of the average duration of the cardiac cycle (0% – 100%), the latter 2 being equivalent. While timing values expressed in milliseconds have been considered more clinically relevant with echocardiography, they are also directly dependent on the heart rate, potentially rendering comparison of studies acquired with different heart rates problematic.[23] Hence, for this study all timing values are expressed in degrees.

2D Echocardiography

Transthoracic resting 2D echocardiography was performed with a commercially available system (Vivid Seven, General Electric-Vingmed, Milwaukee, Wisconsin, USA) with the patient in left lateral decubitus position. A 3.5 MHz transducer was used to obtain images at a depth of 16 cm in parasternal and apical views (standard long- and short-axis, 2- and 4-chamber images). From apical 2- and 4-chamber images, LV end-systolic (LVESV) and LV end-diastolic (LVEDV) volumes along with LVEF were calculated using the biplane Simpson's approach.[24] In addition, TDI was performed to assess LV dyssynchrony. For TDI (triggered to the QRS complex) color Doppler frame rates exceeded 80 frames/s and pulse repetition frequencies varied between 500 Hz and 1 KHz, yielding aliasing velocities between 16 cm/s and 32 cm/s. TDI images and conventional echo images were saved in cine-loop format and analyzed by 2 experienced observers blinded to the GMPS and clinical patient data. All analyses were performed using commercially available software (Echopac 6.0.1 General Electric-Vingmed, Milwaukee, Wisconsin, USA). To determine LV dyssynchrony, the sample volume was placed in the basal portions of the septum and lateral wall; peak systolic velocities and time-to-peak systolic velocities were obtained and the delay in peak systolic velocity between the septum and the lateral wall was calculated as an indicator of LV dyssynchrony.[25] Reliable tissue Doppler curves for assessment of septal-to-lateral delay were obtained in 39 patients. The peak systolic velocity analysis was limited to the LV ejection

phase (marked by opening and closure of aortic valve). Inter- and intraobserver agreement for assessment of LV dyssynchrony were 90% and 96%, respectively.[26] Substantial LV dyssynchrony on TDI was defined as a delay in peak systolic velocity ≥65 ms between the basal septum and lateral wall.[7]

CRT Implantation

The LV pacing lead was inserted transvenously via the subclavian route as reported previously.[25] A coronary sinus venogram was obtained during occlusion of the coronary sinus using a balloon catheter. The LV pacing lead was inserted in the coronary sinus with an 8 Fr guiding catheter, and positioned as far as possible in the venous system, preferably in the (postero-) lateral vein. The right atrial and right ventricular leads were positioned conventionally. For each patient the atrio-ventricular interval was adjusted to maximize the mitral inflow duration using pulsed-wave Doppler echocardiography. No adjustments were made to the V-V interval during the first 6 months of CRT. CRT device and LV lead implantation were successful in all patients without major complications; all patients received a CRT-D device (Contak Renewal, Guidant, USA; InSync III, InSync Marquis or InSync Sentry, Medtronic Inc., USA; Atlas HF, St. Jude Medical, USA) and four types of pacemaker leads were used (Acuity 4554 or Easytrak 4517-4524, Guidant; Attain 4193-4194, Medtronic; Quicksite 1056T, St. Jude Medical).

Statistical Analysis

Continuous data are expressed as mean ± SD and categorical data are presented as percentages (or numbers). When appropriate, 2-tailed paired or unpaired Student's t test and the Chi-square test were used for numerical or categorical data.

Pearson's correlation analysis was performed to evaluate the relation between histogram bandwidth and phase SD derived from GMPS and LV dyssynchrony derived from TDI. Next, univariate and multivariate analyses were performed to determine predictors of response to CRT. Receiver operating characteristic (ROC) curve analyses were performed to determine the optimal cutoff values of histogram bandwidth and phase SD to predict response to CRT. The highest sum of sensitivity and specificity was considered as the optimal cutoff value for prediction of response to CRT. For all analyses, a p-value <0.05 was considered statistically significant.

Results

Study Population

Baseline characteristics of the 40 patients (32 men, mean age 63±8 years) are summarized in Table 1. The etiology of heart failure was ischemic cardiomyopathy in 70% of patients and idiopathic dilated cardiomyopathy in 30%. Medication consisted of diuretics (90% of patients), ACE inhibitors (90% of patients) and beta-blockers (75% of patients) in maximum tolerated dosages. Prior to CRT implantation, the mean NYHA functional class was 3.1±0.4 and the mean QoL score was 38±19. On the surface ECG, the mean QRS interval was 156±34 ms and the 6-minute walking distance was 323±96 m. On 2D echocardiography, the mean LVESV was 193±79 ml, with a mean LVEDV of 252±84 ml and a mean LVEF of 25±8%. Mean heart rate during GMPS was 68.6±12.9 beats/min, whereas mean heart rate during TDI was 68.5±13.2 beats/min (p=NS). The mean number of cardiac segments with a perfusion defect was 6±3.

Table 1. Baseline characteristics of the study population (n=40)

Age (yrs)	63±8
Gender (M/F)	32/8
Etiology of heart failure	
Ischemic cardiomyopathy	28 (70%)
Idiopathic dilated cardiomyopathy	12 (30%)
NYHA functional class	3.1±0.4
QoL score	38±19
6-min walking distance (m)	323±96
QRS duration (ms)	156±34
LVEDV (ml)	252±84
LVESV (ml)	193±79
LVEF (%)	25±8
Cardiac segments with perfusion defect	6±3

Data are presented as mean ± standard deviation or as number (%). LVEDV = left ventricular end-diastolic volume; LVEF = left ventricular ejection fraction; LVESV = left ventricular end-systolic volume; NYHA = New York Heart Association; QoL = quality of life.

LV Dyssynchrony: Gated Myocardial Perfusion SPECT versus Tissue Doppler Imaging

Phase analysis on GMPS yielded a mean histogram bandwidth of 84±26° (range 40° to 152°) and a mean phase SD of 23±7° (range 12° to 41°). On TDI, the mean LV dyssynchrony was 53±35 ms (range 0 to 130 ms). Pearson's correlation showed a significant correlation between LV dyssynchrony on TDI and histogram bandwidth on GMPS ($r=0.69$, $r^2=0.48$, SEE 25.4, n=39, $p<0.01$, Figure 1A). Also, a significant correlation between LV dyssynchrony on

TDI and phase SD on GMPS was demonstrated (r=0.65, r^2=0.42, SEE = 26.8, n=39, p<0.01, Figure 1B). Finally, pearson correlation showed a good correlation between histogram bandwidth and phase SD (r=0.95, r^2=0.91, SEE 8.0, p<0.01).

Importantly, patients with LV dyssynchrony ≥65 ms on TDI (indicating substantial LV dyssynchrony) had significantly larger histogram bandwidth and phase SD as compared to patients with LV dyssynchrony <65 ms on TDI (Figure 2).

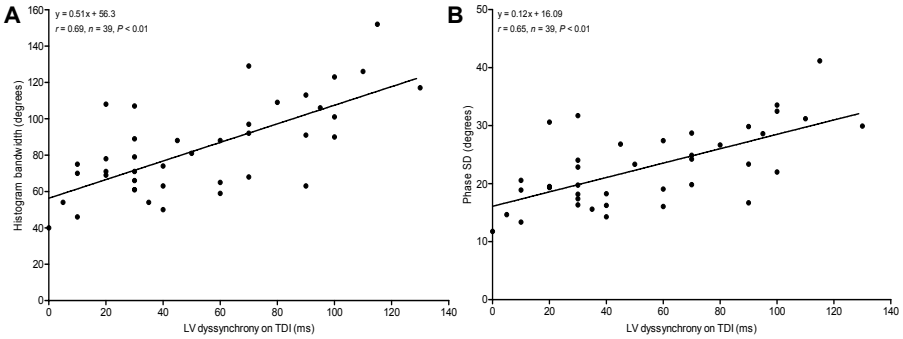

Figure 1. Agreement between left ventricular (LV) dyssynchrony on tissue Doppler imaging (TDI) and histogram bandwidth (A) or phase standard deviation (SD) (B) derived from gated myocardial perfusion single photon emission computed tomography (SPECT). Significant correlation between LV dyssynchrony on TDI and histogram bandwidth or phase SD as assessed with gated myocardial perfusion SPECT was observed.

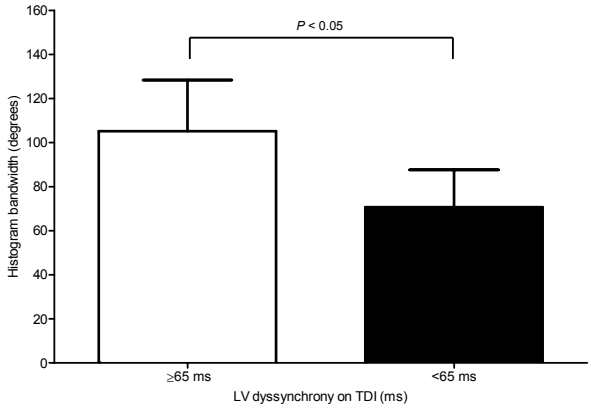

Figure 2A. The histogram bandwidth was significantly larger in patients with substantial left ventricular (LV) dyssynchrony on tissue Doppler imaging (TDI) (defined as mechanical delay between the basal septum and lateral wall ≥65 ms) as compared to patients without LV dyssynchrony (delay <65 ms) on TDI (105±23 versus 71±17, p <0.05).

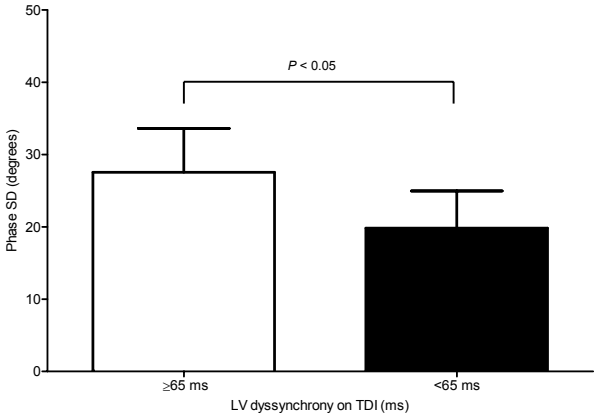

Figure 2B. The phase standard deviation (SD) was significantly larger in patients with substantial left ventricular (LV) dyssynchrony on tissue Doppler imaging (TDI) (defined as mechanical delay between the basal septum and lateral wall ≥65 ms) as compared to patients without LV dyssynchrony (delay <65 ms) on TDI (28±6 versus 20±5, p<0.05).

Clinical Responders and Non-responders

At 6 months follow-up, 24 (60%) patients showed an improvement of 1 or more grades in NYHA functional class and were considered responders to CRT. Among the 16 (40%) non-responders, 5 patients died within 6 months of CRT due to progressive heart failure.

In Table 2, baseline clinical and imaging variables are summarized for responders and non-responders. Responders showed a significantly longer 6-minute walking distance and larger LVEDV. Furthermore, responders had significantly more LV dyssynchrony on TDI (Figure 3).

Concerning the GMPS data, responders showed significantly larger histogram bandwidth (94±23° vs. 68±21°, p<0.01) and phase SD (26±6° vs. 18±5°, p<0.01) as compared to non-responders. Responders to CRT showed significantly lower number of cardiac segments with perfusion defects as compared to non-responders to CRT (5±2 vs. 8±2, p<0.01). Examples of GMPS data in patients with and without response to CRT are shown in Figure 4.

Table 2. Baseline characteristics clinical responders and non-responders

Baseline characteristics	Responders (n=24)	Non-responders (n=16)	p-value
Age (yrs)	62±8	64±9	NS
Gender (M/F)	20/4	12/4	NS
Ischemic etiology	16 (67)	12 (75)	NS
Clinical evaluation			
NYHA class	3.0±0.2	3.2±0.5	NS
QoL score	34±17	45±20	NS
6-MWT (m)	354±81	272±99	0.01
QRS (ms)	162±35	146±31	NS
2D echocardiographic parameters			
LVEDV (ml)	274±79	219±83	0.04
LVESV (ml)	211±75	167±78	NS
LVEF (%)	24±8	25±8	NS
LV dyssynchrony (ms)	62±37	40±26	0.04
Phase distribution			
Bandwidth (°)	94±23	68±21	<0.01
Phase SD (°)	26±6	18±5	<0.01
Segments with perfusion defect	5±2	8±2	<0.01

Data are presented as mean ± standard deviation or as number (%). 2D = 2-dimensional; LVEDV = left ventricular end-diastolic volume; LVEF = left ventricular ejection fraction; LVESV = left ventricular end-systolic volume; 6-MWT = 6-minute walk test; NYHA = New York Heart Association; QoL = quality of life; SD = standard deviation.

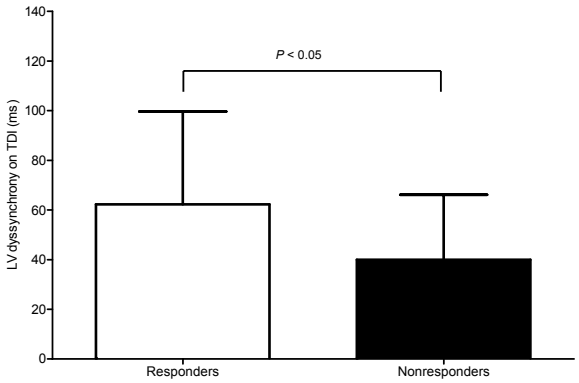

Figure 3. The extent of left ventricular (LV) dyssynchrony on tissue Doppler imaging (TDI) at baseline was significantly larger in responders to cardiac resynchronization therapy (CRT) as compared to non-responders (62±37 ms versus 40±26 ms, p<0.05).

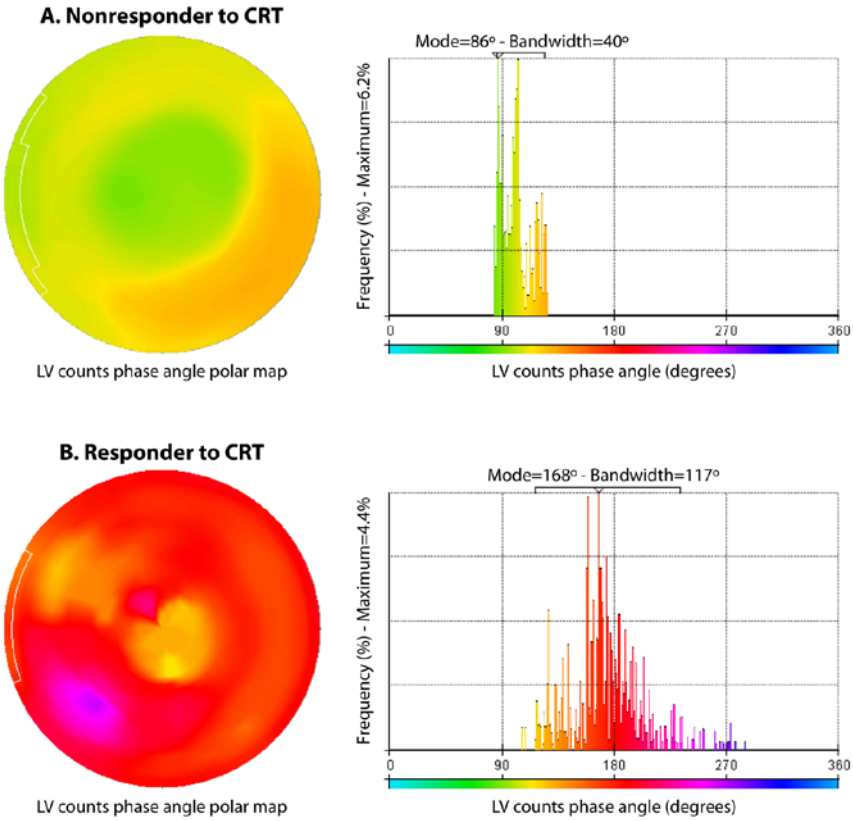

Figure 4. A: Example of a patient without left ventricular (LV) dyssynchrony on gated myocardial perfusion SPECT (GMPS). Synchronous contraction pattern is reflected by a homogeneous phase angle distribution of the polar map (left) and the narrow highly-peaked histogram (right). At 6 months follow-up, no improvement in NYHA functional class was observed and LV ejection fraction remained unchanged (32% at baseline versus 33% at 6 months follow-up).
B: Example of a patient with extensive LV dyssynchrony on GMPS. LV dyssynchrony is indicated by the heterogeneous phase angle distribution of the polar map (left) and the wide histogram (right). At 6 months follow-up, NYHA functional class improved from 3 to 2, with an increase in LV ejection fraction from 21% to 33%.

Baseline and 6 months Follow-up Data

At 6 months follow-up, responders showed significant improvement in NYHA functional class, quality of life score and 6-minute walk distance, whereas non-responders did not show significant improvement in any of the clinical parameters (Table 3). Furthermore, only responders demonstrated a significant decrease in LVEDV and LVESV with a significant increase in LVEF at 6 months follow-up.

Univariate analysis was performed on clinical, echocardiographic and GMPS variables and demonstrated that 6-minute walk distance, LVEDV and LV dyssynchrony on TDI were

predictors of response to CRT at 6 months follow-up. In addition, histogram bandwidth and phase SD were predictive of CRT response at 6 months follow-up. Multivariate analysis showed that 6-minute walk distance and phase SD were the only independent predictors for response to CRT. ROC curve analysis was used to define the optimal threshold for prediction of response to CRT. For histogram bandwidth, optimal cutoff value was defined at 72.5° which yielded a sensitivity of 83% and a specificity of 81%; the area under the curve was 0.83 (Figure 5A). For phase SD, optimal cutoff value was defined at 19.6° yielding a sensitivity of 83% and a specificity of 81%; the area under the curve was 0.85 (Figure 5B).

Table 3. Baseline and 6 months follow-up characteristics: responders versus non-responders

Baseline characteristics	Responders (n=24)	Non-responders (n=16)	p-value
NYHA class			
Baseline	3.0±0.2	3.2±0.5	NS
Follow-up	1.7±0.5*	3.2±0.5	<0.01
QoL score			
Baseline	34.4±17.4	44.9±20.4	NS
Follow-up	21.6±19.2*	40.0±16.3	<0.05
6-MWT (m)			
Baseline	353.9±80.9	272.2±99.4	<0.05
Follow-up	439.8±102.9*	326.8±108.6	<0.05
LVEDV (mL)			
Baseline	274.4±79.2	219.3±82.8	<0.05
Follow-up	243.7±77.0*	180.7±56.5	<0.05
LVESV (mL)			
Baseline	210.5±75.4	167.1±78.4	NS
Follow-up	166.8±76.8*	129.3±50.1	NS
LVEF (%)			
Baseline	23.9±7.5	25.4±8.1	NS
Follow-up	33.8±12.7*	30.0±8.1	NS
LV dyssynchrony (ms)			
Baseline	62.3±37.4	40.0±26.1	<0.05
Follow-up	40.4±32.5	33.2±31.6	NS

Data are presented as mean ± standard deviation or as absolute number (%). Abbreviations as in Table 2. * $p<0.05$ follow-up versus baseline.

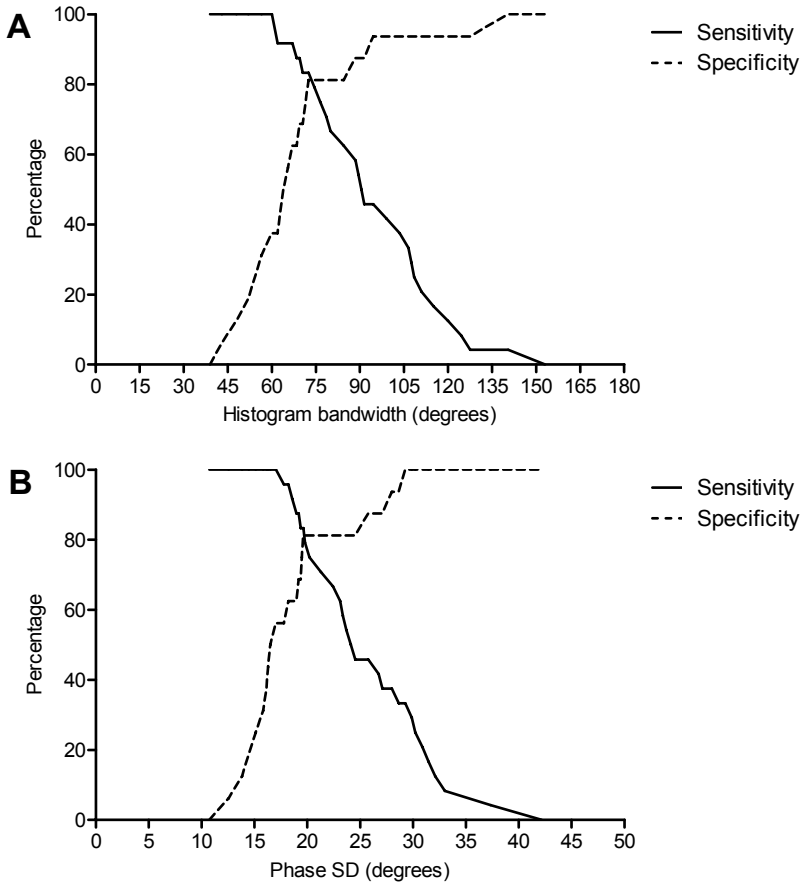

Figure 5. ROC curve analysis for histogram bandwidth (A) and phase standard deviation (SD) (B) for prediction of response to cardiac resynchronization therapy (CRT). ROC curve analysis for histogram bandwidth showed a good predictive value (AUC 0.83) for prediction of response to CRT. Optimal cutoff value was defined at 72.5° yielding a sensitivity of 83% with a specificity of 81%. For phase SD, ROC curve analysis demonstrated a good predictive value (AUC 0.85) for prediction of response to CRT. Optimal cutoff value was defined at 19.6° yielding a sensitivity of 83% with a specificity of 81%.

Discussion

The main observations are as follows: phase analysis on GMPS and echocardiography using TDI showed significant correlation for assessment of LV dyssynchrony. Moreover, both histogram bandwidth and phase SD derived from GMPS were predictive of CRT response at 6 months follow-up. For histogram bandwidth, an optimal cutoff value of 72.5° yielded a sensitivity of 83% with a specificity of 81% to predict response to CRT; for phase SD, a cutoff value of 19.6° yielded similar sensitivity and specificity.

LV Dyssynchrony Derived from GMPS

The current selection criteria for CRT have selected patients meeting the current American Heart Association/American college of Cardiology/European Society of Cardiology guidelines which recommend CRT in patients with NYHA class III or IV, LVEF ≤35%, and a prolonged QRS interval ≥120 ms.[6-10]

However, a substantial amount of the selected patients do not show response to CRT.[2, 5-8] As a consequence, efforts have been made to improve current selection criteria on CRT and previous studies have demonstrated that LV dyssynchrony is related to CRT response and may have additional value in the selection of potential candidates for CRT.[6-8] One of the potential explanations of non-response in patients meeting contemporary guidelines is the fact that a wide QRS complex may reflect interventricular rather than intraventricular dyssynchrony.[26]

To detect LV dyssynchrony a variety of imaging techniques can be used, including echocardiography using TDI[6-8], or myocardial strain (rate) imaging[11], magnetic resonance imaging[12] and nuclear imaging using GMPS.[14-18] Most studies on CRT have reported on echocardiographic methods to assess LV dyssynchrony; in particular echocardiography using TDI has been employed as a tool for assessment of LV dyssynchrony.[6-8] Recently, the feasibility of phase analysis on GMPS for detection of LV dyssynchrony has been shown.[27, 28] This approach provides automatically quantitative parameters of LV dyssynchrony using count-based analysis and has been developed to extract amplitude and phase angle from changes in counts per region during the cardiac cycle.[14-17] Amplitude of the phase curve indicates maximal systolic wall thickening, whereas phase angle is indicative of the beginning of mechanical contraction per region, providing information on the degree of hetero- or homogeneity of the mechanical activation pattern within the ventricle. A histogram was constructed that represents the distribution of the phase angle for all sample points of the LV, providing quantitative parameters for LV dyssynchrony including histogram bandwidth (includes 95% of the elements of the phase histogram) and phase SD (SD of phase distribution).[18]

Various studies have shown that this approach can detect LV dyssynchrony in patients with heart failure and wide QRS complex.[27, 28] Subsequent studies have shown the relation

between phase analysis on GMPS and echocardiographic techniques for assessment of LV dyssynchrony.[29, 30] Henneman and colleagues[29] have evaluated 75 heart failure patients with wide QRS complex in a head-to-head comparison between phase analysis on GMPS and 2D echocardiography using TDI. The authors have demonstrated that histogram bandwidth and phase SD derived from GMPS related well with LV dyssynchrony derived from TDI. Marsan et al.[30] have used real-time 3D echocardiography and also demonstrated good relation with phase analysis on GMPS for detection of LV dyssynchrony in 40 patients with heart failure. In the current study, GMPS data were processed with the QGS algorithm which was expanded to provide quantitative parameters for the assessment of LV dyssynchrony. It was shown that LV dyssynchrony derived from TDI related significantly with histogram bandwidth and phase SD obtained with the QGS algorithm.

GMPS for Prediction of Response to CRT

Many studies performed with echocardiography have shown that LV dyssynchrony is predictive for response to CRT.[6-8] Only 1 study has reported on the use of GMPS for prediction of response to CRT[31]; 42 patients with heart failure, NYHA class III-IV, LVEF <35%, QRS >120 ms underwent GMPS before CRT implantation. In the patients, reflectors of LV dyssynchrony (phase SD and histogram bandwidth) were identified as predictors of response to CRT over a 6 months follow-up period. Particularly, a cutoff value of 43° for phase SD yielded a sensitivity and specificity of 74% for prediction of response to CRT; a cutoff value of 135° for histogram bandwidth had a sensitivity and specificity of 70%. In the current study, a different algorithm was used derived from the QGS program, for assessment of phase SD and histogram bandwidth. In line with previous work[31], histogram bandwidth and phase SD were significantly larger in CRT responders as compared to non-responders (Table 2). When ROC curve analysis was applied, a cutoff value of 19.6° for phase SD yielded a sensitivity of 83% with a specificity of 81% (with area under the curve 0.85) to predict response to CRT at 6 months follow-up. For histogram bandwidth a similar sensitivity and specificity were obtained at a cutoff value of 72.5° (with area under the curve 0.83). The accuracy to predict response to CRT in the current study is in line with earlier work using different software to analyze GMPS.[31] The optimal cutoff values for phase SD and histogram bandwidth in the present study are not identical to the values obtained in the study by Henneman et al.[31], and this may be related to differences in software packages or to differences in study populations. One of the major differences between these packages is the fact that QGS uses an ellipsoidal sampling system[21], as opposed to the hybrid cylindrical-spherical coordinate system used by the Emory Cardiac Toolbox.[32]

In both the study by Henneman et al.[31] and the current study, accuracy of GMPS to predict response to CRT was not perfect. In comparison to TDI, however, GMPS has advantages of providing global measurements and that the measurements are automatically derived. Given these advantages and the accuracy demonstrated by this and previous work, GMPS

may provide a reasonable alternative for clinical use to TDI in predicting CRT response. It is not realistic to expect a perfect accuracy for prediction of CRT response based solely on LV dyssynchrony. Indeed, recent work has indicated that other issues than LV dyssynchrony are important for response to CRT. Scar tissue has been identified as an important factor limiting the response to CRT.[33, 34] It has been shown that the extent of scar tissue was inversely related to the response to CRT; also, patients with scar tissue in the region where the LV lead was positioned did not respond well to CRT and the extent (the total scar burden) of scar tissue have been shown to prevent response to CRT. It would therefore be preferred to not only assess the presence of LV dyssynchrony, but also the extent and location of scar tissue in the left ventricle. In this perspective, GMPS has the potential to provide both these parameters from the same dataset.

Finally, it has been shown that patients with the LV lead positioned outside the region of latest mechanical activation had less benefit from CRT, as compared to patients with the lead positioned in the area of latest activation.[35] More recently, Ypenburg et al.[36] have reported on the outcome of patients undergoing CRT with the LV lead positioned at or outside the region of latest mechanical activation and demonstrated that long-term survival was better when the LV pacing lead was positioned at the site of latest mechanical activation.

Limitations

The current study should be considered as a feasibility study, validating a new algorithm on phase analysis with QGS. As indicated above, patients with extensive scar tissue in the left ventricle benefit less from CRT. In addition, patients with the LV pacing lead located outside the region of latest mechanical activation will have a less favorable response to CRT. In the current study, only the number of cardiac segments with a perfusion defect was integrated, but to provide a meaningful analysis on all these issues, a much larger study population is needed. Whether integration of all this information will result in superior prediction of response to CRT needs further testing in future studies.

Conclusion

Phase analysis on GMPS using QGS software, correlated significantly with TDI for assessment of LV dyssynchrony. In addition, both phase SD and histogram bandwidth were predictive of response to CRT. Larger studies are needed to confirm these findings and to explore the relative clinical effectiveness of GMPS and TDI in prediction of response to TDI.

Reference List

1 Cazeau S, Leclercq C, Lavergne T, et al. Effects of multisite biventricular pacing in patients with heart failure and intraventricular conduction delay. N Engl J Med. 2001;344:873-880.

2 Abraham WT, Fisher WG, Smith AL, et al. Cardiac resynchronization in chronic heart failure. N Engl J Med. 2002;346:1845-1853.

3 Cleland JG, Daubert JC, Erdmann E, et al. The effect of cardiac resynchronization on morbidity and mortality in heart failure. N Engl J Med. 2005;352:1539-1549.

4 Bristow MR, Saxon LA, Boehmer J, et al. Cardiac-resynchronization therapy with or without an implantable defibrillator in advanced chronic heart failure. N Engl J Med. 2004;350:2140-2150.

5 Bax JJ, Van der Wall EE, Schalij MJ. Cardiac resynchronization therapy for heart failure. N Engl J Med. 2002;347:1803-1804.

6 Yu CM, Fung WH, Lin H, Zhang Q, Sanderson JE, Lau CP. Predictors of left ventricular reverse remodeling after cardiac resynchronization therapy for heart failure secondary to idiopathic dilated or ischemic cardiomyopathy. Am J Cardiol. 2003;91:684-688.

7 Bax JJ, Bleeker GB, Marwick TH, et al. Left ventricular dyssynchrony predicts response and prognosis after cardiac resynchronization therapy. J Am Coll Cardiol. 2004;44:1834-1840.

8 Bax JJ, Abraham T, Barold SS, et al. Cardiac resynchronization therapy: Part 1--issues before device implantation. J Am Coll Cardiol. 2005;46:2153-2167.

9 Hunt SA, Abraham WT, Chin MH, et al. ACC/AHA 2005 Guideline Update for the Diagnosis and Management of Chronic Heart Failure in the Adult: a report of the American College of Cardiology/American Heart Association Task Force on Practice Guidelines: developed in collaboration with the American College of Chest Physicians and the International Society for Heart and Lung Transplantation: endorsed by the Heart Rhythm Society. Circulation. 2005;112:154-235.

10 Swedberg K, Cleland J, Dargie H, et al. Guidelines for the diagnosis and treatment of chronic heart failure: executive summary: The Task Force for the Diagnosis and Treatment of Chronic Heart Failure of the European Society of Cardiology. Eur Heart J. 2005;26:1115-1140.

11 Delgado V, Ypenburg C, van Bommel RJ, et al. Assessment of left ventricular dyssynchrony by speckle tracking strain imaging comparison between longitudinal, circumferential, and radial strain in cardiac resynchronization therapy. J Am Coll Cardiol. 2008;51:1944-1952.

12 Westenberg JJ, Lamb HJ, van der Geest RJ, et al. Assessment of left ventricular dyssynchrony in patients with conduction delay and idiopathic dilated cardiomyopathy: head-to-head comparison between tissue doppler imaging and velocity-encoded magnetic resonance imaging. J Am Coll Cardiol. 2006;47:2042-2048.

13 Vilain D, Daou D, Casset-Senon D, Faraggi M, Le GD. Optimal 3-dimensional method for right and left ventricular fourier phase analysis in electrocardiography-gated blood-pool SPECT. J Nucl Cardiol. 2001;8:371-378.

14 Germano G, Erel J, Lewin H, Kavanagh PB, Berman DS. Automatic quantitation of regional myocardial wall motion and thickening from gated technetium-99m sestamibi myocardial perfusion single-photon emission computed tomography. J Am Coll Cardiol. 1997;30:1360-1367.

15 Chen J, Garcia EV, Folks RD, et al. Onset of left ventricular mechanical contraction as determined by phase analysis of ECG-gated myocardial perfusion SPECT imaging: development of a diagnostic tool for assessment of cardiac mechanical dyssynchrony. J Nucl Cardiol. 2005;12:687-695.

16 Garcia EV, Faber TL, Cooke CD, Folks RD, Chen J, Santana C. The increasing role of quantification in clinical nuclear cardiology: the Emory approach. J Nucl Cardiol. 2007;14:420-432.

17 Germano G, Kavanagh PB, Slomka PJ, Van Kriekinge SD, Pollard G, Berman DS. Quantitation in gated perfusion SPECT imaging: the Cedars-Sinai approach. J Nucl Cardiol. 2007;14:433-454.

18 Van Kriekinge SD, Nishina H, Ohba M, Berman DS, Germano G. Automatic Global and Regional Phase Analysis from Gated Myocardial Perfusion SPECT Imaging: Application to the

Characterization of Ventricular Contraction in Patients with Left Bundle Branch Block. J Nucl Med. 2008;49:1790-1797.
19 Rector TS, Kubo SH, Cohn JN. Validity of the Minnesota Living with Heart Failure questionnaire as a measure of therapeutic response to enalapril or placebo. Am J Cardiol. 1993;71:1106-1107.
20 Cerqueira MD, Weissman NJ, Dilsizian V, et al. Standardized myocardial segmentation and nomenclature for tomographic imaging of the heart. A statement for healthcare professionals from the Cardiac Imaging Committee of the Council on Clinical Cardiology of the American Heart. Association. Int J Cardiovasc Imaging. 2002;18:539–542.
21 Germano G, Kiat H, Kavanagh PB, et al. Automatic quantification of ejection fraction from gated myocardial perfusion SPECT. J Nucl Med. 1995; 36:2138-2147.
22 O'Connell JW, Schreck C, Moles M, et al. A unique method by which to quantitate synchrony with equilibrium radionuclide angiography. J Nucl Cardiol. 2005;12:441-450.
23 Kapetanakis S, Kearney MT, Siva A, Gall N, Cooklin M, Monaghan MJ. Real-time three-dimensional echocardiography: a novel technique to quantify global left ventricular mechanical dyssynchrony. Circulation. 2005;112:992-1000.
24 Schiller NB, Shah PM, Crawford M, et al. Recommendations for quantitation of the left ventricle by two-dimensional echocardiography. American Society of Echocardiography Committee on Standards, Subcommittee on Quantitation of Two-Dimensional Echocardiograms. J Am Soc Echocardiogr. 1989;2:358-367.
25 Bleeker GB, Kaandorp TA, Lamb HJ, et al. Effect of posterolateral scar tissue on clinical and echocardiographic improvement after cardiac resynchronization therapy. Circulation. 2006;113:969-976.
26 Bleeker GB, Schalij MJ, Molhoek SG, et al. Relationship between QRS duration and left ventricular dyssynchrony in patients with end-stage heart failure. J Cardiovasc Electrophysiol. 2004;15:544-549.
27 Trimble MA, Borges-Neto S, Smallheiser S, et al. Evaluation of left ventricular mechanical dyssynchrony as determined by phase analysis of ECG-gated SPECT myocardial perfusion imaging in patients with left ventricular dysfunction and conduction disturbances. J Nucl Cardiol. 2007;14:298-307.
28 Trimble MA, Velazquez EJ, Adams GL, et al. Repeatability and reproducibility of phase analysis of gated single-photon emission computed tomography myocardial perfusion imaging used to quantify cardiac dyssynchrony. Nucl Med Commun. 2008;29:374-381.
29 Henneman MM, Chen J, Ypenburg C, et al. Phase analysis of gated myocardial perfusion single-photon emission computed tomography compared with tissue Doppler imaging for the assessment of left ventricular dyssynchrony. J Am Coll Cardiol. 2007;49:1708-1714.
30 Marsan NA, Henneman MM, Chen J, et al. Real-time 3-dimensional Echocardiography as a Novel Approach to Quantify Left Ventricular Dyssynchrony: A Comparison Study with Phase Analysis of Gated Myocardial Perfusion Single Photon Emission Computed Tomography. J Am Soc Echocardiogr. 2008;21:801-807.
31 Henneman MM, Chen J, Dibbets-Schneider P, et al. Can LV dyssynchrony as assessed with phase analysis on gated myocardial perfusion SPECT predict response to CRT? J Nucl Med. 2007;48:1104-1111.
32 Faber TL, Cooke CD, Folks RD, Vansant JP, Nichols KJ, DePuey EG, Pettigrew RI, Garcia EV. Left ventricular function and perfusion from gated SPECT perfusion images: an integrated method. J Nucl Med 1999; 40:650-659.
33 White JA, Yee R, Yuan X, et al. Delayed enhancement magnetic resonance imaging predicts response to cardiac resynchronization therapy in patients with intraventricular dyssynchrony. J Am Coll Cardiol. 2006;48:1953-1960.

34 Adelstein EC, Saba S. Scar burden by myocardial perfusion imaging predicts echocardiographic response to cardiac resynchronization therapy in ischemic cardiomyopathy. Am Heart J. 2007;153:105-112.

35 Murphy RT, Sigurdsson G, Mulamalla S, et al. Tissue synchronization imaging and optimal left ventricular pacing site in cardiac resynchronization therapy. Am J Cardiol. 2006;97:1615-1621.

36 Ypenburg C, van Bommel RJ, Delgado V, et al. Optimal left ventricular lead position predicts reverse remodeling and survival after cardiac resynchronization therapy. J Am Coll Cardiol. 2008;52:1402-1409.

Chapter **8**

Optimal Left Ventricular Lead Position Assessed with Phase Analysis on Gated Myocardial Perfusion SPECT

Mark J. Boogers, MD[1,2], Ji Chen, PhD[3], Rutger J. van Bommel, MD[1], C. Jan Willem Borleffs, MD[1], Petra Dibbets-Schneider, MSc[4], Bernies van der Hiel, MD[4]; Imad Al Younis, MD[4], Martin J. Schalij, MD, PhD[1], Ernst E. van der Wall, MD, PhD[1], Ernest V. Garcia, PhD[3], Jeroen J. Bax, MD, PhD[1].

[1]Department of Cardiology, Leiden University Medical Center, Leiden, the Netherlands; [2]The Interuniversity Cardiology Institute of the Netherlands, Utrecht, the Netherlands; [3]Department of Radiology, Emory University School of Medicine, Atlanta, Georgia, USA; [4]Department of Nuclear Medicine, Leiden University Medical Center, Leiden, the Netherlands.

Abstract

Purpose The current study aimed to evaluate the relation between the site of latest mechanical activation as assessed with gated myocardial perfusion SPECT (GMPS), left ventricular (LV) lead position and response to cardiac resynchronization therapy (CRT).

Methods The patient population consisted of consecutive advanced heart failure patients currently indicated for CRT. Before implantation, 2D echocardiography and GMPS were performed. 2D echocardiography was performed to assess LV end-systolic volume (LVESV), LV end-diastolic volume (LVEDV) and LV ejection fraction (LVEF). The site of latest mechanical activation was assessed by phase analysis on GMPS and related to LV lead position on fluoroscopy. Echocardiography was repeated after 6 months of CRT. CRT response was defined as >15% decrease in LVESV.

Results Ninety patients (72% men, 67±10 yrs) with advanced heart failure were enrolled. In 52 (58%) patients, the LV lead was positioned at the site of latest mechanical activation (concordant), whereas the LV lead was positioned outside the site of latest mechanical activation (discordant) in 38 (42%) patients. CRT response was significantly more often documented in patients with concordant LV lead position than in patients with discordant LV lead position (79% vs. 26%, $p<0.01$). After 6 months, patients with concordant LV lead position showed significant improvement in LVEF, LVESV and LVEDV ($p<0.05$), whereas patients with discordant LV lead position showed no significant improvement in these variables.

Conclusions Patients with concordant LV lead position showed significant improvement in LV volumes and LV systolic function, whereas patients with discordant LV lead position showed no significant improvements.

Introduction

Cardiac resynchronization therapy (CRT) represents an established therapeutic option for patients with drug-refractory advanced heart failure and ventricular conduction delay.[1, 2] The merits of CRT have been demonstrated for morbidity and mortality in several randomized clinical trials which have currently included more than 4,000 patients diagnosed with moderate-to-severe heart failure.[3-6] Even though promising results have been reported, individual response to CRT varies with up to one-third of the heart failure patients showing no success to CRT.[5, 7]

Different mechanisms play an important role in the response to CRT, such as pre-existent mechanical dyssynchrony, location and extent of scarred myocardium and the position of the left ventricular (LV) pacing lead.[7, 8] The region of LV pacing and the area of latest mechanical activation, seem to be important factors in the prediction of outcome to CRT.[9-14] To date, the LV pacing lead is usually positioned in the lateral or posterolateral vein of the coronary sinus, since the largest hemodynamic response was observed when pacing the free lateral wall.[9] However, recent studies have also demonstrated that the region of latest mechanical activation may vary significantly in patients eligible for CRT.[10, 14-16] Previous studies using echocardiography have reported that patients with the LV lead positioned at the site of latest mechanical activation (concordant LV lead) showed superior response to CRT when compared to patients with the LV lead positioned outside the area of latest mechanical activation (discordant LV lead).[10, 14-16]

Phase analysis on gated myocardial perfusion single photon emission computed tomography (SPECT) (GMPS) has been developed to evaluate the presence and extent of mechanical dyssynchrony using an automatic and standardized approach.[17, 18] Recent developments have resulted in an integrated evaluation of mechanical dyssynchrony, regional mechanical activation pattern and the site of latest mechanical activation using the same SPECT data set. Hence, GMPS with phase analysis may provide important information for assessment of optimal LV lead position in patients referred for CRT. Currently, no study has been performed evaluating the use of GMPS to assess the preferred LV lead position. Moreover, the relation between the site of latest mechanical activation as derived from GMPS, LV lead position and CRT response is unknown. Accordingly, the current study sought to evaluate the feasibility of GMPS to assess the preferred LV lead position. In addition, the study aimed to evaluate the relation between the site of latest mechanical activation, LV lead position and CRT response in patients with CRT.

Materials and Methods

Patient Population and Protocol

Patients with advanced drug-refractory heart failure (New York Heart Association (NYHA) functional class III-IV), reduced LV systolic function (left ventricular ejection fraction (LVEF) ≤35%), prolonged QRS interval (≥120 ms) and sinus rhythm were consecutively included for implantation of a CRT device.[1, 2] Patients with decompensated heart failure, recent myocardial infarction (within 3 months of CRT device implantation) or who died during 6-months follow-up were excluded. Ischemic cardiomyopathy was defined as the presence of ≥50% stenosis in one or more of the major epicardial coronary arteries and/or previous myocardial infarction or percutaneous coronary intervention.

Prior to CRT device implantation, resting GMPS with ^{99m}technetium tetrofosmin and transthoracic 2D echocardiography were performed in all patients. Clinical status was evaluated by assessment of NYHA functional class. Resting myocardial perfusion imaging was performed to assess the presence and extent of myocardial infarction, whereas phase analyses of GMPS studies was used to assess the site of latest mechanical activation. Resting transthoracic 2D echocardiography was performed to measure LVEF and LV volumes. Additionally, speckle tracking radial strain analysis on 2D echocardiography was performed in a subset of 50 patients to validate the assessment of the site of latest mechanical activation as derived from GMPS.

After 6 months of CRT, assessment of clinical status and resting 2D transthoracic echocardiography were repeated. Patients with a decrease of >15% in LV end-systolic volume (LVESV) were classified as responders to CRT, whereas patients with a <15% decrease in LVESV were classified as non-responders to CRT.[19] Consecutively, the relation between the site of latest mechanical activation on GMPS, LV lead position and CRT response was evaluated.

Gated Myocardial Perfusion SPECT: Acquisition

GMPS with ^{99m}technetium tetrofosmin (500 MBq, MYOVIEW, General Electric Healthcare, United Kingdom) was performed at rest using a triple-head SPECT camera system (GCA 9300/HG; Toshiba Corporation, Tokyo, Japan) equipped with low-energy high-resolution collimators. A 20% window was used around the 140-KeV energy peak of ^{99m}technetium tetrofosmin and 90 projections (step and shoot method, 35 s/projection, 64 x 64 matrix, total imaging time 23 minutes) were obtained over a 360° circular orbit. Acquisition involved 16 frames per cardiac cycle. Data were reconstructed by filtered back projection and reoriented into long- and short-axis projections perpendicular to the heart axis.[20] The short-axis slices were displayed in polar map format and they were normalized for maximal myocardial activity (100%). No attenuation correction was used in this study. Two

experienced observers who were blinded to other study data evaluated the SPECT studies. Cardiac segments with <50% tracer uptake were considered as segments with a perfusion defect. The extent of myocardial perfusion defects (<50% tracer uptake) was expressed as a percentage of the myocardium. Consecutively, reoriented gated short-axis images were submitted to the Emory Cardiac Toolbox (Emory University, Atlanta, Georgia, USA) for phase analysis processing. Phase analysis measurements were performed at the Emory University (blinded to echocardiographic and clinical data).

Phase Analysis

Phase analysis on GMPS was used to obtain the site of latest mechanical activation. Phase analysis of GMPS studies is based on the partial-volume effect wherein alterations in regional maximum counts are relative to myocardial wall thickening.[21, 22] A 3D sampling algorithm is used to determine regional maximal counts per cardiac frame and is used to generate count-based wall thickening curves by approximation of first Fourier harmonics (FFH) function. The phase angle represents the onset of mechanical activation per segment. The distribution of phase angles within the LV can be displayed in polar map or histogram format and provides quantitative parameters of global LV dyssynchrony; histogram bandwidth (includes 95% of the phase angles) and phase standard deviation (SD) (standard deviation of phase distribution).[17, 18] In addition, phase analysis provides information on regional mechanical activation. For the current study, the area of latest mechanical activation was determined on GMPS studies using the 6-segment model (septal, anteroseptal, anterior, lateral, posterior and inferior).[23] Regions of interests (ROI) corresponding to the 6-segment model were automatically placed on the phase polar map as shown in Figure 1. Each ROI covered 45° and 6 short-axis slices starting from the middle slice toward the base. As the 3D sampling algorithm collected one sample for every 9°, each ROI contains 5 x 6 = 30 samples. The mean phases of the 6 segments were calculated by averaging the phases of their 30 samples and then compared. The latest mechanically activated segment had the largest phase angles.

The intra- and interobserver reproducibility of phase analysis for assessment of the site of latest mechanical activation was determined in a subset of 30 patients, randomly selected from the patient population.

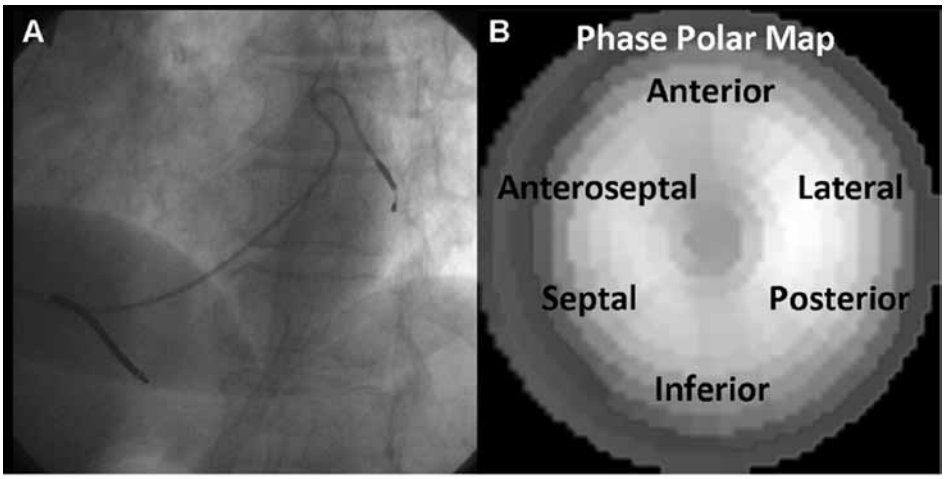

Figure 1 The site of latest mechanical activation was assessed on gated myocardial perfusion single photon emission computed tomography (SPECT) (GMPS) (panel B) and related to the left ventricular (LV) lead position on fluoroscopy (panel A).

A. Panel A shows an example of a patient with the LV lead positioned in the lateral cardiac region.

B. The region of latest mechanical activation was automatically calculated using phase analysis on GMPS. The region of latest mechanical activation was located on the phase polar map using the 6-segment model.[23]

Resting Transthoracic Echocardiography: Acquisition

Echocardiographic images were obtained with a commercially available system (Vivid Seven, General Electric-Vingmed, Milwaukee, Wisconsin, USA) in patients lying in left lateral decubitus position. With a 3.5 MHz transducer data acquisition was performed at a depth of 16 cm in the parasternal and apical views (standard long- and short-axis, 2- and 4-chamber images). Conventional 2D images were obtained during breath hold and saved in cine-loop format from three consecutive beats for offline analysis (Echopac version 7.0.0, General Electric-Vingmed, Milwaukee, Wisconsin, USA). From apical 2- and 4-chamber views, LVESV and LV end-diastolic volume (LVEDV) along with LVEF were measured using the biplane Simpson's approach.[24] Semi-quantitative assessment of mitral regurgitation was performed from color-flow Doppler images using the apical 4-chamber views. The severity was scored according to the following scale: (1) mild jet (area/left atrial area <20%), (2) moderate (jet area/left atrial area 20-45%) and (3) severe (jet area/left atrial area >45%).[25]

In 50 patients, the site of latest mechanical activation was assessed using 2D speckle tracking radial strain analysis on baseline mid-ventricular short-axis images. Images were recorded at a frame rate of at least 30 frames/sec and time-frame curves were generated for 6 cardiac segments (Echopac version 7.0.0, General Electric-Vingmed, Milwaukee, Wisconsin, USA) similar as for GMPS studies. Finally, the time between QRS onset and peak radial strain of the cardiac segments was used to assess the site of latest mechanical activation.[23]

CRT Implantation

All leads were placed via the subclavian route and the right atrial and ventricular lead were placed conventionally.[26] With the use of a balloon catheter, a sinus venogram was obtained after occlusion of the coronary sinus. Subsequently, the LV pacing lead was inserted with an 8 Fr guiding catheter in the coronary sinus, preferably in the lateral or posterolateral vein. The positioning of the LV pacing lead was performed by an electrophysiologist who was blinded to other data. The V-V interval was not adjusted during the first 6 months of CRT.

LV Lead Position and the Site of Latest Activation

LV lead positions were determined by an independent observer who was blinded to other data. The LV lead position was assessed on biplane fluoroscopy (which was obtained during implantation procedure) using the left anterior oblique (LAO 60˚) and right anterior oblique (RAO 30˚) view. For this analysis, LV pacing leads that were positioned in the basal or midregion of the LV were included and LV leads positioned at the cardiac apex were excluded from further analysis. Using the 6-segment model[23], the LV lead positions were scored as anterior, lateral, posterior or inferior. Subsequently, the LV lead positions were related to the area of latest activation (6-segment model) as assessed with GMPS using phase analysis.

The LV lead position was considered concordant if the LV lead was positioned at the area of latest activation, whereas the LV lead position was considered discordant if the LV lead was positioned outside the area of latest activation.

Intra- and interobserver reproducibility for assessment of LV lead position was evaluated in a randomly selected subset of 30 patients. To assess intraobserver reproducibility, the position of the LV lead on biplane fluoroscopy was assessed twice by the same observer. To assess interobserver reproducibility, a second blinded observer assessed the LV lead position on biplane fluoroscopy.

Statistical Analysis

Continuous data are presented as mean ± standard deviation and categorical data are presented as numbers and percentages. Differences in baseline characteristics between patients with concordant or discordant LV lead positions were studied with the unpaired Student's *t* test (continuous data) and Chi-square or Fisher exact tests (categorical data). During follow-up, changes in continuous data were studied using the paired Student's *t* test for both study groups. Agreement between GMPS with phase analysis and 2D speckle tracking radial strain analysis for assessment of the site of latest mechanical activation was evaluated using Cohen's Kappa statistics, and *k* values were qualified as poor (<0.40), moderate (0.40-0.75) or good (>0.75) agreement. In addition, Cohen's Kappa statistics were used to evaluate intra- and interobserver reproducibility for assessment of the site of latest mechanical activation using phase analysis in a subset of 30 randomly selected patients. Similarly, Cohen's Kappa statistics were used to evaluate the intra- and interobserver reproducibility for assessment

of the LV lead position on biplane fluoroscopy in 30 randomly selected patients. All tests were two-sided and for all analyses a p-value <0.05 was considered statistically significant. Statistical analyses were performed with SPSS software package, version 16.0 (SPSS Inc., Chicago, Illinois, USA).

Results

Patient Population

A total of 95 consecutive patients were derived from our ongoing clinical heart failure registry, of which 50 patients were part of previous work. Five patients were excluded because of apical LV lead position (n=3) or cardiac death during 6-months follow-up (n=2). The baseline characteristics of 90 heart failure patients (72% men, mean age 67±10 yrs) are listed in Table 1. The mean NYHA functional class was 3.0±0.4. Sixty-two (69%) patients were diagnosed with ischemic cardiomyopathy, whereas 28 (31%) patients had non-ischemic cardiomyopathy. Patients showed reduced LV systolic function, with a mean LVEF of 26±8%. The extent of myocardial perfusion defect was 26±16% on average. Medication consisted of diuretics (90% of patients), angiotensin-converting enzyme (ACE) inhibitors or angiotensin (AT) II antagonists (88% of patients) and beta-blockers (69% of patients).

GMPS with Phase Analysis and LV Lead Position

The mean value of histogram bandwidth and phase SD was 139±77˚ and 41±21˚. The region of latest mechanical activation as assessed with GMPS was located in the posterior (42.2%), lateral (23.3%), inferior (13.3%), anterior (15.6%), anteroseptal (3%) or septal (2.3%) region. Furthermore, a good agreement was found between GMPS and 2D speckle tracking radial strain analysis for assessment of the site of latest mechanical activation (total agreement of 86%, *k* value=0.79). A good intraobserver (*k*=0.96, total agreement of 93%) and interobserver (*k*=0.92, total agreement of 87%) reproducibility of phase analysis was observed for assessment of the site of latest mechanical activation. CRT device and LV lead implantation were successful in all patients without major complications. The LV pacing lead was positioned in the lateral (44.4% of patients), posterior (50.0% of patients) or anterior (5.6% of patients) region. A good intraobserver (*k*=0.82, total agreement of 90%) and interobserver (*k*=0.76, total agreement of 87%) reproducibility for assessment of LV lead position on fluoroscopy was observed.

Fifty-two (58%) patients showed a concordant LV lead position and 38 (42%) patients showed a discordant LV lead position, as shown in Table 2. No significant differences were observed for demographic, clinical and echocardiographic variables between patients with concordant or discordant LV lead position. In addition, no difference was found for

Table 1. Baseline characteristics of the patient population (n=90)

Age (yrs)	67±10
Male	65 (72)
Ischemic heart failure	62 (69)
NYHA functional class	3.0±0.4
QRS duration (ms)	161±36
Echocardiographic parameters	
LVEDV (mL)	214±64
LVESV (mL)	160±57
LVEF (%)	26±8
Scintigraphic parameters	
Perfusion defect in LV pacing region	17 (19)
Extent of perfusion defect (%)	26±16
Histogram bandwidth (°)	139±77
Phase SD (°)	41±21
Medication	
Diuretics	81 (90)
ACE inhibitors / AT II antagonists	79 (88)
Beta-blockers	62 (69)
Spironolactone	40 (44)
Statins	55 (61)

Data are presented as mean ± standard deviation or as number (%).
NYHA = New York Heart Association; LVEDV = left ventricular end-diastolic volume; LVESV = left ventricular end-systolic volume; LVEF = left ventricular ejection fraction; GMPS = gated myocardial perfusion single photon emission computed tomography; SD = standard deviation; ACE = angiotensin-converting enzyme; AT II = angiotensin II.

histogram bandwidth and phase SD between both groups. Patients with concordant and discordant LV lead position showed no significant difference in perfusion defects located in the LV pacing region (13% vs. 26%, p=NS). Additionally, no difference was found between patients with concordant and discordant LV lead position in the extent of myocardial perfusion defects (22.9±14.1% vs. 29.3±18.1%, p=NS). The extent of myocardial perfusion defects was significantly smaller in patients with CRT response as compared to patients without CRT response (21.1±12.3% vs. 31.6±18.7%, $p<0.05$). Furthermore, the percentage CRT responders was significantly higher in patients with concordant LV lead position when compared to patients with discordant LV lead position (79% vs. 26%, $p<0.01$). Patient examples with a concordant and discordant LV lead position are shown in Figure 2. Of note, 11 patients with concordant LV lead position showed no response to CRT after 6 months. In these patients, 7 patients showed severe perfusion defects at the region of LV pacing.

Table 2. Baseline characteristics between patients with concordant and discordant LV lead positions

Baseline characteristics	Concordant LV lead position (n=52)	Discordant LV lead position (n=38)	p-value
Age (yrs)	68±10	66±11	0.5
Gender (male)	37 (71)	28 (74)	0.8
Ischemic heart failure	38 (73)	24 (63)	0.4
NYHA functional class	3.0±0.4	3.0±0.4	1.0
QRS duration (ms)	168±35	153±33	0.1
LVEDV (mL)	214±67	213±62	1.0
LVESV (mL)	160±57	161±57	0.9
LVEF (%)	27±8	26±8	0.7
Mitral regurgitation (moderate/ severe)	19 (37)	19 (50)	0.2
Histogram bandwidth (°)	126±67	157±86	0.1
Phase SD (°)	38±20	45±21	0.1
Perfusion defect LV pacing region	7 (13)	10 (26)	0.2
Extent perfusion defect (%)	23±14	29±18	0.1
CRT response after 6 months	41 (79)	10 (26)	<0.01

Data are presented as mean ± standard deviation or as number (%).
NYHA = New York Heart Association; LVEDV = left ventricular end-diastolic volume; LVESV = left ventricular end-systolic volume; LVEF = left ventricular ejection fraction; SD = standard deviation; CRT = cardiac resynchronization therapy.

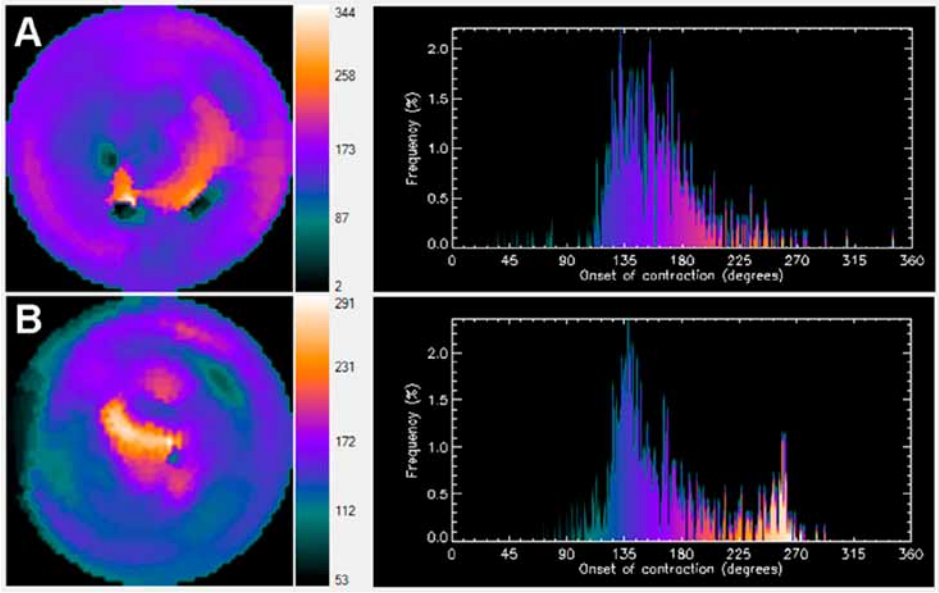

Figure 2 Area of latest mechanical activation as assessed with phase analysis on gated myocardial perfusion single photon emission computed tomography (SPECT) (GMPS).

A. Example of a patient with the left ventricular (LV) lead positioned at the area of latest activation (concordant LV lead position). The area of latest activation was located in the lateral segment. The patient showed a significant improvement in LV end-systolic volume (LVESV) (139 mL vs. 86 mL) and LV ejection fraction (LVEF) (32% vs. 44%) after 6 months of cardiac resynchronization therapy (CRT).

B. Example of a patient with the LV lead positioned outside the area of latest activation (discordant LV lead position). The area of latest activation was located in the anterior segment, whereas the LV lead was positioned in the posterior segment. The patient showed no improvement in LVESV (124 mL vs. 153 mL) and LVEF (27% vs. 22%) after 6 months of CRT.

Baseline and 6-months Follow-up

The total patient population showed a significant improvement in NYHA functional class from 3.0±0.4 to 2.5±0.7 ($p<0.05$). In addition, patients showed a significant improvement in echocardiographic variables, including LVESV (160±57 mL vs. 137±55 mL, $p<0.05$), LVEDV (214±64 mL vs. 197±64 mL, $p<0.05$) and LVEF (26±8% vs. 32±11%, $p<0.05$). After 6 months of CRT, patients with a concordant LV lead position showed significant improvement in LVESV (159±57 mL vs. 125±54 mL, $p<0.05$), LVEDV (214±67 mL vs. 188±62 mL, $p<0.05$) and LVEF (27±8% vs. 35±12%, $p<0.05$), as illustrated in Figure 3. Additionally, an improvement in NYHA functional class was observed in patients with a concordant LV lead position (3.0±0.4 vs. 2.3±0.7, $p<0.05$). However, patients with the LV lead positioned outside the region of latest mechanical activation (discordant LV lead position) showed no improvement in NYHA functional class (3.0±0.4 vs. 2.7±0.7, p=NS). In addition, LVESV

(161±57 mL vs. 153±53 mL, p=NS), LVEDV (213±62 mL vs. 210±65 mL, p=NS) and LVEF (26±8% vs. 28±9%, p=NS) showed no significant improvement after 6 months of CRT in patients with a discordant LV lead position, as depicted in Figure 3.

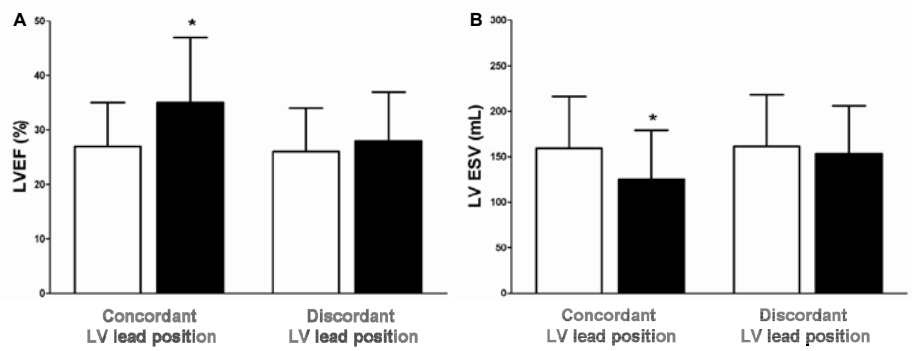

Figure 3 Response to cardiac resynchronization therapy (CRT) in patients with concordant (n=52) and discordant (n=38) left ventricular (LV) lead positions. Baseline (white bars) and 6 months follow-up (black bars) echocardiographic measurements are depicted below.

A. Patients with concordant LV lead position showed significant improvement in LV ejection fraction (LVEF) (27±8% vs. 35±12%, p<0.05), whereas patients with discordant LV lead position showed no significant improvement in LVEF (26±8% vs. 28±9%, p=NS).

B. Patients with concordant LV lead position showed significant improvement in LV end-systolic volume (LVESV) (159±57 mL vs. 125±54 mL, p<0.05), whereas patients with discordant LV lead position showed no significant improvement in LVESV (161±57 mL vs. 153±53 mL, p=NS).

Discussion

The main findings of the current study can be summarized as follows: patients with concordant LV lead position showed significant LV reverse remodeling and improvement in LV systolic function, whereas patients with discordant LV lead position showed no significant improvements. Accordingly, GMPS with phase analysis represents a feasible technique to identify the preferred LV lead position in patients referred for CRT.

Resynchronization therapy is based on the rationale to improve the intrinsic electrical ventricular conductance by pacing the ventricles in a synchronized manner.[1, 2] To optimize synchronicity of the LV contraction, the LV pacing lead should be targeted at the region of latest mechanical activation.[9-13] In this perspective, it is important to note that the region of latest mechanical activation may vary significantly in heart failure patients, with the posterolateral region as the most common site of latest activation.[10,14-16] The study by Becker et al.[16], who sought to determine the effect of LV lead position on reverse remodeling and

LV function as assessed with echocardiography, has shown that the site of latest mechanical activation differed significantly among 47 heart failure patients. The site of latest mechanical activation was predominantly located in the posterolateral region of the ventricle (60% of patients). Likewise, the current study showed that the posterolateral cardiac segments represented the most common site of latest mechanical activation (66% of patients).

Additionally, the relation between LV lead position, the site of mechanical delay and CRT outcome has been evaluated in several studies.[9-16] An important study was performed by Becker et al.[16] who evaluated the efficacy of CRT in patients with optimal (n=28) or suboptimal (n=19) LV lead position. The position of the LV lead was considered optimal if the LV lead was concordant with the cardiac segment showing the latest mechanical contraction (≤1 segment between the LV pacing region and the segment with latest mechanical activation). Circumferential strain analysis on echocardiography was used to assess the site of delayed mechanical activation. After 10 months follow-up, patients with an optimal LV lead position showed a significantly larger decrease in LVESV and LVEDV as well as a significant improvement in LVEF, as compared to patients with suboptimal LV lead position (all, $p<0.01$).

Recently, Ypenburg et al.[14] have evaluated 6-month echocardiograhic response to CRT as well as long-term outcome in patients with concordant (n=153) and discordant (n=91) LV lead position. Speckle tracking radial strain analysis on 2D echocardiography was used to determine the region of latest mechanical delay. After 6 months of CRT, patients with concordant LV lead position showed a significant decrease in LV volumes as well as a significant improvement in LVEF as compared to patients with discordant LV lead position (all, $p<0.01$). Importantly, a concordant LV lead position was an independent predictor of combined endpoint of hospitalization and all-cause mortality. Similarly, the current study has demonstrated that patients with concordant LV lead position showed superior improvement in LVEF after 6 months of CRT (27±8% vs. 35±12%, $p<0.05$) when compared to patients with discordant LV lead position (26±8% vs. 28±9%, p=NS). Additionally, considerable reverse remodeling, as reflected by a significant decrease in LVESV and LVEDV, was observed in patients with the LV lead positioned at the site of latest activation as derived from GMPS with phase analysis. The findings demonstrate that CRT response is related to LV lead position and the region of latest mechanical contraction. More specifically, these observations support the hypothesis that resynchronization of the LV, induced by pacing at the region of latest mechanical activation, exerts positive effects on ventricular geometry and function.

Of interest, a small number of patients with the LV lead placed outside the region of latest activation responded positively to CRT. In these patients, the distance between the region of latest activation and the LV lead position (as reflected by the number of cardiac segments in between) was minimal (≤2 cardiac segments). As a consequence, the contraction pattern may have become less dyssynchronous in these patients. Additionally, 11 (21%) patients did

not show CRT response despite the fact that the LV lead was positioned at the latest activated area. This observation may be explained by the fact that extensive perfusion defects were located at or near the site of latest mechanical activation in this subset of patients. It has been demonstrated that the extent and location of scarred myocardium play an important role in CRT response.[26-28] Bleeker et al.[26] have performed an important study evaluating the effect of posterolateral scar tissue on CRT response in 40 consecutive advanced heart failure patients. The study has shown that patients with posterolateral scar tissue on magnetic resonance imaging showed a significantly lower response rate as compared to patients without posterolateral scar tissue (14% vs. 81%, $p<0.05$). Similarly, the current study has demonstrated that severe perfusion defects at or adjacent to the region of latest mechanical activation were associated with non-response to CRT. Patients with a concordant LV lead position but with severe perfusion defects at the region of LV pacing showed no response to CRT. Furthermore, the study has shown that the extent of myocardial perfusion defects was significantly smaller in patients with response to CRT as compared to patients without CRT response. Accordingly, location and extent of scarred myocardium play an important role in the likelihood of response to CRT.

At present, non-response to CRT has been associated with the absence of pre-existent mechanical dyssynchrony, location and extent of scarred myocardium (particularly at LV pacing region) and suboptimal LV lead position.[7, 8, 26-28] For this reason, phase analysis on GMPS has gained increasingly interest for the evaluation of CRT patients as it allows an integrated evaluation of mechanical dyssynchrony, regional activation pattern and myocardial infarction.[17, 18] More specifically, the presence of infarcted myocardium at or adjacent to the region of maximal mechanical delay can be evaluated using the SPECT data sets. Accordingly, phase analysis on GMPS represents a feasible technique to identify the preferred LV lead position.

At present, different non-invasive imaging techniques are available for the evaluation of patients referred for CRT, including echocardiography, magnetic resonance imaging as well as nuclear imaging. A comprehensive evaluation of CRT patients can be performed by each of these imaging techniques as they provide information on pre-existent LV mechanical dyssynchrony, presence and location of myocardial infarction as well as the site of latest mechanical activation. As they all provide useful information, the choice for one of these techniques is eventually determined by the local expertise and availability.

Some study limitations need to be acknowledged. First of all, the study findings are based on a relatively small number of patients who were referred for CRT. The current study however, represents only a feasibility study evaluating the role of phase analysis on GMPS for assessment of optimal LV lead position in advanced heart failure patients. The novelty of the present study relates to the evaluation of CRT response in patients with concordant and discordant LV lead position as assessed with phase analysis on GMPS. A second limitation is the fact that long-term effects of resynchronization therapy on mortality and/or morbidity

rates were not reported in the current study as the patient population was too small for long-term outcome analysis.

Conclusion

Patients with concordant LV lead position showed significant improvements in LV volumes and LV systolic function, whereas patients with discordant LV lead position showed no significant improvement in LV volumes and LV systolic function. Accordingly, phase analysis on GMPS represents a feasible technique to identify the preferred LV lead position in patients indicated for CRT.

Reference List

(1) Hunt SA, Abraham WT, Chin MH, Feldman AM, Francis GS, Ganiats TG, Jessup M, Konstam MA, Mancini DM, Michl K, Oates JA, Rahko PS, Silver MA, Stevenson LW, Yancy CW. 2009 focused update incorporated into the ACC/AHA 2005 Guidelines for the Diagnosis and Management of Heart Failure in Adults: a report of the American College of Cardiology Foundation/American Heart Association Task Force on Practice Guidelines: developed in collaboration with the International Society for Heart and Lung Transplantation. Circulation 2009;119(14):e391-e479.

(2) Epstein AE, DiMarco JP, Ellenbogen KA, Estes NA, III, Freedman RA, Gettes LS, Gillinov AM, Gregoratos G, Hammill SC, Hayes DL, Hlatky MA, Newby LK, Page RL, Schoenfeld MH, Silka MJ, Stevenson LW, Sweeney MO, Smith SC, Jr., Jacobs AK, Adams CD, Anderson JL, Buller CE, Creager MA, Ettinger SM, Faxon DP, Halperin JL, Hiratzka LF, Hunt SA, Krumholz HM, Kushner FG, Lytle BW, Nishimura RA, Ornato JP, Page RL, Riegel B, Tarkington LG, Yancy CW. ACC/AHA/HRS 2008 Guidelines for Device-Based Therapy of Cardiac Rhythm Abnormalities: a report of the American College of Cardiology/American Heart Association Task Force on Practice Guidelines: developed in collaboration with the American Association for Thoracic Surgery and Society of Thoracic Surgeons. Circulation 2008;117(21):e350-e408.

(3) Cazeau S, Leclercq C, Lavergne T, Walker S, Varma C, Linde C, Garrigue S, Kappenberger L, Haywood GA, Santini M, Bailleul C, Daubert JC. Effects of multisite biventricular pacing in patients with heart failure and intraventricular conduction delay. N Engl J Med 2001;344(12):873-880.

(4) Abraham WT, Fisher WG, Smith AL, Delurgio DB, Leon AR, Loh E, Kocovic DZ, Packer M, Clavell AL, Hayes DL, Ellestad M, Trupp RJ, Underwood J, Pickering F, Truex C, McAtee P, Messenger J. Cardiac resynchronization in chronic heart failure. N Engl J Med 2002;346(24):1845-1853.

(5) Bristow MR, Saxon LA, Boehmer J, Krueger S, Kass DA, De Marco T, Carson P, DiCarlo L, DeMets D, White BG, DeVries DW, Feldman AM. Cardiac-resynchronization therapy with or without an implantable defibrillator in advanced chronic heart failure. N Engl J Med 2004;350(21):2140-2150.

(6) Cleland JG, Daubert JC, Erdmann E, Freemantle N, Gras D, Kappenberger L, Tavazzi L. The effect of cardiac resynchronization on morbidity and mortality in heart failure. N Engl J Med 2005;352(15):1539-1549.

(7) Bax JJ, Abraham T, Barold SS, Breithardt OA, Fung JW, Garrigue S, Gorcsan J, III, Hayes DL, Kass DA, Knuuti J, Leclercq C, Linde C, Mark DB, Monaghan MJ, Nihoyannopoulos P, Schalij MJ, Stellbrink C, Yu CM. Cardiac resynchronization therapy: Part 1--issues before device implantation. J Am Coll Cardiol 2005;46(12):2153-2167.

(8) Bax JJ, Abraham T, Barold SS, Breithardt OA, Fung JW, Garrigue S, Gorcsan J, III, Hayes DL, Kass DA, Knuuti J, Leclercq C, Linde C, Mark DB, Monaghan MJ, Nihoyannopoulos P, Schalij MJ, Stellbrink C, Yu CM. Cardiac resynchronization therapy: Part 2--issues during and after device implantation and unresolved questions. J Am Coll Cardiol 2005;46(12):2168-2182.

(9) Butter C, Auricchio A, Stellbrink C, Fleck E, Ding J, Yu Y, Huvelle E, Spinelli J. Effect of resynchronization therapy stimulation site on the systolic function of heart failure patients. Circulation 2001;104(25):3026-3029.

(10) Ansalone G, Giannantoni P, Ricci R, Trambaiolo P, Fedele F, Santini M. Doppler myocardial imaging to evaluate the effectiveness of pacing sites in patients receiving biventricular pacing. J Am Coll Cardiol 2002;39(3):489-499.

(11) Gasparini M, Mantica M, Galimberti P, Bocciolone M, Genovese L, Mangiavacchi M, Marchesina UL, Faletra F, Klersy C, Coates R, Gronda E. Is the left ventricular lateral wall the best lead implantation site for cardiac resynchronization therapy? Pacing Clin Electrophysiol 2003;26(1 Pt 2):162-168.

(12) Dekker AL, Phelps B, Dijkman B, van der Nagel T, van der Veen FH, Geskes GG, Maessen JG. Epicardial left ventricular lead placement for cardiac resynchronization therapy: optimal pace site selection with pressure-volume loops. J Thorac Cardiovasc Surg 2004;127(6):1641-1647.
(13) Lane RE, Chow AW, Mayet J, Francis DP, Peters NS, Schilling RJ, Davies DW. The interaction of interventricular pacing intervals and left ventricular lead position during temporary biventricular pacing evaluated by tissue Doppler imaging. Heart 2007;93(11):1426-1432.
(14) Ypenburg C, Van Bommel RJ, Delgado V, Mollema SA, Bleeker GB, Boersma E, Schalij MJ, Bax JJ. Optimal left ventricular lead position predicts reverse remodeling and survival after cardiac resynchronization therapy. J Am Coll Cardiol 2008;52(17):1402-1409.
(15) Murphy RT, Sigurdsson G, Mulamalla S, Agler D, Popovic ZB, Starling RC, Wilkoff BL, Thomas JD, Grimm RA. Tissue synchronization imaging and optimal left ventricular pacing site in cardiac resynchronization therapy. Am J Cardiol 2006;97(11):1615-1621.
(16) Becker M, Kramann R, Franke A, Breithardt OA, Heussen N, Knackstedt C, Stellbrink C, Schauerte P, Kelm M, Hoffmann R. Impact of left ventricular lead position in cardiac resynchronization therapy on left ventricular remodeling. A circumferential strain analysis based on 2D echocardiography. Eur Heart J 2007;28(10):1211-1220.
(17) Chen J, Garcia EV, Folks RD, Cooke CD, Faber TL, Tauxe EL, Iskandrian AE. Onset of left ventricular mechanical contraction as determined by phase analysis of ECG-gated myocardial perfusion SPECT imaging: development of a diagnostic tool for assessment of cardiac mechanical dyssynchrony. J Nucl Cardiol 2005;12(6):687-695.
(18) Chen J, Henneman MM, Trimble MA, Bax JJ, Borges-Neto S, Iskandrian AE, Nichols KJ, Garcia EV. Assessment of left ventricular mechanical dyssynchrony by phase analysis of ECG-gated SPECT myocardial perfusion imaging. J Nucl Cardiol 2008;15(1):127-136.
(19) Bax JJ, Bleeker GB, Marwick TH, Molhoek SG, Boersma E, Steendijk P, van der Wall EE, Schalij MJ. Left ventricular dyssynchrony predicts response and prognosis after cardiac resynchronization therapy. J Am Coll Cardiol 2004;44(9):1834-1840.
(20) Cerqueira MD, Weissman NJ, Dilsizian V, Jacobs AK, Kaul S, Laskey WK, Pennell DJ, Rumberger JA, Ryan T, Verani MS. Standardized myocardial segmentation and nomenclature for tomographic imaging of the heart: a statement for healthcare professionals from the Cardiac Imaging Committee of the Council on Clinical Cardiology of the American Heart Association. Circulation 2002;105(4):539-542.
(21) Hoffman EJ, Huang SC, Phelps ME. Quantitation in positron emission computed tomography: 1. Effect of object size. J Comput Assist Tomogr 1979;3(3):299-308.
(22) Galt JR, Garcia EV, Robbins WL. Effects of myocardial wall thickness on SPECT quantification. IEEE Trans Med Imaging 1990;9(2):144-150.
(23) Suffoletto MS, Dohi K, Cannesson M, Saba S, Gorcsan J, III. Novel speckle-tracking radial strain from routine black-and-white echocardiographic images to quantify dyssynchrony and predict response to cardiac resynchronization therapy. Circulation 2006;113(7):960-968.
(24) Schiller NB, Shah PM, Crawford M, DeMaria A, Devereux R, Feigenbaum H, Gutgesell H, Reichek N, Sahn D, Schnittger I, . Recommendations for quantitation of the left ventricle by two-dimensional echocardiography. American Society of Echocardiography Committee on Standards, Subcommittee on Quantitation of Two-Dimensional Echocardiograms. J Am Soc Echocardiogr 1989;2(5):358-367.
(25) Bonow RO, Carabello BA, Chatterjee K, de Leon AC, Jr., Faxon DP, Freed MD, Gaasch WH, Lytle BW, Nishimura RA, O'Gara PT, O'Rourke RA, Otto CM, Shah PM, Shanewise JS. 2008 Focused update incorporated into the ACC/AHA 2006 guidelines for the management of patients with valvular heart disease: a report of the American College of Cardiology/American Heart Association Task Force on Practice Guidelines (Writing Committee to Revise the 1998 Guidelines for the Management of Patients With Valvular Heart Disease): endorsed by the Society of Cardiovascular

Anesthesiologists, Society for Cardiovascular Angiography and Interventions, and Society of Thoracic Surgeons. Circulation 2008;118(15):e523-e661.

(26) Bleeker GB, Kaandorp TA, Lamb HJ, Boersma E, Steendijk P, de Roos A, van der Wall EE, Schalij MJ, Bax JJ. Effect of posterolateral scar tissue on clinical and echocardiographic improvement after cardiac resynchronization therapy. Circulation 2006;113(7):969-976.

(27) Ypenburg C, Schalij MJ, Bleeker GB, Steendijk P, Boersma E, Dibbets-Schneider P, Stokkel MP, van der Wall EE, Bax JJ. Extent of viability to predict response to cardiac resynchronization therapy in ischemic heart failure patients. J Nucl Med 2006;47(10):1565-1570.

(28) Ypenburg C, Schalij MJ, Bleeker GB, Steendijk P, Boersma E, Dibbets-Schneider P, Stokkel MP, van der Wall EE, Bax JJ. Impact of viability and scar tissue on response to cardiac resynchronization therapy in ischaemic heart failure patients. Eur Heart J 2007;28(1):33-41.

Chapter **9**

Left Ventricular Diastolic Dyssynchrony Assessed with Phase Analysis of Gated Myocardial Perfusion SPECT: A Comparison with Tissue Doppler Imaging

Mark J. Boogers, MD[1, 2]; Ji Chen, PhD[3]; Caroline E. Veltman, MD[1, 2]; Rutger J. van Bommel, MD[1]; Eline A. Q. Mooyaart, MD[1]; Imad Al Younis, MD[4]; Bernies van der Hiel, MD[4]; Petra Dibbets-Schneider, MSc[4]; Ernst E. van der Wall, MD, PhD[1]; Martin J. Schalij, MD, PhD[1]; Ernest V. Garcia, PhD[3]; Jeroen J. Bax, MD, PhD[1]; Victoria Delgado, MD, PhD[1].

[1]Department of Cardiology, Leiden University Medical Center, Leiden, the Netherlands; [2]The Interuniversity Cardiology Institute of the Netherlands, Utrecht, the Netherlands; [3]Department of Radiology, Emory University School of Medicine, Atlanta, Georgia, USA; [4]Department of Nuclear Medicine, Leiden University Medical Center, Leiden, the Netherlands.

Abstract

Purpose The current study aimed to evaluate the feasibility of phase analysis on gated myocardial perfusion SPECT (GMPS) for assessment of left ventricular (LV) diastolic dyssynchrony in a head-to-head comparison with tissue Doppler imaging (TDI).

Methods The patient population consisted of end-stage heart failure (HF) patients (New York Heart Association (NYHA) functional class III or IV) with reduced LV ejection fraction (LVEF) ≤35%. LV diastolic dyssynchrony was calculated using TDI as the maximal time delay between early peak diastolic velocities of 2 opposing LV walls (diastolic mechanical delay). Significant LV diastolic dyssynchrony was defined as a diastolic mechanical delay of >55 ms on TDI. Furthermore, phase analysis on GMPS was performed to evaluate LV diastolic dyssynchrony; diastolic phase standard deviation (SD) and histogram bandwidth (HBW) were used as markers of LV diastolic dyssynchrony.

Results A total of 150 (114 men, mean age 66.0±10.4 yrs) patients with end-stage HF were enrolled. Both diastolic phase SD ($r=0.81$, $p<0.01$) and diastolic HBW ($r=0.75$, $p<0.01$) showed good correlations with LV diastolic dyssynchrony on TDI. Additionally, patients with LV diastolic dyssynchrony on TDI (>55 ms) showed significantly larger diastolic phase SD (68.1±13.4˚ vs. 40.7±14.0˚, $p<0.01$) and diastolic HBW (230.6±54.3˚ vs. 129.0±55.6˚, $p<0.01$) as compared to patients without LV diastolic dyssynchrony on TDI (≤55 ms). Finally, phase analysis on GMPS showed a good intra- and interobserver reproducibility for diastolic phase SD (ICC 0.97 and 0.88) and diastolic HBW (ICC 0.98 and 0.93).

Conclusions Phase analysis on GMPS showed good correlations with TDI for assessment of LV diastolic dyssynchrony.

Introduction

Left ventricular (LV) systolic dyssynchrony is considered an important pathophysiologic condition in patients with heart failure (HF).[1, 2] In addition, it has been shown that a dyssynchronous relaxation pattern of the LV, which is commonly referred to as LV diastolic dyssynchrony, plays an important role in patients with HF.[3-5] In these patients, LV diastolic dyssynchrony has been related to abnormalities in LV diastolic filling and LV filling rate, which may contribute to a further impairment of the hemodynamics of the failing heart.[5] Importantly, it has been recognized that LV diastolic dyssynchrony is a common pathophysiologic condition in HF patients with an estimated prevalence of more than 50%.[3, 6]

At present, the majority of available studies have used echocardiography for the assessment of LV diastolic dyssynchrony in patients with HF.[3, 4, 6-8] Among the echocardiographic techniques, tissue Doppler imaging (TDI) has been used predominantly for the evaluation of diastolic relaxation patterns of the LV.[6-8] Although TDI represents an accurate approach for the assessment of LV diastolic dyssynchrony, the post-processing of Doppler images requires special expertise and standardized protocols to optimize the interobserver variability.

Phase on gated myocardial perfusion single photon emission computed tomography (SPECT) (GMPS) has emerged as a practical technique for assessment of LV mechanical dyssynchrony as it automatically provides robust and reproducible indices of mechanical dyssynchrony.[9, 10] Moreover, phase analysis can be performed on conventional GMPS studies without the use of additional image acquisitions. Although studies have shown that phase analysis on GMPS can be used for assessment of LV systolic dyssynchrony, its feasibility to assess LV diastolic dyssynchrony has not been demonstrated. Accordingly, the current study aimed to demonstrate the feasibility of phase analysis on GMPS for assessment of LV diastolic dyssynchrony in a head-to-head comparison with TDI.

Material and Methods

Patient Population and Protocol

The patient population consisted of end-stage HF patients (New York Heart Association (NYHA) functional class III or IV) with depressed LV ejection fraction (LVEF) ≤35%. Patient data were prospectively collected in the departmental Cardiology Information System (EPD-Vision®, Leiden University Medical Center (LUMC), Leiden, the Netherlands) and retrospectively analyzed. All patients were treated according to the MISSION! - Heart Failure care track operational at the LUMC. All patients were stable on maximum tolerated doses of heart failure medications. Patients with recent myocardial infarction (within 3 months prior to GMPS), atrial fibrillation, decompensated HF or acute coronary syndrome were excluded.

Patients were diagnosed with ischemic cardiomyopathy in the presence of ≥50% stenosis in one or more of the major epicardial coronary arteries, previous myocardial infarction, percutaneous coronary intervention or coronary artery bypass grafting.

Resting GMPS and 2D echocardiography with TDI were performed as part of the clinical evaluation of HF patients to determine therapeutic options. A standard 12-lead electrocardiogram (ECG) was obtained prior to GMPS. GMPS and TDI were compared for assessment of LV diastolic dyssynchrony. TDI was considered the standard of reference for evaluation of LV diastolic dyssynchrony, which was calculated as the maximal time delay between early peak diastolic velocities of 2 opposing LV walls. As previously reported, a cutoff value of 55 ms of diastolic mechanical delay on TDI was used as a marker of significant LV diastolic dyssynchrony.[6]

Phase analysis on GMPS was used to evaluate LV diastolic dyssynchrony and systolic dyssynchrony. Both diastolic phase histogram bandwidth (HBW) and diastolic phase standard deviation (SD) as derived from the onset of mechanical relaxation (OMR) distribution were used as markers of LV diastolic dyssynchrony, whereas systolic HBW and systolic phase SD were used as markers of LV systolic dyssynchrony, as previously described.[11] Consecutively, TDI and phase analysis on GMPS were compared for assessment of LV diastolic dyssynchrony. Additionally, the extent of LV diastolic dyssynchrony on GMPS was evaluated in patients with (>55 ms) and without (≤55 ms) significant LV diastolic dyssynchrony on TDI. Finally, the relation between LV diastolic and systolic dyssynchrony as assessed with GMPS was evaluated.

Gated Myocardial Perfusion SPECT: Acquisition

Resting GMPS with ^{99m}technetium tetrofosmin was performed on a triple-head SPECT camera (GCA 9300/HG; Toshiba Corporation, Tokyo, Japan) equipped with low-energy high-resolution collimators. At rest, an average dose of 500 MBq of ^{99m}technetium tetrofosmin (MYOVIEW, General Electric Healthcare, UK) was administered intravenously. A 20% window was centered around the 140-KeV energy peak of ^{99m}technetium tetrofosmin. A total of 90 projections (step and shoot method, 35 s/projection, 64 x 64 matrix, total imaging time 23 minutes) were obtained over a 360° circular orbit. ECG gating was applied on the cardiac cycle with 16 frames per cardiac cycle using a tolerance window of 50%.

Subsequently, the raw data were uploaded to the Emory Cardiac Toolbox (Emory University, Atlanta, Georgia, USA) for data reconstruction, reorientation and phase analysis processing. All patient studies were reconstructed by ordered subsets expectation maximization (OSEM) with 3 iterations and 10 subsets. A Butterworth filter with a cutoff frequency of 0.35 cycles/cm and a power of 10 was used to filter the gated images. The reconstructed images were thereafter reoriented manually with assistance of the automatic reorientation tool in the Emory Reconstruction Toolbox (Emory University, Atlanta, Georgia, USA) to generate gated short-axis images. The gated short-axis images were sampled for regional maximum

counts using the Emory Cardiac Toolbox (Emory University, Atlanta, Georgia, USA) and then submitted to the multi-harmonic phase analysis tool. Finally, phase analysis processing was performed blinded at Emory University.

Phase Analysis on GMPS

Phase analysis of GMPS studies was performed to derive LV diastolic and systolic dyssynchrony. LV diastolic dyssynchrony was assessed using phase analysis which consisted of several consecutive processing steps, as illustrated in Figure 1. Initially, regional maximal count detection was performed in 3D for each temporal frame using the standard gated

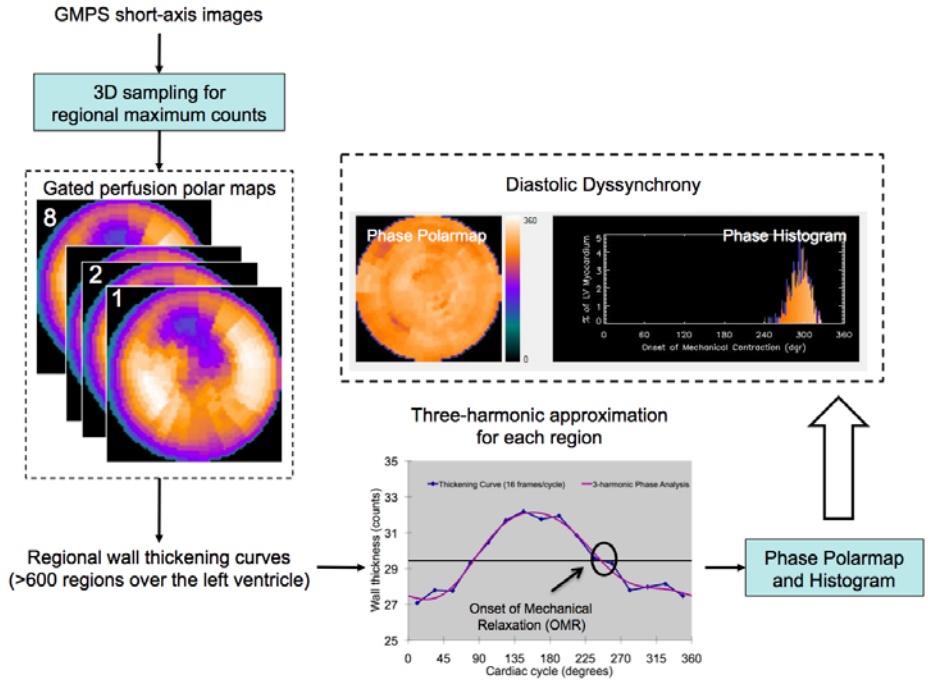

Figure 1 Schematic illustration of the processing steps involved in the assessment of diastolic dyssynchrony using phase analysis of gated myocardial perfusion single photon emission computed tomography (SPECT) (GMPS) studies. For each temporal frame, a regional maximal count detection was performed in 3D using the standard gated short-axis SPECT images. Consecutively, the third Fourier harmonic function was used to approximate the discrete sample points into a continuous wall-thickening curve. The wall-thickening curve provided a phase angle that represented the onset of mechanical relaxation (OMR) of the region (>600 regions for the entire left ventricle (LV)). The OMR phase angles of all LV regions were used to generate a phase distribution, which was displayed in a polar map and histogram. The phase histogram was used to obtain the LV diastolic dyssynchrony indices; diastolic phase standard deviation (SD) (SD of the OMR phase distribution) and diastolic histogram bandwidth (HBW) (the width of the band that includes 95% of the OMR phase angles).

short-axis SPECT image. Phase analysis processing was based on the partial-volume effect wherein alterations in regional maximal counts are proportional to changes in regional myocardial wall thickening over the cardiac cycle.[12, 13] This linear relationship was demonstrated in a phantom study.[13] Consecutively, the third Fourier harmonic function was used to approximate the discrete sample points into a continuous wall-thickening curve. For each region, the wall-thickening curve provided a phase angle that represented the OMR of the particular region. The OMR phase is the time point when the curves crossed the middle line from positive to negative. Once the OMR phase angles of all regions (>600 regions over the entire LV) were obtained, a phase distribution was generated that provided information on the degree of diastolic dyssynchrony for the entire LV. The phase distribution was displayed in a polar map and histogram as shown in Figure 1. The quantitative parameters for LV diastolic dyssynchrony were derived from the phase histogram; diastolic phase SD (SD of the OMR phase distribution) and diastolic HBW (the width of the band that includes 95% of the OMR phase angles), similar to as LV systolic dyssynchrony indices.[11]

Additionally, LV systolic dyssynchrony was evaluated measuring the systolic phase SD and systolic HBW.[11] As previously described[11], the onset of mechanical contraction per cardiac region was measured using count-based wall-thickening curves which were derived from alternations in myocardial counts during the cardiac cycle. Each myocardial segment yielded a phase angle representing the onset of mechanical contraction for that particular segment of the myocardium. Finally, the phase angles of the entire LV (exceeding 600 per LV) were plotted in a polar map and histogram, wherein the phase histogram was used to calculate systolic phase SD and systolic HBW as markers of LV systolic dyssynchrony.[11]

Furthermore, the intra- and interobserver reproducibility of phase analysis for assessment of diastolic phase SD and diastolic HBW was determined in a subset of 25 patients.

Transthoracic Echocardiography with Tissue Doppler Imaging

Transthoracic echocardiography was performed at rest in patients lying in left lateral decubitus position using a commercially available ultrasound device (M3S probe, Vivid 7, GE-Vingmed, Horten, Norway). With a 3.5 MHz transducer data acquisition was performed in the parasternal and apical views (standard long- and short-axis, 2-, 4-chamber and apical long-axis images). Conventional 2D images were obtained during breath hold and saved in cine-loop format from three consecutive beats for offline analysis (EchoPac 108.1.5, GE-Vingmed, Horten, Norway). From apical 2- and 4-chamber views, LV end-systolic volume (LVESV) and LV end-diastolic volume (LVEDV) along with LVEF were measured using the biplane Simpson's approach.[14] Consecutively, color-coded TDI was performed to assess diastolic dyssynchrony of the LV, as shown in Figure 2. In each patient, color-coded TDI of the LV was obtained in the apical 2- and 4-chamber views during end-expiration. The sector size and depth were optimized for the highest possible frame rate (>115 frames/sec). Consecutively, a sample volume (12 x 6 mm) was positioned in the middle of the basal

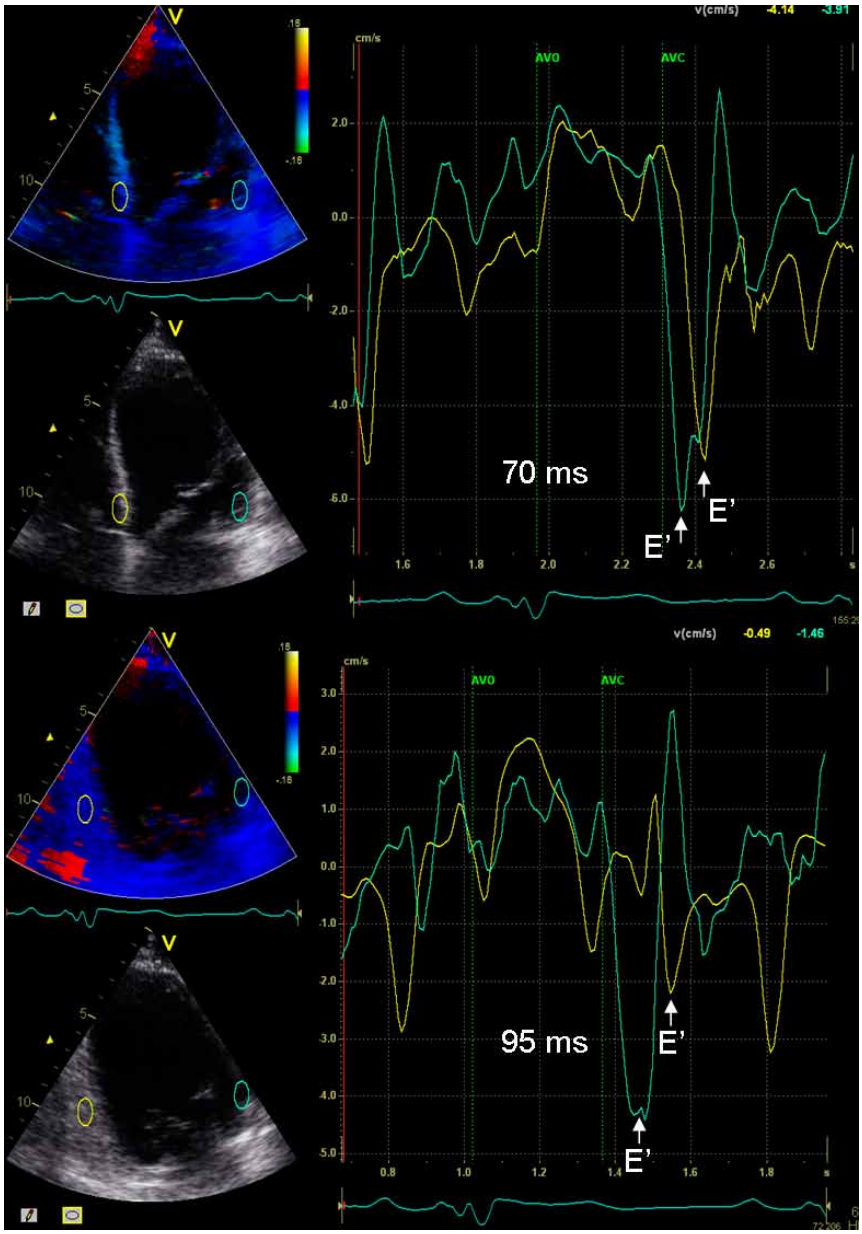

Figure 2 Left ventricular (LV) diastolic dyssynchrony was assessed with color-coded tissue Doppler imaging (TDI). The time between the onset of the QRS complex and the peak early diastolic myocardial velocity (E') of 4 different LV wall segments (anterior, lateral, inferior and septal) was obtained using color-coded TDI. LV dyssynchrony was calculated as the maximal time delay between peak early diastolic velocities of 2 opposing walls (diastolic mechanical delay). In this example, the diastolic mechanical delay was 70 ms between the septal and lateral LV wall (4-chamber view; upper panel) and 95 ms between the anterior and inferior LV wall (2-chamber view; lower panel).

portion of the 4 different LV wall segments (anterior, lateral, inferior and septal) to obtain regional color-coded TDI velocity curves. For each region, the maximal diastolic delay was obtained measuring the time interval between the onset QRS complex and the peak early diastolic myocardial velocity (E′).[7, 15] LV diastolic dyssynchrony was calculated as the time delay between peak early diastolic velocities of 2 opposing walls (diastolic mechanical delay). Significant LV diastolic dyssynchrony was defined as a diastolic mechanical delay of >55 ms.[6] As previously reported[6], the cutoff value of 55 ms was derived from the mean ± 2 SD of the maximal diastolic delay in 38 control patients who had no history of cardiovascular disease. Post-processing of the TDI recordings was performed by two independent observers, who were blinded to the other clinical and phase analysis data.

Statistical Analysis

Continuous variables are expressed as mean ± standard deviation as they were normally distributed when evaluated by Kolmogorov-Smirnov tests. Categorical data are presented as numbers or percentages. Phase analysis on GMPS and TDI were compared using Pearson's linear regression analysis. Furthermore, patients were stratified into patients with and without LV diastolic dyssynchrony using a cutoff value of 55 ms of diastolic mechanical delay on TDI.[6] Phase SD and HBW were compared between patients with LV diastolic dyssynchrony (>55 ms) and without LV diastolic dyssynchrony (≤55 ms) on TDI using the Student's *t* test. LV diastolic dyssynchrony and LV systolic dyssynchrony indices were compared using Pearson's linear regression analyis. Intra- and interobserver reproducibility was evaluated by calculating the intraclass correlation coefficients (ICC). Excellent agreement was defined as an ICC of >0.8. Statistical analyses were performed with SPSS software package, version 16.0 (SPSS Inc., Chicago, Illinois, USA).

Results

Patient Population

A total of 150 end-stage HF patients (114 (76%) men, mean age 66.0±10.4 yrs) were included. Baseline characteristics of the patient population are listed in Table 1. One-hundred-one (67%) patients had ischemic cardiomyopathy, whereas 49 (33%) patients had non-ischemic cardiomyopathy. Patients showed a severely reduced LVEF (27±8%) on 2D echocardiography. Medication consisted of diuretics (87% of patients), angiotensin-converting enzyme inhibitor (ACE-I) or angiotensin (AT) II antagonists (91% of patients) and beta-blockers (73% of patients).

Table 1. Baseline characteristics of the patient population (n=150)

Age (yrs)	66±10
Male gender, n (%)	114 (76)
Ischemic cardiomyopathy	101 (67)
NYHA functional class III (%)	115 (77)
LVEF (%)	27±8
QRS duration (ms)	160±32
Cardiovascular risk factors, n (%)	
Diabetes	32 (21)
Hypertension	59 (39)
Hypercholesterolemia	52 (35)
Smoking	81 (54)
Family history of CAD	58 (39)
Medication, n (%)	
Diuretic	131 (87)
ACE-I / ATII antagonist	137 (91)
Beta-blocker	109 (73)
Statin	99 (66)

Data are presented as mean ± standard deviation or as number (%).
ACE-I = angiotensin converting enzyme - inhibitor; AT = angiotensin; CAD = coronary artery disease; LVEF = left ventricular ejection fraction; NYHA = New York Heart Association.

LV Diastolic Dyssynchrony

The mean values of LV diastolic dyssynchrony indices are shown in Table 2. The patient population showed a mean diastolic mechanical delay of 53.4±21.4 ms on TDI. Phase analysis on GMPS showed a mean diastolic phase SD of 53.3±19.4˚ and diastolic HBW of 175.7±74.7˚. Patient examples of a patient with and without extensive LV diastolic dyssynchrony are provided in Figure 3.

Furthermore, phase analysis on GMPS showed a good correlation with TDI for assessment of LV diastolic dyssynchrony; diastolic phase SD (r=0.81, p<0.01) and diastolic HBW (r=0.75, p<0.01) were well-correlated with LV diastolic dyssynchrony on TDI, as illustrated in Figure 4.

Table 2. Left ventricular (LV) diastolic dyssynchrony indices of the patients (n=150)

Color-coded TDI	
Diastolic mechanical delay (ms)	53.4±21.4
Phase analysis on GMPS	
Diastolic phase SD (˚)	53.3±19.4
Diastolic HBW (˚)	175.7±74.7

GMPS = gated myocardial perfusion single photon emission computed tomography; HBW = histogram bandwidth; SD = standard deviation; TDI = tissue Doppler imaging.

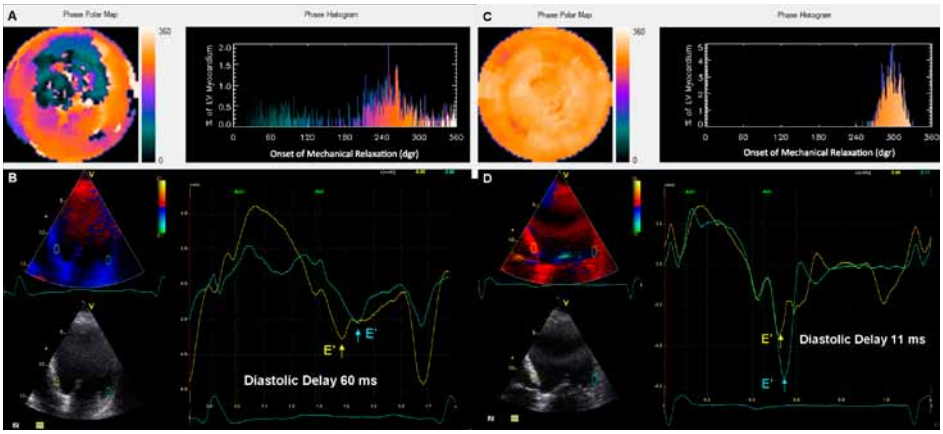

Figure 3 Diastolic left ventricular (LV) dyssynchrony as assessed with phase analysis on gated myocardial perfusion single photon emission computed tomography (SPECT) (GMPS) and 2D echocardiography with tissue Doppler imaging (TDI).

Left panel: Example of a patient with extensive LV diastolic dyssynchrony on GMPS (panel A) and TDI (panel B). Extensive LV diastolic dyssynchrony was reflected by a heterogeneous color-coded phase polar map and a broad phase histogram (panel A); diastolic phase standard deviation (SD) and diastolic histogram bandwidth (HBW) were respectively 90.6˚ and 312.0˚. Similarly, TDI showed extensive LV dyssynchrony with a diastolic mechanical delay of 60 ms (panel B).

Right panel: Example of a patient without LV diastolic dyssynchrony on GMPS (panel C) and TDI (panel D). Phase analysis on GMPS showed a homogeneous color-coded phase polar map and a narrow phase histogram (panel C); diastolic phase SD and diastolic HBW were respectively 14.2˚ and 46.0˚. In this patient, diastolic mechanical delay on TDI was 11 ms (panel D).

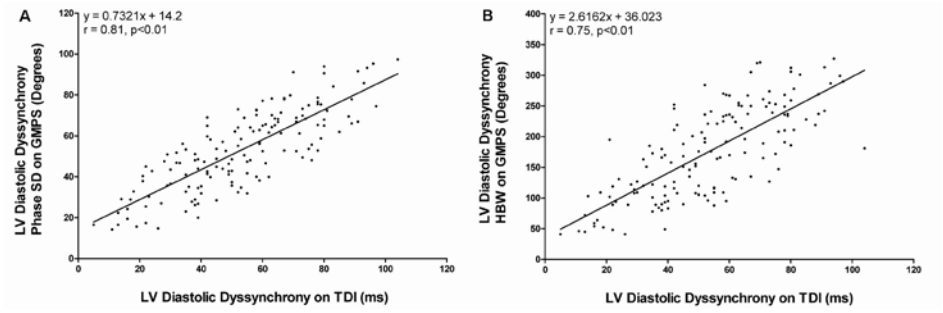

Figure 4 Phase analysis on gated myocardial perfusion single photon emission computed tomography (SPECT) (GMPS) was well-correlated to 2D echocardiography with tissue Doppler imaging (TDI) for assessment of left ventricular (LV) diastolic dyssynchrony. Diastolic phase standard deviation (SD) (panel A; r=0.81, p<0.01) and diastolic histogram bandwidth (HBW) (panel B; r=0.75, p<0.01) showed good correlations with LV diastolic dyssynchrony on TDI.

Additionally, phase analysis on GMPS showed a good correlation with TDI for assessment of LV diastolic dyssynchrony in patients with non-ischemic cardiomyopathy as compared to patients with ischemic cardiomyopathy (diastolic phase SD; r=0.86 vs. r=0.78 and diastolic HBW; r=0.78 vs. r=0.73; p<0.01 for all analyses). Patients with ischemic cardiomyopathy showed more extensive LV diastolic dyssynchrony, as reflected by diastolic phase SD (55.9±18.5˚ vs. 47.9±20.1˚, p=0.2) and diastolic HBW (185.0±72.5˚ vs. 156.6±76.3˚, p=0.4) than patients with non-ischemic cardiomyopathy.

In total, 69 (46%) patients showed LV diastolic dyssynchrony (diastolic mechanical delay >55 ms) on TDI, whereas 81 (54%) patients showed no LV diastolic dyssynchrony (diastolic mechanical delay ≤55 ms). Patients with LV diastolic dyssynchrony showed a significantly larger diastolic phase SD (68.1±13.4˚ vs. 40.7±14.0˚, p<0.01) and diastolic HBW (230.6±54.3˚ vs. 129.0±55.6˚, p<0.01) as compared to patients without LV diastolic dyssynchrony on TDI (Figure 5).

Finally, phase analysis on GMPS showed a good intra- and interobserver reproducibility for diastolic phase SD (ICC 0.97 and 0.88, respectively) and diastolic HBW (ICC 0.98 and 0.93, respectively) in a subset of 25 randomly selected patients.

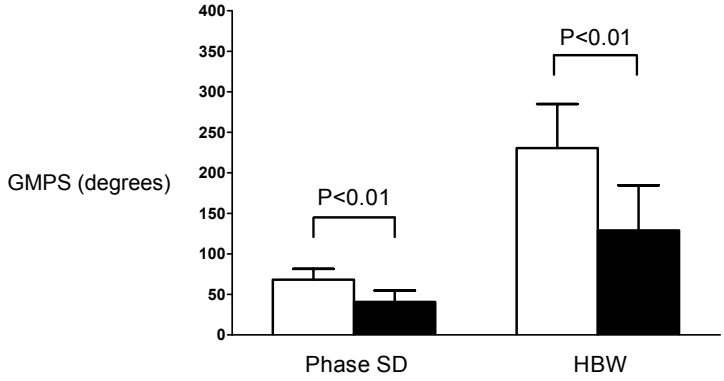

Figure 5 The patient population was divided into patients with and without significant left ventricular (LV) diastolic dyssynchrony on tissue Doppler imaging (TDI) using a cutoff value of 55 ms of diastolic mechanical delay.[6] Gated myocardial perfusion single photon emission computed tomography (SPECT) (GMPS) with phase analysis was used to calculate diastolic phase standard deviation (SD) and diastolic histogram bandwidth (HBW), which were used as markers of LV diastolic dyssynchrony. Patients with significant LV diastolic dyssynchrony on TDI (>55 ms) (white bars) showed significantly higher values of diastolic phase SD (68.1±13.4˚ vs. 40.7±14.0˚, p<0.01) and diastolic HBW (230.6±54.3˚ vs. 129.0±55.6˚, p<0.01) as compared to patients without significant LV diastolic dyssynchrony on TDI (≤55 ms) (black bars).

LV Diastolic Dyssynchrony and QRS Duration

QRS duration was not correlated to LV diastolic dyssynchrony as assessed with phase analysis on GMPS or TDI. Diastolic phase SD (r=0.11, p=NS) and diastolic HBW (r=0.16, p=NS) showed no significant correlation with QRS duration. Similarly, LV diastolic dyssynchrony on TDI (r=0.12, p=NS) showed no significant correlation with QRS duration.

LV Diastolic Dyssynchrony and Systolic Dyssynchrony on GMPS

LV diastolic phase SD (r=0.91, p<0.01) and diastolic HBW (r=0.94, p<0.01) were well-correlated with LV systolic SD and systolic HBW, respectively. In addition, LV diastolic phase SD showed a good correlation with LV systolic HBW (r=0.90, p<0.01). Finally, LV diastolic HBW and systolic phase SD (r=0.92, p<0.01) were well-correlated.

Discussion

The current study showed that phase analysis on GMPS was significantly correlated to TDI for assessment of LV diastolic dyssynchrony. Diastolic phase SD and diastolic HBW as derived from GMPS showed good correlations to diastolic mechanical delay on TDI. Accordingly, phase analysis on GMPS represents a feasible technique for evaluation of LV diastolic dyssynchrony in patients with HF.

Dyssynchrony of the LV contraction pattern, commonly referred to as LV systolic dyssynchrony, is considered an important condition in patients with HF.[1, 2] Previous studies have shown that patients with extensive LV systolic dyssynchrony are at risk for adverse cardiac events.[1, 2] In addition, it has been suggested that LV diastolic dyssynchrony, which is a dyssynchronous relaxation pattern of the LV, plays an important role in patients with HF.[3-5] In patients with HF, it is known that left bundle branch block can cause LV diastolic dyssynchrony and marked diastolic LV filling impairment by inducing a reduced diastolic filling rate, prolonged isovolumic contraction and relaxation times. As a consequence, LV diastolic dyssynchrony is related to abnormalities in diastolic filling pattern of the LV, which may further compromise the hemodynamic function of the failing heart.[3, 4]

At present, TDI echocardiography is a feasible method for evaluation of diastolic relaxation patterns of the LV.[6-8] By measuring the time delays in peak diastolic velocities of LV segments diastolic dyssynchrony can be derived.[6-8] Even though a detailed evaluation of LV diastolic dyssynchrony can be made with TDI, the post-processing of Doppler images remains observer dependent and requires substantial expertise.

Phase analysis on GMPS is another approach for evaluation of mechanical dyssynchrony.[16, 17] In recent years, phase analysis on GMPS has gained increasing interest as it provides robust and reproducible indices of mechanical dyssynchrony using an automated approach.[9, 10] Moreover, GMPS with phase analysis provides integrated information on

mechanical dyssynchrony, regional mechanical activation pattern as well as myocardial perfusion using a single SPECT study. Thus far, several studies have shown its feasibility for assessment of LV systolic dyssynchrony in patients with HF.[16, 17] Henneman et al.[17] have shown that phase analysis on GMPS was well-correlated to 2D echocardiography with TDI for assessment of LV systolic dyssynchrony. Good correlations were found between systolic phase SD ($r=0.80$, $p<0.05$) or systolic HBW ($r=0.89$, $p<0.01$) and LV systolic dyssynchrony on TDI in 75 patients with moderate-to-severe HF. Additionally, phase analysis on GMPS has been compared with real-time 3-dimensional echocardiography (RT3DE) for assessment of LV systolic dyssynchrony in 40 patients with severe HF.[18] Both techniques showed a good agreement for LV systolic dyssynchrony; systolic phase SD ($r=0.80$, $p<0.05$) and systolic HBW ($r=0.76$, $p<0.05$) as derived from GMPS were well-correlated to LV systolic dyssynchrony on RT3DE. Although these studies have shown that phase analysis on GMPS can be used for assessment of LV systolic dyssynchrony, no study has currently evaluated its feasibility to assess LV diastolic dyssynchrony in patients with HF. The present study has shown the feasibility of phase analysis on GMPS for evaluation of LV diastolic dyssynchrony, as reflected by good correlations between LV diastolic dyssynchrony indices on GMPS (phase SD and HBW) and LV diastolic dyssynchrony on TDI. Moreover, patients with LV diastolic dyssynchrony on TDI (diastolic mechanical delay >55 ms) showed significantly larger diastolic phase SD and diastolic HBW as compared to patients without LV diastolic dyssynchrony on TDI (diastolic mechanical delay ≤55 ms). Accordingly, phase analysis on GMPS represents a feasible technique for assessment of both LV diastolic and systolic dyssynchrony in HF patients.

Furthermore, a sub-analysis was performed to evaluate whether phase analysis on GMPS could be used for assessment of LV diastolic dyssynchrony in patients with ischemic and non-ischemic cardiomyopathy. In the current study, the agreement between phase analysis on GMPS and TDI for measuring LV diastolic dyssynchrony was slightly reduced in patients with ischemic cardiomyopathy as compared to patients with non-ischemic cardiomyopathy. One of the potential explanations for this finding could be the fact that the presence of myocardial scar tissue may have influenced the comparison between both techniques. In patients with ischemic cardiomyopathy, the presence of extensive scar tissue may have reduced the accuracy of TDI to assess LV diastolic dyssynchrony. Although the agreement between both techniques was slightly reduced in ischemic HF patients, the study demonstrated that phase analysis on GMPS can also be used for assessment of LV diastolic dyssynchrony in patients with ischemic cardiomyopathy. Finally, the current study has shown that LV diastolic dyssynchrony was a common phenomenon in patients with HF. In the present study, 69 (46%) patients showed LV diastolic dyssynchrony defined as a diastolic mechanical delay of >55 ms on TDI. Similarly, Schuster et al.[3] have reported that diastolic dyssynchrony of the LV was prevalent in patients with HF; 58% of patients showed LV diastolic dyssynchrony on TDI. Furthermore, the current findings were in line with the study from Shanks et al.[6] who

showed that LV diastolic dyssynchrony as assessed with TDI was present in nearly 52% of the patients with HF. Accordingly, phase analysis on GMPS allows detection of LV diastolic dyssynchrony.

LV Diastolic Dyssynchrony and QRS Duration

Several studies have shown that electrical dyssynchrony, as reflected by a prolonged QRS interval, is neither associated with systolic dyssynchrony nor diastolic dyssynchrony of the LV.[3, 19, 20] Schuster et al.[3] have shown that QRS duration was poorly correlated to LV systolic dyssynchrony and LV diastolic dyssynchrony in 108 patients with HF. Similar findings were reported by Wang et al.[7] who revealed that LV diastolic dyssynchrony and QRS interval (r=0.36, p=0.03) were poorly correlated in 60 HF patients. In line with these studies, the present study showed that QRS duration was not correlated to LV diastolic dyssynchrony as assessed with phase analysis on GMPS or TDI.

Limitations

Although the study has demonstrated that phase analysis on GMPS could be used to assess LV diastolic dyssynchrony, some limitations need to be addressed. First, the current findings were based on a relatively small subset of patients, whereas a large cohort of HF patients would have been more preferred to evaluate the feasibility of phase analysis on GMPS for assessment of LV diastolic dyssynchrony. Secondly, even though the current evaluation has shown that phase analysis on GMPS was well-correlated with TDI for assessment of LV diastolic dyssynchrony, some variation was observed between both imaging techniques. This may be explained by the fact that GMPS with phase analysis allows evaluation of the time dispersion of mechanical phenomena (both diastolic relaxation and systolic contraction) in 3D, whereas TDI represents the time difference between 2 opposing walls. For this reason, 3D echocardiography (rather than 2D echocardiography with TDI) would be preferred to evaluate the feasibility of phase analysis on GMPS for assessment of LV diastolic dyssynchrony. At present however, TDI represents the most commonly used technique for the assessment of LV diastolic dyssynchrony. In addition, the implications of GMPS-derived LV diastolic dyssynchrony on response to cardiac resynchronization therapy (CRT) or the effects of CRT on LV diastolic mechanical relaxation were not evaluated. Additional studies are needed in order to establish the accuracy of GMPS-derived LV diastolic dyssynchrony to predict response to CRT or long-term outcome.

Conclusions

Phase analysis on GMPS showed a good correlation with TDI for assessment of LV diastolic dyssynchrony. Accordingly, phase analysis is a feasible technique for evaluation of LV diastolic dyssynchrony in patients with HF.

Reference List

(1) Bader H, Garrigue S, Lafitte S, Reuter S, Jais P, Haissaguerre M, Bonnet J, Clementy J, Roudaut R. Intra-left ventricular electromechanical asynchrony. A new independent predictor of severe cardiac events in heart failure patients. J Am Coll Cardiol. 2004;43:248-56.

(2) Cho GY, Song JK, Park WJ, Han SW, Choi SH, Doo YC, Oh DJ, Lee Y. Mechanical dyssynchrony assessed by tissue Doppler imaging is a powerful predictor of mortality in congestive heart failure with normal QRS duration. J Am Coll Cardiol. 2005;46:2237-43.

(3) Schuster I, Habib G, Jego C, Thuny F, Avierinos JF, Derumeaux G, Beck L, Medail C, Franceschi F, Renard S, Ferracci A, Lefevre J, Luccioni R, Deharo JC, Djiane P. Diastolic asynchrony is more frequent than systolic asynchrony in dilated cardiomyopathy and is less improved by cardiac resynchronization therapy. Journal of american college of cardiology. 2005;46:2250-7.

(4) Xiao HB, Lee CH, Gibson DG. Effect of left bundle branch block on diastolic function in dilated cardiomyopathy. Br Heart J. 1991;66:443-7.

(5) Waggoner AD, Rovner A, de las FL, Faddis MN, Gleva MJ, Sawhney N, vila-Roman VG. Clinical outcomes after cardiac resynchronization therapy: importance of left ventricular diastolic function and origin of heart failure. J Am Soc Echocardiogr. 2006;19:307-13.

(6) Shanks M, Bertini M, Delgado V, Ng ACT, Nucifora G, Van Bommel RJ, Borleffs CJW, Holman ER, Van de Veire NRL, Schalij MJ, Bax JJ. Effect of biventricular pacing on diastolic dyssynchrony. Journal of american college of cardiology. 2010;56:1567-75.

(7) Wang J, Kurrelmeyer KM, Torre-Amione G, Nagueh SF. Systolic and diastolic dyssynchrony in patients with diastolic heart failure and the effect of medical therapy. J Am Coll Cardiol. 2007;49:88-96.

(8) Yu CM, Zhang Q, Yip GW, Lee PW, Kum LC, Lam YY, Fung JW. Diastolic and systolic asynchrony in patients with diastolic heart failure: a common but ignored condition. J Am Coll Cardiol. 2007;49:97-105.

(9) Trimble MA, Velazquez EJ, Adams GL, Honeycutt EF, Pagnanelli RA, Barnhart HX, Chen J, Iskandrian AE, Garcia EV, Borges-Neto S. Repeatability and reproducibility of phase analysis of gated single-photon emission computed tomography myocardial perfusion imaging used to quantify cardiac dyssynchrony. Nucl Med Commun. 2008;29:374-81.

(10) Lin X, Xu H, Zhao X, Folks RD, Garcia EV, Soman P, Chen J. Repeatability of left ventricular dyssynchrony and function parameters in serial gated myocardial perfusion SPECT studies. J Nucl Cardiol. 2010;17:811-6.

(11) Chen J, Garcia EV, Folks RD, Cooke CD, Faber TL, Tauxe EL, Iskandrian AE. Onset of left ventricular mechanical contraction as determined by phase analysis of ECG-gated myocardial perfusion SPECT imaging: development of a diagnostic tool for assessment of cardiac mechanical dyssynchrony. J Nucl Cardiol. 2005;12:687-95.

(12) Hoffman EJ, Huang SC, Phelps ME. Quantitation in positron emission computed tomography: 1. Effect of object size. J Comput Assist Tomogr 1979;3:299-308.

(13) Galt JR, Garcia EV, Robbins WL. Effects of myocardial wall thickness on SPECT quantification. IEEE Trans Med Imaging. 1990;9:144-50.

(14) Schiller NB, Shah PM, Crawford M, DeMaria A, Devereux R, Feigenbaum H, Gutgesell H, Reichek N, Sahn D, Schnittger I. Recommendations for quantitation of the left ventricle by two-dimensional echocardiography. American Society of Echocardiography Committee on Standards, Subcommittee on Quantitation of Two-Dimensional Echocardiograms. J Am Soc Echocardiogr. 1989;2:358-67.

(15) Chang SA, Kim HK, Kim DH, Kim YJ, Sohn DW, Oh BH, Park YB. Left ventricular systolic and diastolic dyssynchrony in asymptomatic hypertensive patients. J Am Soc Echocardiogr. 2009;22:337-42.

(16) Henneman MM, Chen J, Dibbets-Schneider P, Stokkel MP, Bleeker GB, Ypenburg C, van der Wall EE, Schalij MJ, Garcia EV, Bax JJ. Can LV dyssynchrony as assessed with phase analysis on gated myocardial perfusion SPECT predict response to CRT? J Nucl Med. 2007;48:1104-11.

(17) Henneman MM, Chen J, Ypenburg C, Dibbets-Schneider P, Bleeker GB, Boersma E, Stokkel MP, van der Wall EE, Garcia EV, Bax JJ. Phase analysis of gated myocardial perfusion single-photon emission computed tomography compared with tissue Doppler imaging for the assessment of left ventricular dyssynchrony. J Am Coll Cardiol. 2007;49:1708-14.

(18) Marsan NA, Henneman MM, Chen J, Ypenburg C, Dibbets-Schneider P, Ghio S, Bleeker GB, Stokkel MP, van der Wall EE, Tavazzi L, Garcia EV, Bax JJ. Real-time 3-dimensional Echocardiography as a Novel Approach to Quantify Left Ventricular Dyssynchrony: A Comparison Study with Phase Analysis of Gated Myocardial Perfusion Single Photon Emission Computed Tomography. J Am Soc Echocardiogr. 2008;21:801-7.

(19) Bleeker GB, Schalij MJ, Molhoek SG, Holman ER, Verwey HF, Steendijk P, van der Wall EE, Bax JJ. Frequency of left ventricular dyssynchrony in patients with heart failure and a narrow QRS complex. Am J Cardiol. 2005;95:140-2.

(20) Yu CM, Chan YS, Zhang Q, Yip GW, Chan CK, Kum LC, Wu L, Lee AP, Lam YY, Fung JW. Benefits of cardiac resynchronization therapy for heart failure patients with narrow QRS complexes and coexisting systolic asynchrony by echocardiography. J Am Coll Cardiol. 2006;48:2251-7.

Chapter **10**

Left Ventricular Diastolic Dyssynchrony on Gated Myocardial Perfusion SPECT Predicts Response to Cardiac Resynchronization Therapy

Mark J. Boogers, MD[1, 2]; Ji Chen, PhD[3]; Caroline E. Veltman, MD[1, 2]; Nina Ajmone Marsan, MD[1,2]; Rutger J. van Bommel, MD[1]; C. Jan Willem Borleffs, MD[1]; Imad Al Younis, MD[4]; Bernies van der Hiel, MD[4]; Petra Dibbets-Schneider, MSc[4]; Ernst E. van der Wall, MD, PhD[1]; Martin J. Schalij, MD, PhD[1]; Ernest V. Garcia, PhD[3]; Jeroen J. Bax, MD, PhD[1]; Victoria Delgado, MD, PhD[1].

[1]Department of Cardiology, Leiden University Medical Center, Leiden, the Netherlands; [2]The Interuniversity Cardiology Institute of the Netherlands, Utrecht, the Netherlands; [3]Department of Radiology, Emory University School of Medicine, Atlanta, Georgia, USA; [4]Department of Nuclear Medicine, Leiden University Medical Center, Leiden, the Netherlands.

Abstract

Background: Limited information is available about the role of LV diastolic dyssynchrony measured with gated myocardial perfusion single photon emission computed tomography (GMPS) to predict CRT response. Accordingly, the present evaluation explored whether LV diastolic dyssynchrony on GMPS predicts CRT response.

Methods: Heart failure (HF) patients with depressed LV systolic function (LV ejection fraction (LVEF) ≤35%) were included. Before CRT device implantation, patients underwent resting GMPS and real-time 3D echocardiography (RT3DE). GMPS was performed to evaluate myocardial scar (<50% tracer uptake), whereas phase analysis on GMPS was used to assess LV systolic and diastolic dyssynchrony. Systolic histogram bandwidth (HBW) and systolic phase standard deviation (SD) were used as markers of LV systolic dyssynchrony, whereas diastolic HBW and diastolic phase SD were used as LV diastolic dyssynchrony indices. RT3DE was performed to measure LVEF and LV volumes. At 6 months after CRT, RT3DE was repeated and CRT response was defined as a reduction of ≥15% in LV end-systolic volume (LVESV).

Results: A total of 50 patients (36 men, mean age 66.5±9.9 yrs) were included. Thirty-six (72%) patients showed response to CRT, while 14 (28%) were non-responders. Multivariate analyses showed that LV systolic dyssynchrony, LV diastolic dyssynchrony and myocardial scar as assessed with GMPS were independent predictors of CRT response. Receiver operating characteristic curve analyses showed that diastolic HBW and diastolic phase SD were valuable predictors of response to CRT with an area under the curve of 0.79 and 0.80, respectively.

Conclusions: LV diastolic dyssynchrony together with LV systolic dyssynchrony and myocardial scar assessed with GMPS are important determinants of CRT response.

Introduction

Besides improvements in heart failure (HF) symptoms, left ventricular (LV) volumes and LV systolic function, cardiac resynchronization therapy (CRT) has been shown to considerably reduce mortality and morbidity rates in patients with moderate-to-severe HF and prolonged QRS duration.[1, 2]

Even though the benefits of CRT have been demonstrated in several studies, response to CRT may vary significantly among patients referred for CRT.[3, 4] A significant proportion of these patients (approximately 30 to 40%) do not respond to CRT. The lack of response to CRT has been related to several factors such as the absence of pre-existent mechanical dyssynchrony or the presence of (extensive) myocardial scar tissue.[5-7] Previous studies have indicated that pre-existent LV systolic dyssynchrony is associated with a high likelihood of response to CRT.[5, 6]

In addition, LV diastolic dyssynchrony may also be important in patients referred for CRT.[8-10] Thus far, echocardiographic techniques have been commonly used for the assessment of LV diastolic dyssynchrony in patients receiving CRT.[10-13] Although echocardiography provides accurate measurements of LV diastolic dyssynchrony, it requires special expertise along with standardized image and post-processing protocols to achieve good interobserver reproducibility.

Gated myocardial perfusion single photon emission computed tomography (SPECT) (GMPS) with phase analysis is a comprehensive imaging technique that provides automatic and reproducible measures of LV mechanical dyssynchrony, including phase histogram bandwidth (HBW) and phase standard deviation (SD).[14, 15] Although phase analysis on GMPS has been used to predict CRT response using LV systolic dyssynchrony[16], limited information is available about the role of LV diastolic dyssynchrony assessment to predict response to CRT. Accordingly, the current study aimed to investigate whether LV diastolic dyssynchrony as derived from phase analysis on GMPS predicts response to CRT.

Methods

Patient Population and Data Collection

The patient population consisted of patients who were clinically referred for implantation of a CRT device because of drug-refractory HF, reduced LV systolic function (LV ejection fraction (LVEF) ≤35%) and sinus rhythm.[1, 2] Patient data were prospectively collected in the departmental Cardiology Information System (EPD-Vision®, Leiden University Medical Center, Leiden, the Netherlands) and retrospectively analyzed. All patients were stable on maximum tolerated doses of medications. Patients with decompensated heart failure, recent

myocardial infarction (within 3 months of CRT device implantation) or who died during 6 months follow-up after CRT implantation were excluded. Ischemic cardiomyopathy was defined as a ≥50% stenosis in one or more of the major epicardial coronary arteries and/or a history of myocardial infarction, percutaneous coronary intervention or coronary artery bypass grafting.

According to the institutional protocol, the clinical status was evaluated prior to CRT implantation, including New York Heart Association (NYHA) functional class, 6-minute walk test and quality of life score using the Minnesota Quality-of-Life Questionnaire.[17] In addition, patients underwent resting GMPS as well as real-time 3D echocardiography (RT3DE). Resting GMPS was performed to evaluate the presence and extent of myocardial scar. Phase analysis on GMPS was used to assess LV systolic and diastolic dyssynchrony. Systolic HBW and systolic phase SD were used as markers of LV systolic dyssynchrony, whereas diastolic HBW and diastolic phase SD as derived from the diastolic phase distribution were used as LV diastolic dyssynchrony indices. RT3DE was performed to measure LVEF and LV volumes.

After 6 months of CRT, the evaluation of clinical status and RT3DE were repeated. As previously reported, a reduction of ≥15% in LV end-systolic volume (LVESV) at 6 months follow-up defined response to CRT.[18] The value of baseline clinical, echocardiographic and GMPS variables for the prediction of response to CRT was evaluated.

Gated Myocardial Perfusion SPECT

Acquisition

GMPS with ^{99m}technetium tetrofosmin was performed at rest using a triple-head SPECT camera (GCA 9300/HG; Toshiba Corporation, Tokyo, Japan) which was equipped with low-energy high-resolution collimators. An average dose of 500 MBq of ^{99m}technetium tetrofosmin (MYOVIEW, General Electric Healthcare, United Kingdom) was given intravenously per patient. Around the energy peak of ^{99m}technetium tetrofosmin (140 KeV) a 20% window was centered. In total, 90 projections (step and shoot method, 35 s/projection, 64 x 64 matrix, total imaging time 23 minutes) were acquired over a 360° circular orbit. ECG gating was applied on the cardiac cycle with 16 frames per cardiac cycle using a tolerance window of 50%.

Thereafter, the GMPS data sets were uploaded to the Emory Cardiac Toolbox (Emory University, Atlanta, Georgia, USA) for data reconstruction, reorientation and phase analysis processing. All data sets were reconstructed using ordered subsets expectation maximization (OSEM) with 3 iterations and 10 subsets. The gated images were filtered with a Butterworth filter with a cutoff frequency of 0.35 cycles/cm and a power of 10. Subsequently, the reconstructed images were reoriented manually with the use of an automatic reorientation tool in the Emory Reconstruction Toolbox (Emory University, Atlanta, Georgia, USA) to generate gated short-axis images which were sampled for regional maximum counts using the Emory

Cardiac Toolbox (Emory University, Atlanta, Georgia, USA). These sampled data sets were then submitted to the multi-harmonic phase analysis tool for phase analysis processing that was performed blinded at Emory University.

Additionally, GMPS data sets were evaluated for the presence and extent of myocardial scar. Data sets were displayed in polar map format and normalized for maximal myocardial activity (100%). Myocardial scar was defined as myocardium with <50% tracer uptake. Subsequently, the extent of myocardial scar was expressed as a percentage of the myocardium.

Phase Analysis on GMPS

Phase analysis on GMPS was used to assess LV systolic and diastolic dyssynchrony. First, LV systolic dyssynchrony was assessed using gated short-axis SPECT images, as previously described.[16] In brief, the onset of mechanical contraction was detected per cardiac region using count-based wall thickening curves. These count-based wall-thickening curves were derived from changes in myocardial counts during the cardiac cycle. For each cardiac segment, the onset of mechanical contraction was reflected by a phase angle. After the phase angles were obtained for each cardiac segment within the LV (>600 regions over the entire LV), they were displayed in a polar map and phase histogram. Consecutively, the phase histogram was used to derive quantitative parameters of LV systolic dyssynchrony; systolic HBW (reflects 95% of the phase angles) and systolic phase SD (SD of the phase distribution) were used as markers of LV systolic dyssynchrony.

In addition, LV diastolic dyssynchrony was assessed using the same gated short-axis SPECT images. The assessment of LV diastolic dyssynchrony was based on several consecutive processing steps (Figure 1). First, regional maximal count detection was performed on short-axis images in 3D for each temporal frame. Based on the partial volume effect[19, 20], the variation of the regional maximal counts was proportional to changes in regional wall thickening over the cardiac cycle.[20] Consecutively, the third Fourier harmonic function was used to approximate the discrete sample points into a continuous wall-thickening curve. For each region (>600 regions over the entire LV), a wall-thickening curve was generated that provided a phase angle which represented the onset of mechanical relaxation (OMR) of the particular region. The OMR phase is the time point when the curves crossed the middle line from positive to negative. Once the phase angles for the entire LV were obtained, a phase distribution was generated that provided information on the degree of diastolic dyssynchrony of the LV. A polar map and histogram were used to display the phase angle distribution of the LV. LV diastolic dyssynchrony indices were derived from the phase histogram; diastolic HBW (the histogram bandwidth including 95% of the OMR phase angles) and diastolic phase SD (standard deviation of the OMR phase distribution) were used as markers of LV diastolic dyssynchrony.

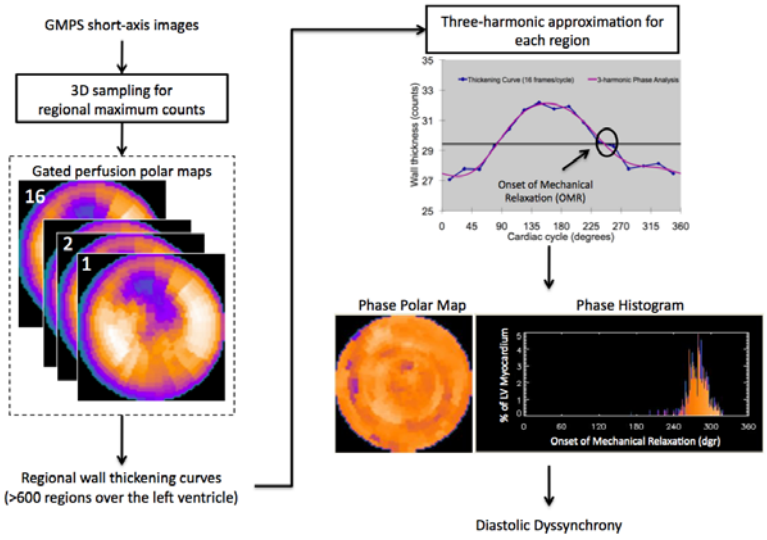

Figure 1. Diastolic mechanical dyssynchrony of the left ventricle (LV) can be assessed with phase analysis on gated myocardial perfusion single photon emission computed tomography (SPECT) (GMPS). At first, GMPS data sets were reoriented and reconstructed into gated short-axis images. A 3D regional maximal count detection was performed for each temporal time frame using reconstructed gated short-axis SPECT images. Subsequently, approximation of discrete sample points into a continuous wall-thickening curve was performed by the third Fourier harmonic function. These wall-thickening curves were generated for each cardiac region (>600 regions for the entire LV). Using the wall-thickening curve, a phase angle was derived which reflected the onset of mechanical relaxation (OMR) per cardiac region. All phase angles (>600 for entire LV) were plotted in a phase polar map or histogram. Finally, LV diastolic dyssynchrony indices were derived from the phase histogram; diastolic phase standard deviation (SD) (SD of the OMR phase distribution) and diastolic histogram bandwidth (HBW) (the width of the band that includes 95% of the OMR phase angles) were used as markers of LV diastolic dyssynchrony.

Real-time 3D Echocardiography

Patients underwent RT3DE with a commercially available system (iE33, Philips Medical Systems, Bothell, Washington, USA) equipped with an X3, fully sampled matrix transducer. Apical full-volume data sets were obtained combining, within 1 breath-hold, 7 real-time ECG-triggered subvolumes into a larger pyramidal volume (101 x 104 degrees). For this study, the frame rate varied between 20 to 35 frames/s. Post-processing of the digitally stored RT3DE data sets was performed off-line using a semi-automated contour tracing algorithm (Q-lab, version 7.0, Philips Medical Systems).

The apical 4-chamber and 2-chamber views as well as the parasternal short-axis views were automatically displayed during the post-processing of the RT3DE data set. Once the cardiac apex and mitral annulus were identified using 5 reference points in the end-diastolic and end-systolic frames, a pre-configured ellipse was fitted to the endocardial border for

each frame. Manual adaptations of the endocardial border could be performed to improve the endocardial border detection. Thereafter, the LV 3D model was automatically generated and used for the assessment of LVEF and LV volumes in each patient.[21] RT3DE data sets were excluded from further analysis if they showed more than 2 LV segments that were not visualized or uninterpretable. RT3DE was performed at baseline and after 6 months of CRT. A decrease of ≥15% in LVESV at 6 months follow-up defined response to CRT.[18]

CRT Implantation

All leads were placed via the subclavian route and the right atrial and ventricular leads were positioned conventionally. Once a coronary sinus venogram was obtained using the balloon catheter, an 8 Fr guiding catheter was used to position the LV pacing lead as far as possible in the coronary venous system, preferably into the lateral or posterolateral vein. All LV leads were connected to a dual-chamber biventricular implantable cardiac device. Simultaneous biventricular pacing was applied in all patients and the interventricular delay was not systematically adjusted during the first 6 months. The optimal atrioventricular delay was set based on echocardiographic transmitral pulsed wave Doppler recordings.

Statistical Analysis

Continuous variables are expressed as mean ± standard deviation and categorical data are presented as numbers or percentages. Kolmogorov-Smirnov tests were used to evaluate whether baseline variables were normally distributed. Changes in clinical, echocardiographic and GMPS variables between baseline and 6 months follow-up were evaluated with paired Student t-tests or Wilcoxon signed-rank tests, as appropriate. Furthermore, differences in baseline variables between responders and non-responders to CRT were evaluated with unpaired Student t-tests and Mann-Whitney U-test, as appropriate (for continuous variables) and Chi-square or Fisher exact tests (for categorical variables).

Consecutively, univariate logistic regression models were constructed to identify significant predictors of response to CRT. All variables that were significantly associated with CRT response at the $p<0.05$ level were included in the multivariate logistic regression model (using enter method). To avoid multi-collinearity different predictive models were created in order to identify significant independent determinants of response to CRT.

Finally, the optimal cutoff values of diastolic HBW and diastolic phase SD for prediction of CRT response were defined using receiver operating characteristic (ROC) curve analyses. Using the ROC curves, the area under the curve (AUC) was calculated for both diastolic HBW and diastolic phase SD. The optimal cutoff value was defined as the value that yielded the maximal sum of sensitivity and specificity. Statistical analyses were performed with SPSS software package, version 16.0 (SPSS Inc., Chicago, Illinois, USA). A p-value <0.05 was considered statistically significant.

Results

Patient Population

From an ongoing registry of HF patients treated with CRT, 63 consecutive HF patients who had undergone GMPS prior to CRT implantation were evaluated.[22] Of these 63 patients, 13 patients were excluded as they did not undergo RT3DE at 6 months follow-up. Accordingly, a total of 50 patients (36 males, mean age 66.5±9.9 yrs) were included in the current analysis. The baseline characteristics of these patients are shown in Table 1. Thirty (60%) patients had ischemic cardiomyopathy, and 20 (40%) patients had non-ischemic cardiomyopathy. In total, 43 (86%) patients were in NYHA functional class III, whereas the remaining 7 (14%) patients were in NYHA functional class IV. RT3DE showed a mean LVEF of 27.7±5.8%. Patients were treated with optimal HF medication, consisting of diuretics (86%), angiotensin converting enzyme-inhibitors (ACE-I) (90%) and beta-blockers (72%).

Furthermore, GMPS with phase analysis showed a mean systolic HBW and systolic phase SD of 160.9±73.1˚ and 47.7±18.6˚, respectively. In addition, mean diastolic HBW

Table 1. Baseline characteristics of the patient population (n=50)

Age (yrs)	66.5±9.9
Male gender	36 (72)
Ischemic cardiomyopathy	30 (60)
Clinical evaluation	
NYHA functional class III/IV	43/7
Quality-of-life score	26.1±15.4
6-minute walk test (m)	358.6±105.9
QRS duration (ms)	164.0±25.5
Real-time 3D echocardiography	
LVEDV (mL)	206.8±48.4
LVESV (mL)	150.5±42.4
LVEF (%)	27.7±5.8
GMPS variables	
Myocardial scar (%)	26.1±14.9
LV systolic dyssynchrony	
HBW (˚)	160.9±73.1
Phase SD (˚)	47.7±18.6
LV diastolic dyssynchrony	
HBW (˚)	183.3±74.2
Phase SD (˚)	56.3±19.8

Data are presented as mean ± standard deviation or as number (%). GMPS = gated myocardial perfusion single photon emission computed tomography; HBW = histogram bandwidth; LVEDV = left ventricular end-diastolic volume; LVEF = left ventricular ejection fraction; LVESV = left ventricular end-systolic volume; NYHA = New York Heart Association; SD = standard deviation.

and diastolic phase SD were 183.3±74.2˚ and 56.3±19.8˚. The extent of myocardial scar on GMPS was on average 26.1±14.9%.

Baseline versus 6 months Follow-up

After 6 months of CRT, 30 (60%) patients showed an improvement of 1 NYHA functional class and 12 (24%) patients showed an improvement of 2 NYHA functional classes at 6 months follow-up. In addition, a marked increase in 6-minute walk distance (from 352.9±108.4 m to 380.1±107.7 m, p<0.01) as well as a significant reduction in quality-of-life score (from 25.5±15.0 to 17.4±14.1, p<0.01) were observed. At 6 months follow-up, patients showed a significant improvement in LVEDV (206.8±48.4 mL vs. 183.8±52.8 mL, p<0.01), LVESV (150.5±42.4 mL vs. 119.9±44.6 mL, p<0.01) and LVEF (27.7±5.8% vs. 35.6±7.5%, p<0.01).

After 6 months of CRT, 36 (72%) patients were classified as responders to CRT (reduction of ≥15% in LVESV at 6 months of CRT), whereas the remaining 14 (28%) patients were classified as non-responders to CRT.

Among responders to CRT, 23 (64%) patients showed an improvement of at least 1 NYHA functional class at 6 months follow-up (baseline vs. follow-up, p<0.05). In addition, CRT responders showed a significant improvement in quality-of-life score (25.3±15.5 vs. 17.8±14.8, p<0.01) and 6-minute walk distance (376.4±98.6 m vs. 409.0±87.3 m, p<0.01) at 6 months of follow-up. Finally, in these patients, a significant improvement in LVEDV (206.6±46.6 mL vs. 175.9±44.9 mL, p<0.01), LVESV (150.1±40.3 mL vs. 108.8±31.6 mL, p<0.01) and LVEF (27.8±5.3% vs. 38.4±6.3%, p<0.01) was observed at 6 months post-CRT.

Even though non-responders to CRT showed an improvement in NYHA functional class (baseline vs. follow-up, p=0.002) and quality-of-life score (25.8±14.2 vs. 16.3±12.7, p=0.009), no improvements were observed in 6-minute walk distance (298.2±114.6 m vs. 312.8±123.9 m, p=0.3), LVEDV (207.4±54.7 mL vs. 204.1±66.8 mL, p=0.2), LVESV (151.7±48.8 mL vs. 148.5±60.0 mL, p=0.2), and LVEF (27.6±7.1% vs. 28.6±6.0%. p=0.5).

Baseline Characteristics: Responders versus Non-Responders to CRT

Baseline characteristics of responders and non-responders to CRT are shown in Table 2. No significant differences were observed for clinical and echocardiographic variables between responders and non-responders to CRT. However, responders to CRT showed a significantly larger systolic HBW (180.8±66.1˚ vs. 109.6±66.9˚, p<0.01) and systolic phase SD (53.2±15.8˚ vs. 33.5±18.1˚, p<0.01) than non-responders to CRT.

Importantly, diastolic HBW (205.3±64.0˚ vs. 126.9±70.5˚, p<0.01) and diastolic phase SD (62.1±16.5˚ vs. 41.2±20.3˚, p<0.01) were also significantly higher in responders to CRT as compared to non-responders to CRT (Figure 2). Examples of a patient with and without extensive LV diastolic dyssynchrony are provided in Figure 3.

Table 2. Baseline characteristics in patients with and without response to cardiac resynchronization therapy (CRT)

Baseline variables	Responders (n=36)	Non-responders (n=14)	p-value
Age (yrs)	65.8±10.5	68.4±8.2	0.3
Male gender	26 (72)	10 (71)	1.0
Ischemic cardiomyopathy	21 (58)	10 (71)	0.7
Clinical evaluation			
NYHA functional class III/IV	29/7	14/0	0.07
Quality-of-life score	26.3±16.2	25.5±13.6	0.9
6-minute walk test (m)	378.7±95.2	310.5±118.5	0.05
QRS duration (ms)	165.4±25.7	160.4±25.5	0.4
Real-time 3D echocardiography			
LVEDV (mL)	206.6±46.6	207.4±54.7	0.8
LVESV (mL)	150.1±40.3	151.7±48.8	0.6
LVEF (%)	27.7±5.3	27.5±7.1	0.9
GMPS variables			
Myocardial scar (%)	24.3±13.3	30.8±17.9	0.2
LV systolic dyssynchrony			
HBW (˚)	180.8±66.1	109.6±66.9	0.001
Phase SD (˚)	53.2±15.8	33.5±18.1	0.001
LV diastolic dyssynchrony			
HBW (˚)	205.3±64.0	126.9±70.5	0.002
Phase SD (˚)	62.1±16.5	41.2±20.3	0.001

Data are presented as mean ± standard deviation or as number (%). GMPS = gated myocardial perfusion single photon emission computed tomography; HBW = histogram bandwidth; LVEDV = left ventricular end-diastolic volume; LVEF = left ventricular ejection fraction; LVESV = left ventricular end-systolic volume; NYHA = New York Heart Association; SD = standard deviation.

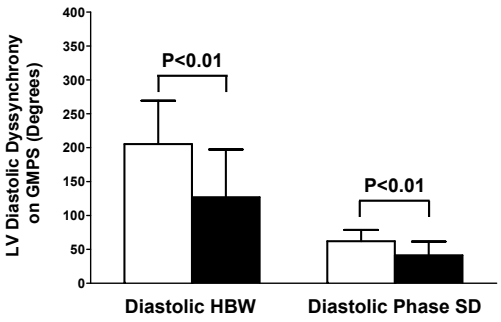

Figure 2. Patients with response to cardiac resynchronization therapy (CRT) showed significantly more left ventricular (LV) diastolic dyssynchrony on gated myocardial perfusion single photon emission computed tomography (SPECT) (GMPS) as compared to patients without response to CRT. Both diastolic histogram bandwidth (HBW) (205.3±64.0˚ vs. 126.9±70.5˚, p<0.01) and diastolic phase standard deviation (SD) (62.1±16.5˚ vs. 41.2±20.3˚, p<0.01) were significantly higher in responders to CRT (white bars) than in non-responders to CRT (black bars).

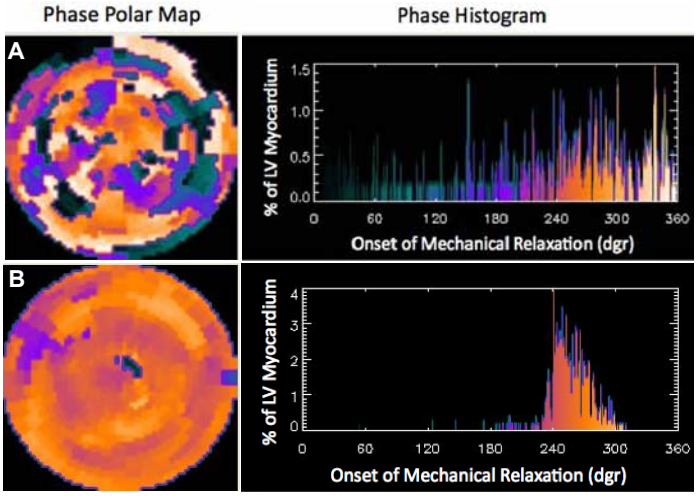

Figure 3. Phase analysis on gated myocardial perfusion single photon emission computed tomography (SPECT) (GMPS) was used for assessment of left ventricular (LV) diastolic dyssynchrony in patients referred for cardiac resynchronization therapy (CRT). Diastolic histogram bandwidth (HBW) and diastolic phase standard deviation (SD) were used as markers of LV diastolic dyssynchrony.

A. Example of a responder to CRT who showed extensive LV diastolic dyssynchrony as reflected by a wide histogram and a heterogenously color-coded diastolic phase polar map. Phase analysis on GMPS showed a diastolic HBW and diastolic phase SD of 313.0˚ and 91.6˚, respectively. After 6 months of CRT, the patient showed a marked improvement in LV ejection fraction (LVEF) (23% vs. 42%).

B. Example of a non-responder to CRT who showed no LV diastolic dyssynchrony on GMPS. Phase analysis showed a narrow histogram and homogenously color-coded diastolic phase polar map. In this patient, the diastolic HBW and diastolic phase SD were on average 64.0˚ and 28.9˚. No improvement in LVEF was observed after 6 months of CRT (32% vs. 30%).

Prediction of Response to CRT

The value of baseline clinical and imaging variables for prediction of CRT response was evaluated (Table 3). Univariate logistic regression analyses showed that systolic HBW (OR=1.02 95% CI 1.01-1.03, p<0.01), systolic phase SD (OR=1.08, 95% CI 1.03-1.13, p<0.01), diastolic HBW (OR=1.02, 95% CI 1.01-1.03, p<0.01) and diastolic phase SD (OR=1.07, 95% CI 1.02-1.11, p<0.01) were significantly associated with CRT response.

To avoid multi-collinearity among several variables, different multivariate models were constructed to determine independent predictors for CRT response, as shown in Table 4. As myocardial scar, electrical dyssynchrony (QRS duration) and age were regarded as important parameters in patients referred for CRT, they were also included in the multivariate model.

Multivariate analyses demonstrated that systolic HBW and systolic phase SD were independent predictors for CRT response. In addition, diastolic HBW and diastolic phase SD as well as myocardial scar were independent predictors for response to CRT.

As shown in Figure 4, ROC curve analyses showed that diastolic HBW (AUC 0.79) and diastolic phase SD (AUC 0.80) could be used for prediction of response to CRT. The optimal cutoff value of diastolic HBW for prediction of CRT response was 157.5˚, yielding a sensitivity of 81% and a specificity of 79%. For diastolic phase SD, the optimal point was defined at 47.0˚ with a sensitivity of 86% and a specificity of 71%.

Table 3. Univariate analyses of baseline variables for prediction of response to cardiac resynchronization therapy (CRT)

Variables	Univariate analysis OR (95% CI)	p-value
Age (yrs)	0.97 (0.91-1.04)	0.4
Male gender	1.04 (0.26-4.09)	1.0
Ischemic cardiomyopathy	0.78 (0.22-2.79)	0.7
Clinical evaluation		
Quality-of-life score	1.00 (0.96-1.05)	0.9
6-minute walk test (m)	1.01 (1.00-1.01)	0.1
QRS duration (ms)	1.01 (0.98-1.03)	0.5
Real-time 3D echocardiography		
LVEDV (mL)	1.00 (0.99-1.01)	1.0
LVESV (mL)	0.99 (0.99-1.01)	0.9
LVEF (%)	1.01 (0.90-1.12)	0.9
GMPS variables		
Myocardial scar (%)	0.97 (0.93-1.01)	0.2
LV systolic dyssynchrony		
HBW (˚)	1.02 (1.01-1.03)	<0.01*
Phase SD (˚)	1.08 (1.03-1.13)	<0.01*
LV diastolic dyssynchrony		
HBW (˚)	1.02 (1.01-1.03)	<0.01*
Phase SD (˚)	1.07 (1.02-1.11)	<0.01*

* Significant association with CRT response at a level of $p<0.05$ in univariate analysis.

CI = confidence interval; GMPS = gated myocardial perfusion single photon emission computed tomography; HBW = histogram bandwidth; LVEDV = left ventricular end-diastolic volume; LVEF = left ventricular ejection fraction; LVESV = left ventricular end-systolic volume; OR = odds ratio; SD = standard deviation.

Table 4. Multivariate analyses of baseline variables for prediction of response to cardiac resynchronization therapy (CRT)

Variables	Multivariate analysis OR (95% CI)	p-value
Model I		
Myocardial scar (%)	0.88 (0.80-0.96)	<0.01*
Systolic HBW (˚)	1.04 (1.02-1.06)	<0.01*
QRS duration (ms)	1.02 (0.98-1.06)	0.4
Age (yrs)	0.97 (0.88-1.08)	0.6
Model II		
Myocardial scar (%)	0.87 (0.79-0.96)	<0.01*
Systolic phase SD (˚)	1.18 (1.07-1.30)	<0.01*
QRS duration (ms)	1.02 (0.98-1.07)	0.3
Age (yrs)	0.99 (0.89-1.10)	0.8
Model III		
Myocardial scar (%)	0.87 (0.79-0.95)	<0.01*
Diastolic HBW (˚)	1.04 (1.02-1.07)	<0.01*
QRS duration (ms)	1.02 (0.98-1.06)	0.3
Age (yrs)	1.00 (0.90-1.11)	1.0
Model IV		
Myocardial scar (%)	0.87 (0.80-0.95)	<0.01*
Diastolic phase SD (˚)	1.16 (1.06-1.26)	<0.01*
QRS duration (ms)	1.03 (0.99-1.08)	0.2
Age (yrs)	1.00 (0.90-1.11)	1.0

* Significant association with CRT response at a level of $p<0.05$ in multivariate analysis. CI = confidence interval; HBW = histogram bandwidth; OR = odds ratio; SD = standard deviation. The increment for systolic HBW, systolic phase SD, diastolic HBW and diastolic phase SD was 1˚.

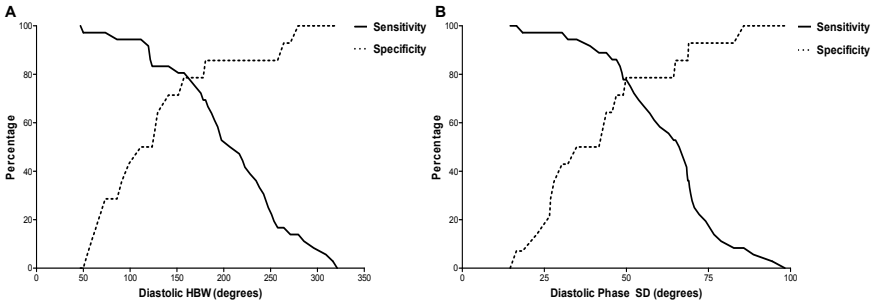

Figure 4. Receiver-operating characteristic (ROC) curve analyses showed that diastolic histogram bandwidth (HBW) (AUC 0.79) and diastolic phase standard deviation (SD) (AUC 0.80) can be used for prediction of response to cardiac resynchronization therapy (CRT). The optimal cutoff value for diastolic HBW (panel A) was defined at 157.5˚ with a sensitivity of 81% and a specificity of 79%. For diastolic phase SD (panel B), the optimal point was 47.0˚, yielding a sensitivity of 86% with a specificity of 71%.

Discussion

The current study showed that LV systolic dyssynchrony, LV diastolic dyssynchrony and myocardial scar are related to response to CRT. More specifically, the study demonstrated that both diastolic HBW and diastolic phase SD (markers of LV diastolic dyssynchrony) as assessed with phase analyses on GMPS can be used for identification of potential responders to CRT.

Resynchronization of the LV contraction pattern by synchronized pacing of both ventricles (CRT) has resulted in substantial improvements in clinical symptoms, LV volumes and LV systolic function of patients with symptomatic HF and intra-ventricular conduction delay.[1, 2] Beyond these beneficial effects, patients with CRT exhibit considerably lower mortality and morbidity rates when compared to patients with conventional HF medication alone.[23, 24] However, on a patient level, it has been shown that around 30 to 40% of patients who fulfill current inclusion criteria for CRT do not show response to CRT.[5-7] Accordingly, a large number of studies have focused on the identification of potential determinants of CRT response.[25] Factors likely to influence CRT response include mechanical dyssynchrony, ischemic heart disease, LV lead position and CRT device programming. Among these factors, pre-existent mechanical dyssynchrony of the LV contraction pattern (LV systolic dyssynchrony) has been identified as one of the important determinants of response to CRT.[5, 6]

In addition, it has been suggested that a dyssynchronous relaxation pattern of the LV (LV diastolic dyssynchrony) may also play a role in patients receiving CRT.[8-10] Although most of the clinical studies have used echocardiographic techniques for assessment of LV diastolic dyssynchrony, echocardiography may show some intra- and interobserver variability as it requires special expertise and dedicated image and post-processing protocols.[10, 11, 26]

GMPS with phase analysis may overcome these limitations as it provides robust indices of mechanical dyssynchrony using an automatic approach with limited manual interference, which can be applied on conventional GMPS images.[14, 15]

The Influence of LV Diastolic Dyssynchrony as Assessed with GMPS on CRT Response

Although previous observations have indicated that GMPS can be used for prediction of CRT response, these studies have only focused on the assessment of pre-existent LV systolic dyssynchrony with phase analysis, rather than LV diastolic dyssynchrony.[16] The current evaluation has shown that LV diastolic dyssynchrony on GMPS can also be used for identification of responders to CRT; patients with extensive LV diastolic dyssynchrony were more likely to respond to CRT as compared to patients without significant LV diastolic dyssynchrony. LV diastolic dyssynchrony may play an important role in CRT patients as resynchronization of the LV contraction pattern may also result in a resynchronization of the diastolic relaxation pattern of the LV. For this reason, CRT may (partially) correct abnormalities in LV diastolic

filling that have been associated with LV diastolic dyssynchrony.[8, 27, 28] As diastolic dyssynchrony of the LV has been linked to a reduced LV diastolic filling time and filling rate[8, 27, 28], a reduction of LV diastolic dyssynchrony by CRT may exert positive effects on LV diastolic filling, and as a consequence, may improve the hemodynamics of the heart. Furthermore, patients with LV diastolic dyssynchrony may benefit from CRT as resynchronization of the LV contraction and filling pattern could result in an improvement of diastolic interventricular interaction, particularly in patients with elevated LV filling pressures.[8, 29]

The current study findings are of interest as previous studies have shown that LV diastolic dyssynchrony represents a common pathophysiologic condition in patients fulfilling the criteria for CRT.[10-13] In these patients, LV diastolic dyssynchrony is at least as common as LV systolic dyssynchrony with a prevalence of more than 50%.[10-13] Moreover, it has been shown that LV diastolic dyssynchrony can be present without co-existence of LV systolic dyssynchrony in a substantial number of patients.[10]

Accordingly, the assessment of LV diastolic dyssynchrony may provide useful information to predict CRT response in a large number of HF patients. The present evaluation demonstrated that both diastolic HBW and diastolic phase SD can be used to predict CRT response. Even though diastolic HBW and diastolic phase SD were both independent predictors of response to CRT, the optimal cutoff values of diastolic HBW and diastolic phase SD to predict CRT response showed suboptimal sensitivity and specificity values; diastolic HBW showed an optimal cutoff value of 157.5˚ with a sensitivity of 81% and a specificity of 79%, whereas diastolic phase SD showed an optimal cutoff value of 47.0˚ with a sensitivity of 86% and a specificity of 71%. This may be related to the fact that other issues may have influenced the likelihood of response to CRT, including the presence of LV systolic dyssynchrony as well as myocardial scar tissue.

The Influence of LV Systolic Dyssynchrony and Myocardial Scar as Assessed with GMPS on CRT Response

A large number of studies have currently indicated that the presence of pre-existent LV systolic dyssynchrony affects the likelihood of response to CRT.[5, 6] Henneman et al.[16] have evaluated the predictive value of LV systolic dyssynchrony as assessed with phase analysis on GMPS in 42 patients with advanced HF. In these patients, both systolic HBW and phase SD were significantly higher in patients with CRT response than in patients without CRT response. Moreover, both markers of LV systolic dyssynchrony were predictive for CRT response, as reflected by an AUC of 0.78 and 0.81 for systolic HBW and systolic phase SD, respectively. The current study has shown that LV systolic dyssynchrony plays an important role in patients with CRT as both systolic HBW and systolic phase SD were independent predictors for response to CRT. Patients with extensive LV systolic dyssynchrony were more likely to respond to CRT when compared to patients with no LV systolic dyssynchrony at baseline.

Furthermore, the presence and location of (transmural) scarred myocardium may have influenced the possibility of CRT response in the current patient population. Previous observations have shown that patients with extensive myocardial scar tissue are less likely to respond to CRT than patients with no myocardial scar tissue.[7, 30] Ypenburg et al.[7] have evaluated whether myocardial infarction as assessed with myocardial perfusion scintigraphy was an important determinant for outcome after 6 months of CRT in 51 patients with ischemic cardiomyopathy. Patients with a low total scar score were more likely to respond to CRT as compared to patients with a high total scar score ($p<0.05$). Similarly, the present study has demonstrated that myocardial scar is an important determinant for prediction of CRT response. Non-responders to CRT showed a considerable higher myocardial scar burden as compared to responders to CRT.

Accordingly, GMPS with phase analysis permits assessment of LV systolic and diastolic dyssynchrony along with information on the presence, location and extent of myocardial infarct tissue. A comprehensive evaluation of CRT patients based upon assessment of LV systolic and diastolic dyssynchrony as well as myocardial scar tissue would improve the identification of potential responders to CRT. One of the major advantages of phase analysis on GMPS is the fact that it permits an integrated assessment of mechanical dyssynchrony and myocardial perfusion using a single SPECT study.

Conclusion

LV systolic dyssynchrony, LV diastolic dyssynchrony and myocardial scar tissue as assessed with GMPS are important determinants of response to CRT. Diastolic HBW and diastolic phase SD are markers of LV diastolic dyssynchrony which can be used for prediction of CRT response.

Reference List

(1) Epstein AE, DiMarco JP, Ellenbogen KA, Estes NA, III, Freedman RA, Gettes LS, Gillinov AM, Gregoratos G, Hammill SC, Hayes DL, Hlatky MA, Newby LK, Page RL, Schoenfeld MH, Silka MJ, Stevenson LW, Sweeney MO, Smith SC, Jr., Jacobs AK, Adams CD, Anderson JL, Buller CE, Creager MA, Ettinger SM, Faxon DP, Halperin JL, Hiratzka LF, Hunt SA, Krumholz HM, Kushner FG, Lytle BW, Nishimura RA, Ornato JP, Page RL, Riegel B, Tarkington LG, Yancy CW. ACC/AHA/HRS 2008 Guidelines for Device-Based Therapy of Cardiac Rhythm Abnormalities: a report of the American College of Cardiology/American Heart Association Task Force on Practice Guidelines: developed in collaboration with the American Association for Thoracic Surgery and Society of Thoracic Surgeons. Circulation 2008;117(21):e350-e408.

(2) Hunt SA, Abraham WT, Chin MH, Feldman AM, Francis GS, Ganiats TG, Jessup M, Konstam MA, Mancini DM, Michl K, Oates JA, Rahko PS, Silver MA, Stevenson LW, Yancy CW. 2009 focused update incorporated into the ACC/AHA 2005 Guidelines for the Diagnosis and Management of Heart Failure in Adults: a report of the American College of Cardiology Foundation/American Heart Association Task Force on Practice Guidelines: developed in collaboration with the International Society for Heart and Lung Transplantation. Circulation 2009;119(14):e391-e479.

(3) Bristow MR, Saxon LA, Boehmer J, Krueger S, Kass DA, De Marco T, Carson P, DiCarlo L, DeMets D, White BG, DeVries DW, Feldman AM. Cardiac-resynchronization therapy with or without an implantable defibrillator in advanced chronic heart failure. N Engl J Med 2004;350(21):2140-2150.

(4) Bax JJ, Ansalone G, Breithardt OA, Derumeaux G, Leclercq C, Schalij MJ, Sogaard P, St John SM, Nihoyannopoulos P. Echocardiographic evaluation of cardiac resynchronization therapy: ready for routine clinical use? A critical appraisal. J Am Coll Cardiol 2004;44(1):1-9.

(5) Yu CM, Fung JW, Zhang Q, Chan CK, Chan YS, Lin H, Kum LC, Kong SL, Zhang Y, Sanderson JE. Tissue Doppler imaging is superior to strain rate imaging and postsystolic shortening on the prediction of reverse remodeling in both ischemic and nonischemic heart failure after cardiac resynchronization therapy. Circulation 2004;110(1):66-73.

(6) Bax JJ, Abraham T, Barold SS, Breithardt OA, Fung JW, Garrigue S, Gorcsan J, III, Hayes DL, Kass DA, Knuuti J, Leclercq C, Linde C, Mark DB, Monaghan MJ, Nihoyannopoulos P, Schalij MJ, Stellbrink C, Yu CM. Cardiac resynchronization therapy: Part 1--issues before device implantation. J Am Coll Cardiol 2005;46(12):2153-2167.

(7) Ypenburg C, Schalij MJ, Bleeker GB, Steendijk P, Boersma E, Dibbets-Schneider P, Stokkel MP, van der Wall EE, Bax JJ. Impact of viability and scar tissue on response to cardiac resynchronization therapy in ischaemic heart failure patients. Eur Heart J 2007;28(1):33-41.

(8) Morris-Thurgood JA, Turner MS, Nightingale AK, Masani N, Mumford C, Frenneaux MP. Pacing in heart failure: improved ventricular interaction in diastole rather than systolic re-synchronization. Europace 2000;2(4):271-275.

(9) Waggoner AD, Rovner A, de las FL, Faddis MN, Gleva MJ, Sawhney N, vila-Roman VG. Clinical outcomes after cardiac resynchronization therapy: importance of left ventricular diastolic function and origin of heart failure. J Am Soc Echocardiogr 2006;19(3):307-313.

(10) Shanks M, Bertini M, Delgado V, Ng ACT, Nucifora G, Van Bommel RJ, Borleffs CJW, Holman ER, Van de Veire NRL, Schalij MJ, Bax JJ. Effect of biventricular pacing on diastolic dyssynchrony. Journal of american college of cardiology 2010;56(19):1567-1575.

(11) Schuster I, Habib G, Jego C, Thuny F, Avierinos JF, Derumeaux G, Beck L, Medail C, Franceschi F, Renard S, Ferracci A, Lefevre J, Luccioni R, Deharo JC, Djiane P. Diastolic asynchrony is more frequent than systolic asynchrony in dilated cardiomyopathy and is less improved by cardiac resynchronization therapy. Journal of american college of cardiology 2005;46(12):2250-2257.

(12) Wang J, Kurrelmeyer KM, Torre-Amione G, Nagueh SF. Systolic and diastolic dyssynchrony in patients with diastolic heart failure and the effect of medical therapy. J Am Coll Cardiol 2007;49(1):88-96.
(13) Yu CM, Zhang Q, Yip GW, Lee PW, Kum LC, Lam YY, Fung JW. Diastolic and systolic asynchrony in patients with diastolic heart failure: a common but ignored condition. J Am Coll Cardiol 2007;49(1):97-105.
(14) Trimble MA, Velazquez EJ, Adams GL, Honeycutt EF, Pagnanelli RA, Barnhart HX, Chen J, Iskandrian AE, Garcia EV, Borges-Neto S. Repeatability and reproducibility of phase analysis of gated single-photon emission computed tomography myocardial perfusion imaging used to quantify cardiac dyssynchrony. Nucl Med Commun 2008;29(4):374-381.
(15) Lin X, Xu H, Zhao X, Folks RD, Garcia EV, Soman P, Chen J. Repeatability of left ventricular dyssynchrony and function parameters in serial gated myocardial perfusion SPECT studies. J Nucl Cardiol 2010;17(5):811-816.
(16) Henneman MM, Chen J, Dibbets-Schneider P, Stokkel MP, Bleeker GB, Ypenburg C, van der Wall EE, Schalij MJ, Garcia EV, Bax JJ. Can LV dyssynchrony as assessed with phase analysis on gated myocardial perfusion SPECT predict response to CRT? J Nucl Med 2007;48(7):1104-1111.
(17) Rector TS, Kubo SH, Cohn JN. Validity of the Minnesota Living with Heart Failure questionnaire as a measure of therapeutic response to enalapril or placebo. Am J Cardiol 1993;71(12):1106-1107.
(18) Bax JJ, Bleeker GB, Marwick TH, Molhoek SG, Boersma E, Steendijk P, van der Wall EE, Schalij MJ. Left ventricular dyssynchrony predicts response and prognosis after cardiac resynchronization therapy. J Am Coll Cardiol 2004;44(9):1834-1840.
(19) Hoffman EJ, Huang SC, Phelps ME. Quantitation in positron emission computed tomography: 1. Effect of object size. J Comput Assist Tomogr 1979;3(3):299-308.
(20) Galt JR, Garcia EV, Robbins WL. Effects of myocardial wall thickness on SPECT quantification. IEEE Trans Med Imaging 1990;9(2):144-150.
(21) Marsan NA, Bleeker GB, Ypenburg C, Van Bommel RJ, Ghio S, Van de Veire NR, Delgado V, Holman ER, van der Wall EE, Schalij MJ, Bax JJ. Real-time three-dimensional echocardiography as a novel approach to assess left ventricular and left atrium reverse remodeling and to predict response to cardiac resynchronization therapy. Heart Rhythm 2008;5(9):1257-1264.
(22) Van Bommel RJ, Mollema SA, Borleffs CJ, Bertini M, Ypenburg C, Marsan NA, Delgado V, van der Wall EE, Schalij MJ, Bax JJ. Impaired renal function is associated with echocardiographic nonresponse and poor prognosis after cardiac resynchronization therapy. J Am Coll Cardiol 2011;57(5):549-555.
(23) Bristow MR, Feldman AM, Saxon LA. Heart failure management using implantable devices for ventricular resynchronization: Comparison of Medical Therapy, Pacing, and Defibrillation in Chronic Heart Failure (COMPANION) trial. COMPANION Steering Committee and COMPANION Clinical Investigators. J Card Fail 2000;6(3):276-285.
(24) Cleland JG, Daubert JC, Erdmann E, Freemantle N, Gras D, Kappenberger L, Tavazzi L. The effect of cardiac resynchronization on morbidity and mortality in heart failure. N Engl J Med 2005;352(15):1539-1549.
(25) Fornwalt BK, Sprague WW, BeDell P, Suever JD, Gerritse B, Merlino JD, Fyfe DA, Leon AR, Oshinski JN. Agreement is poor among current criteria used to define response to cardiac resynchronization therapy. Circulation 2010;121(18):1985-1991.
(26) Chung ES, Leon AR, Tavazzi L, Sun JP, Nihoyannopoulos P, Merlino J, Abraham WT, Ghio S, Leclercq C, Bax JJ, Yu CM, Gorcsan J, III, St John SM, De Sutter J, Murillo J. Results of the Predictors of Response to CRT (PROSPECT) trial. Circulation 2008;117(20):2608-2616.
(27) Yu CM, Lin H, Zhang Q, Sanderson JE. High prevalence of left ventricular systolic and diastolic asynchrony in patients with congestive heart failure and normal QRS duration. Heart 2003;89(1):54-60.

(28) Burgess MI, Fang ZY, Marwick TH. Role of diastolic dyssynchrony in the delayed relaxation pattern of left ventricular filling. J Am Soc Echocardiogr 2007;20(1):63-69.
(29) Atherton JJ, Moore TD, Lele SS, Thomson HL, Galbraith AJ, Belenkie I, Tyberg JV, Frenneaux MP. Diastolic ventricular interaction in chronic heart failure. Lancet 1997;349(9067):1720-1724.
(30) Adelstein EC, Saba S. Scar burden by myocardial perfusion imaging predicts echocardiographic response to cardiac resynchronization therapy in ischemic cardiomyopathy. Am Heart J 2007;153(1):105-112.
(31) Adelstein EC, Tanaka H, Soman P, Miske G, Haberman SC, Saba SF, Gorcsan J, III. Impact of scar burden by single-photon emission computed tomography myocardial perfusion imaging on patient outcomes following cardiac resynchronization therapy. Eur Heart J 2011;32(1): 93-103.

Part III

123-I MIBG for Risk Stratification of Patients with Cardiovascular Disease

Chapter **11**

Cardiac Iodine-123 Metaiodobenzylguanidine Imaging for Risk Stratification in Heart Failure Patients

A report on behalf of the European Council of Nuclear Cardiology (ECNC)

Mark M. Boogers, MD[1, 2], Frank M. Bengel, MD[3], Juhani Knuuti[4], MD, PhD, Jeroen J. Bax, MD, PhD[1]; Leiden, and Utrecht, the Netherlands; Baltimore, USA; Turku, Finland

[1]Department of Cardiology, Leiden University Medical Center, Leiden, the Netherlands; [2]The Interuniversity Cardiology Institute of the Netherlands, Utrecht, the Netherlands; [3]Department of Nuclear Medicine, Johns Hopkins University, Baltimore, USA; [4]Turku PET Centre, Turku University, Turku, Finland.

Introduction

Chronic heart failure is an important health care problem in the developed world as incidence and prevalence numbers have increased rapidly over the last decades. Recently, the American Heart Association Statistics and Stroke Statistics committee reported that chronic heart failure affects 5.3 million patients in the USA, with approximately 660,000 newly diagnosed patients each year.[1] In western Europe, approximately 4 million patients have been diagnosed with chronic heart failure.[2]

Moreover, in the USA, one million hospital admissions for (decompensated) heart failure have been reported annually, resulting in an exponential increase in direct and indirect cost involved with chronic heart failure.[1] Even though significant progress in prevention, diagnostic and therapeutic strategies for chronic heart failure has been made, mortality rate still exceeds 50%.

Coronary artery disease was found to be the main cause of heart failure in nearly 70% of patients, and despite rapid developing treatment options for ischemic and non-ischemic heart failure, long-term prognosis remains poor.[3-6] In 7,599 patients with NYHA class II-IV heart failure, originating from the CHARM study, cardiovascular outcome was studied over a mean follow-up of 3 years. In patients with a LV ejection fraction <33%, all-cause and cardiac mortality were 34% and 28%, respectively.[6] Even higher mortality rates were reported by Levy et al.[4] in the Framingham-based study population; cardiac mortality rate was more than 50%, over a mean follow-up of 5 years. These high mortality rates along with an increasing number of hospitalizations due to (decompensated) heart failure emphasize the need for better risk stratification.

Heart failure represents a complex clinical syndrome resulting from a reduced cardiac pump function. Progressive deterioration in cardiac function is based upon several interacting pathophysiologic mechanisms, in which particularly the neurohormonal system (consisting of the adrenergic nervous system and renin-angiotensin-aldosteron system) plays an important role in chronic heart failure. Initially, neurohormonal feedback mechanisms tend to compensate hemodynamic consequences of cardiac dysfunction via positive inotropic and chronotropic effects. However, in a chronic state these neurohormonal effects are detrimental and may cause cardiac hypertrophy and fibrosis, eventually resulting in remodeling. Moreover, desensitization and downregulation of myocardial beta-adrenoceptors, and alterations of postsynaptic signaling lead to further decline in cardiac function.[7]

In addition, a dysfunctional cardiac autonomic nervous system may also be related to the development of ventricular arrhythmias.[8-11] In this respect, exact mechanisms have to be elucidated and it has been suggested that regions with impaired innervation may be viable and hypersensitive to catecholamines, resulting in increased automaticity and enhanced triggering.[8, 12, 13] In particular, the borderzone of myocardial scar tissue may be predisposed to develop reentrant circuits because these regions are viable but may have damaged

sympathetic nerves.[14-18] The viable peri-infarct region can be (partially) denervated because sympathetic nerve fibers are more vulnerable to ischemia as compared to cardiomyocytes.[19]

Consequently, important clinical and prognostic information in heart failure patients can be provided by assessment of cardiac sympathetic innervation and function. Single photon emission computed tomography (SPECT) and positron emission tomography (PET) are presently the only 2 imaging modalities to allow assessment of myocardial sympathetic nerve activation and innervation by visualization of uptake and storage of radiolabeled neurotransmitters into presynaptic nerve endings. Both imaging techniques can be used to assess global and regional myocardial sympathetic nerve innervation.

Presently, several PET tracers have been used to visualize sympathetic neurotransmission, including carbon-11 hydroxyephedrine (HED), C-11 epinephrine and F-18 fluorodopamine. At present, HED is the most frequently used PET tracer and allows absolute quantification of tracer uptake into sympathetic nerve terminals. One of the major advantages of HED is its capability to detect regional abnormalities in myocardial sympathetic innervation. Hartmann and colleagues[20] have performed an important study which demonstrated regional heterogeneity of impaired cardiac sympathetic innervation in 29 patients with idiopathic dilated cardiomyopathy as compared to patients with normal cardiac function. In heart failure patients, PET with HED has also been used to evaluate the prognostic value of sympathetic nerve innervation. In an elegant study, Pietila et al.[21] have demonstrated that global reduced HED accumulation was an independent predictor of adverse outcome in 46 patients with NYHA class II-III heart failure.

Cardiac 123-I MIBG Scintigraphy

Most studies on cardiac sympathetic innervation have been performed with 123-iodine metaiodobenzylguanidine (MIBG) scintigraphy. The labeling of MIBG with 123-iodine permits visualization of myocardial sympathetic neuronal uptake. MIBG is a false neurotransmitter, an analog of norepinephrine, which uses similar uptake mechanisms in the presynaptic nerve terminals as norepinephrine. The tracer is primarily transported into the presynaptic nerve terminal by sodium- and ATP-dependent transporters, referred to as uptake-1. In the nerve terminal, no degradation of MIBG takes places resulting in an accumulation of MIBG with high signal intensity. These signals are used for planar and tomographic (SPECT) imaging. Early planar imaging and SPECT are performed at 10-20 min after MIBG administration, whereas delayed planar imaging and SPECT are performed 3-4 h after tracer injection. From planar images, global cardiac MIBG uptake can be assessed visually or semi-quantitatively using early and late heart-to-mediastinum (H/M) ratio (Figure 1). To calculate H/M ratio, regions of interest are manually drawn over the heart and upper mediastinum and the mean of myocardial counts per pixel is divided by the mean of mediastinal counts per pixel. Another planar-based parameter is the cardiac washout rate which indicates the rate by which MIBG is released from the myocardium between early

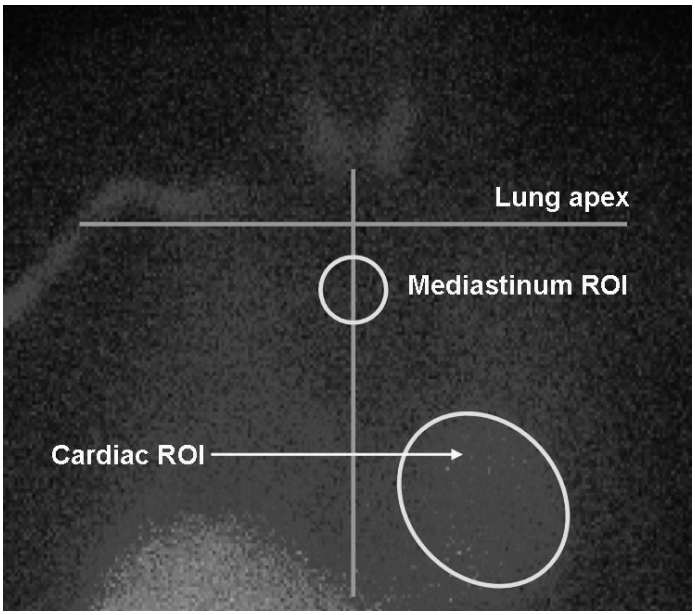

Figure 1. Planar MIBG imaging provides semi-quantitative parameters for assessment of global cardiac sympathetic innervation. Regions of interests are manually drawn within the heart and upper mediastinum. To calculate the heart-to-mediastinum ratio, the mean of cardiac counts per pixel is divided by the mean of counts per pixel within upper mediastinum.

and delayed imaging. To calculate cardiac washout rate, late H/M ratio is subtracted from the early H/M ratio and divided by the early H/M ratio.

These planar-based parameters have been studied extensively in heart failure patients.[22-28] In particular, the prognostic value of global MIBG uptake has been studied by Merlet and colleagues.[22, 23, 25] Initially, these authors[22] have studied 90 patients with moderate-to-severe heart failure, who underwent MIBG scintigraphy, chest X-ray, echocardiography and radionuclide angiography. After follow-up of 27 months, cardiac death and cardiac transplantations were reported in 22 and 10 patients, respectively. H/M ratio on delayed images was found to be the best independent predictor for cardiovascular death. Of note, patients with cardiac transplants were discarded from the survival analysis, whereas the second prognostic study performed by Merlet et al.[25] included patients who underwent cardiac transplantation. In this study, 112 patients with NYHA class II-IV heart failure and LV ejection fraction <40% (measured with radionuclide angiography), underwent MIBG scintigraphy, right-sided invasive angiography, and routine clinical care (echocardiography, chest X-ray and peak exercise testing). After a mean follow-up of 27±20 months, cardiac death was noted in 25 patients, and cardiac transplantation was performed in 19. As illustrated in Figure 2, late H/M ratio was significantly lower in patients with major cardiac events as compared to patients without major cardiac events. Furthermore, the authors

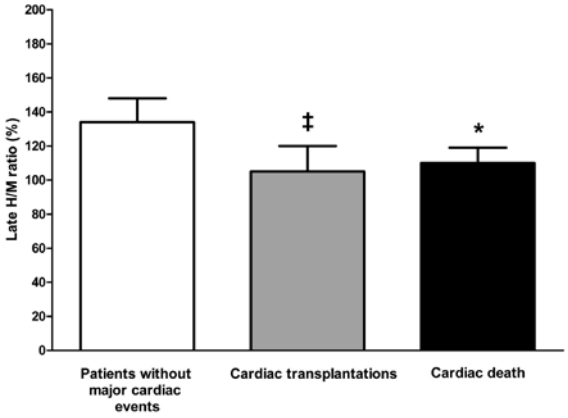

Figure 2. Differences in late heart-to-mediastinum (H/M) ratio among heart failure patients with and without major cardiac events (cardiac death or cardiac transplantation), data based on reference 25. Patients with major cardiac events showed significantly lower H/M ratio on delayed images as compared to patients without major cardiac events (134±14% vs. 105±15% or 110±9%, $p<0.05$ (‡, *).

have demonstrated that the only independent predictors for adverse outcome were reduced myocardial MIBG uptake on delayed planar images and depressed LV ejection fraction.

Besides the prognostic value of global MIBG uptake on delayed images, several studies have reported on cardiac washout rate as a potential predictor for adverse cardiovascular outcome.[29-32] In 59 patients with NYHA class II-IV and dilated cardiomyopathy, the predictive value of MIBG parameters was studied by Momose and coworkers[29]; among all planar MIBG parameters cardiac washout rate was the most powerful predictor of cardiac death, over a mean follow-up of 25±13 months. For cardiac washout rate, a threshold level of 52% showed optimal predictive value for cardiac death. In addition, similar results were demonstrated by Yamada et al.[31] in 65 heart failure patients. Over a mean follow-up of 34±19 months, cardiac washout rate was the only independent predictor for cardiac events. Furthermore, patients with cardiac events showed significant higher myocardial washout rate in comparison to patients without cardiac events, as illustrated in Figure 3. However, importantly, different threshold levels for cardiac washout rate were used in these two studies. Yamada et al.[31] used a cutoff value of 27% for myocardial washout rate, whereas Momose and coworkers[29] used a threshold level of 52%.

Presently, no consensus exists on the optimal cutoff values for early and late H/M ratios, cardiac washout rate, or the defect score on SPECT for prediction of outcome. Agostini et al.[33] have performed in this respect an important retrospective study on 290 heart failure patients from 6 centers across Europe. According to the study protocol, planar and SPECT examinations were re-analyzed in a core laboratory by 3 independent observers who were

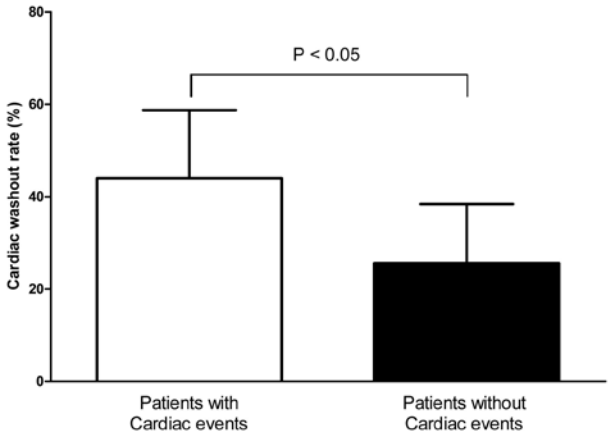

Figure 3. Difference in myocardial washout rate between heart failure patients with adverse cardiac outcome (cardiac death or hospitalization) and heart failure patients without adverse cardiac outcome (data based on reference 31). Patients with adverse cardiac outcome demonstrated significant higher myocardial washout rate as compared to patients without adverse cardiac outcome (44.0±14.7% vs. 25.6±12.8%, p<0.05).

blinded to all other data. Over a follow-up of 2 year, major cardiac events were noted, including cardiac death, cardiac transplantation, potential lethal ventricular arrhythmias or appropriate ICD therapy. The authors showed that patients with a major cardiac event had significant lower H/M ratio on delayed images as compared to patients without a major cardiac event within the 2-year follow-up period. Moreover, for late H/M ratio, the optimal threshold to predict cardiac events was defined at 1.75, and yielded a sensitivity of 84% and specificity of 60%.

The available studies have focused on an index MIBG study and its relation to cardiac outcome. However, several studies used imaging before and after heart failure therapy and demonstrated improved MIBG uptake after optimization of heart failure medication; currently, limited information is available on the predictive value of serial MIBG studies.[34-37] Recently, Kasama et al.[38] have reported on the predictive value of serial MIBG imaging in 208 heart failure patients with a LV ejection fraction <45%. According to the study design, MIBG scintigraphy was performed at baseline and at 6 months follow-up. During a mean follow-up of 5±2 months, cardiac death was reported in 56 patients. The authors have reported that a 6-month change in washout rate >5%, was an independent predictor for all-cause cardiac death and sudden cardiac death.

Prediction of Ventricular Arrhythmia

Although most prognostic studies used all-cause mortality, cardiac mortality (progressive heart failure), or cardiac transplantation as endpoints, some studies suggested that MIBG imaging can also be used for prediction of ventricular arrhythmias and sudden cardiac death.[39-41] At present, it is known that parasympathetic stimulation of the ventricles exerts anti-fibrillatory effects on the myocardium, whereas sympathetic activation of the ventricles appears to have a pro-arrhythmogenic effect on the myocardium. In patients with heart failure, the increased sympathetic tone along with a decreased parasympathetic activation can cause ventricular arrhythmias by enhancing cardiomyocyte pacemaker activity and reentrant excitation.[39-41] Moreover, the presence of sympathetic denervated regions alongside regions with preserved sympathetic innervation can lead to an inhomogeneous neuronal release of norepinephrine, which subsequently, can cause marked alterations in action potential duration and configuration of the cardiomyocytes. Therefore, the electrical signaling of the heart becomes non-uniform (electrophysiologic heterogeneity) which contributes to its vulnerability for development of ventricular arrhythmias.

Arora et al.[39] have evaluated the role of MIBG imaging in 17 patients with an implantable cardioverter-defibrillator (ICD). In total, 10 patients received appropriate ICD discharges (reflecting potential lethal ventricular arrhythmias or sudden cardiac death) and these patients showed significant lower global (early) and regional (early and late) MIBG uptake as compared to patients who did not receive appropriate ICD discharges. Furthermore, comparable results were reported by Nagahara and colleagues[41] who evaluated whether MIBG scintigraphy was useful for prediction of appropriate ICD therapy in 54 patients, after a mean follow-up of 15 months. Ten patients who received appropriate ICD therapy showed significantly lower late MIBG uptake as compared to patients who did not receive appropriate ICD therapy. Moreover, H/M ratio on delayed images was found to be an independent predictor for appropriate ICD therapy.

MIBG studies have reported on planar imaging as a potential tool for risk stratification in heart failure patients. Although some innervation studies have employed regional MIBG uptake as a prognostic marker, the role of SPECT for prognostification of heart failure patients is unclear.[42-44] In particular, the role of regional sympathetic denervated myocardium in the genesis of spontaneous ventricular arrhythmias has to be further elucidated.[14-18] Bax et al.[45] have studied whether abnormalities in sympathetic innervation on MIBG SPECT could predict inducibility of ventricular arrhythmias on electrophysiological testing in 50 patients with coronary artery disease and LV ejection fraction ≤40%. The MIBG SPECT defect score was significantly larger in the 30 patients with a positive electrophysiologic test as compared to patients without inducible ventricular arrhythmias, as illustrated in Figure 4.

In conclusion, the available studies have shown that cardiac innervation imaging holds great potential for risk stratification of heart failure patients. Recent studies suggest that particularly MIBG imaging may play a major role in identifying patients with LV dysfunction

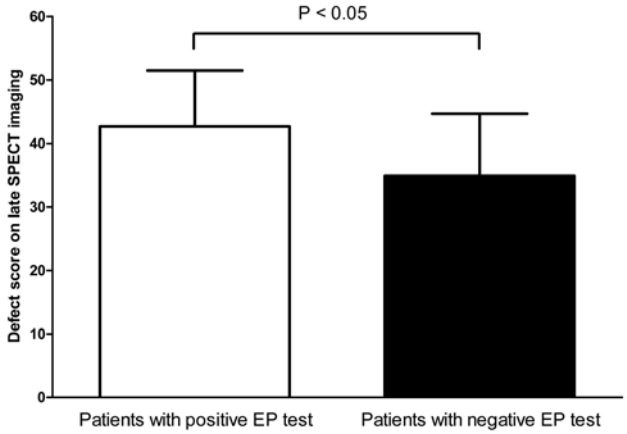

Figure 4. Defect score on late single photon emission computed tomography (SPECT) in patients with positive and negative electrophysiologic (EP) test (data based on reference 45). Patients with inducible ventricular tachyarrhythmias during EP testing showed significantly higher defect score on SPECT as compared to patients without inducible ventricular arrhythmias (42.7±8.8 vs. 34.9±9.8, $p<0.05$).

at elevated risk of heart failure death or arrhythmic death. The results of these initial studies are promising, and more studies will help to determine the precise role of innervation imaging in risk stratification of heart failure patients.

Reference List

(1) Rosamond W, Flegal K, Furie K et al. Heart disease and stroke statistics-2008 update: a report from the American Heart Association Statistics Committee and Stroke Statistics Subcommittee. Circulation 2008; 117(4):e25-146.

(2) Cowie MR, Mosterd A, Wood DA et al. The epidemiology of heart failure. Eur Heart J 1997; 18(2):208-25.

(3) Gheorghiade M, Bonow RO. Chronic heart failure in the United States: a manifestation of coronary artery disease. Circulation 1998; 97(3):282-9.

(4) Levy D, Kenchaiah S, Larson MG et al. Long-term trends in the incidence of and survival with heart failure. N Engl J Med 2002; 347(18):1397-402.

(5) Roger VL, Weston SA, Redfield MM et al. Trends in heart failure incidence and survival in a community-based population. JAMA 2004; 292(3):344-50.

(6) Solomon SD, Anavekar N, Skali H et al. Influence of ejection fraction on cardiovascular outcomes in a broad spectrum of heart failure patients. Circulation 2005; 112(24):3738-44.

(7) Bristow MR. The adrenergic nervous system in heart failure. N Engl J Med 1984; 311(13):850-1.

(8) Zipes DP. Sympathetic stimulation and arrhythmias. N Engl J Med 1991; 325(9):656-7.

(9) Barron HV, Lesh MD. Autonomic nervous system and sudden cardiac death. J Am Coll Cardiol 1996; 27(5):1053-60.

(10) Barron HV, Viskin S. Autonomic markers and prediction of cardiac death after myocardial infarction. Lancet 1998; 351(9101):461-2.

(11) Yukinaka M, Nomura M, Ito S, Nakaya Y. Mismatch between myocardial accumulation of 123I-MIBG and 99mTc-MIBI and late ventricular potentials in patients after myocardial infarction: association with the development of ventricular arrhythmias. Am Heart J 1998; 136(5):859-67.

(12) Podrid PJ, Fuchs T, Candinas R. Role of the sympathetic nervous system in the genesis of ventricular arrhythmia. Circulation 1990; 82(2 Suppl):I103-I113.

(13) Sasano T, Abraham MR, Chang KC et al. Abnormal sympathetic innervation of viable myocardium and the substrate of ventricular tachycardia after myocardial infarction. J Am Coll Cardiol 2008; 51(23):2266-75.

(14) Kammerling JJ, Green FJ, Watanabe AM et al. Denervation supersensitivity of refractoriness in noninfarcted areas apical to transmural myocardial infarction. Circulation 1987; 76(2):383-93.

(15) Minardo JD, Tuli MM, Mock BH et al. Scintigraphic and electrophysiological evidence of canine myocardial sympathetic denervation and reinnervation produced by myocardial infarction or phenol application. Circulation 1988; 78(4):1008-19.

(16) Tomoda H, Yoshioka K, Shiina Y, Tagawa R, Ide M, Suzuki Y. Regional sympathetic denervation detected by iodine 123 metaiodobenzylguanidine in non-Q-wave myocardial infarction and unstable angina. Am Heart J 1994; 128(3):452-8.

(17) Bengel FM, Barthel P, Matsunari I, Schmidt G, Schwaiger M. Kinetics of 123I-MIBG after acute myocardial infarction and reperfusion therapy. J Nucl Med 1999; 40(6):904-10.

(18) Simoes MV, Barthel P, Matsunari I et al. Presence of sympathetically denervated but viable myocardium and its electrophysiologic correlates after early revascularised, acute myocardial infarction. Eur Heart J 2004; 25(7):551-7.

(19) Matsunari I, Schricke U, Bengel FM et al. Extent of cardiac sympathetic neuronal damage is determined by the area of ischemia in patients with acute coronary syndromes. Circulation 2000; 101(22):2579-85.

(20) Hartmann F, Ziegler S, Nekolla S et al. Regional patterns of myocardial sympathetic denervation in dilated cardiomyopathy: an analysis using carbon-11 hydroxyephedrine and positron emission tomography. Heart 1999; 81(3):262-70.

(21) Pietila M, Malminiemi K, Ukkonen H et al. Reduced myocardial carbon-11 hydroxyephedrine retention is associated with poor prognosis in chronic heart failure. Eur J Nucl Med 2001; 28(3):373-6.
(22) Merlet P, Valette H, Dubois-Rande JL et al. Prognostic value of cardiac metaiodobenzylguanidine imaging in patients with heart failure. J Nucl Med 1992; 33(4):471-7.
(23) Merlet P, Valette H, Dubois-Rande JL et al. Iodine 123-labeled metaiodobenzylguanidine imaging in heart disease. J Nucl Cardiol 1994; 1(2 Pt 2):S79-S85.
(24) Nakata T, Miyamoto K, Doi A et al. Cardiac death prediction and impaired cardiac sympathetic innervation assessed by MIBG in patients with failing and nonfailing hearts. J Nucl Cardiol 1998; 5(6):579-90.
(25) Merlet P, Benvenuti C, Moyse D et al. Prognostic value of MIBG imaging in idiopathic dilated cardiomyopathy. J Nucl Med 1999; 40(6):917-23.
(26) Cohen-Solal A, Esanu Y, Logeart D et al. Cardiac metaiodobenzylguanidine uptake in patients with moderate chronic heart failure: relationship with peak oxygen uptake and prognosis. J Am Coll Cardiol 1999; 33(3):759-66.
(27) Carrio I. Cardiac neurotransmission imaging. J Nucl Med 2001; 42(7):1062-76.
(28) Anastasiou-Nana MI, Terrovitis JV, Athanasoulis T et al. Prognostic value of iodine-123-metaiodobenzylguanidine myocardial uptake and heart rate variability in chronic congestive heart failure secondary to ischemic or idiopathic dilated cardiomyopathy. Am J Cardiol 2005; 96(3):427-31.
(29) Momose M, Kobayashi H, Iguchi N et al. Comparison of parameters of 123I-MIBG scintigraphy for predicting prognosis in patients with dilated cardiomyopathy. Nucl Med Commun 1999; 20(6):529-35.
(30) Ogita H, Shimonagata T, Fukunami M et al. Prognostic significance of cardiac (123)I metaiodobenzylguanidine imaging for mortality and morbidity in patients with chronic heart failure: a prospective study. Heart 2001; 86(6):656-60.
(31) Yamada T, Shimonagata T, Fukunami M et al. Comparison of the prognostic value of cardiac iodine-123 metaiodobenzylguanidine imaging and heart rate variability in patients with chronic heart failure: a prospective study. J Am Coll Cardiol 2003; 41(2):231-8.
(32) Verberne HJ, Brewster LM, Somsen GA, Van Eck-Smit BL. Prognostic value of myocardial 123I-metaiodobenzylguanidine (MIBG) parameters in patients with heart failure: a systematic review. Eur Heart J 2008; 29(9):1147-59.
(33) Agostini D, Verberne HJ, Burchert W et al. I-123-mIBG myocardial imaging for assessment of risk for a major cardiac event in heart failure patients: insights from a retrospective European multicenter study. Eur J Nucl Med Mol Imaging 2008; 35(3):535-46.
(34) Takeishi Y, Atsumi H, Fujiwara S, Takahashi K, Tomoike H. ACE inhibition reduces cardiac iodine-123-MIBG release in heart failure. J Nucl Med 1997; 38(7):1085-9.
(35) Toyama T, Aihara Y, Iwasaki T et al. Cardiac sympathetic activity estimated by 123I-MIBG myocardial imaging in patients with dilated cardiomyopathy after beta-blocker or angiotensin-converting enzyme inhibitor therapy. J Nucl Med 1999; 40(2):217-23.
(36) Toyama T, Hoshizaki H, Seki R et al. Efficacy of carvedilol treatment on cardiac function and cardiac sympathetic nerve activity in patients with dilated cardiomyopathy: comparison with metoprolol therapy. J Nucl Med 2003; 44(10):1604-11.
(37) Kasama S, Toyama T, Kumakura H et al. Effect of spironolactone on cardiac sympathetic nerve activity and left ventricular remodeling in patients with dilated cardiomyopathy. J Am Coll Cardiol 2003; 41(4):574-81.
(38) Kasama S, Toyama T, Sumino H et al. Prognostic value of serial cardiac 123I-MIBG imaging in patients with stabilized chronic heart failure and reduced left ventricular ejection fraction. J Nucl Med 2008; 49(6):907-14.
(39) Arora R, Ferrick KJ, Nakata T et al. I-123 MIBG imaging and heart rate variability analysis to predict the need for an implantable cardioverter defibrillator. J Nucl Cardiol 2003; 10(2):121-31.

(40) Paul M, Schafers M, Kies P et al. Impact of sympathetic innervation on recurrent life-threatening arrhythmias in the follow-up of patients with idiopathic ventricular fibrillation. Eur J Nucl Med Mol Imaging 2006; 33(8):866-70.
(41) Nagahara D, Nakata T, Hashimoto A et al. Predicting the need for an implantable cardioverter defibrillator using cardiac metaiodobenzylguanidine activity together with plasma natriuretic peptide concentration or left ventricular function. J Nucl Med 2008; 49(2):225-33.
(42) Patel AD, Iskandrian AE. MIBG imaging. J Nucl Cardiol 2002; 9(1):75-94.
(43) Flotats A, Carrio I. Cardiac neurotransmission SPECT imaging. J Nucl Cardiol 2004; 11(5):587-602.
(44) Mitrani RD, Klein LS, Miles WM et al. Regional cardiac sympathetic denervation in patients with ventricular tachycardia in the absence of coronary artery disease. J Am Coll Cardiol 1993; 22(5):1344-53.
(45) Bax JJ, Kraft O, Buxton AE et al. ^{123}-I-MIBG scintigraphy to predict inducibility of ventricular arrhythmias on cardiac electrophysiology testing. Circ Cardiovasc Imaging. 2008; 1(1):131-140.

Chapter **12**

Cardiac Sympathetic Denervation Assessed with 123-iodine Metaiodobenzylguanidine Imaging Predicts Ventricular Arrhythmias in Implantable Cardioverter-Defibrillator Patients

Mark J. Boogers, MD[1, 2], C. Jan Willem Borleffs, MD[1], Maureen M. Henneman, MD[1], Rutger J. van Bommel, MD[1], Jan van Ramshorst, MD[1], Eric Boersma, PhD[3], Petra Dibbets-Schneider, MSc[4], Marcel P. Stokkel, MD, PhD[4], Ernst E. van der Wall, MD, PhD[1], Martin J. Schalij, MD, PhD[1], Jeroen J. Bax, MD, PhD[1].

[1]Department of Cardiology, Leiden University Medical Center, Leiden, the Netherlands; [2]The Interuniversity Cardiology Institute of the Netherlands, Utrecht, the Netherlands; [3]Department of Epidemiology and Statistics, Erasmus University, Rotterdam, the Netherlands; [4]Department of Nuclear Medicine, Leiden University Medical Center, Leiden, the Netherlands.

Abstract

Objectives To evaluate whether 123-iodine metaiodobenzylguanidine (123-I MIBG) imaging predicts ventricular arrhythmias causing appropriate implantable cardioverter-defibrillator (ICD) therapy (primary endpoint) and the composite of appropriate ICD therapy or cardiac death (secondary endpoint).

Background Although cardiac sympathetic denervation is associated with ventricular arrhythmias, limited data are available on the predictive value of sympathetic nerve imaging with 123-I MIBG on the occurrence of arrhythmias.

Methods Before ICD implantation, patients underwent 123-I MIBG and myocardial perfusion imaging. Early and late 123-I MIBG (planar and SPECT) imaging was performed to assess cardiac innervation (heart-to-mediastinum ratio, cardiac washout rate and 123-I MIBG SPECT defect score). Stress-rest myocardial perfusion imaging was performed to assess myocardial infarction and perfusion abnormalities (perfusion defect scores). During follow-up, appropriate ICD therapy and cardiac death were documented.

Results One-hundred sixteen heart failure patients referred for ICD therapy were enrolled. During a mean follow-up of 23±15 months, appropriate ICD therapy (primary endpoint) was documented in 24 (21%) patients and appropriate ICD therapy or cardiac death (secondary endpoint) in 32 (28%) patients. Late 123-I MIBG SPECT defect score was an independent predictor for both endpoints. Patients with a large late 123-I MIBG SPECT defect (summed score >26) showed significantly more appropriate ICD therapy (52% vs. 5%, $p<0.01$) and appropriate ICD therapy or cardiac death (57% vs. 10%, $p<0.01$) than patients with a small defect (summed score ≤26) at 3-year follow-up.

Conclusions Cardiac sympathetic denervation predicts ventricular arrhythmias causing appropriate ICD therapy as well as the composite of appropriate ICD therapy or cardiac death.

Introduction

Sudden cardiac death (SCD) represents a leading cause of death in the developed world with an estimated annual incidence of 300,000 to 350,000 patients in the United States.[1] Implantable cardioverter-defibrillator (ICD) treatment is well established in patients at high risk for arrhythmic death. Initially, ICD treatment was indicated in survivors of sustained ventricular tachycardia or ventricular fibrillation and more recently, in a population at high risk, regardless of prior ventricular tachyarrhythmias.[2, 3] Based on large randomized trials, current guidelines recommend ICD treatment based solely on a poor left ventricular (LV) systolic function with or without nonsustained ventricular tachycardia as a class I indication.[4]

Post-hoc analysis of the second Multicenter Automated Defibrillator Implantation Trial (MADIT II) population showed that only 35% of patients received appropriate ICD therapy after 3-year follow-up.[5] Additionally, the majority of arrhythmic deaths occurs in a population without ICD indication.[6] Although the benefits of ICD treatment have been demonstrated, the question has been raised whether improvements in patient selection can be made.

Dysfunction of the autonomic nervous system (which can be assessed with 123-iodine metaiodobenzylguanidine (123-I MIBG) imaging) is thought to play an important role in the development of ventricular tachyarrhythmias.[7, 8] Observational studies have demonstrated that cardiac denervation (as evidenced by reduced 123-I MIBG uptake) is associated with the occurrence of ventricular tachyarrhythmias.[9, 10] Moreover, it was recently shown that inducibility of ventricular tachyarrhythmias was related to regional cardiac sympathetic denervation as assessed with 123-I MIBG imaging.[10]

At present, limited data are available on the role of 123-I MIBG imaging for prediction of ventricular arrhythmias. Moreover, the value of 123-I MIBG imaging in identification of patients who may benefit from ICD treatment is unclear. Accordingly, this study evaluated the role of cardiac sympathetic nerve imaging with 123-I MIBG for the prediction of ventricular arrhythmias causing appropriate ICD therapy (primary endpoint) and the composite of appropriate ICD therapy or cardiac death (secondary endpoint).

Methods

Patient Population and Protocol

The patient population consisted of consecutive advanced heart failure patients undergoing cardiac 123-I MIBG imaging for heart failure risk stratification. The patients were clinically referred for ICD implantation based on poor LV function with or without nonsustained ventricular tachycardia (primary prevention) or prior sustained ventricular tachycardia or ventricular fibrillation (secondary prevention).[4]

Prior to ICD implantation, patients underwent 123-I MIBG imaging and gated myocardial perfusion single photon emission computed tomography (SPECT) with 99m-technetium tetrofosmin (^{99m}Tc-tetrofosmin). 123-I MIBG imaging was clinically performed to assess cardiac sympathetic innervation for risk stratification of heart failure patients.[11] Stress-rest myocardial perfusion imaging was performed to assess myocardial infarction (location and extent) and perfusion abnormalities (ischemia). All patients received optimal pharmacologic and revascularization therapy prior to ICD implantation. Patient's medication was continued during cardiac imaging.

During follow-up, ventricular arrhythmia with subsequent ICD therapy (appropriate ICD therapy) and cardiac mortality were documented. The occurrence of primary endpoints (appropriate ICD therapy) and secondary endpoints (the composite of appropriate ICD therapy or cardiac death) was assessed for all patients. Subsequently, the value of 123-I MIBG and myocardial perfusion imaging variables in the prediction of endpoints was studied.

123-I MIBG Imaging

Patients were pretreated with 120 mg sodium iodide to block uptake of free iodine-123 by the thyroid gland. Sodium iodide was given orally one hour before intravenous administration of 185 MBq 123-I MIBG (AdreView, General Electric Healthcare, United Kingdom). 123-I MIBG planar imaging and SPECT were performed in supine position. A 10-minute planar image was acquired from an anterior thoracic view (256 x 256 matrix) 10-15 minutes after tracer administration.

Thereafter, a SPECT study (step and shoot mode, 90 projections, imaging time 30 minutes) was performed using a dual-head camera system (GCA-7200, Toshiba Corp., Tokyo, Japan) equipped with low-energy, parallel-hole high-resolution collimators. A 128 x 128 matrix was used for SPECT studies and a 20% energy peak was centered around the 159-keV energy peak of 123-I MIBG. Planar imaging and SPECT were repeated after 3 to 4 hours of tracer administration.

Heart-to-mediastinum (H/M) ratio was calculated from planar imaging using regions of interest, placed over the entire heart and upper mediastinum.[10]

123-I MIBG SPECT studies were processed with filtered back-projection and reconstructed into standard long- and short-axis, perpendicular to the heart axis.[12] Three late SPECT studies were uninterpretable and excluded from evaluation of late 123-I MIBG SPECT.

From planar images, the H/M ratio was computed by dividing the mean counts per pixel within the myocardium by the mean counts per pixel within the mediastinum. H/M ratio was computed for early and late planar imaging. Cardiac washout rate was calculated using the following formula: [(early H/M ratio) – (delayed H/M ratio)] / (early H/M ratio) x 100. No background correction was performed in this study.

From SPECT images, the 123-I MIBG SPECT defect score was calculated by assessment of patient's segmental 123-I MIBG tracer uptake score using the 17-segment model.[12] Each

myocardial segment was scored according to the following tracer uptake scale: 0 = normal tracer uptake, 1 = mildly reduced tracer uptake, 2 = moderately reduced tracer uptake, 3 = severely reduced tracer uptake, 4 = no tracer uptake. Subsequently, the 123-I MIBG SPECT defect score was calculated by summation of segmental tracer uptake scores. The 123-I MIBG SPECT defect score was calculated for early and delayed SPECT. Data analysis was performed by 2 blinded and independent observers. Both readers scored all study segments and disagreements were resolved by consensus. There was no association between the myocardial perfusion and 123-I MIBG SPECT images as the different SPECT images were evaluated in separate sessions.

Reproducibility of the scoring system was evaluated by assessment of intra- and interobserver variability. To assess intraobserver variability myocardial segments were scored twice by the same observer in a subset of 30 randomly selected patients. To assess interobserver variability, the second SPECT reader independently graded the myocardial segments from the same subset of patients.

Gated Myocardial Perfusion SPECT

Stress-rest gated myocardial perfusion SPECT with ^{99m}Tc-tetrofosmin (500 MBq, MYOVIEW, General Electric Healthcare, United Kingdom) was performed as previously described.[13] Myocardial perfusion images were analyzed by 2 observers who were blinded to 123-I MIBG images. The myocardium was divided into 17 segments and patient's segmental perfusion score was assessed using a similar tracer uptake scale as used for 123-I MIBG images.[12] The rest perfusion defect score was calculated by summation of segmental perfusion scores on resting myocardial perfusion imaging. Stress perfusion defect score was calculated by summation of segmental perfusion scores on stress myocardial perfusion imaging. Accordingly, both rest and stress perfusion defect scores could range from 0 to 68 (17 x 4) points. Subsequently, the summed perfusion difference score (indicating the extent of reversible myocardial perfusion defects) was calculated by subtracting the rest perfusion defect score from the stress perfusion defect score. Finally, the 123-I MIBG/perfusion mismatch score was calculated by subtracting the rest perfusion defect score from the late 123-I MIBG SPECT defect score.

ICD Implantation

ICDs were implanted transvenously and without thoracotomy. Testing of sensing and pacing thresholds and defibrillation threshold testing was performed during implantation. In case of patient eligibility for cardiac resynchronization therapy (CRT), a combined CRT-D device was implanted.[14]

Clinical Follow-up and Endpoints

Clinical follow-up was performed by evaluation of device interrogation printouts and patient medical record data every 3 to 6 months.

The primary endpoint was defined as the occurrence of appropriate ICD therapy. Appropriate ICD therapy was defined as anti-tachycardia pacing (ATP) or shock triggered by ventricular tachycardia or ventricular fibrillation. ICD discharges were evaluated at the outpatient pacemaker clinic using ICD stored electrocardiographic data by 2 experienced electrophysiologists, blinded to other study data.

The secondary endpoint was a combined endpoint consisting of appropriate ICD therapy or cardiac death. Cardiac mortality included death caused by progressive heart failure or acute myocardial infarction.

Statistical Analysis

Continuous variables are expressed as mean ± standard deviation, and categorical data are expressed in numbers and percentages. Intra- and interobserver agreements were evaluated by calculating the intraclass correlation coefficients (ICC). Excellent agreement was defined as an intraclass correlation coefficient of >0.8. Cox proportional hazards regression analysis was performed to evaluate which variables were associated with the primary or secondary endpoint. At first, univariable analysis of baseline characteristics was performed to determine significant predictors for both endpoints. All variables that were significantly associated with the primary or secondary endpoint at the $p<0.15$ level were included in a multivariable analysis. When early and late 123-I MIBG imaging variables showed strong interrelation (Pearson's correlation coefficient >0.8), early 123-I MIBG imaging variables were excluded from multivariable analysis. Only late 123-I MIBG imaging variables were included in the multivariable analysis as they are the most commonly used 123-I MIBG imaging parameters.[11] For each variable, a hazard ratio (HR) with a 95% confidence interval (CI) was calculated.

Cumulative event rates were assessed using the method of Kaplan-Meier and log rank test. Additionally, late 123-I MIBG SPECT defect score was subdivided using the prospectively selected median value as a cutoff. The median value was selected to ensure that the number of patients was equally distributed across the two groups. Additionally, receiver-operating-characteristic (ROC) curve analysis was performed to determine the optimal cutoff point of 123-I MIBG SPECT defect score for prediction of appropriate ICD therapy. The optimal cutoff point was defined as the highest sum of sensitivity and specificity. All analyses were two-sided and a p-value <0.05 was considered statistically significant. Statistical analyses were performed with SPSS software package, version 15.0 (SPSS Inc., Chicago, Illinois, USA).

Results

Patient Population

A total of 116 patients (80 men, mean age 65±9 yrs) were enrolled. Baseline characteristics of all patients are summarized in Table 1. One-hundred three (89%) patients received an ICD as primary prevention and 13 (11%) patients as secondary prevention for SCD. Eighty-six (74%) patients were diagnosed with ischemic cardiomyopathy and 30 (26%) patients with nonischemic cardiomyopathy. The mean New York Heart Association (NYHA) functional class was 2.9±0.6 and the mean LV ejection fraction (LVEF) was 28±8%. A combined CRT-D device was implanted in 101 patients. Medication consisted of beta-blockers (71% of patients), amiodarone (19% of patients), angiotensin converting enzyme - inhibitors (ACE-I) or angiotensin II (AT II) antagonists (85% of patients) and diuretics (88% of patients).

Table 1. Baseline characteristics of the study population (n=116)

Characteristics	Values
Age (yrs)	65±9
Male gender	80 (69)
CRT-D	101 (87)
ICD indication	
Primary prevention	103 (89)
Secondary prevention	13 (11)
Ischemic cardiomyopathy	86 (74)
NYHA functional class	2.9±0.6
LVEF (%)	28±8
Cardiovascular risk factors	
Diabetes	16 (14)
Hypertension	37 (32)
Hypercholesterolemia	30 (26)
Smoking	31 (27)
Family history of CAD	35 (30)
Medication use	
Beta-blocker	82 (71)
Amiodarone	22 (19)
ACE-I / AT II antagonist	98 (85)
Oral anticoagulant	76 (66)
Statin	79 (68)
Diuretic	102 (88)

Data are presented as mean ± standard deviation or as number (%).

ACE-I = angiotensin converting enzyme - inhibitor; AT = angiotensin; CAD = coronary artery disease; CRT-D = cardiac resynchronization therapy - defibrillator; ICD = implantable cardioverter-defibrillator; LVEF = left ventricular ejection fraction; NYHA = New York Heart Association.

123-I MIBG and Myocardial Perfusion Imaging

Baseline variables of 123-I MIBG and myocardial perfusion imaging are shown in Table 2. Mean values of early and late H/M ratio were 1.58±0.18 and 1.47±0.18. Accordingly, the mean value of cardiac washout rate was 6.80±6.37. Furthermore, the early 123-I MIBG SPECT defect score had a mean value of 21.6±10.1 and the late 123-I MIBG SPECT defect score had a mean value of 26.8±10.0.

The mean rest perfusion defect score was 16.8±10.3, whereas the mean stress perfusion defect score was 18.3±10.6. Accordingly, the mean summed perfusion difference score was 1.4±2.8.

The mean 123-I MIBG/perfusion mismatch score was 9.9±12.3, indicating larger 123-I MIBG defects as compared to perfusion defects (26.8±10.0 vs. 16.8±10.3, $p<0.01$).

An excellent reproducibility was observed for early (ICC 0.98, 95% CI 0.94-0.99) and late (ICC 0.98, 95% CI 0.95-0.99) 123-I MIBG SPECT defect score. Furthermore, both SPECT readers showed an excellent agreement for early (ICC 0.97, 95% CI 0.95-0.99) and late (ICC 0.98, 95% CI 0.96-0.99) 123-I MIBG SPECT defect score.

Figure 1 shows an example of normal resting myocardial perfusion with a defect on late 123-I MIBG SPECT in a patient who received appropriate ICD therapy after 18 months of follow-up.

Table 2. Baseline variables of 123-I MIBG and myocardial perfusion imaging

123-I MIBG imaging	
Early planar H/M ratio	1.58±0.18
Late planar H/M ratio	1.47±0.18
Cardiac washout rate (%)	6.80±6.37
Early 123-I MIBG SPECT defect score	21.6±10.1
Late 123-I MIBG SPECT defect score	26.8±10.0
Myocardial perfusion imaging	
Rest perfusion defect score	16.8±10.3
Stress perfusion defect score	18.3±10.6
Summed perfusion difference score	1.4±2.8
123-I MIBG/perfusion mismatch score	9.9±12.3

Data are presented as mean ± standard deviation. H/M ratio = heart-to-mediastinum ratio; 123-I MIBG = 123-iodine metaiodobenzylguanidine; SPECT = single photon emission computed tomography.

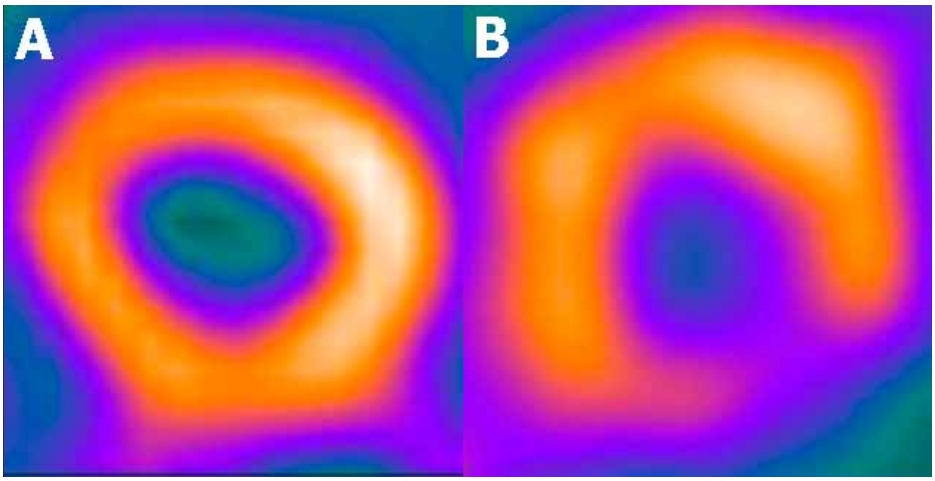

Figure 1 Example of resting myocardial perfusion (panel A) and late 123-I MIBG (panel B) imaging in an ICD patient. In this patient, showing normal myocardial perfusion and abnormal 123-I MIBG imaging, an appropriate ICD therapy (ATP) was documented after 18 months of follow-up.

Primary Endpoint: Appropriate ICD Therapy

During 23±15 months follow-up, 86 episodes of ventricular tachycardia or ventricular fibrillation were terminated by appropriate ICD therapy in 24 (21%) patients. Appropriate ICD therapy consisted of 44 episodes of ATP in 16 (14%) patients and 42 ICD shocks in 15 (13%) patients.

Univariable analyses demonstrated that ICD indication (secondary vs. primary prevention), ischemic cardiomyopathy, early 123-I MIBG SPECT defect score, late 123-I MIBG SPECT defect score, summed perfusion difference score, and the 123-I MIBG/perfusion mismatch score were significantly associated with appropriate ICD therapy (Table 3). The early 123-I MIBG SPECT defect score was excluded for multivariable analysis as it showed strong interrelation (r=0.82) with the late 123-I MIBG SPECT defect score.

Subsequently, multivariable analysis demonstrated that ICD indication (secondary vs. primary prevention) (HR 3.85, 95% CI 1.43-10.37, p<0.01) and late 123-I MIBG SPECT defect score (HR 1.13, 95% CI 1.05-1.21, p<0.01) were independent predictors for appropriate ICD therapy.

Table 3. Univariable and multivariable analyses of baseline variables for appropriate ICD therapy (primary endpoint)

	Univariable analysis		Multivariable analysis	
Characteristics	HR (95% CI)	p-value	HR (95% CI)	p-value
Age (yrs)	1.02 (0.98-1.08)	0.3		
Male gender	1.52 (0.57-4.06)	0.4		
CRT-D	1.15 (0.34-3.86)	0.8		
ICD indication	4.55 (1.95-10.65)	<0.01*	3.85 (1.43-10.37)	<0.01**
Ischemic cardiomyopathy	3.16 (0.94-10.60)	0.06*	2.10 (0.58-7.64)	0.3
NYHA functional class	1.10 (0.54-2.24)	0.8		
LVEF (%)	1.02 (0.97-1.07)	0.5		
Cardiovascular risk factors				
Diabetes	0.60 (0.14-2.54)	0.5		
Hypertension	1.13 (0.48-2.65)	0.8		
Hypercholesterolemia	1.08 (0.43-2.73)	0.9		
Smoking	1.39 (0.61-3.19)	0.4		
Positive family history of CAD	0.87 (0.36-2.09)	0.7		
Medication use				
Beta-blockade	1.03 (0.43-2.47)	1.0		
Amiodarone	1.64 (0.65-4.12)	0.3		
ACE-I / AT II antagonist	1.23 (0.37-4.14)	0.7		
Oral anticoagulant	0.61 (0.27-1.37)	0.2		
Statin	1.45 (0.57-3.65	0.4		
Diuretic	1.13 (0.27-4.8)	0.9		
123-I MIBG imaging				
Early H/M ratio	0.35 (0.04-3.30)	0.4		
Late H/M ratio	0.27 (0.03-2.32)	0.2		
Cardiac washout rate (%)	1.02 (0.95-1.09)	0.6		
Early 123-I MIBG SPECT defect score	1.07 (1.03-1.12)	<0.01*		
Late 123-I MIBG SPECT defect score	1.14 (1.08-1.20)	<0.01*	1.13 (1.05-1.21)	<0.01**
Myocardial perfusion imaging				
Rest perfusion defect score	1.02 (0.98-1.06)	0.4		
Stress perfusion defect score	1.03 (0.99-1.07)	0.2		
Summed perfusion difference score	1.09 (0.98-1.22)	0.12*	0.93 (0.83-1.05)	0.3
123-I MIBG/perfusion mismatch score	1.06 (1.02-1.09)	<0.01*	1.01 (0.97-1.06)	0.5

* Significant association with appropriate ICD therapy at a level of $p<0.15$ in univariate analysis.
**Significant association with appropriate ICD therapy in multivariate analysis. ACE-I = angiotensin converting enzyme - inhibitor; AT = angiotensin; CAD = coronary artery disease; CRT-D = cardiac resynchronization therapy - defibrillator; H/M ratio = heart-to-mediastinum ratio; 123-I MIBG = 123-iodine metaiodobenzylguanidine; LVEF = left ventricular ejection fraction; NYHA = New York Heart Association; SPECT = single photon emission computed tomography.

Risk Stratification for Appropriate ICD Therapy

Patients were stratified according to the prospectively selected median value of the 123-I MIBG SPECT defect score (summed score of 26) into patients with large (summed score >26) or small (summed score ≤26) late 123-I MIBG SPECT defect. Twenty-two (40%) patients with a large late 123-I MIBG SPECT defect (summed score >26) versus 2 (3%) patients with a small late 123-I MIBG SPECT defect (summed score ≤26) received appropriate ICD therapy ($p<0.01$).

The cumulative event rate at 3-year follow-up for appropriate ICD therapy was 52% (95% CI 36-68%) for patients with a large late 123-I MIBG SPECT defect versus 5% (95% CI 0-11%) for patients with a small late 123-I MIBG SPECT defect (Figure 2). Appropriate ICD therapy was significantly more often documented in patients with a large late 123-I MIBG SPECT defect when compared to patients with a small late 123-I MIBG SPECT defect during a mean follow-up of 23±15 months (log rank test, $p<0.01$). Moreover, the risk for appropriate ICD therapy was 13 times higher in patients with a large late 123-I MIBG SPECT defect as compared to patients with a small defect (HR 12.81, 95% CI 3.01-54.50, $p<0.01$).

ROC curve analysis showed an excellent predictive value of late 123-I MIBG SPECT defect score (AUC 0.87). The optimal cutoff value of 123-I MIBG SPECT defect score was defined at 31, which yielded a sensitivity of 75% and a specificity of 82% for prediction of appropriate ICD therapy. Patients with large 123-I MIBG SPECT defect (>31) showed

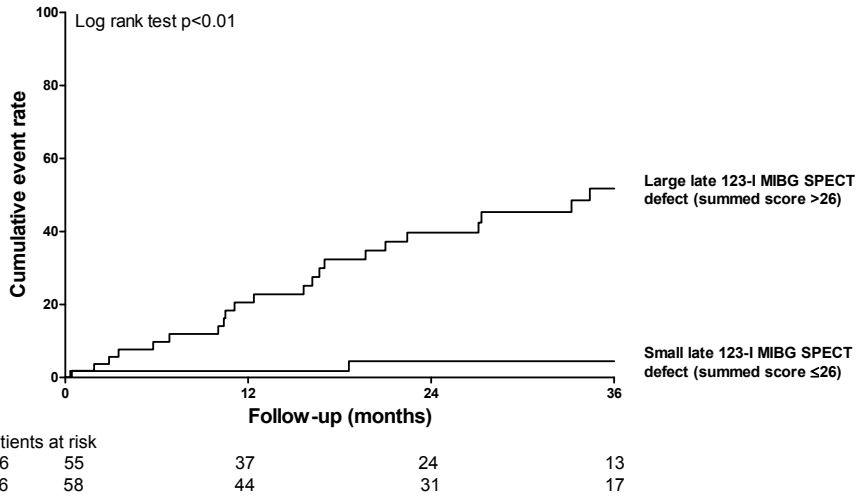

Figure 2. Kaplan-Meier curve showing the difference in appropriate ICD therapy (primary endpoint) between patients with a large (summed score >26) and small (summed score ≤26) late 123-I MIBG SPECT defect.

significantly more appropriate ICD therapy as compared to patients with small late 123-I MIBG SPECT defect (≤31) at 3-year follow-up (9% vs. 66%, p<0.01).

Secondary Endpoint: Appropriate ICD Therapy or Cardiac Mortality

Appropriate ICD therapy or cardiac mortality was documented in 32 (28%) patients. In total, 24 (21%) patients received appropriate ICD therapy and 8 (7%) patients died of progressive heart failure without previous appropriate ICD therapy. In total, cardiac death was documented in 13 (11%) patients, including 5 (4%) patients who received appropriate ICD therapy before cardiac death.

Univariable analysis demonstrated that ICD indication (secondary vs. primary prevention), ischemic cardiomyopathy, delayed H/M ratio, early 123-I MIBG SPECT defect score, late 123-I MIBG SPECT defect score and 123-I MIBG/perfusion mismatch score were significant predictors for the secondary endpoint. Since early and late 123-I MIBG SPECT defect score were strongly interrelated (r=0.82), early 123-I MIBG SPECT defect score was excluded for multivariable analysis.

Late 123-I MIBG SPECT defect score (HR 1.12, 95% CI 1.05-1.19, p<0.01) was the only independent predictor in multivariable analysis.

Risk Stratification for Appropriate ICD Therapy or Cardiac Mortality

Appropriate ICD therapy or cardiac mortality was documented in 28 (51%) patients with a large late 123-I MIBG SPECT defect (summed score >26) and in 4 (7%) patients with a small late 123-I MIBG SPECT defect (summed score ≤26) (p<0.01).

The cumulative event rate at 3-year follow-up for appropriate ICD therapy or cardiac mortality was 57% (95% CI 43-72%) for patients with a large late 123-I MIBG SPECT defect as compared to 10% (95% CI 0-20%) for patients with a small defect. Appropriate ICD therapy or cardiac death was significantly more documented in patients with a large late 123-I MIBG SPECT defect as compared to patients with a small defect during a mean follow-up of 23±15 months (log rank test, p<0.01). Moreover, the risk for appropriate ICD therapy or cardiac death was 8 times higher in patients with a large late 123-I MIBG SPECT defect than patients with a small defect (HR 8.29, 95% CI 2.91-23.63, p<0.01).

Discussion

The main findings of the study can be summarized as follows. Late 123-I MIBG SPECT defect score was an independent predictor for ventricular arrhythmias causing appropriate ICD therapy (primary endpoint) as well as the composite of appropriate ICD therapy or cardiac death (secondary endpoint). In addition, cumulative event rates for appropriate ICD therapy (52% vs. 5%, p<0.01) and appropriate ICD therapy or cardiac death (57% vs. 10%, p<0.01)

were significantly higher in patients with a large late 123-I MIBG SPECT defect (summed score >26) as compared to patients with a small late 123-I MIBG SPECT defect (summed score ≤26) at 3-year follow-up. Importantly, only 2 (3%) patients with a small late 123-I MIBG SPECT defect received appropriate ICD therapy during follow-up.

Sudden Cardiac Death and Substrate Imaging

ICD therapy has become a cornerstone treatment in patients at high risk for sudden arrhythmic death.[4] Although the benefits of ICD treatment have been demonstrated, the question has been raised whether patient selection according to the current guidelines is adequate, as it is still unclear which patients will benefit from ICD treatment.[2, 3, 5] Post-hoc analysis of the second Multicenter Automated Defibrillator Implantation Trial (MADIT II) population demonstrated that 35% of patients received appropriate ICD therapy after 3-year follow-up.[5] Moreover, the majority of arrhythmic deaths occurs in patients without ICD indication.[6]

Accordingly, attention has shifted towards improved risk stratification of patients currently indicated for ICD therapy. Recently, the AHA/ACC/HRS scientific statement on the noninvasive risk stratification in patients at risk for sudden arrhythmic death was published, indicating that the optimal method for risk stratification is unclear.[15] Although an LVEF of <40% is most commonly used for stratification of patients at risk for ventricular arrhythmias, it does not allow accurate discrimination of patients with or without sudden arrhythmic death.[15] Moreover, sudden arrhythmic death is often occurred in patients with an LVEF of >40%.[6, 15]

Since the majority of patients with documented arrhythmic death is diagnosed with structural heart disease, predominantly coronary artery disease (CAD), risk stratification should focus on further identification of the underlying substrate for arrhythmic death.[15, 16] Although the exact mechanisms of ventricular arrhythmias have been a matter of debate, it has been recognized that scar tissue and myocardial ischemia may serve as important substrates for ventricular arrhythmias. In acute myocardial infarction, ischemia may serve as a substrate for ventricular arrhythmias by inducing electrical instability.[17] In chronic myocardial infarction, areas of slow conduction are present that facilitate the development of reentrant tachycardia.[17]

Different imaging techniques (predominantly myocardial perfusion imaging) have been used to provide information on the underlying substrate. Borger van der Burg et al.[18] have evaluated the occurrence of ventricular arrhythmia and cardiac death in relation to ischemia, viability and scar tissue in 156 survivors of sudden arrhythmic death. Extent of scar tissue and reduced LV function (LVEF ≤30%) were significantly associated with occurrence of ventricular arrhythmias and cardiac death in univariable and multivariable analysis. In the present study, ischemia (summed perfusion difference score) was significantly associated with appropriate ICD therapy in univariable analysis. However, myocardial infarction (resting perfusion defect score) and ischemia were not significantly associated with both

endpoints in multivariable analysis. One of the potential explanations for these findings is the fact that the current study included patients with nonischemic cardiomyopathy, whereas in the study performed by Borger van der Burg et al.[18] all patients were diagnosed with significant CAD. In the present study, a small amount of myocardial ischemia was observed which can be explained by the fact that these patients received optimal pharmacologic and revascularization therapy prior to ICD implantation.

The autonomic nervous system may also play an important role in the pathogenesis of ventricular arrhythmias.[7, 8] Observational studies have associated the occurrence of ventricular arrhythmias with abnormalities in cardiac sympathetic innervation.[9, 10] Although the pathophysiologic mechanisms are unclear, it has been suggested that denervated but viable myocardium may be hypersensitive to circulating catecholamines. As compared to regions with normal cardiac innervation, denervated myocardium may respond differently to sympathetic activation with increased automaticity and enhanced triggering.[7] In particular, the borderzone of infarct tissue may be predisposed to develop reentrant circuits as these regions are viable but may have damaged sympathetic nerves. Viable myocardium may already exhibit areas of denervation (innervation/perfusion mismatch), as sympathetic nerve fibers are more susceptible to myocardial ischemia than cardiac tissue.[19, 20]

Recently, the innervation/perfusion mismatch score was assessed in 50 patients with LV systolic dysfunction referred for electrophysiologic testing.[10] The innervation/perfusion mismatch score was not significantly associated with inducibility of tachyarrhythmias in univariable and multivariable analysis.[10] Although the current study showed that 123-I MIBG/perfusion mismatch score was associated with the occurrence of ventricular arrhythmias in univariable analysis, no significant association was found in multivariable analysis. The lack of prognostic value of 123-I MIBG/perfusion mismatch score may be related to the relatively small extent of 123-I MIBG/perfusion mismatch observed in the patient population.

Risk Stratification in Heart Failure Patients with 123-I MIBG Imaging

Several studies using 123-I MIBG imaging have demonstrated that abnormalities in global cardiac innervation were predictive for overall cardiac mortality in heart failure patients.[21, 22] Merlet et al.[22] have shown that impaired cardiac sympathetic innervation, as assessed with planar 123-I MIBG imaging, was associated to adverse cardiac outcomes in 112 patients with heart failure and a poor LV function. Over a mean follow-up of 27±20 months, the only independent predictors for mortality were low 123-I MIBG uptake ($p<0.01$) and LV function ($p=0.02$). Recently, Agostini et al.[11] have confirmed the predictive value of cardiac 123-I MIBG imaging in 290 patients with moderate-to-severe heart failure. Most important, the study has shown that patients with normal 123-I MIBG uptake had a significantly higher 2-year event-free survival as compared to patients with reduced 123-I MIBG uptake (95% vs. 62%, $p<0.01$).

123-I MIBG Imaging to Predict Ventricular Arrhythmia

Abnormalities in the autonomic nervous system have been related to the occurrence of ventricular arrhythmias.[9, 10] Arora et al.[23] have performed a pilot study that evaluated cardiac sympathetic innervation in 17 patients with ICD treatment. ICDs were implanted because of sustained ventricular tachycardia or ventricular fibrillation. Patients with a documented ICD discharge showed significantly more global (early H/M ratio) and regional sympathetic denervation (early and late 123-I MIBG defect score) than patients without an ICD discharge. In addition, Nagahara et al.[24] have evaluated in a small study population whether abnormalities in cardiac sympathetic innervation were related to appropriate ICD therapy or lethal cardiac events. During a mean follow-up of 15 months, global cardiac sympathetic innervation (assessed with delayed H/M ratio) was independently associated with appropriate ICD therapy.

Tamaki et al.[25] have shown that myocardial washout rate was significantly associated with the occurrence of sudden arrhythmic death in 106 heart failure patients. In the current study however, myocardial washout rate was not predictive for appropriate ICD therapy. One of the explanations for these different findings may be the fact that myocardial washout rate was significantly lower in the current population when compared to the study by Tamaki et al.[25] Although both studies enrolled individuals with heart failure and severely reduced LV systolic function, patient's medication use was different. The number of patients receiving ACE-inhibitors (or AT II antagonists) was higher in the current study (85%) when compared to the study by Tamaki et al. (71%).[25] Moreover, patients received beta-blockade therapy during 123-I MIBG SPECT in this study, whereas Tamaki et al.[25] have excluded patients who had been receiving beta-blocking agents. It has been demonstrated that the use of ACE-inhibitors or beta-blockers is associated with beneficial modulation of cardiac sympathetic activity.[26, 27] Accordingly, changes in pharmacologic regime may lead to differences in myocardial washout of 123-I MIBG.

The relation between cardiac sympathetic innervation and inducibility of ventricular arrhythmias during electrophysiologic testing was recently evaluated in 50 patients with previous myocardial infarction and reduced LV systolic function.[10] Although no significant association between global cardiac denervation and inducible ventricular arrhythmias was found, regional cardiac denervation was significantly higher in patients with positive electrophysiologic tests than patients with negative electrophysiologic tests. In addition, Mitrani et al.[9] have evaluated whether patients with documented ventricular arrhythmias showed abnormal sympathetic innervation. Patients with ventricular tachycardia showed significantly more regional sympathetic denervation as compared to patients without ventricular tachycardia. Likewise, this study has demonstrated that regional cardiac sympathetic denervation derived from late 123-I MIBG SPECT was significantly associated with ventricular arrhythmias causing appropriate ICD therapy. Moreover, late 123-I MIBG SPECT defect score was an independent predictor for appropriate ICD therapy. Importantly, the risk for

appropriate ICD therapy was 13 times higher in patients with a large late 123-I MIBG SPECT defect than patients with a small defect.

Limitations

Although the current study has clearly demonstrated that cardiac sympathetic denervation on late 123-I MIBG SPECT was predictive for both study endpoints, some limitations need to be considered. In this study, a heterogeneous patient population was enrolled, including patients with ischemic and nonischemic cardiomyopathy. Additional studies are needed to establish the specific role of 123-I MIBG imaging in these subpopulations. In addition, innervation and perfusion scans were scored visually, whereas an automatic quantitative approach would be preferred. Finally, 123-I MIBG SPECT in patients with severe LV dysfunction can be limited by reduced myocardial tracer uptake, hampering the acquisition of tomographic images of the heart. These limitations have been compensated by a long acquisition time and the use of a dual-head SPECT camera equipped with low-energy, parallel-hole high-resolution collimators.

Conclusions

Cardiac sympathetic denervation on late 123-I MIBG imaging predicts ventricular arrhythmia causing appropriate ICD therapy (primary endpoint) as well as the composite of appropriate ICD therapy or cardiac death (secondary endpoint). Cardiac sympathetic denervation as assessed with delayed 123-I MIBG SPECT may improve risk stratification for arrhythmic death in patients who have an indication for ICD treatment.

Reference List

(1) Zipes DP, Camm AJ, Borggrefe M, et al. ACC/AHA/ESC 2006 Guidelines for Management of Patients With Ventricular Arrhythmias and the Prevention of Sudden Cardiac Death: a report of the American College of Cardiology/American Heart Association Task Force and the European Society of Cardiology Committee for Practice Guidelines: developed in collaboration with the European Heart Rhythm Association and the Heart Rhythm Society. Circulation 2006;114:e385-e484.

(2) Moss AJ, Hall WJ, Cannom DS, et al. Improved survival with an implanted defibrillator in patients with coronary disease at high risk for ventricular arrhythmia. Multicenter Automatic Defibrillator Implantation Trial Investigators. N Engl J Med 1996;335:1933-40.

(3) Moss AJ, Zareba W, Hall WJ, et al. Prophylactic implantation of a defibrillator in patients with myocardial infarction and reduced ejection fraction. N Engl J Med 2002;346:877-83.

(4) Epstein AE, DiMarco JP, Ellenbogen KA, et al. ACC/AHA/HRS 2008 Guidelines for Device-Based Therapy of Cardiac Rhythm Abnormalities: a report of the American College of Cardiology/American Heart Association Task Force on Practice Guidelines: developed in collaboration with the American Association for Thoracic Surgery and Society of Thoracic Surgeons. Circulation 2008;117:e350-e408.

(5) Moss AJ, Greenberg H, Case RB, et al. Long-term clinical course of patients after termination of ventricular tachyarrhythmia by an implanted defibrillator. Circulation 2004;110:3760-5.

(6) Myerburg RJ, Kessler KM, Castellanos A. Sudden cardiac death. Structure, function, and time-dependence of risk. Circulation 1992;85(1 Suppl):I2-10.

(7) Podrid PJ, Fuchs T, Candinas R. Role of the sympathetic nervous system in the genesis of ventricular arrhythmia. Circulation 1990;82(2 Suppl):I103-I113.

(8) Zipes DP. Sympathetic stimulation and arrhythmias. N Engl J Med 1991;325:656-7.

(9) Mitrani RD, Klein LS, Miles WM, et al. Regional cardiac sympathetic denervation in patients with ventricular tachycardia in the absence of coronary artery disease. J Am Coll Cardiol 1993;22:1344-53.

(10) Bax JJ, Kraft O, Buxton AE, et al. 123-MIBG scintigraphy to predict inducibility of ventricular arrhythmias on cardiac electrophysiologic testing. A prospective multicenter pilot study. Circ Cardiovasc imaging 2009;1:131-140.

(11) Agostini D, Verberne HJ, Burchert W, et al. I-123-mIBG myocardial imaging for assessment of risk for a major cardiac event in heart failure patients: insights from a retrospective European multicenter study. Eur J Nucl Med Mol Imaging 2008;35:535-46.

(12) Cerqueira MD, Weissman NJ, Dilsizian V, et al. Standardized myocardial segmentation and nomenclature for tomographic imaging of the heart: a statement for healthcare professionals from the Cardiac Imaging Committee of the Council on Clinical Cardiology of the American Heart Association. Circulation 2002;105:539-42.

(13) van Ramshorst J, Bax JJ, Beeres SL, et al. Intramyocardial bone marrow cell injection for chronic myocardial ischemia: a randomized controlled trial. JAMA 2009;301:1997-2004.

(14) Hunt SA, Abraham WT, Chin MH, et al. 2009 focused update incorporated into the ACC/AHA 2005 Guidelines for the Diagnosis and Management of Heart Failure in Adults: a report of the American College of Cardiology Foundation/American Heart Association Task Force on Practice Guidelines: developed in collaboration with the International Society for Heart and Lung Transplantation. Circulation 2009;119:e391-e479.

(15) Goldberger JJ, Cain ME, Hohnloser SH, et al. American Heart Association/American College of Cardiology Foundation/Heart Rhythm Society scientific statement on noninvasive risk stratification techniques for identifying patients at risk for sudden cardiac death: a scientific statement from the American Heart Association Council on Clinical Cardiology Committee on Electrocardiography and Arrhythmias and Council on Epidemiology and Prevention. Circulation 2008;118:1497-1518.

(16) Zipes DP, Wellens HJ. Sudden cardiac death. Circulation 1998;98:2334-51.

(17) de Bakker JM, van Capelle FJ, Janse MJ, et al. Slow conduction in the infarcted human heart. 'Zigzag' course of activation. Circulation 1993;88:915-26.
(18) Borger van der Burg AE, Bax JJ, Boersma E, Pauwels EK, van der Wall EE, Schalij MJ. Impact of viability, ischemia, scar tissue, and revascularization on outcome after aborted sudden death. Circulation 2003;108:1954-9.
(19) Zipes DP. Influence of myocardial ischemia and infarction on autonomic innervation of heart. Circulation 1990;82:1095-1105.
(20) Matsunari I, Schricke U, Bengel FM, et al. Extent of cardiac sympathetic neuronal damage is determined by the area of ischemia in patients with acute coronary syndromes. Circulation 2000;101:2579-85.
(21) Merlet P, Valette H, Dubois-Rande JL, et al. Prognostic value of cardiac metaiodobenzylguanidine imaging in patients with heart failure. J Nucl Med 1992;33:471-7.
(22) Merlet P, Benvenuti C, Moyse D, et al. Prognostic value of MIBG imaging in idiopathic dilated cardiomyopathy. J Nucl Med 1999;40:917-23.
(23) Arora R, Ferrick KJ, Nakata T, et al. I-123 MIBG imaging and heart rate variability analysis to predict the need for an implantable cardioverter defibrillator. J Nucl Cardiol 2003;10:121-31.
(24) Nagahara D, Nakata T, Hashimoto A, et al. Predicting the need for an implantable cardioverter defibrillator using cardiac metaiodobenzylguanidine activity together with plasma natriuretic peptide concentration or left ventricular function. J Nucl Med 2008;49:225-33.
(25) Tamaki S, Yamada T, Okuyama Y, et al. Cardiac iodine-123 metaiodobenzylguanidine imaging predicts sudden cardiac death independently of left ventricular ejection fraction in patients with chronic heart failure and left ventricular systolic dysfunction: results from a comparative study with signal-averaged electrocardiogram, heart rate variability, and QT dispersion. J Am Coll Cardiol 2009;53:426-35.
(26) Takeishi Y, Atsumi H, Fujiwara S, Takahashi K, Tomoike H. ACE inhibition reduces cardiac iodine-123-MIBG release in heart failure. J Nucl Med 1997;38:1085-9.
(27) Yamazaki J, Muto H, Kabano T, Yamashina S, Nanjo S, Inoue A. Evaluation of beta-blocker therapy in patients with dilated cardiomyopathy--Clinical meaning of iodine 123-metaiodobenzylguanidine myocardial single-photon emission computed tomography. Am Heart J 2001;141:645-52.

Chapter **13**

123-I MIBG/perfusion Scintigraphy in Comparison with Contrast-enhanced Magnetic Resonance Imaging for Assessment of Infarct Size and Infarct Border Zone

Mark J. Boogers, MD[1, 2]; Rob J van der Geest, PhD[3]; Stijntje D. Roes, MD[1]; Petra Dibbets-Schneider, MSc[4]; Victoria Delgado, MD, PhD[1]; Imad Al Younis, MD[4]; Bernies van der Hiel, MD[4]; Albert de Roos, MD, PhD[5]; Johan H. C. Reiber, PhD[3]; Martin J. Schalij, MD, PhD[1]; Jeroen J. Bax, MD, PhD[1]; Ernst E. van der Wall, MD, PhD[1]

[1]Department of Cardiology, Leiden University Medical Center, Leiden, the Netherlands; [2]The Interuniversity Cardiology Institute of the Netherlands, Utrecht, the Netherlands; [3]Division of Image Processing, Leiden University Medical Center, Leiden, the Netherlands; [4]Department of Nuclear Medicine, Leiden University Medical Center, Leiden, the Netherlands; [5]Department of Radiology, Leiden University Medical Center, Leiden, the Netherlands.

Abstract

Background: Contrast-enhanced magnetic resonance imaging (MRI) allows assessment of total infarct size and infarct border zone, which can be used as markers of vulnerable myocardium for ventricular arrhythmias. Combined 123-iodine metaiodobenzylguanidine (123-I MIBG) and myocardial perfusion scintigraphy may also be used for infarct tissue characterization. However, at present, contrast-enhanced MRI and 123-I MIBG/perfusion scintigraphy have not been compared for characterization of infarct tissue. Accordingly, this descriptive study evaluated the relation between contrast-enhanced MRI and 123-I MIBG/perfusion scintigraphy for assessment of infarct size and infarct border zone.

Methods: Ischemic heart failure patients who underwent contrast-enhanced MRI and 123-I MIBG/myocardial perfusion scintigraphy were included. Contrast-enhanced MRI and myocardial perfusion scintigraphy were compared for assessment of infarct size. Infarct tissue was defined as myocardium with signal intensity (SI) ≥50% of the maximum SI on contrast-enhanced MRI. The total perfusion defect score was used to assess infarct size on myocardial perfusion scintigraphy. Additionally, contrast-enhanced MRI was compared to 123-I MIBG/perfusion scintigraphy for assessment of infarct border zone. On contrast-enhanced MRI, a significant infarct border zone (myocardium with ≥35% SI <50% of the maximum SI) was defined as an infarct border zone of >16.7 grams. On 123-I MIBG/perfusion scintigraphy, the total 123-I MIBG SPECT defect score and the innervation/perfusion mismatch score (infarct border zone) were used to assess vulnerable myocardium for ventricular arrhythmias.

Results: Forty patients (29 men, mean age 66±10 yrs) with ischemic heart failure were included. Contrast-enhanced MRI and myocardial perfusion scintigraphy showed good correlations for infarct size ($r=0.72$, $p<0.01$). In addition, patients with a significant infarct border zone on contrast-enhanced MRI showed a significantly higher total 123-I MIBG SPECT defect score (48.2±12.5% vs. 32.1±9.5%, $p<0.05$) and innervation/perfusion mismatch score (13.9±11.0% vs. 6.8±6.0%, $p<0.05$) than patients without a significant infarct border zone.

Conclusions: Contrast-enhanced MRI and myocardial perfusion scintigraphy showed good correlations for infarct size. Importantly, patients with a significant infarct border zone on contrast-enhanced MRI showed significantly larger areas of infarct border zone on 123-I MIBG/perfusion scintigraphy.

Introduction

Assessment of myocardial infarct tissue has shown to play an important role to risk stratify patients for adverse cardiac events.[1, 2] Infarct tissue may show considerable spatial heterogeneity due to the presence of necrotic areas that are intermingled with bundles of viable cardiomyocytes.[3, 4] These regions of infarct tissue heterogeneity are primarily present in the periphery of the infarcted myocardium, which is commonly referred to as the infarct border zone or peri-infarct region. Previous studies have postulated that peri-infarct regions may serve as an important substrate for the development of potential life-threatening ventricular arrhythmias through the presence of reentrant circuits originating from slow-conduction pathways.[4-7]

With its high spatial resolution and signal-to-image noise ratio, contrast-enhanced magnetic resonance imaging (MRI) allows an accurate delineation of myocardial infarct tissue.[3-6, 8] More specifically, contrast-enhanced MRI enables the discrimination between myocardial infarct core and peri-infarct regions using marked differences in contrast-media hyperenhancement.[3-6, 8] Accordingly, contrast-enhanced MRI permits the assessment of vulnerable myocardium at risk for ventricular arrhythmias by assessment of infarct border zone.[4-6]

In addition, nuclear imaging can be used for evaluation of myocardial infarct tissue.[9] Myocardial perfusion scintigraphy can be used for assessment of infarct size, whereas cardiac 123-iodine metaiodobenzylguanidine (123-I MIBG) imaging permits assessment of myocardial sympathetic denervation.[9-11] It has been shown that viable myocardium may already exhibit areas of sympathetic denervation, as sympathetic nerve fibers are more prone to the detrimental effects of myocardial ischemia than cardiomyocytes.[10, 12] Thus, regions with deprived sympathetic innervation may reflect the total extent of injured myocardium, rather than the myocardial perfusion defect alone.

At present, regions with cardiac sympathetic denervation as assessed with 123-I MIBG imaging have been marked as myocardium at risk for ventricular arrhythmias.[11, 13, 14] Areas of sympathetic denervation may show an enhanced triggering and automaticity when compared to adjacent regions with preserved sympathetic innervation.[14]

Furthermore, it has been shown that the mismatch between cardiac sympathetic innervation and myocardial perfusion, which is referred to as the innervation/perfusion mismatch or infarct border zone, may be used as a marker of pro-arrhythmogenic myocardium.[15-17]

Contrast-enhanced MRI and 123-I MIBG/perfusion scintigraphy have currently not been compared for characterization of infarct tissue. More specifically, the relation between contrast-enhanced MRI and 123-I MIBG/perfusion scintigraphy for assessment of infarct border zone as a marker of vulnerable myocardium for ventricular arrhythmias has not been evaluated. Accordingly, this descriptive study aimed to explore the relation between

contrast-enhanced MRI and 123-I MIBG/perfusion scintigraphy for assessment of infarct size and infarct border zone, as markers for vulnerable myocardium for ventricular arrhythmias.

Materials and Methods

Patient Population and Protocol

The patient population consisted of patients with ischemic heart failure who were clinically referred for cardiac MRI, myocardial perfusion single photon emission computed tomography (SPECT) and cardiac 123-iodine metaiodobenzylguanidine (123-I MIBG) imaging for risk stratification of heart failure. Patient data were prospectively collected in the departmental Cardiology Information System (EPD-Vision®, Leiden University Medical Center, Leiden, the Netherlands) and retrospectively analyzed. All patients were treated according to the MISSION! - Heart Failure care track operational at the LUMC.[18] Patients with unstable angina or acute coronary syndromes were excluded from study analysis.

Ischemic etiology was based on the presence of previous (1) myocardial infarction, (2) percutaneous coronary intervention, (3) coronary artery bypass grafting or (4) evidence of coronary artery disease (CAD) on previous diagnostic tests. Risk factors for CAD were derived from patient medical record data.

First, contrast-enhanced MRI and myocardial perfusion scintigraphy were compared for the assessment of myocardial infarct size. On contrast-enhanced MRI, infarct size was assessed with signal intensity (SI) analyses on short-axis images, in which infarct tissue was defined as myocardium with SI ≥50% of the maximum SI. On myocardial perfusion scintigraphy, the total perfusion defect score was used to assess myocardial infarct size (Table 1).

Consecutively, contrast-enhanced MRI and nuclear imaging were compared for assessment of infarct border zone (Table 1). Contrast-enhanced MRI was used to assess infarct border zone which was used as a marker of vulnerable myocardium for ventricular arrhythmias (pro-arrhythmogenic myocardium).[4-6] As previously reported, a cutoff value of 16.7 grams of infarct border zone allows identification of patients at risk for potential lethal ventricular arrhythmias.[6] Accordingly, patients with >16.7 grams of infarct border zone were considered to have a significant infarct border zone on contrast-enhanced MRI.

In addition, both total 123-I MIBG SPECT defect score as derived from late 123-I MIBG SPECT and the mismatch between cardiac sympathetic innervation and myocardial perfusion (the innervation/perfusion mismatch) were used to identify the infarct border zone (Table 1).

Thereafter, the total 123-I MIBG SPECT defect score and the innervation/perfusion mismatch score (infarct border zone) were evaluated in patients with (>16.7 grams) and without (≤16.7 grams) a significant infarct border zone on contrast-enhanced MRI.

Table 1. Baseline imaging variables of the patient population (n=40)

Baseline variables	Definition
Myocardial infarct Size	
Contrast-enhanced MRI (%)	Myocardium with SI ≥50% of maximum SI
Myocardial perfusion imaging (%)	Total perfusion defect score
Myocardium at risk for ventricular arrhythmias	
Contrast-enhanced MRI (%)	Myocardium with ≥35% SI <50% of maximum SI
123-I MIBG imaging (%)	Total 123-I MIBG SPECT defect score
123-I MIBG/perfusion imaging (%)	Innervation/perfusion mismatch score

Data are presented as percentages (%). 123-I MIBG = 123-iodine metaiodobenzylguanidine; MRI = magnetic resonance imaging; SI = signal intensity; SPECT = single photon emission computed tomography.

Magnetic Resonance Imaging

Acquisition and Analysis

Contrast-enhanced images were acquired with a 1.5-T Gyroscan ACS-NT/Intera MRI scanner (Philips Medical Systems, Best, the Netherlands) equipped with powertrack 6000 gradients in combination with a 5-element cardiac synergy coil. Using vector electrocardiographic (ECG) gating, cardiac images were acquired in patients in supine position during breath holds of approximately 15 seconds. Using 10-12 imaging levels (one slice per breath hold), the entire heart was imaged from apex to cardiac base[19] in short-axis view with the use of a balanced turbo-field echo sequence with parallel imaging (SENSE, acceleration factor 2). Subsequently, contrast-enhanced imaging was performed 15 minutes after bolus infusion of 0.15 mmol/kg of gadolinium diethylenetriamine penta-acetic (Magnevist, Schering/Berlin, Germany) using an inversion-recovery 3D turbo-field echo sequence with parallel imaging (SENSE, acceleration factor 2). The entire heart was imaged in short-axis view during one breath-hold with 20-24 imaging levels. The number of imaging levels was dependent on the size of the heart. The inversion time was assessed by real-time plan scan to null normal myocardial signal. The cardiac images were send to a remote off-line workstation with dedicated in-house developed MASS research software (Mass V2008-EXP, LKEB, Leiden, the Netherlands).[20]

At first, contrast-enhanced short-axis images were evaluated by an independent observer to assess infarct size as well as infarct border zone, as shown in Figure 1. For this purpose, endocardial and epicardial contours were manually outlined on contrast-enhanced short-axis images. After the contour detection, the region with maximal SI within the scarred myocardium was defined on short-axis images. Myocardial infarct tissue was defined as myocardium with SI ≥50% of the maximum SI, whereas the infarct border zone was defined as myocardium with ≥35% SI <50% of the maximum SI. The full-width at half maximum (FWHM) criterion was used to define myocardial infarct tissue.[21, 22] As previously reported,

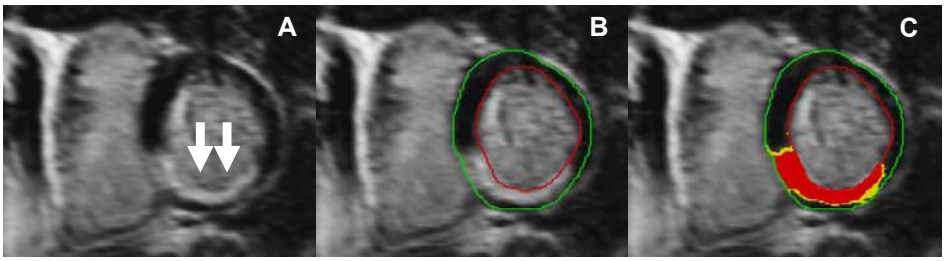

Figure 1. Contrast-enhanced magnetic resonance imaging (MRI) was used for assessment of infarct tissue heterogeneity, which consisted of myocardial infarct tissue and infarct border zone. The infarct border zone was used as a marker of myocardium at risk for ventricular arrhythmias (pro-arrhythmogenic myocardium).[5, 6] At first, contrast-enhanced short-axis images were used to evaluate the presence of myocardial infarct tissue (panel A, white arrows). Consecutively, endocardial (red) and epicardial (green) contours were manually outlined on short-axis images (panel B). With the use of the maximum signal intensity (SI) within the infarcted myocardium, the infarct tissue (red area) and the infarct border zone (yellow area) were assessed (panel C). Infarct tissue was defined as myocardium with SI ≥50% of the maximum SI, whereas the infarct border zone (area at risk) was defined as myocardium with ≥35% SI <50% of the maximum SI.

the threshold for infarct border zone was based on the ratio of 2:3 for threshold SI of infarct border zone versus infarct core.[5, 6] Myocardial infarct size and infarct border zone were expressed in percentages of the myocardium.

Patients with >16.7 grams of infarct border zone were classified as patients with a significant infarct border zone, whereas patients with ≤16.7 grams of infarct border zone were classified as patients without a significant infarct border zone.[6] As previously reported, a cutoff of 16.7 grams of infarct border zone allows identification of patients at risk for potential lethal ventricular arrhythmias.[6]

Sympathetic Nerve Imaging with 123-I MIBG

Acquisition and Analysis

One hour prior to intravenous administration of 185 MBq 123-I MIBG (AdreView, General Electric Healthcare, United Kingdom), patients were pretreated with 120 mg sodium iodide to block the thyroid uptake of free iodine-123. In all patients, 123-I MIBG SPECT was performed on a dual-head camera system (GCA-7200, Toshiba Corp., Tokyo, Japan) equipped with low-energy, parallel-hole high-resolution collimators. SPECT images were acquired using a step and shoot mode (90 projections, imaging time 30 minutes). A 128 x 128 matrix was used for SPECT studies and the energy window was symmetrically centered to 20% of the 159-keV energy peak of 123-I MIBG. SPECT was repeated 3-4 hours after intravenous injection of 123-I MIBG. After the SPECT studies were processed with iterative reconstruction, they were reconstructed into short-, vertical and horizontal long-axis according to the standard recommendations.[23]

The late 123-I MIBG SPECT images were used to calculate the total 123-I MIBG SPECT defect score by two independent observers. Using the 17-segment model[23], each myocardial segment was scored using the following tracer uptake scale: 0 = normal tracer uptake, 1 = mildly reduced tracer uptake, 2 = moderately reduced tracer uptake, 3 = severely reduced tracer uptake, 4 = no tracer uptake. The total 123-I MIBG SPECT defect score was calculated by the summation of each segmental uptake score. Accordingly, the total 123-I MIBG defect score could range from 0 to 68 (0-100%). As previously reported[11], a low intra-observer (ICC 0.98, 95% CI 0.95-0.99) as well as a low inter-observer (ICC 0.98, 95% CI 0.96-0.99) variability was demonstrated for late 123-I MIBG SPECT defect score.[11] The total 123-I MIBG SPECT defect score (%) was used as a measure of vulnerable myocardium for ventricular arrhythmias, as shown in Table 1.

Gated Myocardial Perfusion SPECT

Acquisition and Analysis

Resting ECG-gated myocardial perfusion SPECT with ^{99m}Tc-tetrofosmin (500 MBq, injected at rest) was performed using a triple-head SPECT camera system (GCA 9300/HG; Toshiba Corp., Tokyo, Japan) equipped with high-resolution, low-energy collimators. A 20% window was centered around the 140-keV energy peak of ^{99m}Tc-tetrofosmin. Ninety projections were acquired according to the step and shoot method (35 s/projection, 64 x 64 matrix, total imaging time 23 minutes) over a 360-degree circular orbit. ECG gating was applied on the cardiac cycle with 16 frames per cardiac cycle using a tolerance window of 50%. After the pre-filtration was performed using a Butterworth filter, images were reconstructed into long- and short-axis projections perpendicular to the heart axis using a filtered back projecting algorithm. No attenuation correction was used.[23]

Thereafter, resting myocardial SPECT images were evaluated by two independent observers who were unaware of the 123-I MIBG and contrast-enhanced MRI data. Based on the 17-segment model[23], each myocardial segment was scored using the similar tracer uptake scale as applied for 123-I MIBG SPECT images. Subsequently, patient's segmental scores were summed, yielding a total perfusion defect score per patient, which could range from 0 to 68 (0-100%). As shown in Table 1, the total perfusion defect score was used as a measure of myocardial infarct size.

Finally, the innervation/perfusion mismatch score (infarct border zone) was assessed by subtracting the total perfusion defect score from total 123-I MIBG SPECT defect score.[11] The innervation/perfusion mismatch score was used as a measure of vulnerable myocardium for ventricular arrhythmias (Table 1). The innervation/perfusion mismatch score could vary between 0 and 68 (0-100%). Figure 2 provides an example of a patient with a considerable innervation/perfusion mismatch, in which the sympathetic nerve defect as assessed with late

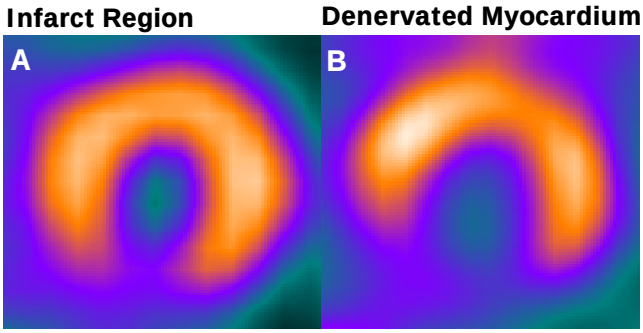

Figure 2. Nuclear imaging techniques were used for assessment of myocardial infarct size as well as myocardium at risk for ventricular arrhythmias.

A. Myocardial scar tissue was assessed with ^{99m}Tc-tetrofosmin resting myocardial perfusion single photon emission computed tomography (SPECT). The total perfusion defect score on myocardial perfusion scintigraphy was used as a marker of myocardial infarct size.

B. The total 123-iodine metaiodobenzylguanidine (123-I MIBG) SPECT defect score as derived from late 123-I MIBG SPECT as well as the innervation/perfusion mismatch score (the difference between resting perfusion imaging and late 123-I MIBG SPECT) were used as markers of myocardium at risk for ventricular arrhythmias.

123-I MIBG SPECT (panel B) was significantly larger than the myocardial perfusion defect (panel A).

Statistical Analysis

Continuous variables were expressed as mean ± SD, and categorical data as numbers or percentages. Kolmogorov-Smirnov tests were used to evaluate the distribution of the data. When non-normally distributed, data were presented as medians and 25th and 75th percentiles. Contrast-enhanced MRI and myocardial perfusion scintigraphy were compared for assessment of infarct size using Pearson's linear regression analyses and paired *t* tests. Paired *t* tests were used to compare contrast-enhanced MRI with 123-I MIBG imaging and myocardial perfusion scintigraphy for assessment of infarct border zone.

Furthermore, patients were stratified according to the prospectively selected cutoff value of 16.7 grams of infarct border zone on contrast-enhanced MRI into patients with (>16.7 grams) and without (≤16.7 grams) significant infarct border zone. As previously reported, a cutoff value of 16.7 grams of infarct border zone allows identification of patients at risk for potential lethal ventricular arrhythmias.[6] Student's *t* tests were used to evaluate the total 123-I MIBG SPECT defect score and the innervation/perfusion mismatch score in patients with (>16.7 grams) and without (≤16.7 grams) a significant infarct border zone on contrast-enhanced MRI. All p-values were two-sided and a p-value <0.05 was considered to indicate statistical significance. Statistical analyses were performed with the use of dedicated software (SPSS version 16.0, SPSS inc., Chicago, Illinois, USA).

Results

Patient Population

A total of 40 patients (29 men, mean age 66±10 yrs) with ischemic heart failure were enrolled. Baseline characteristics of the patient population are summarized in Table 2. The mean New York Heart Association (NYHA) functional class was 2.6±0.7. Medication consisted of diuretics (78% of patients), angiotensin converting enzyme - inhibitors (ACE-I) or angiotensin II (AT II) antagonists (88% of patients) or beta-blockers (68% of patients). Contrast-enhanced MRI and 123-I MIBG imaging were performed within a mean period of 8.1±47.3 days. No acute coronary events or change in medication was documented between both examinations. Contrast-enhanced MRI showed a mean LV mass of 149.7±55.1 grams.

Table 2. Baseline characteristics of the study population (n=40)

Characteristics	Values
Age (yrs)	66±10
Male gender	29 (73)
LVEF (%)	27±10
NYHA functional class	2.6±0.7
Previous MI	27 (68)
Previous PCI	17 (43)
Previous CABG	15 (38)
Cardiovascular risk factors	
Diabetes	5 (13)
Hypertension	14 (35)
Hypercholesterolemia	18 (45)
Family history of CAD	14 (35)
Current smoking	8 (20)
Obesity	8 (20)
Medication	
Diuretic	31 (78)
ACE-I / AT II antagonist	35 (88)
Beta-blocker	27 (68)
Statin	36 (90)
Nitrate	14 (35)

Data are presented as mean ± standard deviation or as number (%).

ACE-I = angiotensin converting enzyme - inhibitor; AT = angiotensin; CABG = coronary artery bypass graft surgery; CAD = coronary artery disease; LVEF = left ventricular ejection fraction; MI = myocardial infarction; NYHA = New York Heart Association; PCI = percutaneous coronary intervention.

Assessment of Myocardial Infarct Size

The infarct size on myocardial perfusion scintigraphy was significantly larger as compared to the infarct size on contrast-enhanced MRI; the mean infarct size as assessed with myocardial perfusion scintigraphy and contrast-enhanced MRI were 30.6±12.6% and 16.9±11.8%, respectively ($p<0.05$). Contrast-enhanced MRI and myocardial perfusion scintigraphy were well-correlated for assessment of infarct size ($r=0.72$, $n=40$, $p<0.01$), as shown in Figure 3.

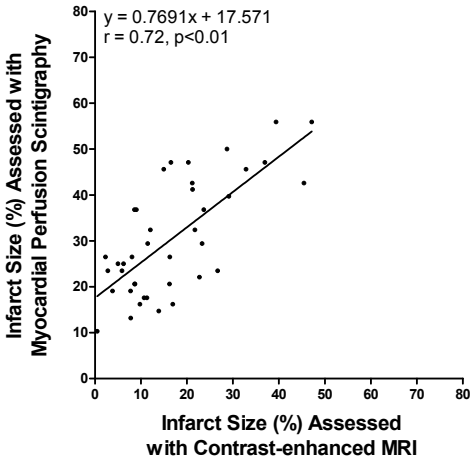

Figure 3. Contrast-enhanced magnetic resonance imaging (MRI) and myocardial perfusion scintigraphy were compared for the assessment of myocardial infarct size. Contrast-enhanced MRI and myocardial perfusion scintigraphy were well-correlated for the assessment of infarct size ($r=0.72$, $p<0.01$).

Assessment of Infarct Border Zone

Contrast-enhanced MRI showed a mean infarct border zone of 16.1±7.3%. The mean total 123-I MIBG SPECT defect score was 41.4±13.8%, whereas the mean innervation/perfusion mismatch score (infarct border zone) was 10.9±9.8%. The total 123-I MIBG SPECT defect score ($p<0.05$) and the innervation/perfusion mismatch score (infarct border zone) ($p<0.05$) were significantly different when compared to the infarct border zone on contrast-enhanced MRI. Additionally, patients were stratified according to the prospectively selected value of 16.7 grams of infarct border zone (as derived from contrast-enhanced MRI) into patients with (>16.7 grams) and without (≤16.7 grams) significant infarct border zone.[6] In total, 23 (58%) patients showed a significant infarct border zone on contrast-enhanced MRI, whereas 17 (42%) patients showed no significant infarct border zone on contrast-enhanced MRI.

As shown in Figure 4, patients with a significant infarct border zone on contrast-enhanced MRI (>16.7 grams) showed a significantly larger total 123-I MIBG SPECT defect score as

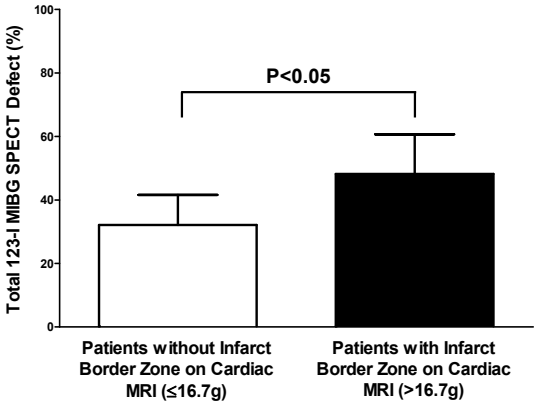

Figure 4. The infarct border zone (myocardium at risk for ventricular arrhythmias) can be assessed with contrast-enhanced magnetic resonance imaging (MRI). As previously reported, a cutoff of 16.7 grams of infarct border zone allows identification of patients at risk for life-threatening ventricular arrhythmias.[6] Patients with a significant infarct border zone on contrast-enhanced MRI (infarct border zone >16.7 grams) showed a significantly larger total 123-iodine metaiodobenzylguanidine (123-I MIBG) single photon emission computed tomography (SPECT) defect as compared to patients without a significant infarct border zone on contrast-enhanced MRI (infarct border zone ≤16.7 grams) (48.2±12.5% vs. 32.1±9.5%, p<0.05).

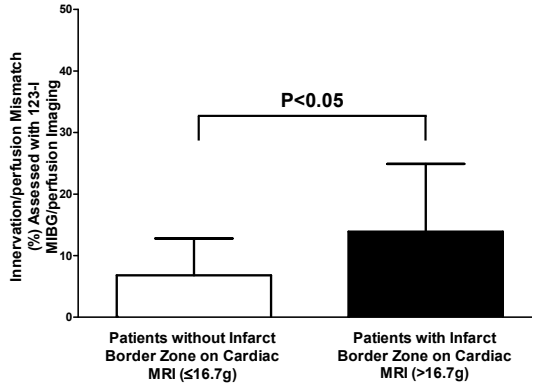

Figure 5. Contrast-enhanced magnetic resonance imaging (MRI) permits assessment of infarct border zone, which was used as a marker of myocardium at risk for ventricular arrhythmias. A cutoff value of 16.7 grams of infarct border zone was used to define a significant infarct border zone.[6] Patients with a significant infarct border zone on contrast-enhanced MRI (infarct border zone >16.7 grams) showed a significantly larger innervation/perfusion mismatch as assessed with 123-iodine metaiodobenzylguanidine (123-I MIBG) imaging and myocardial perfusion scintigraphy as compared to patients without a significant infarct border zone on contrast-enhanced MRI (infarct border zone ≤16.7 grams) (13.9±11.0% vs. 6.8±6.0%, p<0.05).

compared to patients without a significant infarct border zone on contrast-enhanced MRI (48.2±12.5% vs. 32.1±9.5%, $p<0.05$). Similarly, the innervation/perfusion mismatch (infarct border zone) was significantly larger in patients with an infarct border zone of >16.7 grams than in patients with an infarct border zone of ≤16.7 grams on contrast-enhanced MRI (13.9±11.0% vs. 6.8±6.0%, $p<0.05$) (Figure 5).

Discussion

The current study showed that infarct size as assessed with contrast-enhanced MRI was significantly correlated to infarct size on myocardial perfusion scintigraphy. Importantly, this descriptive study is the first showing that patients with a significant infarct border zone on contrast-enhanced MRI showed a significantly larger innervation/perfusion mismatch (infarct border zone) on 123-I MIBG/perfusion scintigraphy when compared to patients without a significant infarct border zone on contrast-enhanced MRI.

Infarct tissue may exhibit substantial heterogeneity as necrotic myocardium can be present along with different stages of healed myocardial infarction.[3, 4] Myocardial necrosis is primarily located in the middle of the infarct region, while bundles of viable cardiomyocytes bordered by dense fibrosis (referred to as tissue heterogeneity) can be found in the periphery of the infarct region, the so-called peri-infarct zone or border zone.[4-6] Thus far, cardiac MRI and 123-I MIBG/perfusion scintigraphy have not been related for infarct tissue characterization, nor have these imaging techniques been compared for assessment of infarct border zone, which can be used as a marker of vulnerable myocardium for ventricular arrhythmias.[4, 6]

Myocardial Infarct Size

Myocardial infarct tissue can be assessed with several non-invasive imaging techniques, including contrast-enhanced MRI, echocardiography as well as nuclear imaging. Among these techniques, contrast-enhanced MRI is considered the standard of reference for evaluation of infarct tissue as it allows an accurate delineation of infarct area and border zone using marked differences in contrast-media hyperenhancement within the infarcted myocardium.[3-6, 8]

Beyond contrast-enhanced MRI, nuclear imaging is another reliable imaging technique for assessment of myocardial infarct tissue.[9] Moreover, nuclear imaging techniques, such as myocardial perfusion scintigraphy have been used frequently for evaluation of myocardial infarct tissue in clinical practice. Previous studies have shown that myocardial perfusion scintigraphy was significantly correlated to contrast-enhanced MRI for assessment of infarct size.[3, 24, 25] In 12 post-infarct patients, Lima et al.[3] have demonstrated good correlations between contrast-enhanced MRI and myocardial perfusion imaging for myocardial infarct

size (r=0.92, p<0.01). More recently, Ibrahim et al.[25] have shown that infarct size as assessed with contrast-enhanced MRI was well-correlated with infarct size as derived from myocardial perfusion SPECT (r=0.86, p<0.05). Moreover, infarct size was significantly overestimated by myocardial perfusion SPECT (7% of the LV, p<0.03) at 42 minutes post-injection using a constant inversion time of 300 ms. Similarly, the current study has shown that myocardial infarct size on contrast-enhanced MRI was significantly correlated to infarct size as assessed with myocardial perfusion scintigraphy. Moreover, both studies showed an overestimation of infarct size on myocardial perfusion SPECT as compared to contrast-enhanced MRI. This finding may be related to differences in spatial resolution between both techniques; myocardial perfusion SPECT has a markedly lower spatial resolution than contrast-enhanced MRI, which may have introduced partial volume effects with an overestimation of infarct size. In addition, both techniques used a different approach for quantification of infarct size. In the current study, the infarct size on contrast-enhanced MRI was defined as myocardium with SI ≥50% of the maximum SI (expressed as a percentage of the total myocardium), whereas the infarct size on myocardial perfusion SPECT was assessed using the semi-quantitative resting perfusion defect score (expressed as a percentage of the total perfusion defect).

Infarct Border Zone

Beyond the assessment of infarct size, contrast-enhanced MRI allows evaluation of infarct tissue heterogeneity by demarcation of infarct core and border zone.[4-6] The infarct border zone is considered an important infarct region as it may serve as substrate for development of ventricular arrhythmias; patients with a large infarct border zone showed an increased susceptibility for ventricular arrhythmias as compared to patients with small infarct border zone.[4, 6]

Nuclear imaging may also be used for evaluation of arrhythmogenic myocardium by assessment of total denervated myocardium and the innervation/perfusion mismatch, which is referred to as the infarct border zone.[11, 13, 14] Previous studies have indicated that regions with deprived cardiac sympathetic innervation as assessed with 123-I MIBG imaging may play an important role in ventricular arrhythmogenesis as they show an enhanced triggering and automaticity when compared to adjacent regions with relatively intact sympathetic innervation of the myocardium.[14] In addition, the mismatch between cardiac sympathetic innervation and myocardial perfusion (innervation/perfusion mismatch) can be used as a marker for pro-arrhythmogenic myocardium as it reflects the infarct border zone.[15-17] Regions with cardiac sympathetic denervation but preserved myocardial viability can be present as neural tissue exhibits an increased susceptibility to hypoxia as compared to cardiomyocytes.[10] Simoes et al.[16] have shown that the innervation/perfusion mismatch as assessed with 123-I MIBG imaging and 201-thallium perfusion scintigraphy was significantly correlated to prolonged ventricular repolarization and delayed depolarization in 67 patients with ischemic heart disease. Based upon these initial studies, it has been suggested that

nuclear imaging with 123-I MIBG/perfusion scintigraphy can be used to identify patients at risk for arrhythmic events.

The current descriptive study has shown that patients with a significant infarct border zone on contrast-enhanced MRI exhibited a significantly higher total 123-I MIBG SPECT defect score and innervation/perfusion mismatch score (infarct border zone) as compared to patients without a significant infarct border zone on contrast-enhanced MRI. This is an important finding as it indicates that 123-I MIBG/perfusion scintigraphy permits identification of patients with a significant infarct border zone, and for this reason may help to identify patients at risk for adverse arrhythmic events. Eventually, the assessment of arrhythmogenic substrate (infarct border zone) may be used for identification of patients indicated for implantable cardioverter-defibrillator (ICD) therapy.

Although contrast-enhanced MRI and 123-I MIBG/perfusion scintigraphy allowed identification of vulnerable myocardium for ventricular arrhythmia by assessment of infarct border zone, both techniques showed differences in the size of the infarct border zone. This may be related to the superior spatial resolution of contrast-enhanced MRI when compared to the nuclear imaging techniques. In addition, the differences between both imaging techniques for assessment of infarct border zone may be related to the fact that the infarct border zone on contrast-enhanced MRI can be calculated using several approaches. At present, additional studies are needed that determine the optimal criterion for assessment of infarct border zone.

Although the study showed that 123-I MIBG/perfusion scintigraphy can be used to assess infarct border zone, some limitations need to be acknowledged. First, the study findings are based on a relatively small patient population consisting of 40 patients with ischemic heart failure, whereas a larger patient population would have been preferred for comparison of both techniques. Moreover, the prognostic value of infarct size and infarct border zone has not been evaluated as the current study was only designed to describe the relation between contrast-enhanced MRI and 123-I MIBG/perfusion scintigraphy for assessment of infarct size and infarct border zone.

Conclusion

Contrast-enhanced MRI and myocardial perfusion scintigraphy were significantly correlated for infarct size. Importantly, patients with a significant infarct border zone on contrast-enhanced MRI showed a significantly larger innervation/perfusion mismatch (infarct border zone) on 123-I MIBG/perfusion scintigraphy.

Reference List

(1) Braunwald E, Fauci AS, Kasper DL, Hauser SL, Longo DL, Jameson JL. Principles of internal medicine. Harrison's 15 ed. 2001:1316-1323.

(2) Kannel WB, Abbott RD. Incidence and prognosis of unrecognized myocardial infarction. An update on the Framingham study. N Engl J Med 1984;311(18):1144-1147.

(3) Lima JA, Judd RM, Bazille A, Schulman SP, Atalar E, Zerhouni EA. Regional heterogeneity of human myocardial infarcts demonstrated by contrast-enhanced MRI. Potential mechanisms. Circulation 1995;92(5):1117-1125.

(4) Schmidt A, Azevedo CF, Cheng A, Gupta SN, Bluemke DA, Foo TK, Gerstenblith G, Weiss RG, Marban E, Tomaselli GF, Lima JA, Wu KC. Infarct tissue heterogeneity by magnetic resonance imaging identifies enhanced cardiac arrhythmia susceptibility in patients with left ventricular dysfunction. Circulation 2007;115(15):2006-2014.

(5) Yan AT, Shayne AJ, Brown KA, Gupta SN, Chan CW, Luu TM, Di Carli MF, Reynolds HG, Stevenson WG, Kwong RY. Characterization of the peri-infarct zone by contrast-enhanced cardiac magnetic resonance imaging is a powerful predictor of post-myocardial infarction mortality. Circulation 2006;114(1):32-39.

(6) Roes SD, Borleffs CJ, van der Geest RJ, Westenberg JJ, Marsan NA, Kaandorp TA, Reiber JH, Zeppenfeld K, Lamb HJ, de Roos A, Schalij MJ, Bax JJ. Infarct tissue heterogeneity assessed with contrast-enhanced MRI predicts spontaneous ventricular arrhythmia in patients with ischemic cardiomyopathy and implantable cardioverter-defibrillator. Circ Cardiovasc Imaging 2009;2(3):183-190.

(7) de Bakker JM, van Capelle FJ, Janse MJ, Wilde AA, Coronel R, Becker AE, Dingemans KP, van Hemel NM, Hauer RN. Reentry as a cause of ventricular tachycardia in patients with chronic ischemic heart disease: electrophysiologic and anatomic correlation. Circulation 1988;77(3):589-606.

(8) Wu E, Judd RM, Vargas JD, Klocke FJ, Bonow RO, Kim RJ. Visualisation of presence, location, and transmural extent of healed Q-wave and non-Q-wave myocardial infarction. Lancet 2001;357(9249):21-28.

(9) Underwood SR, Anagnostopoulos C, Cerqueira M, Ell PJ, Flint EJ, Harbinson M, Kelion AD, Al-Mohammad A, Prvulovich EM, Shaw LJ, Tweddel AC. Myocardial perfusion scintigraphy: the evidence. Eur J Nucl Med Mol Imaging 2004;31(2):261-291.

(10) Matsunari I, Schricke U, Bengel FM, Haase HU, Barthel P, Schmidt G, Nekolla SG, Schoemig A, Schwaiger M. Extent of cardiac sympathetic neuronal damage is determined by the area of ischemia in patients with acute coronary syndromes. Circulation 2000;101(22):2579-2585.

(11) Boogers MJ, Borleffs CJW, Henneman MM, Van Bommel RJ, Van Ramshorst J, Boersma E, Dibbets-Schneider P, Stokkel MP, van der Wall EE, Schalij MJ, Bax JJ. Cardiac Sympathetic Denervation Assessed with 123-I MIBG Imaging Predicts Ventricular Arrhythmias in Implantable Cardioverter-Defibrillator Patients. J Am Coll Cardiol 2010;55(24):2769-2777.

(12) McGhie AI, Corbett JR, Akers MS, Kulkarni P, Sills MN, Kremers M, Buja LM, Durant-Reville M, Parkey RW, Willerson JT. Regional cardiac adrenergic function using I-123 meta-iodobenzylguanidine tomographic imaging after acute myocardial infarction. Am J Cardiol 1991;67(4):236-242.

(13) Jacobson AF, Senior R, Cerqueira MD, Wong ND, Thomas GS, Lopez VA, Agostini D, Weiland F, Chandna H, Narula J. Myocardial Iodine-123 Meta-Iodobenzylguanidine Imaging and Cardiac Events in Heart Failure Results of the Prospective ADMIRE-HF (AdreView Myocardial Imaging for Risk Evaluation in Heart Failure) Study. J Am Coll Cardiol 2010;55(20):2212-2221.

(14) Podrid PJ, Fuchs T, Candinas R. Role of the sympathetic nervous system in the genesis of ventricular arrhythmia. Circulation 1990;82(2 Suppl):I103-I113.

(15) Yukinaka M, Nomura M, Ito S, Nakaya Y. Mismatch between myocardial accumulation of 123I-MIBG and 99mTc-MIBI and late ventricular potentials in patients after myocardial infarction: association with the development of ventricular arrhythmias. Am Heart J 1998;136(5):859-867.
(16) Simoes MV, Barthel P, Matsunari I, Nekolla SG, Schomig A, Schwaiger M, Schmidt G, Bengel FM. Presence of sympathetically denervated but viable myocardium and its electrophysiologic correlates after early revascularised, acute myocardial infarction. Eur Heart J 2004;25(7):551-557.
(17) Bax JJ, Kraft O, Buxton AE, Fjeld JG, Parizek P, Agostini D, Knuuti J, Flotats A, Arrighi J, Muxi A, Alibelli MJ, Banerjee G, Jacobsen AF. 123-MIBG scintigraphy to predict inducibility of ventricular arrhythmias on cardiac electrophysiologic testing. A prospective multicenter pilot study. Circ Cardiovasc imaging 2008;(2):131-140.
(18) Haeck ML, Hoogslag GE, Rodrigo SF, Atsma DE, Klautz RJ, van der Wall EE, Schalij MJ, Verwey HF. Treatment options in end-stage heart failure: where to go from here? Neth Heart J 2011.
(19) Lamb HJ, Doornbos J, van der Velde EA, Kruit MC, Reiber JH, de Roos A. Echo planar MRI of the heart on a standard system: validation of measurements of left ventricular function and mass. J Comput Assist Tomogr 1996;20(6):942-949.
(20) van der Geest RJ, Reiber JH. Quantification in cardiac MRI. J Magn Reson Imaging 1999;10(5):602-608.
(21) Hoffmann KR, Dmochowski J, Nazareth DP, Miskolczi L, Nemes B, Gopal A, Wang Z, Rudin S, Bednarek DR. Vessel size measurements in angiograms: manual measurements. Med Phys 2003;30(4):681-688.
(22) Amado LC, Gerber BL, Gupta SN, Rettmann DW, Szarf G, Schock R, Nasir K, Kraitchman DL, Lima JA. Accurate and objective infarct sizing by contrast-enhanced magnetic resonance imaging in a canine myocardial infarction model. J Am Coll Cardiol 2004;44(12):2383-2389.
(23) Cerqueira MD, Weissman NJ, Dilsizian V, Jacobs AK, Kaul S, Laskey WK, Pennell DJ, Rumberger JA, Ryan T, Verani MS. Standardized myocardial segmentation and nomenclature for tomographic imaging of the heart: a statement for healthcare professionals from the Cardiac Imaging Committee of the Council on Clinical Cardiology of the American Heart Association. Circulation 2002;105(4):539-542.
(24) Mahrholdt H, Wagner A, Holly TA, Elliott MD, Bonow RO, Kim RJ, Judd RM. Reproducibility of chronic infarct size measurement by contrast-enhanced magnetic resonance imaging. Circulation 2002;106(18):2322-2327.
(25) Ibrahim T, Nekolla SG, Hornke M, Bulow HP, Dirschinger J, Schomig A, Schwaiger M. Quantitative measurement of infarct size by contrast-enhanced magnetic resonance imaging early after acute myocardial infarction: comparison with single-photon emission tomography using Tc99m-sestamibi. J Am Coll Cardiol 2005;45(4):544-552.

Summary, Conclusions and Future Perspectives

Cardiovascular Disease

Cardiovascular disease remains one of the leading health care issues these days, even though considerable advances in diagnosis, therapeutic options and prognostification of patients with cardiovascular disease have been made in the last couple of decades.[1-3]

Novel insights into cardiac imaging and post-processing techniques can be used to further improve currently applied diagnostic, therapeutic and prognostic algorithms for patients with cardiovascular disease.

The general introduction of the thesis (**chapter 1**) describes novel insights into cardiac imaging for evaluation of patients with cardiovascular disease, predominantly in the setting of coronary artery disease (CAD) and chronic heart failure.

The aim of the thesis was to evaluate the role of novel insights into cardiac imaging for diagnosis (Part I), treatment (Part II) and risk stratification (Part III) of patients with cardiovascular disease.

Part I: Dedicated Automated Quantitative Computed Tomography in Patients with Coronary Artery Disease

Chapter 2 provides an overview of the currently available approaches for cardiac computed tomography (CT) to quantify coronary atherosclerosis. In addition, it reviews the potential value of quantitative cardiac CT to guide percutaneous coronary intervention procedures.

The study described in **chapter 3** was designed to demonstrate the feasibility of a novel dedicated algorithm for automated quantification of stenosis severity on cardiac CT in a direct comparison to quantitative coronary angiography (QCA). In 100 patients (53 men, 59.8±8.0 yrs), cardiac CT and QCA showed good correlations for percentage diameter stenosis on a vessel-basis (n=282, r=0.83, p<0.01) and a patient-basis (n=93, r=0.86, p<0.01). Furthermore, a good agreement was observed between cardiac CT and QCA for semi-quantitative assessment of diameter stenosis (accuracy of 95%). Moreover, quantitative CT showed a significantly higher positive predictive value (100% vs. 78%, p<0.05) and higher diagnostic accuracy (95% vs. 87%, p=0.08) for assessment of ≥50% diameter stenosis when compared to visual analysis. In summary, quantitative CT was well-correlated to QCA for assessment of stenosis severity. Importantly, the study showed an improved diagnostic accuracy and positive predictive value of quantitative CT when compared to visual analysis of CT images.

Chapter 4 describes the feasibility of automated coronary plaque quantification on cardiac CT using dedicated software with a novel 3D coregistration algorithm of CT and intravascular ultrasound (IVUS). A total of 51 patients (40 men, 58±11 yrs, 103 coronary arteries) with 146 lesions were evaluated. Quantitative CT and IVUS showed good correlation for minimal lumen area (MLA) (n=146, r=0.75, p<0.001). Both quantitative techniques were well-correlated for lumen area stenosis (n=146, r=0.79, p<0.001) and plaque burden (n=146, r=0.70, p<0.001) at the level of the MLA. Finally, mean plaque burden (n=146,

r=0.64, p<0.001) and remodeling index (n=146, r=0.56, p<0.001) showed significant correlations between QCT and IVUS. In conclusion, automated quantification of coronary plaque using CT with a dedicated quantitative software and a novel 3D registration algorithm is feasible.

In **chapter 5**, the value of cardiac CT for assessment of diastolic function in comparison with 2D echocardiography using tissue Doppler imaging (TDI) is evaluated. A total of 70 patients (46 men, mean age 55±11 yrs) who had undergone both cardiac CT and 2D echocardiography with TDI were included. Cardiac CT and 2D echocardiography were well-correlated for early transmitral peak velocity (E) (r=0.73, p<0.01), E/A (r=0.87, p<0.01), peak mitral septal tissue velocity (Ea) (r=0.82, p<0.01) and E/Ea (r=0.81, p<0.01). Furthermore, a good agreement was observed between cardiac CT and 2D echocardiography with TDI for assessment of diastolic function (agreement of 79%). Accordingly, cardiac CT can be used to provide information on LV diastolic dysfunction in addition to coronary atherosclerosis.

Part II: Myocardial Perfusion SPECT for Selection of Heart Failure Patients Referred for Cardiac Resynchronization Therapy

The potentials of nuclear imaging with gated myocardial perfusion single photon emission computed tomography (SPECT) (GMPS) in heart failure patients referred for cardiac resynchronization therapy (CRT) are evaluated in **chapter 6**. The review concluded that GMPS with phase analysis allows detailed assessment of myocardial ischemia, infarct tissue and viability along with left ventricular (LV) mechanical dyssynchrony using a single SPECT data set. A comprehensive evaluation of heart failure patients referred for CRT with the use of GMPS and phase analysis can improve the selection of patients who will benefit from CRT.

In **chapter 7**, the QGS algorithm for phase analysis on GMPS is validated in a direct comparison with echocardiography using TDI for assessment of LV systolic dyssynchrony. Additionally, the prediction of response to CRT using GMPS with phase analysis is evaluated in chapter 7. In 40 heart failure patients (32 men, mean age 63±8 yrs), phase analysis on GMPS was significantly correlated with TDI for assessment of LV systolic dyssynchrony (histogram bandwidth (HBW) (r=0.69, p<0.01) and phase standard deviation (SD) (r=0.65, p<0.01). Moreover, phase analysis on GMPS allowed prediction of CRT response, in which the optimal cutoff value for HBW was defined at 72.5°, yielding a sensitivity of 83% and a specificity of 81%. The area under the curve for HBW was 0.83. The optimal cutoff value for phase SD was set at 19.6°, which yielded a sensitivity of 83% and a specificity of 81%. The area under the curve for phase SD was 0.85.

Chapter 8 evaluates the relation between the site of latest mechanical activation on GMPS, LV lead position and response to CRT. A total of 90 heart failure patients (72% men, mean age 67±10 yrs) were included, of which 52 (58%) patients showed a concordant LV lead position and 38 (42%) patients showed a discordant LV lead position. GMPS and 2D speckle tracking radial strain analysis agreed well for assessment of the site of latest

mechanical activation (total agreement of 86%, *k* value=0.79). Furthermore, the study has demonstrated that response to CRT was significantly more often documented in patients with concordant LV lead position as compared to patients with discordant LV lead position (79% vs. 26%, p<0.01). Moreover, patients with concordant LV lead position showed significant improvement in LV volumes and LV systolic function (p<0.05) at 6 months follow-up, whereas patients with discordant LV lead position showed no significant improvement in LV volumes and LV systolic function. In conclusion, GMPS with phase analysis can be used to assess the site of latest mechanical activation. Importantly, a concordant LV lead position was associated with significant improvement in LV volumes and LV systolic function.

The study in **chapter 9** has evaluated the feasibility of phase analysis on GMPS for assessment of LV diastolic dyssynchrony in comparison with TDI. In 150 heart failure patients (114 men, mean age 66.0±10.4 yrs), diastolic HBW (r=0.75, p<0.01) and diastolic phase SD (r=0.81, p<0.01) showed good correlations with LV diastolic dyssynchrony on TDI. In addition, patients with LV diastolic dyssynchrony on TDI (>55 ms) showed significantly larger diastolic phase SD (68.1±13.4˚ vs. 40.7±14.0˚, p<0.01) and diastolic HBW (230.6±54.3˚ vs. 129.0±55.6˚, p<0.01) as compared to patients without LV diastolic dyssynchrony on TDI (≤55 ms). Accordingly, phase analysis on GMPS allows assessment of LV diastolic dyssynchrony.

Finally, **chapter 10** describes whether LV diastolic dyssynchrony on GMPS allows prediction of response to CRT. A total of 50 moderate-to-severe heart failure patients (36 men, mean age 66.5±9.9 yrs) with depressed LV systolic function (LV ejection fraction (LVEF) ≤35%) were included. Thirty-four (68%) patients showed response to CRT, while 16 (32%) patients were non-responders. CRT responders showed a significant improvement in New York Heart Association (NYHA) functional class, quality-of-life score, 6-minute walk distance, LV volumes and LVEF at 6 months follow-up (p<0.05). Multivariate analyses showed that LV diastolic dyssynchrony along with LV systolic dyssynchrony and myocardial scar were independent predictors of CRT response (p<0.05).

Part III: Cardiac Sympathetic Nerve Scintigraphy with 123-I Metaiodobenzylguanidine for Risk Stratification of Patients with Cardiovascular Disease

The role of cardiac sympathetic nerve imaging with 123-iodine metaiodobenzylguanidine (123-I MIBG) scintigraphy for risk stratification of patients with cardiovascular disease is described in **chapter 11**. The review concludes that cardiac innervation imaging with 123-I MIBG holds great potential for risk stratification and prognostification of heart failure patients. Cardiac 123-I MIBG imaging can be used to identify patients with heart failure at risk for (cardiac) death, worsening heart failure as well as ventricular arrhythmias or sudden cardiac death.

The potentials of 123-I MIBG scintigraphy for prediction of ventricular arrhythmias are evaluated in **chapter 12**. In total, 116 heart failure patients (80 men, mean age 65±9 yrs) referred for implantable cardioverter-defibrillator (ICD) therapy were included. During a mean follow-up of 23±15 months, appropriate ICD therapy was documented in 24 (21%) patients and appropriate ICD therapy or cardiac death in 32 (28%) patients. The study showed that late 123-I MIBG SPECT defect score was an independent predictor for appropriate ICD therapy and the combined endpoint of appropriate ICD therapy or cardiac death. More specifically, patients with a large late 123-I MIBG SPECT defect (summed score >26) showed significantly more appropriate ICD therapy (52% vs. 5%, $p<0.01$) and appropriate ICD therapy or cardiac death (57% vs. 10%, $p<0.01$) when compared to patients with a small late 123-I MIBG SPECT defect (summed score ≤26) at 3-year follow-up. Thus, cardiac sympathetic denervation allowed prediction of ventricular arrhythmias causing appropriate ICD therapy.

Chapter 13 describes the relation between contrast-enhanced magnetic resonance imaging (MRI) and 123-I MIBG/perfusion scintigraphy for assessment of myocardial infarct size and infarct border zone, referred to as myocardium at risk for ventricular arrhythmias. In 40 patients with ischemic heart failure (29 men, mean age 66±10 yrs), contrast-enhanced MRI and myocardial perfusion scintigraphy showed good correlations for infarct size ($r=0.72$, $p<0.01$). Moreover, the 123-I MIBG SPECT defect score (48.2±12.5% vs. 32.1±9.5%, $p<0.05$) and innervation/perfusion mismatch score (13.9±11.0% vs. 6.8±6.0%, $p<0.05$), which were used as markers of myocardium at risk for ventricular arrhythmias, were significantly larger in patients with an infarct border zone on contrast-enhanced MRI (≤16.7 grams of infarct border zone) than in patients without an (≤16.7 grams of infarct border zone) infarct border zone on contrast-enhanced MRI. In conclusion, the study has demonstrated that contrast-enhanced MRI and 123-I MIBG/perfusion scintigraphy correlated for assessment of infarct size and infarct border zone, which are commonly referred to as myocardium at risk for ventricular arrhythmias.

Conclusions and Future Perspectives

The purpose of the thesis was to explore the role of novel insights into cardiac imaging for diagnosis (Part I), treatment (Part II) and risk stratification (Part III) of patients with cardiovascular disease. Rapid developments in cardiac imaging techniques have already contributed significantly in the evaluation of patients with a broad spectrum of cardiovascular disease, predominantly in the setting of coronary artery disease and chronic heart failure.[4-7]

New insights in cardiac imaging and post-processing technologies can further refine currently applied diagnostic, therapeutic and prognostic algorithms for patients with cardiovascular disease. Moreover, further developments in cardiac imaging can help to generate a patient-tailored health care system, which in turn should result in an improved cost-effectiveness as patients are more appropriately selected for diagnostic procedures and

therapeutic interventions, such as (percutaneous) coronary intervention procedures and dedicated cardiac device therapies.

At first, the value of automated quantitative CT for evaluation of coronary atherosclerosis has been demonstrated in this thesis. As the feasibility of quantitative CT has been shown in several studies presented in this thesis, new developments in quantitative software should further improve its diagnostic accuracy for quantification of coronary plaque, particularly for coronary lesions with severe calcifications. Additionally, refinements in quantitative algorithms for cardiac CT may help to solve difficulties regarding quantification of in-stent stenosis and bifurcation lesions. Consecutively, the value of quantitative CT to guide coronary intervention procedures as well as to monitor progression of coronary atherosclerosis (e.g. once pharmacologic treatment has been started) can be prospectively validated in future studies. Moreover, further improvements in quantitative CT algorithms should reduce the amount of post-processing time required for evaluation of CAD.

Secondly, the thesis has shown that GMPS with phase analysis provides important information in heart failure patients referred for CRT. GMPS with phase analysis allows integrated assessment of myocardial infarction, viability and ischemia along with LV mechanical dyssynchrony and site of latest mechanical activation, which altogether play an important role in response to CRT. Accordingly, phase analysis on GMPS provides information that can be used to improve the currently applied algorithm for selection of patients who will benefit from CRT. As the value of GMPS with phase analysis has been demonstrated in patients referred for CRT, additional studies are needed that prospectively validate selection algorithms including GMPS with phase analysis for identification of responders to CRT. Ultimately, one should demonstrate the improved cost-effectiveness of these comprehensive algorithms for selection of heart failure patients for CRT.

Finally, the thesis has demonstrated that cardiac 123-I MIBG scintigraphy can be used for selection of patients prone for ventricular arrhythmias or sudden cardiac death. Although the benefits of cardiac 123-I MIBG scintigraphy have been demonstrated in patients at risk for ventricular arrhythmias, the incremental value of cardiac 123-I MIBG scintigraphy in relation to other non-invasive risk markers for ventricular arrhythmias or sudden cardiac death should be addressed more thoroughly in future studies. Implementation of cardiac 123-I MIBG scintigraphy in currently applied risk models for ventricular arrhythmias would provide important information on the incremental value of 123-I MIBG imaging over already existing risk markers for ventricular arrhythmias or sudden cardiac death. In addition, the role of cardiac 123-I MIBG scintigraphy for prediction of clinical outcome in patients with unstable clinical conditions, such as acute coronary syndromes, needs to be further elucidated. Currently, cardiac 123-I MIBG imaging has only been used in patients with prior myocardial infarction or acute coronary syndrome for assessment of sympathetic denervation patterns.[8-10] In this subset of patients, regions with deprived sympathetic innervation may be present which reach beyond the peripheral border of myocardial necrosis,

indicating the presence of viable but denervation myocardium.[8-10] Accordingly, beyond the setting of chronic heart failure, cardiac 123-I MIBG scintigraphy may provide incremental information to risk stratify patients with ischemic heart disease.

Samenvatting, Conclusies en Toekomstperspectief

Hart- en vaatziekten zijn één van de belangrijkste problemen voor de volksgezondheid, ondanks vele ontwikkelingen die in de afgelopen decennia hebben plaatsgevonden op het gebied van diagnostiek, therapie en risicostratificatie van patiënten met hart- en vaatziekten.[1-3]

Nieuwe ontwikkelingen op het gebied van cardiale beeldvorming en post-processing kunnen gebruikt worden om de huidige diagnostische, therapeutische en prognostische algoritmen voor patiënten met hart- en vaatziekten te verbeteren.

De algemene inleiding van het proefschrift (**hoofdstuk 1**) beschrijft nieuwe inzichten in cardiale beeldvormingstechnieken die kunnen worden toegepast voor de evaluatie van patiënten met hart- en vaatziekten, in het bijzonder voor patiënten met coronairlijden (aderverkalking van de kransslagaderen) en chronisch hartfalen.

De doelstelling van dit proefschrift was om nieuwe ontwikkelingen op het gebied van cardiale beeldvorming voor diagnostiek (Deel I), therapie (Deel II) en risicostratificatie (Deel III) van patiënten met hart- en vaatziekten te evalueren.

Deel I: Automatische Computed Tomografie in Patiënten met Coronairlijden

Hoofdstuk 2 beschrijft een overzicht van de huidige methoden voor het kwantificeren van coronairlijden met cardiale computed tomografie (CT). Voorts beschrijft hoofdstuk 2 de rol die kwantitatieve CT kan spelen bij percutane coronaire interventies.

De studie beschreven in **hoofdstuk 3** is destijds opgezet om de toepasbaarheid te demonstreren van een specifiek algoritme voor automatische kwantificatie van coronairstenose op cardiale CT in een directe vergelijking met kwantitatieve coronair angiografie (quantitative coronary angiography, QCA). In 100 patiënten (53 mannen 59.8±8.0 jaar), lieten cardiale CT en QCA een goede correlatie zien voor percentage diameter stenose bij analyse naar de culprit lesie per coronair (n=282, r=0.83, p<0.01) of per patiënt (n=93, r=0.86, p<0.01). Tevens, werd er een goede *agreement* gevonden tussen cardiale CT en QCA voor semikwantitatieve analyse naar diameter stenose (diagnostische nauwkeurigheid van 95%). Bovendien liet kwantitatieve CT een significante hogere positief voorspellende waarde (100% vs. 78%, p<0.05) en diagnostische nauwkeurigheid (95% vs. 87%, p=0.08) zien voor ≥50% diameter stenose in vergelijking met visuele CT analyse. Samenvattend, kwantitatieve CT liet een goede correlatie zien met QCA voor het evalueren van coronairstenose. In aanvulling, liet de studie een verbetering zien in de diagnostische nauwkeurigheid en positief voorspellende waarde van kwantitatieve CT ten opzichte van visuele CT.

In **hoofdstuk 4** wordt de uitvoerbaarheid van automatische kwantificatie van coronairlijden met behulp van cardiale CT en speciale software met een nieuw 3D coregistratie CT algoritme voor CT en *intravascular ultrasound (IVUS)* beschreven. Een cohort van 51 patiënten (40 mannen, 58±11 jaar, 103 coronairen) met 146 coronair lesies werd geëvalueerd. Kwantitatieve CT en IVUS lieten een goede correlatie zien voor *minimal lumen*

area (MLA) (n=146, r=0.75, p<0.001). Beide kwantitatieve technieken lieten eveneens een goede correlatie zien voor *lumen area stenose* (n=146, r=0.79, p<0.001) en *plaque burden* (n=146, r=0.70, p<0.001) op het niveau van de MLA. Tenslotte, de *mean plaque burden* (n=146, r=0.64, p<0.001) en *remodeling index* (n=146, r=0.56, p<0.001) lieten significante correlaties zien tussen kwantitatieve CT en IVUS. Samenvattend liet de studie zien dat automatische kwantificatie van coronairlijden op cardiale CT mogelijk is met behulp van nieuwe kwantificatie software met een 3D registratie algoritme.

De waarde van cardiale CT voor het bepalen van de diastolische hartfunctie in vergelijking met 2D echocardiografie met *tissue Doppler imaging (TDI)* werd in **hoofdstuk 5** geëvalueerd. Een cohort van 70 patiënten (46 mannen, 55±11 jaar), welke cardiale CT en 2D echocardiografie met TDI hadden ondergaan, werd geïncludeerd. Cardiale CT en 2D echocardiografie lieten een goede correlatie zien voor *early transmitral peak velocity* (E) (r=0.73, p<0.01), E/A (r=0.87, p<0.01), *peak mitral septum velocity* (Ea) (r=0.82, p<0.01) en E/Ea (r=0.81, p<0.01). In aanvulling lieten beide technieken een goede *agreement* zien voor het vaststellen van diastolische disfunctie (*agreement* van 79%). Op basis van deze onderzoeksresultaten werd geconcludeerd dat cardiale CT kan worden gebruikt voor de evaluatie van diastolische hartfunctie.

Deel II: Myocard Perfusie Scintigrafie voor de Selectie van Hartfalen Patiënten Verwezen voor Cardiale Resynchronizatie Therapie

The rol van nucleaire beeldvorming met gated myocard perfusie scintigrafie (*myocardial perfusion single photon emission computed tomography (SPECT)*, *GMPS*) in patiënten met hartfalen, die verwezen werden voor cardiale resynchronizatie therapie (CRT) is geëvalueerd in **hoofdstuk 6**. De review concludeerde dat GMPS met fase analyse gebruikt kan worden voor het evalueren van cardiale ischemie, infarcering, viabiliteit van het myocard alsmede linker kamer (LV) mechanische dyssynchronie. Tenslotte kan een complete en uitgebreide evaluatie van patiënten met hartfalen met GMPS en fase analyse de selectie van patiënten voor CRT verbeteren.

In **hoofdstuk 7** werd het QGS algoritme voor fase analyse van GMPS gevalideerd voor LV mechanische dyssynchronie in een directe vergelijking met echocardiografie met TDI. In hoofdstuk 7 werd eveneens onderzocht of GMPS met fase analyse kon worden gebruikt om response op CRT te voorspellen. In 40 patiënten met hartfalen (32 mannen, 63±8 jaar), liet GMPS met fase analyse significante correlaties zien met TDI voor LV systolische dyssynchronie (histogram bandbreedte (HBW) (r=0.69, p<0.01) en fase standaard deviatie (SD) (r=0.65, p<0.01). Bovendien liet de studie zien dat GMPS met fase analyse kan worden gebruikt om CRT response te voorspellen, waarbij de optimale *cutoff* waarde voor HBW 72.5° was met een sensitiviteit van 83% en een specificiteit van 81%. De *area under the curve* (AUC) voor HBW was 0.83. De optimale *cutoff* waarde voor fase SD was 19.6° met een sensitiviteit van 83% en een specificiteit van 81%. De AUC voor fase SD was 0.85.

In **Hoofdstuk 8** wordt de relatie tussen het myocard met laatste mechanische activatie (met behulp van GMPS met fase analyse), LV lead positie en response op CRT geëvalueerd. Een groep van 90 patiënten met hartfalen (72% mannen, 67±10 jaar) werd geïncludeerd. Van deze groep patiënten waren er 52 (58%) met een concordante *LV lead positie* en 38 (42%) met een discordante *LV lead* positie. GMPS en *2D speckle tracking radial strain* analyse lieten een goede *agreement* zien voor het bepalen van het myocard met laatste mechanische activatie (*agreement* van 86%, *k*=0.79). Daarnaast liet de studie zien dat response op CRT significant vaker werd geobserveerd in patiënten met een concordante *LV lead* positie in vergelijking met patiënten met een discordante *LV lead* positie (79% vs. 26%, p<0.01). Bovendien lieten patiënten met een concordante *LV lead* positie significante verbeteringen zien in LV volumina en LV systolische functie (p<0.05) na 6 maanden follow-up, terwijl patiënten met een discordante *LV lead* positie geen significante verbetering lieten zien in LV volumina en LV systolische functie. Concluderend liet deze studie zien dat GMPS met fase analyse kan worden gebruikt om het laatste geactiveerde myocard vast te stellen. Dit is belangrijk aangezien een concordante *LV lead* positie geassocieerd was met significante *reverse remodeling* evenals een verbetering van de LV systolische functie.

De studie in **hoofdstuk 9** onderzocht de toepasbaarheid van GMPS met fase analyse voor het evalueren van LV diastolische dyssynchronie in vergelijking met TDI. In 150 patiënten met hartfalen (114 mannen, 66.0±10.4 jaar), lieten diastolisch HBW (r=0.75, p<0.01) en diastolisch fase SD (r=0.81, p<0.01) goede correlaties zien met LV diastolische dyssynchronie op TDI. Tevens lieten patiënten met LV diastolische dyssynchronie op TDI (>55 ms) significant grotere diastolische fase SD (68.1±13.4˚ vs. 40.7±14.0˚, p<0.01) en HBW (230.6±54.3˚ vs. 129.0±55.6˚, p<0.01) zien in vergelijking met patiënten zonder LV diastolische dyssynchronie op TDI (≤55 ms). Deze studie liet zien dat fase analyse op GMPS gebruikt kan worden voor het evalueren van LV diastolische dyssynchronie.

In **hoofdstuk 10** wordt de voorspellende waarde van LV diastolisch dyssynchronie op GMPS voor response op CRT beschreven. Vijftig patiënten met matig tot ernstig hartfalen (36 mannen, 66.5±9.9 jaar) met verminderde LV systolische functie (LV ejectie fractie (LVEF) ≤35%) werden geïncludeerd. In totaal lieten 34 (68%) patiënten response op CRT (responders) zien, terwijl 16 (32%) patiënten geen response lieten zien op CRT (non-responders). Response werd gedefinieerd als ≥15% reductie in LV eind-systolisch volume na 6 maanden follow-up. CRT responders lieten een significante verbetering zien in *New York Heart Association (NYHA)* functionele klasse, kwaliteit van leven, 6-minuten looptest, LV volumina en LVEF na 6 maanden follow-up (p<0.05). Multivariate analyse liet zien dat LV diastolische dyssynchronie, LV systolische dyssynchronie en myocard infarct onafhankelijke voorspellers waren voor response op CRT (p<0.05).

Deel III: Cardiale Sympathische Scintigrafie met 123-I Metaiodobenzylguanidine voor Risicostratificatie van Patiënten met Hart- en Vaatziekten

De rol van cardiale sympathische beeldvorming met 123-iodine metaiodobenzylguanidine (123-I MIBG) scintigrafie voor risicostratificatie van patiënten met hart- en vaatziekten is beschreven in **hoofdstuk 11.** De review concludeert dat cardiale innervatie beeldvorming met 123-I MIBG kan worden gebruikt voor risicostratificatie van patiënten met hartfalen. Cardiale 123-I MIBG scintigrafie kan worden gebruikt voor het identificeren van patiënten met hartfalen die een verhoogd risico hebben op (cardiale) dood, progressief hartfalen en ventriculaire aritmiëen of plotse hartdood.

De rol van cardiale 123-I MIBG scintigrafie in het voorspellen van ventriculaire aritmieen wordt geëvalueerd in **hoofdstuk 12**. Er werden 116 hartfalen patiënten (80 mannen, 65±9 jaar), die werden verwezen voor *implantable cardioverter-defibrillator* (ICD) therapie geëvalueerd. Tijdens een gemiddelde follow-up duur van 23±15 maanden, werd terechte ICD therapie in 24 (21%) patiënten geobjectiveerd en terechte ICD therapie of cardiale dood in 32 (28%) patiënten. De studie liet zien dat *123-I MIBG SPECT defect score* op late 123-I MIBG scintigrafie een onafhankelijke voorspeller was voor het optreden van terechte ICD therapie evenals het gecombineerde eindpunt terechte ICD therapie of cardiale dood. In het bijzonder lieten patiënten met een groot *123-I MIBG SPECT defect (summed score van >26)* significant vaker terechte ICD therapie (52% vs. 5%, p<0.01) en terechte ICD therapie of cardiale dood (57% vs. 10%, p<0.01) zien, dan patiënten met een klein *123-I MIBG SPECT defect (summed score ≤26)* op 3-jaar follow-up. Samenvattend liet de studie zien dat cardiale sympathische denervatie belangrijke informatie geeft voor het voorspellen van ventriculaire aritmiëen resulterend in ICD therapie.

Hoofdstuk 13 evalueert de relatie tussen *contrast-enhanced magnetic resonance imaging* (MRI) and 123-I MIBG/perfusie scintigrafie in het kwantificeren van infarct grootte en *infarct border zone*, gebruikt als surrogaat voor myocard met een verhoogd risico op het ontstaan van ventriculaire aritmiëen. In 40 patiënten met hartfalen (29 mannen, 66±10 jaar), lieten *contrast-enhanced* MRI en myocard perfusie scintigrafie, een goede relatie zien voor infarct grootte (r=0.72, p<0.01). Bovendien, liet de studie zien dat de *123-I MIBG SPECT defect score* (48.2±12.5% vs. 32.1±9.5%, p<0.05) en de *innervatie/perfusie mismatch score* (13.9.±11.0% vs. 6.8±6.0%), markers voor myocard met een verhoogd risico op ventriculaire aritmiëen, significant groter waren in patiënten met een *infarct border zone* op *contrast-enhanced* MRI in vergelijking met patiënten zonder *infarct border zone* op *contrast-enhanced* MRI. Concluderend, liet de studie zien dat 123-I MIBG/perfusie scintigrafie kon worden gebruikt voor het evalueren van infarct grootte en *infarct border zone*.

Conclusies en Toekomstperspectief

Het doel van dit proefschrift was om nieuwe ontwikkelingen op het gebied van cardiale beeldvorming te evalueren voor diagnostiek (Deel I), therapie (Deel II) en risicostratificatie (Deel III) van patiënten met hart- en vaatziekten. Nieuwe ontwikkelingen in cardiale beeldvormingstechnieken hebben tot op heden significant bijgedragen aan de evaluatie van patiënten met hart- en vaatziekten, in het bijzonder in patiënten met coronairlijden en chronisch hartfalen.[4-7]

Nieuwe inzichten in cardiale beeldvorming en *post-processing* technologie kunnen de huidige diagnostische, therapeutische en prognostische algoritmen voor patiënten met hart- en vaatziekten verder verbeteren. Voortschrijdend inzicht in cardiale beeldvorming kan bovendien worden gebruikt om de kosten-effectiviteit van de huidige gezondheidszorg verder te optimaliseren door patiënten beter te selecteren voor diagnostische en therapeutische interventies, zoals (percutane) coronaire interventies of cardiale pacemaker of ICD therapie.

Ten eerste werd in dit proefschrift de waarde van automatische kwantitatieve CT voor de evaluatie van coronairlijden beschreven. Aangezien de beschreven studies de toepasbaarheid van kwantitatieve CT voor het evalueren van coronairlijden hebben laten zien, kunnen toekomstige studies zich gaan richten op het verbeteren van de nauwkeurigheid van kwantitatieve CT in het evalueren van ernstige verkalkte coronair lesies alsmede de in-stent stenoses of bifurcatie lesies. Door verbeterde kwantitatieve CT, kan cardiale CT mogelijkerwijs een grotere rol gaan spelen bij het voorbereiden van percutane coronaire interventies alsmede in het monitoren van progressie van coronairlijden (bijvoorbeeld na starten medicamenteuze therapie). Bovendien kunnen ontwikkelingen in kwantitatieve CT algoritmen mogelijkerwijs de tijd, welke nodig is voor de post-processing van cardiale CT, verkorten.

Ten tweede laten de studies in dit proefschrift zien dat GMPS met fase analyse kan worden gebruikt ter analyse van patienten met hartfalen die verwezen worden voor CRT. GMPS met fase analyse biedt de mogelijkheid om (1) myocard infarct, (2) viabiliteit van het myocard, (3) ischemie, (4) LV mechanische dyssynchronie en (5) myocard met de laatste mechanische activatie te evalueren in een enkel SPECT onderzoek. Met behulp van deze informatie kan een goede inschatting worden gemaakt welke patienten respons op CRT laten zien en kan derhalve de selectie van patiënten voor CRT worden geoptimaliseerd.

Alhoewel de waarde van GMPS met fase analyse in patiënten met hartfalen verwezen voor CRT is beschreven in diverse studies, zijn additionele onderzoeken geïndiceerd die de selectie algoritmen met GMPS en fase analyse prospectief gaan valideren. Vervolgens moeten studies de kosten-effectiviteit van dergelijke selectie algoritmen voor hartfalen patiënten gaan aantonen.

Tenslotte laat dit proefschrift zien dat cardiale 123-I MIBG scintigrafie kan worden gebruikt voor de selectie van patiënten met een verhoogd risico op ventriculaire aritmiëen of plotse hartdood. Ondanks het feit dat de prognostische waarde van cardiale 123-I MIBG

scintigrafie voor het optreden van ventriculaire aritmiëen of plotse hartdood is aangetoond, is de waarde van 123-I MIBG scintigrafie in relatie tot andere niet-invasieve risicomarkers voor plotse hartdood onvoldoende onderzocht. Daarnaast zijn er additionele studies nodig die de prognostische waarde van cardiale 123-I MIBG scintigrafie in patiënten met instabiele klinische condities (acuut coronair syndroom) gaan evalueren. Tot op heden is cardiale 123-I MIBG scintigrafie enkel gebruikt voor het evalueren van sympathische denervatie patronen in patiënten met status na myocardinfarct of acuut coronair syndroom.[8-10] De prognostische waarde van 123-I MIBG scintigrafie in patienten met acuut coronair syndroom is onvoldoende onderzocht. In deze patiënten, kunnen gebieden met sympathische denervatie zich uitstrekken tot voorbij het geïnfarceerde myocard (de *innervatie/perfusie mismatch* of *infarct border zone*).[8-10] Dientengevolge, kan cardiale 123-I MIBG scintigrafie additionele informatie geven voor risicostratificatie in patiënten met ischemische hartziekten.

Reference List

(1) Yusuf S, Reddy S, Ounpuu S, Anand S. Global burden of cardiovascular diseases: part I: general considerations, the epidemiologic transition, risk factors, and impact of urbanization. Circulation 2001;104(22):2746-2753.

(2) Sanz J, Fayad ZA. Imaging of atherosclerotic cardiovascular disease. Nature 2008;451(7181):953-957.

(3) World Health Organization. Report on global burden of disease. 2008.

(4) Mark DB, Berman DS, Budoff MJ, Carr JJ, Gerber TC, Hecht HS, Hlatky MA, Hodgson JM, Lauer MS, Miller JM, Morin RL, Mukherjee D, Poon M, Rubin GD, Schwartz RS. ACCF/ACR/AHA/NASCI/SAIP/SCAI/SCCT 2010 expert consensus document on coronary computed tomographic angiography: a report of the American College of Cardiology Foundation Task Force on Expert Consensus Documents. Circulation 2010;121(22):2509-2543.

(5) Achenbach S, Raggi P. Imaging of coronary atherosclerosis by computed tomography. Eur Heart J 2010;31(12):1442-1448.

(6) Hendel RC, Berman DS, Di Carli MF, Heidenreich PA, Henkin RE, Pellikka PA, Pohost GM, Williams KA. ACCF/ASNC/ACR/AHA/ASE/SCCT/SCMR/SNM 2009 appropriate use criteria for cardiac radionuclide imaging: a report of the American College of Cardiology Foundation Appropriate Use Criteria Task Force, the American Society of Nuclear Cardiology, the American College of Radiology, the American Heart Association, the American Society of Echocardiography, the Society of Cardiovascular Computed Tomography, the Society for Cardiovascular Magnetic Resonance, and the Society of Nuclear Medicine. Circulation 2009;119(22):e561-e587.

(7) Willerson JT. Imaging in electrical cardiac devices. J Am Coll Cardiol 2011;57(7):829-830.

(8) Bengel FM, Barthel P, Matsunari I, Schmidt G, Schwaiger M. Kinetics of 123I-MIBG after acute myocardial infarction and reperfusion therapy. J Nucl Med 1999;40(6):904-910.

(9) Matsunari I, Schricke U, Bengel FM, Haase HU, Barthel P, Schmidt G, Nekolla SG, Schoemig A, Schwaiger M. Extent of cardiac sympathetic neuronal damage is determined by the area of ischemia in patients with acute coronary syndromes. Circulation 2000;101(22):2579-2585.

(10) Simoes MV, Barthel P, Matsunari I, Nekolla SG, Schomig A, Schwaiger M, Schmidt G, Bengel FM. Presence of sympathetically denervated but viable myocardium and its electrophysiologic correlates after early revascularised, acute myocardial infarction. Eur Heart J 2004;25(7):551-557.

List of publications

1. Automated quantification of coronary plaque with computed tomography: comparison with intravascular ultrasound using a dedicated registration algorithm for fusion-based quantification.
   Boogers MJ, Broersen A, van Velzen JE, de Graaf FR, El-Naggar HM, Kitslaar PH, Dijkstra J, Delgado V, Boersma E, de Roos A, Schuijf JD, Schalij MJ, Reiber JH, Bax JJ, Jukema JW.
   Eur Heart J. 2012;33:1007-16.

2. Left ventricular diastolic dyssynchrony assessed with phase analysis of gated myocardial perfusion SPECT: a comparison with tissue Doppler imaging.
   Boogers MJ, Chen J, Veltman CE, van Bommel RJ, Mooyaart EA, Al Younis I, van der Hiel B, Dibbets-Schneider P, van der Wall EE, Schalij MJ, Garcia EV, Bax JJ, Delgado V.
   Am J Cardiol. 2011;108:968-72.

3. Prognostic Value of Renal Dysfunction for the Prediction of Outcome Versus Results of Computed Tomographic Coronary Angiography.
   Yiu KH, de Graaf FR, Schuijf JD, van Werkhoven JM, van Velzen JE, Boogers MJ, Roos CJ, de Bie MK, Pazhenkottil A, Kroft LJ, Boersma E, Herzog B, de Roos A, Kaufmann PA, Bax JJ, Jukema JW.
   Am J Cardiol. 2011;108:968-72.

4. Automatic centerline extraction of coronary arteries in coronary computed tomographic angiography.
   Yang G, Kitslaar P, Frenay M, Broersen A, Boogers MJ, Bax JJ, Reiber JH, Dijkstra J.
   Int J Cardiovasc Imaging. 2011.

5. Positive remodeling on coronary computed tomography as a marker for plaque vulnerability on virtual histology intravascular ultrasound.
   Kröner ES, van Velzen JE, Boogers MJ, Siebelink HM, Schalij MJ, Kroft LJ, de Roos A, van der Wall EE, Jukema JW, Reiber JH, Schuijf JD, Bax JJ.
   Am J Cardiol. 2011;107(12):1725-9.

6. Feasibility of diastolic function assessment with cardiac CT: feasibility study in comparison with tissue Doppler imaging.
   Boogers MJ, van Werkhoven JM, Schuijf JD, Delgado V, El-Naggar HM, Boersma E, Nucifora G, van der Geest RJ, Paelinck BP, Kroft LJ, Reiber JH, de Roos A, Bax JJ, Lamb HJ.
   JACC Cardiovasc Imaging. 2011;4(3):246-56.

7. Multimodality imaging in diabetic heart disease.
Ng AC, Delgado V, Djaberi R, Schuijf JD, Boogers MJ, Auger D, Bertini M, de Roos A, van der Meer RW, Lamb HJ, Bax JJ.
Curr Probl Cardiol. 2011;36(1):9-47.

8. Subclinical left ventricular dysfunction and coronary atherosclerosis in asymptomatic patients with type 2 diabetes.
Scholte AJ, Nucifora G, Delgado V, Djaberi R, Boogers MJ, Schuijf JD, Kharagjitsingh AV, Jukema JW, van der Wall EE, Kroft LJ, de Roos A, Bax JJ.
Eur J Echocardiogr. 2011;12(2):148-55.

9. Can cardiac [123I]m-iodobenzylguanidine imaging be used for risk stratification of patients with acute myocardial infarction?
Boogers MJ, Bax JJ.
Heart. 2011;97(1):1-3.

10. Impact of clinical presentation and pretest likelihood on the relation between calcium score and computed tomographic coronary angiography.
van Werkhoven JM, de Boer SM, Schuijf JD, Cademartiri F, Maffei E, Jukema JW, Boogers MJ, Kroft LJ, de Roos A, Bax JJ.
Am J Cardiol. 2010;106(12):1675-9.

11. Diagnostic performance of non-invasive multidetector computed tomography coronary angiography to detect coronary artery disease using different endpoints: detection of significant stenosis vs. detection of atherosclerosis.
van Velzen JE, Schuijf JD, de Graaf FR, Boersma E, Pundziute G, Spanó F, Boogers MJ, Schalij MJ, Kroft LJ, de Roos A, Jukema JW, van der Wall EE, Bax JJ.
Eur Heart J. 2011;32(5):637-45.

12. Optimal left ventricular lead position assessed with phase analysis on gated myocardial perfusion SPECT.
Boogers MJ, Chen J, van Bommel RJ, Borleffs CJ, Dibbets-Schneider P, van der Hiel B, Al Younis I, Schalij MJ, van der Wall EE, Garcia EV, Bax JJ.
Eur J Nucl Med Mol Imaging. 2011;38(2):230-8.

13. The role of nuclear imaging in the failing heart: myocardial blood flow, sympathetic innervation, and future applications.
Boogers MJ, Fukushima K, Bengel FM, Bax JJ.
Heart Fail Rev. 2011;16(4):411-23.

14. Incremental prognostic value of left ventricular function analysis over non-invasive coronary angiography with multidetector computed tomography.
de Graaf FR, van Werkhoven JM, van Velzen JE, Antoni ML, Boogers MJ, Kroft LJ, de Roos A, Schalij MJ, Jukema JW, van der Wall EE, Schuijf JD, Bax JJ.
J Nucl Cardiol. 2010;17(6):1034-40.

15. Automated quantification of stenosis severity on 64-slice CT: a comparison with quantitative coronary angiography.
Boogers MJ, Schuijf JD, Kitslaar PH, van Werkhoven JM, de Graaf FR, Boersma E, van Velzen JE, Dijkstra J, Adame IM, Kroft LJ, de Roos A, Schreur JH, Heijenbrok MW, Jukema JW, Reiber JH, Bax JJ.
Cardiovasc Ther. 2011;29(6):43-53.

16. Coronary Artery Calcium Scoring in Cardiovascular Risk Assessment.
Nucifora G, Bax JJ, van Werkhoven JM, Boogers MJ, Schuijf JD.
Cardiovasc Ther. 2011;29(6):43-53.

17. Quantification of stenosis severity on multidetector row computed tomography.
Boogers MJ, Schuijf JD.
EuroIntervention. 2010;6 Suppl G:G57-64.

18. Cardiac sympathetic denervation assessed with 123-iodine metaiodobenzylguanidine imaging predicts ventricular arrhythmias in implantable cardioverter-defibrillator patients.
Boogers MJ, Borleffs CJ, Henneman MM, van Bommel RJ, van Ramshorst J, Boersma E, Dibbets-Schneider P, Stokkel MP, van der Wall EE, Schalij MJ, Bax JJ.
J Am Coll Cardiol. 2010;55(24):2769-77.

19. The use of nuclear imaging for cardiac resynchronization therapy.
Chen J, Boogers MJ, Bax JJ, Soman P, Garcia EV.
Curr Cardiol Rep. 2010;12(2):185-91.

20. Diagnostic accuracy of 320-row multidetector computed tomography coronary angiography to noninvasively assess in-stent restenosis.
de Graaf FR, Schuijf JD, van Velzen JE, Boogers MJ, Kroft LJ, de Roos A, Reiber JH, Sieders A, Spanó F, Jukema JW, Schalij MJ, van der Wall EE, Bax JJ.
Invest Radiol. 2010;45(6):331-40.

21. Increased accuracy in computed tomography coronary angiography; a new body surface area adapted protocol.
van der Wall EE, van Velzen JE, de Graaf FR, Boogers MM, Schuijf JD, Bax JJ.
Int J Cardiovasc Imaging. 2010;26(5):601-4.

22. Should mechanical dyssynchrony be assessed in patients with implantable cardioverter-defibrillators?
Boogers MJ, Schalij MJ, Bax JJ.
J Nucl Cardiol. 2010;17(3):354-8.

23. Diagnostic accuracy of 64-slice multislice computed tomographic coronary angiography in patients with an intermediate pretest likelihood for coronary artery disease.
van Werkhoven JM, Heijenbrok MW, Schuijf JD, Jukema JW, Boogers MM, van der Wall EE, Schreur JH, Bax JJ.
Am J Cardiol. 2010;105(3):302-5.

24. Quantitative gated SPECT-derived phase analysis on gated myocardial perfusion SPECT detects left ventricular dyssynchrony and predicts response to cardiac resynchronization therapy.
Boogers MM, Van Kriekinge SD, Henneman MM, Ypenburg C, Van Bommel RJ, Boersma E, Dibbets-Schneider P, Stokkel MP, Schalij MJ, Berman DS, Germano G, Bax JJ.
J Nucl Med. 2009;50(5):718-25.

25. Nuclear imaging in heart failure.
Bax JJ, Boogers MM, Schuijf JD.
Cardiol Clin. 2009;27(2):265-76.

26. Role of nuclear imaging in cardiac resynchronization therapy.
Boogers MM, Chen J, Bax JJ.
Expert Rev Cardiovasc Ther. 2009;7(1):65-72.

27. Is nuclear imaging a viable alternative technique to assess dyssynchrony?
Chen J, Bax JJ, Henneman MM, Boogers MJ, Garcia EV.
Europace. 2008;10 Suppl 3:101-5.

28. Myocardial perfusion single photon emission computed tomography for the assessment of mechanical dyssynchrony.
Boogers MM, Chen J, Bax JJ.
Curr Opin Cardiol. 2008;23(5):431-9.

29. Measuring left ventricular mechanical dyssynchrony from ECG-gated SPECT myocardial perfusion imaging.
Chen J, Garcia EV, Henneman MM, Bax JJ, Boogers MJ, Trimble MA, Borges-Neto S, Velazquez EJ, Iskandrian AE.
Minerva Cardioangiol. 2008;56(2):227-35.

30. Can cardiac iodine-123 metaiodobenzylguanidine imaging contribute to risk stratification in heart failure patients?
Bax JJ, Boogers M, Henneman MM.
Eur J Nucl Med Mol Imaging. 2008;35(3):532-4.

Acknowledgements

Dit proefschrift is gebaseerd op studies die zijn uitgevoerd op de afdelingen cardiologie, radiologie en nucleaire geneeskunde van het Leids Universitair Medisch Centrum.

Ik zou graag mijn dank willen uitspreken aan degenen die direct of indirect betrokken zijn geweest bij de totstandkoming van mijn proefschrift.

In het bijzonder wil ik mijn dank uitspreken aan:
Degenen die hebben meegeholpen aan de selectie van onderzoekspatiënten en aan degenen die beeldvormend onderzoek in deze patiëntpopulaties hebben verricht.

De laboranten, clinici en technici van de afdelingen cardiologie, radiologie en nucleaire geneeskunde! In het bijzonder: Petra, dank voor je steun in (soms) turbulente onderzoeksperioden en Bea, dank voor het verstrekken van de 'CRT patiëntenlijsten', waarmee ik mijn inclusie rate op peil kon houden.

Het stafsecretariaat cardiologie: (Talitha, Cora, Monique en Marina) voor de secretariële ondersteuning tijdens mijn promotieonderzoek.

Mijn 'tuincollega's: Joanne, Sjoerd, Laurens, Maaike, Ivo, Gabya, Roxane, Hadrian, Dennis, Jan, Rutger, Roderick, Jael, Ellen, Stijntje, Jaap, Fleur, Joëlla, Carine, Sum-Che, Louisa, Mihály, Hans, Cees, Joep, Noor, Sander, Eline, Jeffrey, Georgette. We zagen elkaar niet alleen in de 'tuin', maar ook tijdens '070- en 071' borrels! Dank voor de gezelligheid en mooie herinneringen!

Joanne: wat ben ik je ongelofelijk dankbaar voor alle tijd en energie die je in mijn promotieonderzoek hebt gestoken. Wellicht komen we elkaar nog eens tegen op wetenschappelijke podia. Succes met je huidige carrière!
Caroline: voor het voortzetten van het onderzoek op de nucleaire afdeling.
Victoria en Nina: for your ongoing support during my thesis.

Het CT-team: Jaap, Joëlla, Fleur, Cees, Noor, Caroline, Robert, Michiel en Agnieska en Prof. dr. J.W. Jukema voor de leerzame CT-sessies!

Het LKEB: Hans, Jouke, Pieter, Alexander, Michel en Gyanyu, voor de prettige samenwerking. Daarnaast prof. dr. E. Boersma voor de geboden statistische hulp.

Mijn huidige collega's in het Bronovo ziekenhuis: voor de flexibiliteit en steun bij het afronden van mijn proefschrift. We hebben een leuke assistentengroep! Mede gezien de goede supervisie in het Bronovo ziekenhuis heb ik de juiste balans kunnen vinden tussen kliniek, het promotieonderzoek en mijn sociale leven.

Gevat: Bob, Died, Muis, Spoel, Onno, LJ, Ex-Ray, Lucas, IJs, Wouter, Mud,
Daan, Jan-Maarten en GP: we hebben 10 mooie jaren achter de rug! Ik denk terug aan vele mooie herinneringen.

Bob en Died, dank dat jullie mijn paranimfen willen zijn! And last but not least: wellicht hebben we in 2012 wel drie doctoren in onze groep, chapot heren!

Lieve pap en mam, lieve ouders, jullie hebben me altijd gestimuleerd, zodat ik het beste in mezelf naar boven kon halen. Jullie hebben me eveneens de mogelijkheid gegeven om te gaan studeren in Leiden en daar mijn proefschrift te verwezenlijken. Dank voor het begrip dat jullie hebben getoond voor het soms drukke bestaan van een promovendus. Ik hoop nu wat meer tijd te krijgen om samen leuke dingen te doen.
Linda, lieve zus, ik wil je bedanken voor je steun tijdens mijn promotieonderzoek!

Lieve Antoine en Willemien, lieve schoonouders, wat een geluk dat jullie in mijn leven zijn gekomen! Antoine, onze 'brainstormsessies' tijdens de Zeeuwse avondwandelingen zal ik nooit vergeten! Het is voor mij erg inspirerend om jouw levensvisie en filosofie te mogen ervaren. Willemien, wat een positivisme en levensenergie straal je uit! Ik denk dat menigeen zo'n schoonmoeder zou wensen! Ik kijk altijd uit naar onze gesprekken over de medische wereld; jouw interesse is erg groot! Ik hoop nu wat meer tijd te krijgen om samen leuke dingen te gaan doen.

Anne-Marie en Jean-Luc, dank voor de gestelde interesse en steun tijdens mijn promotieonderzoek!

Lieve Sophie, jij bent het grootste geluk in mijn leven! Zonder jou was ik nooit zo ver gekomen. Dank voor je liefde en begrip tijdens mijn promotie. Schat, ik wil je nogmaals zeggen: ik houd heel veel van je! Ik zie de toekomst samen met veel plezier tegemoet.

Curriculum Vitae

De auteur van dit proefschrift werd geboren op 16 maart 1983, te Tilburg. In 2001 behaalde hij zijn eindexamen aan het Koning Willem II College, te Tilburg. Van 2001 tot en met 2008 studeerde hij geneeskunde aan de Rijksuniversiteit Leiden. Tijdens zijn doctoraalfase was hij betrokken bij klinisch wetenschappelijk onderzoek naar het cardiovasculaire risicoprofiel van Hindoestanen onder leiding van dr. P.V. Oemrawsingh, Medisch Centrum Haaglanden, 's Gravenhage en dr. J.H.M. Schreur, Medisch Centrum Haaglanden, 's Gravenhage. Na het behalen van zijn artsexamen in 2008, startte zijn promotieonderzoek op de afdeling cardiologie in het Leids Universitair Medisch Centrum onder leiding van Prof. dr. J.J. Bax en Prof. dr. J.W. Jukema. De onderzoeksresultaten staan beschreven in dit proefschrift. Daarnaast heeft hij deelgenomen aan het klinisch uitvoeren en beoordelen van cardiale CT, MRI en nucleaire scans in patiënten met cardiovasculaire ziekten. Per 1 januari 2011 is hij begonnen aan de klinische opleiding cardiologie aan het Leids Universitair Medisch Centrum (opleider: Prof. M.J. Schalij). Momenteel volgt hij zijn vooropleiding interne geneeskunde in het Bronovo Ziekenhuis te 's Gravenhage (opleider: Dr. J.W. van 't Wout), waarna hij zijn opleiding zal voortzetten op de afdeling cardiologie van het Groene Hart Ziekenhuis (opleider: Dr. M.W.J. van Hessen).